



National Library
of Canada

Acquisitions and
Bibliographic Services Branch

395 Wellington Street
Ottawa, Ontario
K1A 0N4

Bibliothèque nationale
du Canada

Direction des acquisitions et
des services bibliographiques

395, rue Wellington
Ottawa (Ontario)
K1A 0N4

Your file *Votre référence*

Our file *Notre référence*

NOTICE

The quality of this microform is heavily dependent upon the quality of the original thesis submitted for microfilming. Every effort has been made to ensure the highest quality of reproduction possible.

If pages are missing, contact the university which granted the degree.

Some pages may have indistinct print especially if the original pages were typed with a poor typewriter ribbon or if the university sent us an inferior photocopy.

Reproduction in full or in part of this microform is governed by the Canadian Copyright Act, R.S.C. 1970, c. C-30, and subsequent amendments.

AVIS

La qualité de cette microforme dépend grandement de la qualité de la thèse soumise au microfilmage. Nous avons tout fait pour assurer une qualité supérieure de reproduction.

S'il manque des pages, veuillez communiquer avec l'université qui a conféré le grade.

La qualité d'impression de certaines pages peut laisser à désirer, surtout si les pages originales ont été dactylographiées à l'aide d'un ruban usé ou si l'université nous a fait parvenir une photocopie de qualité inférieure.

La reproduction, même partielle, de cette microforme est soumise à la Loi canadienne sur le droit d'auteur, SRC 1970, c. C-30, et ses amendements subséquents.

**VERTICAL DYNAMICS
OF RAILWAY VEHICLE-TRACK SYSTEM**

by

RENGUANG DONG

**A Thesis
in
The Department
of
Mechanical Engineering**

**Presented in Partial Fulfillment of the Requirements
for the Degree of Doctor of Philosophy
at
Concordia University
Montreal, Quebec, Canada**

November 1994



National Library
of Canada

Bibliothèque nationale
du Canada

Acquisitions and
Bibliographic Services Branch

Direction des acquisitions et
des services bibliographiques

395 Wellington Street
Ottawa, Ontario
K1A 0N4

395, rue Wellington
Ottawa (Ontario)
K1A 0N4

Your file *Votre référence*

Our file *Notre référence*

THE AUTHOR HAS GRANTED AN IRREVOCABLE NON-EXCLUSIVE LICENCE ALLOWING THE NATIONAL LIBRARY OF CANADA TO REPRODUCE, LOAN, DISTRIBUTE OR SELL COPIES OF HIS/HER THESIS BY ANY MEANS AND IN ANY FORM OR FORMAT, MAKING THIS THESIS AVAILABLE TO INTERESTED PERSONS.

L'AUTEUR A ACCORDE UNE LICENCE IRREVOCABLE ET NON EXCLUSIVE PERMETTANT A LA BIBLIOTHEQUE NATIONALE DU CANADA DE REPRODUIRE, PRETER, DISTRIBUER OU VENDRE DES COPIES DE SA THESE DE QUELQUE MANIERE ET SOUS QUELQUE FORME QUE CE SOIT POUR METTRE DES EXEMPLAIRES DE CETTE THESE A LA DISPOSITION DES PERSONNE INTERESSEES.

THE AUTHOR RETAINS OWNERSHIP OF THE COPYRIGHT IN HIS/HER THESIS. NEITHER THE THESIS NOR SUBSTANTIAL EXTRACTS FROM IT MAY BE PRINTED OR OTHERWISE REPRODUCED WITHOUT HIS/HER PERMISSION.

L'AUTEUR CONSERVE LA PROPRIETE DU DROIT D'AUTEUR QUI PROTEGE SA THESE. NI LA THESE NI DES EXTRAITS SUBSTANTIELS DE CELLE-CI NE DOIVENT ETRE IMPRIMES OU AUTREMENT REPRODUITS SANS SON AUTORISATION.

ISBN 0-612-01282-4

Canada

Name _____

Dissertation Abstracts International is arranged by broad, general subject categories. Please select the one subject which most nearly describes the content of your dissertation. Enter the corresponding four-digit code in the spaces provided.

--	--	--	--

U·M·I

SUBJECT TERM

SUBJECT CODE

Subject Categories

THE HUMANITIES AND SOCIAL SCIENCES

COMMUNICATIONS AND THE ARTS

Architecture	0729
Art History	0377
Cinema	0900
Dance	0378
Fine Arts	0357
Information Science	0723
Journalism	0391
Library Science	0399
Mass Communications	0708
Music	0413
Speech Communication	0459
Theater	0465

Psychology	0525
Reading	0535
Religious	0527
Sciences	0714
Secondary	0533
Social Sciences	0534
Sociology of	0340
Special	0529
Teacher Training	0530
Technology	0710
Tests and Measurements	0288
Vocational	0747

PHILOSOPHY, RELIGION AND THEOLOGY

Philosophy	0422
Religion	
General	0318
Biblical Studies	0321
Clergy	0319
History of	0320
Philosophy of	0322
Theology	0469

Ancient	0579
Medieval	0581
Modern	0582
Black	0328
African	0331
Asia, Australia and Oceania	0332
Canadian	0334
European	0335
Latin American	0336
Middle Eastern	0333
United States	0337
History of Science	0585
Law	0398
Political Science	
General	0615
International Law and Relations	0616
Public Administration	0617
Recreation	0814
Social Work	0452
Sociology	
General	0626
Criminology and Penology	0627
Demography	0938
Ethnic and Racial Studies	0631
Individual and Family Studies	0628
Industrial and Labor Relations	0629
Public and Social Welfare	0630
Social Structure and Development	0700
Theory and Methods	0344
Transportation	0709
Urban and Regional Planning	0999
Women's Studies	0453

EDUCATION

General	0515
Administration	0514
Adult and Continuing	0516
Agricultural	0517
Art	0273
Bilingual and Multicultural	0282
Business	0688
Community College	0275
Curriculum and Instruction	0727
Early Childhood	0518
Elementary	0524
Finance	0277
Guidance and Counseling	0519
Health	0680
Higher	0745
History of	0520
Home Economics	0278
Industrial	0521
Language and Literature	0279
Mathematics	0280
Music	0522
Philosophy of	0998
Physical	0523

LANGUAGE, LITERATURE AND LINGUISTICS

Language	
General	0679
Ancient	0289
Linguistics	0290
Modern	0291
Literature	
General	0401
Classical	0294
Comparative	0295
Medieval	0297
Modern	0298
African	0316
American	0591
Asian	0305
Canadian (English)	0352
Canadian (French)	0355
English	0593
Germanic	0311
Latin American	0312
Middle Eastern	0315
Romance	0313
Slavic and East European	0314

SOCIAL SCIENCES

American Studies	0323
Anthropology	
Archaeology	0324
Cultural	0326
Physical	0327
Business Administration	
General	0310
Accounting	0272
Banking	0770
Management	0454
Marketing	0338
Canadian Studies	0385
Economics	
General	0501
Agricultural	0503
Commerce-Business	0505
Finance	0508
History	0509
Labor	0510
Theory	0511
Folklore	0358
Geography	0366
Gerontology	0351
History	
General	0578

THE SCIENCES AND ENGINEERING

BIOLOGICAL SCIENCES

Agriculture	
General	0473
Agronomy	0285
Animal Culture and Nutrition	0475
Animal Pathology	0476
Food Science and Technology	0359
Forestry and Wildlife	0478
Plant Culture	0479
Plant Pathology	0480
Plant Physiology	0817
Range Management	0777
Wood Technology	0746
Biology	
General	0306
Anatomy	0287
Biostatistics	0308
Botany	0309
Cell	0379
Ecology	0329
Entomology	0353
Genetics	0369
Limnology	0793
Microbiology	0410
Molecular	0307
Neuroscience	0317
Oceanography	0416
Physiology	0433
Radiation	0821
Veterinary Science	0778
Zoology	0472
Biophysics	
General	0786
Medical	0760

Geodesy	0370
Geology	0372
Geophysics	0373
Hydrology	0388
Mineralogy	0411
Paleobotany	0345
Paleoecology	0426
Paleontology	0418
Paleozoology	0985
Palynology	0427
Physical Geography	0368
Physical Oceanography	0415

HEALTH AND ENVIRONMENTAL SCIENCES

Environmental Sciences	0768
Health Sciences	
General	0566
Audiology	0300
Chemotherapy	0992
Dentistry	0567
Education	0350
Hospital Management	0769
Human Development	0758
Immunology	0982
Medicine and Surgery	0564
Mental Health	0347
Nursing	0569
Nutrition	0570
Obstetrics and Gynecology	0380
Occupational Health and Therapy	0354
Ophthalmology	0381
Pathology	0571
Pharmacology	0419
Pharmacy	0572
Physical Therapy	0382
Public Health	0573
Radiology	0574
Recreation	0575

Speech Pathology	0460
Toxicology	0383
Home Economics	0386

PHYSICAL SCIENCES

Pure Sciences

Chemistry	
General	0485
Agricultural	0749
Analytical	0486
Biochemistry	0487
Inorganic	0488
Nuclear	0738
Organic	0490
Pharmaceutical	0491
Physical	0494
Polymer	0495
Radiation	0754
Mathematics	0405
Physics	
General	0605
Acoustics	0986
Astronomy and Astrophysics	0606
Atmospheric Science	0608
Atomic	0748
Electronics and Electricity	0607
Elementary Particles and High Energy	0798
Fluid and Plasma	0759
Molecular	0609
Nuclear	0610
Optics	0752
Radiation	0756
Solid State	0611
Statistics	0463

Applied Sciences

Applied Mechanics	0346
Computer Science	0984

Engineering

General	0537
Aerospace	0538
Agricultural	0539
Automotive	0540
Biomedical	0541
Chemical	0542
Civil	0543
Electronics and Electrical	0544
Heat and Thermodynamics	0348
Hydraulic	0545
Industrial	0546
Marine	0547
Materials Science	0794
Mechanical	0548
Metallurgy	0743
Mining	0551
Nuclear	0552
Packaging	0549
Petroleum	0765
Sanitary and Municipal	0554
System Science	0790
Geotechnology	0428
Operations Research	0796
Plastics Technology	0795
Textile Technology	0994

PSYCHOLOGY

General	0621
Behavioral	0384
Clinical	0622
Developmental	0620
Experimental	0623
Industrial	0624
Personality	0625
Physiological	0989
Psychobiology	0349
Psychometrics	0632
Social	0451



ABSTRACT

VERTICAL DYNAMICS OF RAILWAY VEHICLE-TRACK SYSTEM

Renguang Dong

A comprehensive finite element (FE) model of railway vehicle-track system is developed to study the dynamic interaction between the vehicle and track. The vehicle is represented by a lumped parameter system. The track is modeled as a Timoshenko beam on discrete pad-tie-ballast supports. The tie is considered either as a rigid body or a non-uniform beam. The rail-pad and ballast are modeled as distributed spring-damper elements. The non-linear factors such as loss of wheel/rail contact, rail lift-off from the tie and tie lift-off from the ballast are taken into account. A cutting and merging method along with a set of special boundary conditions is established to extend finite length of track to infinitely long track so that a vehicle can be modeled to travel on the track indefinitely with a time-dependent speed. A numerical direct integration technique is employed to solve the equations of motions of the vehicle and track systems. An adaptive multi-point wheel/rail contact model is proposed and used to calculate the normal and geometrical longitudinal forces due to irregularities in the wheel/rail contact region. The developed FE model is validated using the experimental data obtained from British Rail and Canadian Pacific (CP) Rail. The FE results such as natural frequencies of concrete ties, the wheel/rail contact forces, the rail-pad forces and dynamic strains in the rail, generally show good correlation to the experimental data. The validated model is applied to investigate the characteristics of impact loads due to wheel/rail tread defects such as wheel flats, wheel shells and rail joints. The steady-state interaction between the vehicle and

track, and the dynamic force due to rail corrugations are also evaluated for high speed operation.

The results of this study show that the impact load is maximum at the ties, and is strongly influenced by the axle load, vehicle speed, actual shape of the defect, and rail equivalent mass. Elastomeric shear pads on the wheelset bearing, and reduced rail-pad stiffness, can potentially reduce dynamic bearing force and tie dynamic load, respectively. The magnitude of resonant force for vehicle-track system in a steady-state interaction mainly depends on the unsprung mass, tie spacing, vehicle primary and track ballast damping, and rail stiffness. In the presence of rail corrugation, the energy consumption due to longitudinal force increases quadratically with the depth of rail corrugation. The dynamic contact forces at neighboring wheels are influenced by each other and the basic mechanism that controls such an interaction is the superposition of the dynamic responses. Stable solution in the speed range 0 to 1440 km/h demonstrates the effectiveness of the model for high speed simulation.

ACKNOWLEDGMENTS

First of all, the author would like to thank Dr. S. Sankar for initiating the project, and providing guidance, support and supervision throughout the course of this study until his departure in June 1994. The author would also like to thank Dr. A.K.W. Ahmed, whose supervision finally lead to the completion of the thesis. Sincere thanks are also due to Dr. R.V. Dukkupati of National Research Council of Canada for his co-supervision throughout the course of this study.

The author is grateful to visiting scientist, Prof. Y.S. Hu for his collaboration on the study of freight car dynamic forces due to dipped rail joints. Valuable discussion and encouragement provided by Mr. W. Pak of CP Rail System on many aspects of the study is gratefully acknowledged.

Thanks are due to the faculty members, staff, and other graduate students of CONCAVE Research Center, and the Department of Mechanical Engineering for their help during the course of this work.

Finally, the author would like to express his special thanks to his wife, Jin Wang, parents and other family members for their love, encouragement and support.

TABLE OF CONTENTS

	PAGE
LIST OF FIGURES	x
LIST OF TABLES	xvi
NOMENCLATURE	xvii

CHAPTER 1

INTRODUCTION & LITERATURE REVIEW

1.1 Introduction	1
1.2 Literature review	6
1.2.1 Vehicle models	9
1.2.2 Wheel/rail contact models	12
1.2.3 Modeling of track components	14
1.2.4 Track system models	18
1.2.5 Irregularity representation and track length	24
1.2.6 Frequency-domain solution methods	26
1.2.7 Time-domain solution methods	30
1.3 Scope of the investigation	33

CHAPTER 2

MODELING OF RAILWAY VEHICLE-TRACK SYSTEM

2.1 Introduction	38
2.2 Vehicle system models	39

2.3	Finite elements of track components	43
2.3.1	Finite element for rail	43
2.3.2	Finite elements for ties	49
2.3.3	Finite elements for rail-pad	50
2.3.4	Finite element for ballast and subgrade	55
2.3.5	Finite element for fasteners	56
2.4	Track system model	56
2.4.1	Basic track system model	56
2.4.2	Extension of finite length of track to infinite track	59
2.5	Representation of wheel/rail contact force	62
2.5.1	Calculation of vertical contact force	62
2.5.2	Calculation of geometric longitudinal force	65
2.6	Procedures of vehicle/track interaction calculation	67
2.7	Summary	69

CHAPTER 3

NATURAL FREQUENCIES OF VEHICLE-TRACK SYSTEM

3.1	Introduction	72
3.2	Natural frequencies of concrete ties and wheelsets	72
3.2.1	CN Type-A bridge concrete Tie	75
3.2.2	CT-3 track concrete Tie	78
3.2.3	Natural frequencies of a wheelset	82
3.3	Natural frequencies of vehicle-track system	85
3.3.1	Wheel-track system	85
3.3.2	Car(body)-wheel-track system	93

3.4 Summary	93
-------------	----

CHAPTER 4

IMPACT LOADS DUE TO WHEEL FLATS AND SHELLS

4.1 Introduction	97
4.2 Description of wheel defects	102
4.3 Validations of FE model	104
4.3.1 Validation against BR's experimental data	104
4.3.2 Validation against CP Rail's experimental data	120
4.3.3 Verifications of the adaptive contact model	128
4.4 Dynamic response characteristic due to wheel defect	134
4.5 A parametric study on impact loads	137
4.5.1 Effect of axle load	138
4.5.2 Effect of unsprung mass and vehicle primary stiffness	140
4.5.3 Effect of vehicle speed	140
4.5.4 Effect of rail-pad stiffness	143
4.5.5 Effect of ballast stiffness	143
4.5.6 Equivalent tie mass	147
4.5.7 Effect of rail type	147
4.5.8 Impact position	147
4.5.9 Effect of flat size	147
4.5.10 Effect of lift-offs of rail from tie and tie from ballast	150
4.5.11 Effect of longitudinal force	150
4.6 Dynamic interaction between two wheels due to wheel tread defects	152
4.7 Summary	156

CHAPTER 5
THE DYNAMIC EFFECTS OF CONVENTIONAL FREIGHT CAR
RUNNING OVER A DIPPED RAIL JOINT

5.1 Introduction	158
5.2 Vehicle-track system model	159
5.3 Dynamic response	161
5.4 Parametric studies	169
5.5 Summary	179

CHAPTER 6
STEADY-STATE INTERACTION
BETWEEN RAILWAY VEHICLE AND TRACK

6.1 Introduction	180
6.2 Steady state dynamic response	182
6.3 Track deflection in steady-state interaction	190
6.4 Effects of vehicle speed and acceleration on W/R contact force	195
6.5 Influence of system parameters on resonance force	198
6.6 An application of the FE model to hard spot and void problem	205
6.7 Summary	207

CHAPTER 7
WHEEL/RAIL DYNAMIC CONTACT FORCES
DUE TO RAIL CORRUGATIONS

7.1 Introduction	209
------------------	-----

7.2 Vertical and geometrical longitudinal dynamic forces	212
7.3 Dynamic interaction between two wheels	221
7.3.1 The mechanism of interaction	221
7.3.2 Phase relationship among dynamic forces and excitation sources	225
7.4 Summary	233

CHAPTER 8

CONCLUSIONS AND RECOMMENDATIONS

8.1 Highlight of the thesis	235
8.2 Specific conclusions	237
8.2.1 Natural frequencies of vehicle-track system	237
8.2.2 Impact loads due to wheel flats and shells	238
8.2.3 Dynamic force due to a dipped-rail joint	239
8.2.4 Steady-state interaction between vehicle and track	239
8.2.5 Response to rail corrugation	240
8.3 Recommendations for further studies	241
REFERENCES	244

LIST OF FIGURES

CHAPTER 1

Figure 1.1	Railway vehicles and tracks	3
Figure 1.2	Basic compositions of railway vehicle-track system	3
Figure 1.3	A general vehicle-track interaction system	9
Figure 1.4	Hierarchy of track models	19

CHAPTER 2

Figure 2.1	Vehicle models employed in the FE system model	40
Figure 2.2	A Timoshenko FE beam model	44
Figure 2.3	The relationship between local and global coordinates	51
Figure 2.4	Rail-pad, tie and ballast finite elements	53
Figure 2.5	Physical track system in the FE system model	57
Figure 2.6	Extension of finite length of track to infinite track	60
Figure 2.7	An adaptive contact model	66
Figure 2.8	The relationship between W/R overlap and vertical static force	66
Figure 2.9	Geometric longitudinal force	68

CHAPTER 3

Figure 3.1	Imposing a pair of springs to a free-free beam	74
Figure 3.2	Effects of spring stiffness and support locations on frequencies of a concrete tie	74
Figure 3.3	Dimension of CN Type-A bridge concrete tie	76
Figure 3.4	Dimension of CT-3 concrete tie	76
Figure 3.5	Dimension of wheelset axle system	84

Figure 3.6	Wheelset model	84
Figure 3.7	Dispersion relation for a wheel-track system	88
Figure 3.8	Comparison of the mode shape of the wheel/track fundamental frequency with the deflection shape of track	90
Figure 3.9	Car-wheel-track system	93

CHAPTER 4

Figure 4.1	Wheel flats at the same "o'clock" position on a single wheelset	98
Figure 4.2	A fully shelled wheel	99
Figure 4.3	Configuration used in British Rail experiment	106
Figure 4.4	Wheel/rail contact force due to wheel flat	108
Figure 4.5	Effect of rail equivalent mass on impact load (Calculated from the TBEF track model)	110
Figure 4.6	Dynamic wheel/rail and pad force factor factors due to a wheel flat	111
Figure 4.7	Rail foot bending strains	113
Figure 4.8	Rail shear strains	114
Figure 4.9	Rail foot bending strains calculated from refined FE model	115
Figure 4.10	Rail shear strains calculated from refined FE model	116
Figure 4.11	Effect of boundary conditions on the impact response due to a haversine wheel flat	118
Figure 4.12	Effect of speed on dynamic response	119
Figure 4.13	Location of defective wheels on the consist	122
Figure 4.14	Changes in effective rolling radius of wheel with defects	123
Figure 4.15	Simulation of a wheel impact detector	125

Figure 4.16 Wheel/rail contact force in a drop test	127
Figure 4.17 Impact loads due to wheel flats (L11 and L12 in [36])	129
Figure 4.18 Impact loads due to a wheel shell (L22 in [36])	130
Figure 4.19 Wheel/rail contact force due to a haversine flat	132
Figure 4.20 Dynamic forces and strains calculated from different contact models	133
Figure 4.21 Dynamic forces calculated from different contact models due to a wheel tread defect (L11 in Ref. [36])	135
Figure 4.22 Dynamic forces calculated from different contact models due to a wheel tread defect (L12 in Ref. [36])	135
Figure 4.23 Response of forces and displacements	136
Figure 4.24 Effect of static load on impact load	139
Figure 4.25 Effect of unsprung mass on impact load	141
Figure 4.26 Effect of speed on dynamic force	142
Figure 4.27 Effect of rail-pad stiffness on impact force	144
Figure 4.28 Dropping response on a concrete-tie track (calculated with CPR parameters in Table 4.2)	145
Figure 4.29 Effect of ballast stiffness on impact force	146
Figure 4.30 Effect of equivalent tie mass on impact load (BR parameters)	148
Figure 4.31 Effect of rail type on impact force (CPR parameters)	148
Figure 4.32 Effect of impact position on impact load (CPR parameters)	149
Figure 4.33 Effect of flat size on impact load (CPR parameters)	149
Figure 4.34 Effect of lift-offs on impact load	151
Figure 4.35 Effect of longitudinal force on impact load (BR parameters)	151
Figure 4.36 Across-wheel force due to a wheel flat	153

Figure 4.37 Dynamic force superposition	155
CHAPTER 5	
Figure 5.1 Vehicle/track model at dipped rail joint	160
Figure 5.2 Impact response calculated from an Euler beam on elastic foundation	163
Figure 5.3 Impact response for different track models	165
Figure 5.4 Impact forces at two wheels	167
Figure 5.5 Dynamic forces on leading and trailing wheels	168
Figure 5.6 Effect of wheel mass	170
Figure 5.7 Effect of bearing pad stiffness	170
Figure 5.8 Effect of axle load	171
Figure 5.9 Effect of increasing stiffness of rail pad	171
Figure 5.10 Effect of rail mass	173
Figure 5.11 Effect of ballast stiffness	173
Figure 5.12 Effect of bearing pad stiffness	174
Figure 5.13 Effect of different profiles	175
Figure 5.14 Effect of raising the tie height	176
Figure 5.15 Effect of tie height and pad stiffness	177
Figure 5.15 Impact response of high speed vehicle	178
CHAPTER 6	
Figure 6.1 Wheel, rail and tie displacements, W/R contact force in a steady-state interaction	185
Figure 6.2 A resonance in a steady-state interaction (BR parameters in Table 4.1)	186

Figure 6.3	Effect of rail finite element length on dynamic force	187
Figure 6.4	Effect of tie mass on short wave fluctuation	187
Figure 6.5	Steady-state dynamic forces on leading and trailing wheels	189
Figure 6.6	Dynamic deflection of a non-linear track system in a steady-state interaction (BR parameters in Table 5.1)	191
Figure 6.7	Track deflection at different speeds	193
Figure 6.8	Effect of vehicle speed on maximum deflection of rail	194
Figure 6.9	Steady-state dynamic W/R contact force (3-DOF vehicle model, 0.7 m tie spacing)	196
Figure 6.10	Steady-state dynamic W/R contact force (5-DOF vehicle model, 0.6096 m tie spacing)	196
Figure 6.11	Effect of vehicle speed on W/R contact force	197
Figure 6.12	Effect of step-changed vehicle speed on W/R contact force	197
Figure 6.13	Effect of vehicle unsprung mass	199
Figure 6.14	Effect of rail-pad width	199
Figure 6.15	Effect of damping on primary suspension, rail-pad and ballast	201
Figure 6.16	Effect of equivalent tie mass	201
Figure 6.17	Effect of ballast stiffness	203
Figure 6.18	Effect of rail-pad stiffness	203
Figure 6.19	Effect of tie spacing	204
Figure 6.20	Effect of rail type	204
Figure 6.21	Representation of hard spot and void	206
Figure 6.22	Dynamic force due to hard spot and void	206

CHAPTER 7

Figure 7.1	Rail corrugation	210
Figure 7.2	Dynamic responses due to rail corrugation	214
Figure 7.3	Dynamic force due to rail corrugation	217
Figure 7.4	Work consumed per unit time on one wheel due to geometrical longitudinal force caused by rail corrugation	217
Figure 7.5	Effect of corrugation depth on energy consumption	218
Figure 7.6	Effects of corrugation wavelength on dynamic force	218
Figure 7.7	Effects of speed on dynamic force due to rail corrugation	220
Figure 7.8	Initiating and across-wheel forces due to a corrugation	220
Figure 7.9	Superposition of dynamic forces (linearized contact model)	223
Figure 7.10	Superposition of dynamic forces (adaptive contact model)	224
Figure 7.11	Phase relationship among dynamic forces and exciting sources	226
Figure 7.12	Effect of wheelset axle spacing on maximum dynamic force due to a sinusoidal rail corrugation	228
Figure 7.13	Effect of wheelset axle spacing on phase lag of across-wheel force due to a sinusoidal rail corrugation	230
Figure 7.14	The maximum peak dynamic force on trailing wheel purely due to a rail corrugation under trailing wheel	231

LIST OF TABLES

Table 1.1	Problems of vehicle-track interaction	7
Table 3.1	Natural frequencies of CN Type-A concrete bridge tie	77
Table 3.2	Natural frequencies of CT-3 concrete track tie	80
Table 3.3	Natural frequencies of a wheelset	86
Table 3.4	Natural frequencies of a car(body)-wheel-track system	95
Table 4.1	Nominal parameter values for British Rail's vehicle-track system (based on Ref. [109])	107
Table 4.2	Nominal parameter values for CP Rail's vehicle-track system (based on Ref. [36])	124
Table 6.1	Nominal parameter values	183
Table 7.1	Nominal parameter values	213

NOMENCLATURE

<u>SYMBOL</u>	<u>DESCRIPTION</u>
A_r	Cross-sectional area of rail
BG1, BG2	Rail bending strains defined in Ref. [107]
C_1	Primary damping of vehicle
C_2	Secondary damping of vehicle
C_b	Ballast damping
c_b	Ballast damping per unit length ($=C_p/L_p$)
C_H	Wheel/rail Hertzian spring constant
C_m	Mutual interaction coefficient
C_p	Rail-pad damping
c_p	Rail-pad damping per unit length ($=C_p/L_p$)
C_s	Self interaction coefficient
c_v	Extra damping per unit length added at every rail end
[C]	Damping matrix
D_1, D_2	Parameters used to define irregularity of rail joint (see Eqs. 5.3 and 5.4)
D_f	Depth of haversine wheel flat
E_{ct}	Young's modulus for concrete tie
E_r	Young's modulus for rail steel
E_w	Young's modulus for wheelset axle steel
f	Haversine wheel flat function
F_{Li}	Geometrical longitudinal force on an element contact spring
f_n	Natural frequency
f_{p-p}	Natural frequency for pinned-pinned model of rail

$f_{w/t}$	Coupled wheel/track natural frequency
$\{F\}$	Force vector
G_{ct}	Shear modulus for concrete tie
G_r	Shear modulus for rail steel
G_w	Shear modulus for wheelset axle steel
h	Finite element length
h_i	The raising height of the i th counted from the joint point
I_r	Rail second moment of area
J_b	Bogie pitch initial moment
J_w	Wheel rotational initial
K_1	Primary spring stiffness of vehicle
K_2	Secondary spring stiffness of vehicle
K_b	Ballast spring stiffness
k_b	Ballast spring stiffness per unit length ($=K_b/L_b$)
K_c	Wheel/rail contact stiffness
k_e	Stiffness of contact element spring in adaptive contact model
k_f	Foundation stiffness per unit length for beam on Winkler foundation model
K_H	Linearized Hertzian contact stiffness
K_p	Rail-pad stiffness
k_p	Rail-pad stiffness per unit length ($=K_p/L_p$)
k_{pi}	The rail-pad stiffness at i th tie counted from the rail joint
K_r	Rail end rotational stiffness
K_v	Rail end vertical stiffness
$[K]$	Stiffness matrix
K_θ	Rotational stiffness between the car-body and bogie

L_1, L_2	Parameters used to define irregularity of rail joint (see Eqs. 5.3 and 5.4)
L_a	Wheelset axle spacing
L_b	Tie bottom width along longitudinal direction
L_{ct}	Total length of concrete tie
L_f	Length of haversine wheel flat
L_p	Rail-pad width along longitudinal direction
L_r	Total length of rail used in the calculation
L_t	Tie spacing
L_w	Total length of wheelset
M_b	Bogie mass
M_c	Car body mass
m_{ct}	Tie mass per unit length
M_f	Sideframe mass
m_r	Rail mass per unit length
m_{TR}	Track effective mass per unit length
M_w	Wheel mass
M_{w1}	Leading wheel mass
M_{w2}	Trailing wheel mass
$[M]$	Mass matrix
N_a	Axial force in rail (x direction)
P_1	The first peak impact load
P_2	The second peak impact load
P_{12}	The peak impact load located between P_1 and P_2 (see Fig. 5.2)
P_{b1}	The first peak ballast load
P_{b2}	The second peak ballast load
P_{p1}	The first peak load on rail-pad

P_{p2}	The second peak load on rail-pad
P_{1f}	The first impact load of the leading wheel at the rail joint
P_{1r}	The first impact load of the trailing wheel at the rail joint
P_{01f}	The contact force of the leading wheel before impacting (see Fig.5.5)
P_{01r}	The contact force of the trailing wheel before impacting (see Fig.5.5)
P_c	Wheel/rail contact force
P_{CT}	Wheel/rail contact force at the trailing wheel
P_{CL}	Wheel/rail contact force at the leading wheel
P_{c1}	The first peak of wheel-rail contact force
P_{c2}	The second peak of wheel-rail contact force
p_i	Vertical contact force on a element contact spring
P_i	Wheel/Rail maximum contact force directly caused by a irregularity, where i may be L (leading wheel) or T (trailing wheel).
P_{i-j}	Across-wheel contact force at Wheel j (L or T) due to initiating force at Wheel i (L or T)
$P_L(x,t)$	Wheel/rail total contact force on leading wheel
P_m	Maximum contact force
P_0	Static load per wheel
P_{p1}	The first peak force between the rail and tie (Pad force)
P_{p2}	The second peak force between the rail and tie (Pad force)
$P_T(x,t)$	Wheel/rail total contact force on trailing wheel
R	Wheel rolling radius
$SG2, SG3,$	
$SG4$	Rail shear strains defined in ref. [107]
T	Rail temperature

T_{ct}	Timoshenko shear coefficient for concrete tie
T_r	Timoshenko shear coefficient for rail
T_w	Timoshenko shear coefficient for wheelset axle
u	Coordinate in the vertical direction
U	Kinetic energy
V	Vehicle traveling speed or potential energy
V_{cr}	Vehicle critical traveling speed
V_m	Wave propagation speed in rail
x	Coordinate in the longitudinal direction
Y	The vertical position on the cross-section of rail relative to neutral plane
Y_b	Ballast relative support height ("minus" for under-supported and "plus" for over-supported)
α	Rail joint angle
α_i	FE beam shape function for u
α_t	Temperature coefficient of rail steel expansion
α_{gi}	Wheel/rail geometrical contact angle in the longitudinal direction
β_i	FE beam shape function for ϕ
β_{pi}	The phase of initiating force (p_i) relative to the input corrugation
β_{i-j}	The phase of across-wheel force (p_{i-j}) relative to the initiating force
γ	The angle between a local and global coordinates
γ_{xy}	Shear strain of rail at the neutral plane
ξ	Non-dimension coordinate of FE beam element
ε_y	Normal strain of rail at the vertical position of Y on the cross-section
$\{\eta\}$	Displacement vector
θ_b	Bogie rotational angle

θ_{ct}	Concrete tie rotational angle
ϕ	Rotational angle in a FE beam element
ϕ_{f-d}	The phase difference between the contact force and the displacement wave of rail
ρ_{ct}	Mass density of concrete tie
ρ_w	Mass density of wheelset axle
ρ_r	Mass density of rail steel
λ	Corrugation wavelength
μ	Peak-peak depth of rail corrugation
ν_{ct}	Possion's ratio for concrete tie
ν_w	Possion's ratio for wheelset axle
ν_r	Possion's ratio for rail steel

CHAPTER 1

INTRODUCTION & LITERATURE REVIEW

1.1 INTRODUCTION

Railway transportation system has been in existence for about 170 years and it is still a major mode of transportation all over the world. In the areas with large populations such as in Europe, Asia and many developing countries, railways dominate both the passenger and goods transportation. Even though the highway transportation system is very popular in North America, about 40% (MGT) in U.S.A. and 77% (MGT) in Canada of goods transportation still depend on railways [159]. Railway system is an economical, efficient and environment-friendly transportation mode and it plays very important roles in the world commerce and world development.

However, railway transportation system is under constant pressure to compete with air and road transport systems. Worldwide attention, therefore, has been directed towards improving the efficiency of railway operation in terms of speed and load carrying capacity. In recent years, train speed has reached over 500 km/h [38]. At the same time, the load carrying capacity has been increased significantly approaching 35 tons per axle [118]. These demonstrate that railways will remain one of the major transport systems during the 21st century.

With the increase in operating speed and axle load, there is a growing concern about the track system, its dynamics and dynamic vehicle/track interaction. In recent years, significant attention and studies have been directed towards better understanding of vehicle/track interaction in order to improve the vehicle and

track design, reduce the cost of maintenance and assure safety. The complexity is extreme, but the demands for increased speeds and greater load capacity, which bring new problems of wear, fatigue and stability, have forced railway operators and equipment suppliers to address these problems in a more systematic and fundamental way.

A pictorial view of railway vehicle and track is shown in Fig. 1.1. The various components of the vehicle/track system in the vertical direction is represented by an schematic diagram in Fig. 1.2. Clearly, such a combined system is complex not only because it involves in many components with wide range of mechanical properties, but also because the dynamic variables are function of both time and position. It is therefore, very common that the dynamic studies of the combined system is divided into two subsystems and considered separately. These subsystems are the vehicle system and the track system.

The study of the vehicle subsystem includes car body, secondary suspension, bogie or truck, primary suspension, wheelset and rail which may be rigid or flexible. Such a system is studied on tangent or curves track for rock and roll dynamics, lateral stability (hunting) and curving performance. The track subsystem on the other hand includes the rail, rail-pad, tie, ballast and subgrade, which is mainly considered to study the rail and tie strength, the buckling of track and the deterioration of the track geometry. In these studies, the dynamic interactions between track and vehicle are either ignored or idealized as some form of given functions. Such simplified approach is valid to some extent for many of the investigations carried out to evaluate vehicle system design and track design.



Figure 1.1 Railway vehicles and tracks

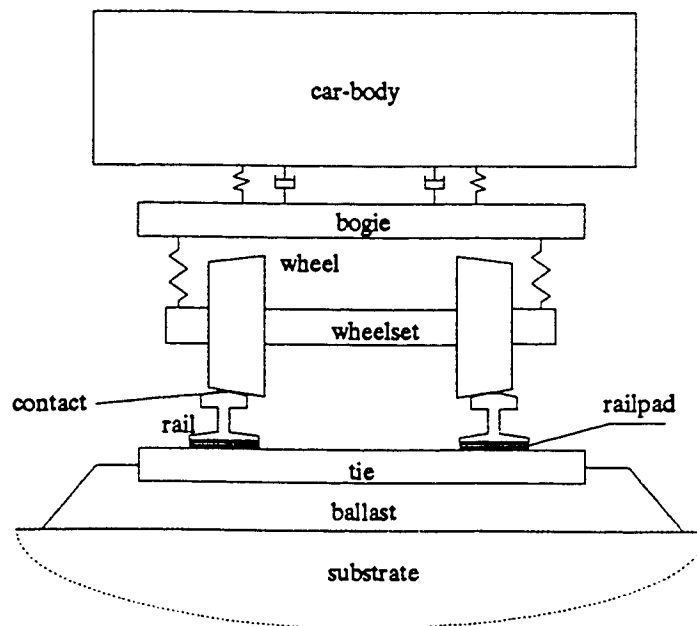


Figure 1.2 Basic compositions of railway vehicle-track system

With the increasing vehicle operating speed and axle load, the interaction between the vehicle and track has become more pronounced than ever before, and can not be ignored or idealized in some cases. Not only the high speed and heavy load operation largely depends on the dynamic responses of the vehicle and track system but also such operating conditions could cause damage to the track and vehicle. A better understanding of the vehicle/track interaction is therefore essential to carry out further development in this area. In the recent years, considerable attention has been directed towards problems associated with wheel and rail tread defects, the rail corrugations and wheel/rail wear and noise. These problems and their influence on the dynamic behavior of vehicle and track can only be investigated through comprehensive modeling of combined vehicle/track system.

This investigation is aimed at developing a comprehensive vehicle/track model as a tool to obtain an in-depth understanding of the interaction between vehicle and track. The versatile Finite element (FE) method has been widely used in many scientific fields and several commercial FE software packages are available. This method can conveniently deal with the complex structures and boundary conditions so that the wheel and track can be considered more realistically even at very high frequencies. However, it is difficult to use these commercial FE software packages to simulate the vehicle/track dynamic interaction if the vehicle is considered as a moving system on the stationary track. A comprehensive FE model of the railway vehicle-track system has been developed for this study. This development is a major contribution that provides a practical approach to simulate a moving system on an infinite structure using standard FE method.

Although such model can be used to study almost any aspects of railway vehicle-track system, this study focuses on some important aspects of vehicle/track interaction problems. Most damage to the vehicle and track is caused by the dynamic forces generated at the wheel/rail interface. Wheel and rail irregularities such as wheel flats, wheel shells, rail joints and rail corrugations are the major sources that cause severe dynamic forces. Railway administrations are currently advocating them as priority areas in railway problems. This study therefore, investigates the characteristics of the dynamic forces due to these defects or irregularities, which may lead to a better understanding and treatment of these problems.

In this study, the developed vehicle/track model is validated wherever possible by comparing the simulated results with available experimental data. The validated model is utilized to investigate the characteristics of impact loads due to wheel tread defects such as wheel flats, shells and bolted rail joints. Simulation is also carried out to investigate the steady-state vehicle-track interaction forces and deflections. Finally, the dynamic forces due to rail corrugations are evaluated and discussed.

1.2 LITERATURE REVIEW

In the last three decades, extensive research work has been carried out on various aspects of railway vehicle dynamics, with prime objective of increasing operating speed, improving safety, improving ride quality, and reducing wear and maintenance. Table 1.1 lists the areas that are of concern in the study of railway vehicle-track system. Among these, the items 1, 2 and 3 have been studied extensively over the years where the vehicle and bogie system studies consider idealized track and the track system studies consider idealized vehicle. In general, the dynamic behaviors of these systems are well understood for most practical purposes.

Items 4, 5 and 6 in Table 1.1, are of increasing concern with the advancement of vehicle speed and load capacity. Some of these problem such as wheel flats and rail joints have been of concern for some time but many aspects have not been fully understood. Rail corrugations are also old problem but further effort is required to search for their mechanisms of formation and development. So far a satisfactory theory about the short-wave corrugation found on many fast lines and transit system has not been established.

The last two items in Table 1.1 dealing with noise and ground-borne vibration are considered new problems because of increasing concern for environmental quality, especially on the transit systems.

TABLE 1.1 PROBLEMS OF VEHICLE-TRACK INTERACTION

	AREA OF CONCERN	FREQUENCY (HZ)	REFS.
1	Vehicle (a) lateral stability (b) vertical stability (c) curving and derailment	0-20	[58]
2	Bogie and unsprung mass (a) wheel bearings (b) fatigue of axles, brake gear etc.	0-500	[157]
3	Steady-state response of track due to a moving load	0-1000	[2,17,19,21, 22,41,46,81 87,88,105, 106,113,142, 151,158]
4	Steady-state vehicle-track interaction		[12,108,144, 145]
5	Irregular running surfaces of wheel and rail (a) wheel flats (b) out-of-round wheels (c) wheel corrugation (d) "long wavelength" rail corrugation (e) "short wavelength" rail corrugation (f) dipped welds and joints (g) pitting, shelling (h) random wheel and rail irregularities	0-2000	[18,36,37,40,49,107] [4,5] [91] [99-102] [23,24,70,75,86,160] [77,80,98,119] [36,37] [5,30]
6	Track components (a) fatigue of rail in bending (b) railpads (c) concrete ties (d) ballast and track geometry	0-1500	[31]
7	Wheel/rail noise (a) rolling noise (b) impact noise (c) squeal	0-5000	[12,123, 131,149]
8	Structure-borne noise and vibration (a) ground-borne vibration (b) viaducts	0-500	[33,43,112,125]

The literature in this field has been reviewed by many researchers and several good surveys have been published. Knothe and Grassie [92] have recently given a detail review of the modeling of railway track and vehicle-track interaction in the high frequency range. The historical surveys, general problems and most of the dynamic models in this field have been covered in the review. Fryba [55] and Kerr [90] have, respectively, given historical surveys and solution method reviews on the steady-state response of infinite beams subjected to moving loads. State of art paper on railway vehicle dynamics has been written by Sankar and Samaha [126]. Fryba [54] has also given a brief review of the dynamic interaction of vehicles with tracks. A literature survey on the dynamic interaction between train and track has also been reported by Dahlberg [27]. A review on vehicle-guideway interactions has been written by Taheri and et al. [146].

Two books have appeared in the scientific field of dynamics of vehicle-track system. The book written by Garg and Dukkipati [58] deals with the vehicle and train system dynamics. In this book, the track vibrations and the interactions are not considered and the effects of the track are usually idealized as some kinds of input functions in the modeling. On the other hand, Fryba [55] considered the vehicle as simplified as constant moving forces and the vibrations of solids and structures are discussed. The main part of this book deals with the vibrations of one-dimensional solids such as beams and frames subjected to moving loads but it also discusses the two-and three-dimensional solids and special problems.

As mentioned earlier, there is a very wider interest in the study of vehicle-track interaction in high speed operation. Such study combining vehicle and track model has become feasible with the advancement of computational tools. Such

study must consider all important aspects of vehicle and track system within the model. The dynamic interactions between the railway vehicle and track generally involve in four main components as presented in Fig. 1.3. These components namely, vehicle model, wheel/rail contact model, track model, and wheel/rail irregularity representation should be combined and solved using efficient numerical technique for realistic simulation. A brief review of literature on each aspects of vehicle-track interaction modeling shown in Fig. 1.3 along with simulation technique is presented in the following subsections so as to develop the scope of the present investigation.

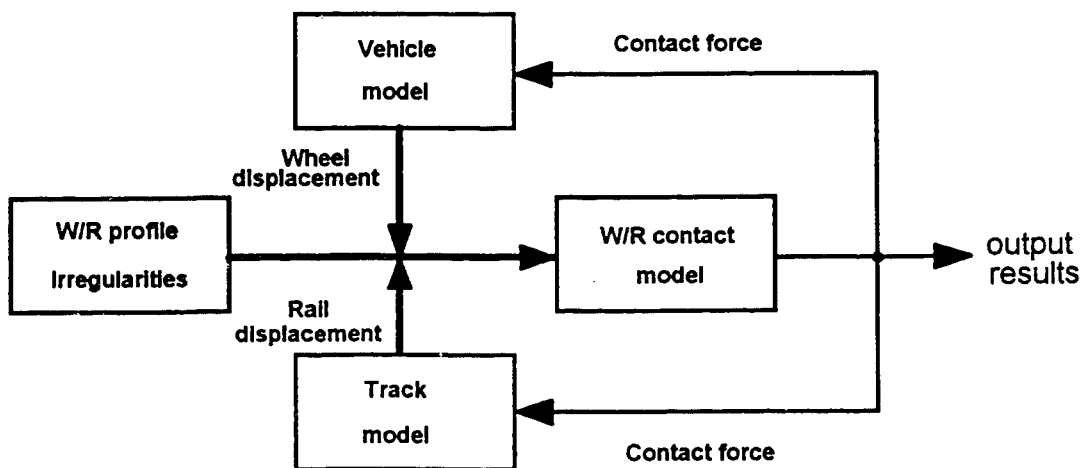


Fig. 1.3 A general vehicle-track interaction system

1.2.1 VEHICLE MODELS

The vehicle is often divided into sprung mass and unsprung mass systems in the analysis. The sprung mass system includes the car body and bogie (see Fig.

1.2) (on a freight car with three-piece-truck, the sprung mass system includes the car body and bolster). The unsprung mass may consist of the wheelset, bearings, axle-hung traction motor and gearing.

The type of the vehicle model employed in a dynamic study mainly depends on the frequency range involved in the specific problem that is under investigation. As indicated in [92], in the low frequency range (less than 20 Hz), the major problems in the system are the vehicle curving, stability and, ride quality for passenger or cargo. Vehicle suspensions are usually designed to ensure that rigid body modes of a vehicle's bogie and body occur at less than 10 Hz in order to isolate the vibration from passengers and to reduce the effective unsprung mass. In this frequency range, the track behaves essentially as a relatively stiff spring and its effect on the vehicle's behavior is small, especially in the vertical direction. Hence, the vehicle is usually modeled as lumped mass systems, as used by many researchers in the vehicle dynamics, e.g. [58]. Several commercial software such as NUCARS, MEDYNA, VAMPIRE and VOCO, have been available to analyze the vehicle behaviors.

At frequencies in the range of 20~100 Hz, the coupled resonance of vehicle-track system may be caused by long wavelength irregularities on the wheels and rail treads, and in the track supports. The dynamic forces on the wheelset bearings and bogie may be strongly affected by the resonance. It is prudent to take into account both the sprung mass and unsprung mass in this case.

When the vertical dynamic forces due to wheel and/or rail irregularities such as wheel flats and rail joints are of concerned, frequencies between 20 to 1500 Hz may be involved in the response. The most active component on the vehicle is

the wheelset or unsprung mass. For this reason, it is adequate to take only an effective wheel mass loaded with a constant force into the model, as used by Newton and Clark [107]. If the dynamic forces on the bearings are of concern, the sprung mass has to be included in the model. If the interaction between wheels on different wheelsets is of concern, half car models with several degrees of freedom may be used. They have been employed by Cai et al. [18], Schwab et al. [133], Nielsen et al. [109], Hu et. al. [77], and in the present work. The two wheels within a wheelset, two side-frames and one bolster have been taken into account as lumped masses by Ahlbeck [3]. An approach has also been suggested by Ahlbeck [3] to include the first four bending modes of wheelset in the vehicle model.

The behaviors of railway wheelsets at high frequencies of excitation both in vertical and lateral plane has been investigated by Grassie et al. [70]. The wheelset is idealized as wheels on a uniform shaft which can extend and bend. Each wheel model is composed of a rigid hub, a thin uniform circular web, and a rim. The hub is encastre on the end of the shaft. The web can deform in bending only and is encastre on the hub and the rim. The rim is a uniform ring of rectangular cross-section.

In the noise studies, very high frequencies (up to 5000 Hz) may be concerned. The elasticity of wheel and wheelset axle have to be taken into account. The major technique used in the simulations is the finite element method. Finite element models of wheels have been reported by Schneider and Popp [131], Thompson [149], and Ganesan and Ramesh [57]. Curved Timoshenko beam on elastic foundation has also been used to model a wheel by Bogacz and Dzula [16].

1.2.2 WHEEL/RAIL CONTACT MODELS

A survey of wheel-rail rolling contact theory has been given by Kalker [84]. State of art paper on the prediction of wheel/rail dynamic contact has been written by Elkins [44]. The book on contact mechanics written by Gladwell [59] deals with contact problems in the classical theory of elasticity. It excludes rolling contacts and is restricted to perfectly elastic solids. Without these limitations, the book written by Johnson [82] includes more aspects of contact problems in engineering applications.

In the vertical dynamics of railway vehicle-track system, the normal contact force is essential. Hertzian contact spring has often been used to represent the wheel/rail relationship, e.g. Newton and Clark [107], Ahlbeck [3], Cai [18]. It is considered as a nonlinear spring which may be expressed as:

$$p = C_H \Delta u^{1.5} \quad (1.1)$$

where p is the total contact force, C_H is the Hertzian contact coefficient and Δu is the wheel/rail overlap. C_H depends on the geometry and materials of wheel and rail.

In some cases, the overlap between the wheel and rail may be small and a linearized contact spring is adequate to represent the wheel/rail relationship. This may largely simplify the modeling of the interaction. The stiffness (K_H) of the linearized spring may be derived from Eq. (1.1) and expressed as:

$$K_H = 1.5C_H\Delta u_0^{0.5} \quad (1.2)$$

where Δu_0 is the wheel/rail overlap under a static load (P_0). The linearized contact spring has been used by Grassie et al. [62] to study rail corrugations, by Sato et al. [130] to study the vibrations due to high frequency irregularities on wheel and rail treads, and by Thompson [149] to study the wheel/rail noises.

The contact point has been usually assumed to be on the center line of the wheel. This may not be always true in some cases. Tunna [152] has indicated that in the case of a wheel flat with a chord shape, the wheel may land on the rail at an angle after a free flight. Tunna [152] has made a modification of the contact assumption. He lets the computer scan around the wheel circumference and find out the maximum overlap, and then calculate the contact force from the maximum overlap with Hertzian spring formulas. A better prediction of time and position of impact has been reported by using this modified Hertzian contact model [152]. However, this model may overestimate the contact stiffness at the corner of a irregularity and overestimate the impact loads [152].

Several complicated non-Hertzian contact models have been developed, e.g. [85, 115]. These models can predict the shape and size of a contact patch but they need enormous computer time. They have not been used to simulate the vehicle/track dynamic interaction.

It is believed that the wheel/rail contact patch may have some influences on the formation of rail corrugations [86]. To take into account the effect of contact patch on the dynamic interaction, a common practice is to filter out the short

waves with wavelengths less than the contact length from the irregularity function before it is used as an input in the calculation. This is a reasonable and simple approach to deal with very short waves. However, the influences of waves with wavelengths about 1-3 times larger than the contact length may also be suppressed to some extent and it is difficult to use such a simple approach to deal with them.

1.2.3 MODELING OF TRACK COMPONENTS

Components in track system include the rail, fasteners, ties, ballast and subballast. The modeling considerations for each of these components are reviewed as follows.

Rail modeling

Rail is the most sensitive component in the vehicle-track interactions because it has a relatively small effective mass and it is located at the interaction interface. A proper representation of the rail is a key to have a good prediction of the dynamic contact force and strains in the rail, which are important for the analyses and designs of tracks.

The simplest way to model a rail is to consider it as a lumped mass [10, 80]. It is impossible to satisfy all the frequencies that could be involved in the dynamic response in lumping the rail mass. The dynamic strains on the rail can not be directly calculated in such a model.

According to Ref. [92], Schwedler began to model the railway track laid on longitudinal ties as a beam on Winkler foundation to calculate the stresses in the

rail more than a century ago. Primarily as a result of Timoshenko's work, it was accepted around 1930 that railway track laid on transverse ties could also be modeled satisfactorily for many purposes by a beam on Winkler foundation. From 1926, starting with Timoshenko's investigation, in which he examined the dynamic effects of wheel flats, there was a growing interest in dynamic loads on track. However, until 1970's there were rather few papers in which dynamic models of track were used to solve practical problems, even though the response of an infinite beam loaded with a moving force had been well established before that time. In recent years, vertical dynamics of vehicle-track system has become a fast growing research area for the railway system.

Rail has been considered as an Euler-Bernoulli beam (or Euler beam) in many analyses. It is adequate to represent the rail's response to vertical dynamic excitation for frequencies of less than about 500 Hz [92, 94]. This model ignores the shear deformation and the rotational inertia of rail, which makes the rail stiffer than it really is and overestimate the dynamic forces in the high frequency range [40,107]. This model may not be suitable for the lateral response due to relative lateral flexibility of the web which ties together the more robust railhead and foot.

Timoshenko-Rayleigh beam (or Timoshenko beam) should be used to model the rail in the predictions of dynamic loads due to wheel and rail imperfections such as wheel flats, and rail joints [40,107]. It has been reported that this beam model is adequate for frequencies up to about 2.5 kHz for vertical responses [92]. For lateral and torsion modes, however, railhead and foot have to be modeled at least as independent Timoshenko beams interconnected by continuous

rotational springs [92]. This double-beam model has been used by Knothe et al. [93] to study rail corrugations.

In the noise studies, frequencies of up to 5 kHz may be of interest and the rail may have to be modeled in much detail. The assumption of the rigid across section used in the beam theories is no longer valid as the rail is excited at very high frequencies. Finite elements have been used by Thompson [149] and Knothe et al. [94] to model the rail to account for the elastic deformation in the across section.

Fastening components

A rail fastening system usually comprises of a rail-pad in parallel with two fastening springs. This system is usually considered as a spring-damper element acting at a point on the railfoot [92]. The rail-pad is made of rubber, plastic or a composite material and its stiffness is usually non-linear. Mostly because it is not convenient to represent the non-linear characteristic of the stiffness in the track system modeling, the stiffness of the rail-pad spring is often considered to be constant and the stiffness value is taken as that at a loaded condition. Little investigation on the dynamic behaviors of the rail-pad has been carried out.

The rail may lose contact with the tie when a train is traveling on the track, especially in the case of wooden-tie track. Both the theoretical and experimental results obtained by Tony [151] have suggested that the rail lift-off from the support has little effect on the maximum deflection of the rail. It is however not quite clear if such a lift-off has influence on the vehicle/track interaction, and the dynamic force.

Tie models

A tie is conventionally modeled as a rigid body or a beam. It has been reported that the dynamic response to forces at the railhead is well represented for frequencies of up to 1 kHz by modeling the tie simply as a rigid body [92]. The FE method has been used to calculate the natural frequencies of concrete ties represented by a Timoshenko beam of variable thickness [31, 92]. The theoretical results have shown very good correlation with the experimental data, as presented in [31,92]. The torsional vibration modes have been observed in the field tests [4], however they have not been considered in the track system model.

Ballast and substrate models

Ballast and substrate systems are actually very complicated. They often show a highly non-linear feature in their load/deflection relationship. Energy dissipated in them are due to friction and wave radiation. There are hard spots and voids in the actual situation. However, the ballast and substrate are relatively far from the wheel/rail interface and they do not show strong effect on the dynamic contact forces excited by wheel and rail tread defects [40], in which only the high-frequency dynamic behavior is of main interest. Most researchers lump the ballast and subballast together and model them as a massless spring-damper element under the tie [18,18,107,109]. The ballast and substrate have also been considered together as an elastic or visco-elastic half-space by some researchers [125]. This is useful for the investigation of the ground-borne vibration, in which the frequencies less than 500 Hz are of concern. Sato [130] and Zhai [158] have considered the ballast as lumped masses below ties which are interconnected by springs and dashpots in shear.

1.2.4 TRACK SYSTEM MODELS

A hierarchy of track models as shown in Fig. 1.4 can be formed by combining the component models described in the previous section. As illustrated in Fig. 1.4, they can be grouped under three basic catalogues, namely: (1) lumped parameter models; (2) models represented by beams on distributed supports; and (3) models represented by beams on discrete supports.

Lumped parameter track models

The simplest track model is a single effective track mass supported on track bed by a linear spring-damper system (Fig. 1.4(1a)). It was the early analytical model used by Meacham and Ahlbeck [103]. The effective mass of the track was derived from the first natural frequency of the rail as an infinite Euler beam on elastic foundation. They found that this single-mass model was adequate to deal with vehicle vibrations at low frequencies associated with the wheel unsprung and sprung masses, but was not sufficient to simulate high frequency wheel/rail impact. Similar models were used by Bjork [14], Kuroda [95], Jenkins et al. [80], and Sato [128]. By improving the work of Bjork [14], a set of simple formulae have been worked out on this simple model by Jenkins et al. [80] to calculate the so-called P_1 and P_2 impact loads developed at a dipped rail joint.

A model consisting of two track masses representing effective rail and tie/ballast has also been used by Ahlbeck [7] (Fig. 1.4(1b)). A non-linear stiffness between the rail and the track structure mass is also used to simulate the stiffening of trackbed under increasing load. Model parameters such as rail and tie effective masses, stiffness, and damping coefficient have been calculated from the beam on elastic foundation model. In the model shown in Fig. 1.4(1c), the tie is

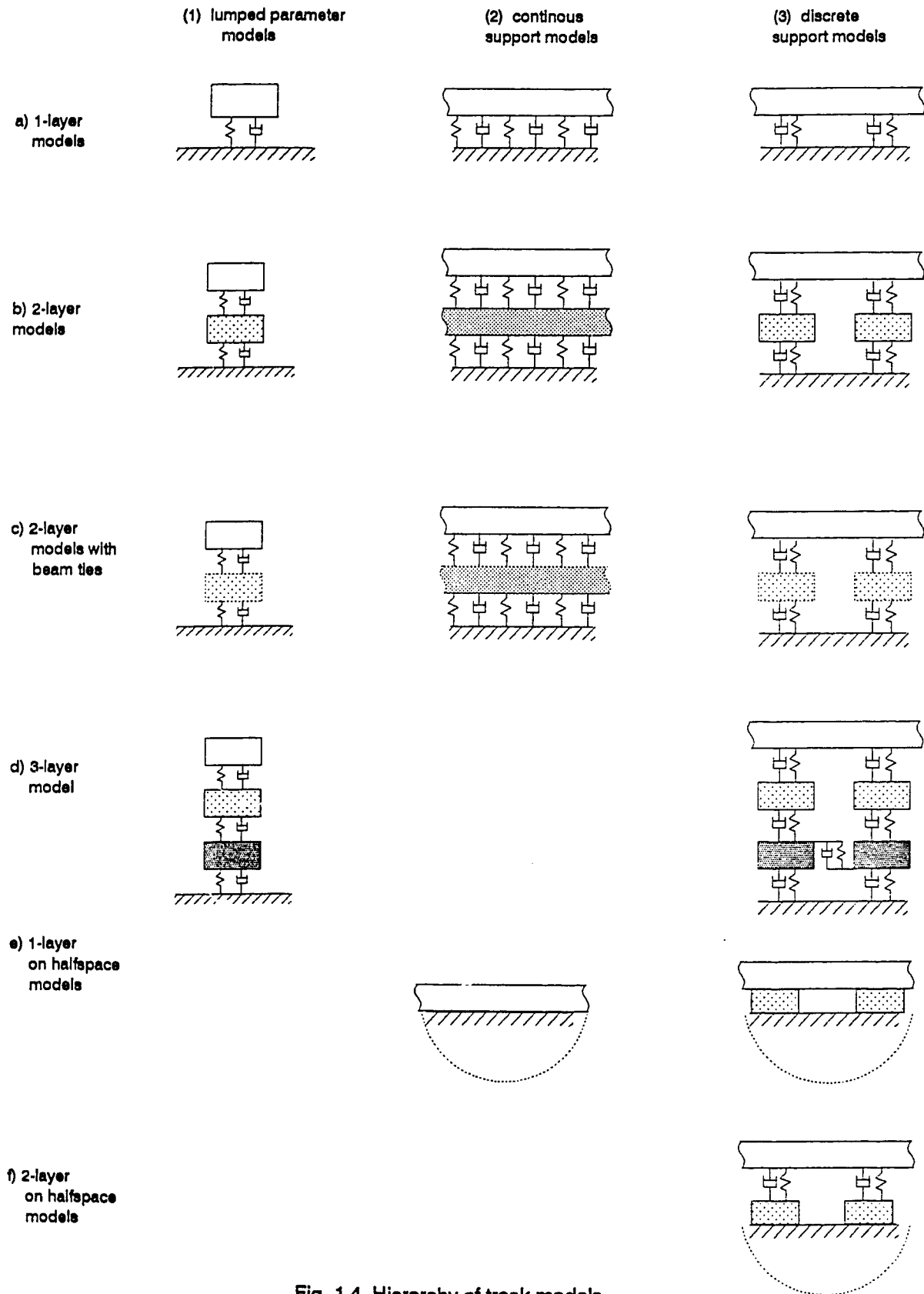


Fig. 1.4 Hierarchy of track models

considered as a beam and the transverse bending modes of concrete ties can be taken into account using the method proposed by Ahlbeck [3].

An effective mass for the separate ballast has been considered by Ehrenbeck and Polcari [42], and Ahlbeck [3] (Fig. 1.4(1d)). In addition, a non-linear rail pad stiffness was incorporated based on laboratory test results. The first four transverse bending modes of the concrete tie have also been incorporated in the model by Ahlbeck [3]. This model has been used to study the wheel/rail impact forces due to wheel tread runout profiles by Harrison and Ahlbeck [9,72], and impact loads on wheelset bearings by Williams, Ahlbeck, Harrison and et al. [73,157].

Generally, a lumped parameter model is simple and fast for the calculation and the computation can be carried out on any PC/AT-type computer. It addresses the major track and wheelset structural modes of response. The non-linear factors can be easily considered in the model. The major drawbacks of the lumped track models are:

- (i). It is difficult to satisfy all the major vibration modes to lump the rail mass;
- (ii). The stresses in the rail can not be directly obtained from the model;
- (iii). The interaction between the wheels on different wheelsets can not be modeled.

Track models represented by beams on distributed supports

Track models in this category cover a large number of publications in the modeling of track and vehicle-track interaction. Such models are popular as

they represent the track system fairly well, without adding much complexity in obtaining solutions. These models are classified as Euler beam on elastic foundation (EBEF), Timoshenko beam on elastic foundation (TBEF) and beams on multi-layer continuous foundation (BMLF).

Euler beam on continuous elastic foundation (Fig. 1.4(2a)) is still the basic model used in the track designs. It was first introduced by Winkler in 1867 [90]. In dynamic analyses, damping is often included in the distributed support and it is referred to as damped Winkler foundation by some researchers. The tie mass is usually absorbed in the rail beam by assuming they are uniformly distributed along the track. The determination of the parameters in the model has been discussed by Mair [99]. The use of this model and also a proper definition of the track modulus, that is the foundation stiffness, has also been discussed by Kerr [89]. Experiments have been performed by Singh and Deepak [138] and El-Sibaie [45] for estimation of track stiffness and track damping. Stewart [143] reported field measurements of the vertical track response under static loading conditions. Track stiffness and damping can also be found in text books written by Fastenrath [48] and Hay [74]. Euler beam on a continuous foundation with random stiffness and damping has been recently used to investigate the moving load problem by Fryba [56].

As mentioned before, Timoshenko beam has a better representation of the rail than Euler beam as high frequencies are of interest, but it takes more efforts to obtain solutions. The shear coefficient in Timoshenko beam theory has been investigated by several researchers and some simple and accurate formulae are available for its calculation [26].

Sato [127] was the first to represent the track as an Euler beam on a layer of distributed mass devoid of bending and shear stiffness (Fig. 1.4(2b)). Both the rail pads and the ballast are modeled as continuous layers of elastic support with viscous damping. The effects of shear and rotational inertia of the rail are accounted for by describing the rail as a Timoshenko beam by Grassie et al. [67]. A similar model has also been employed by Tassilly & Vincent [147] to study rail corrugations. The same concept has also been employed by Thompson [149] to establish his track model in the wheel/rail noise study.

Grassie & Cox [65] has extended their model in [67] by representing the ties as a layer of Timoshenko beam with cross-track flexural rigidity, but having no longitudinal stiffness (Fig. 1.4(2c)). This allows to investigate the dynamic behaviors of the ties in sufficient detail. Both symmetric and asymmetric bending modes of the ties can be taken into account. A further extension of this model by them [66] has been used to investigate the effects of localized track support deterioration, namely those of unsupported ties due to isolated ballast damage.

The track has been considered as a beam on half-space (Fig. 1.4(2e)) to study its natural frequencies by Patil [114]. The effects of foundation mass on different frequencies may be reflected in such a model.

Track models represented by beams on discrete supports

The effects of discrete supports on the static stresses on a rail have been investigated by Birman [13] (Fig. 1.4(3a)). The results for stationary loads indicate a difference between beam on distributed and discrete support

representations of only 3-5 percent in rail stresses. This suggests that it is not essential to represent the track as beams on discrete supports for the static analyses.

A periodically supported track system has been considered by Jezequel [81] to study the response of track due to a moving load. Cai and et al. [17] have found an exact solution for the dynamic response of an infinite Euler beam on rigid and equally spaced supports subjected to a moving force.

Beams on discrete rigid ties (Fig. 1.4(3b)) have been used by some researchers [51] to model the track. This track model has also been employed by Knothe and Ripke [93], and Hempelmann et al. [75] to investigate the mechanism and process of rail corrugation formation. The rail was represented by three separate layer components by Knothe and Ripke [93] in such a model.

In the model developed by Clark and Lowndes [25], the tie has been considered as an Euler beam (Fig. 1.4(3c)). This model has been used by Newton and Clark [107] to study the impact load due to a wheel flat and by Clark et al. [24] to investigate the track behaviors due to a corrugated rail. Tunna [152] has also used this model to study the dynamic loads due to wheel and rail irregularities such as wheel flats and rail joints. A modification made on this model by Tunna is that the concrete tie is discretized into separated elements (12 elements) each with its own mass, bending stiffness and, support stiffness. Both the rail and the tie have been considered as Timoshenko beams by Cai and Raymond [18], Neilsen and Abrahamsson [108].

The three-layer model (Fig. 1.4(3d)) has been used by Sato [130] and Zhai et al. [158]. The major difficulty in this model is to determine the parameters satisfactorily. Zhai et al. [158] have tried to estimate them theoretically.

Beams on halfspace models (Fig. 1.4(3e)) may be useful for studying ground-borne vibrations [125]. The model developed by Ono and Yamada [112] may also be classified in this catalogue. In their model, the elasticity and the mass inertia of the road bed (ballast/subgrade) are taken into consideration by assuming that the road bed is a compressible media in the vertical direction.

1.2.5 IRREGULARITY REPRESENTATION AND TRACK LENGTH

The most realistic representation of vertical excitation arising in the wheel-track interaction is that of a wheel traveling over irregularities on the track, as used in [107, 110, and 152].

If a vehicle (or a load) is assumed to be stationary to the track in the traveling direction, the solution of a model may be much more simple and efficient, especially if a frequency domain solution method is used. In such a model, the irregularities are pulled through the wheel/rail interface at a constant speed to calculate the interactions [3, 51,67,66,62,73,93,130,147,149]. Furthermore, this makes it convenient to consider the track as an infinite system when the receptance method is used in the calculation, which will be described in the next section.

It has not been very clear that in what circumstances the excitation representation with such a moving irregularity is correct. It is expected that the

errors caused by this representation may not be ignored if the speed is high. At a high speed, the contact force may be different from the force on the rail-pad and ballast. This may not be truly reflected in the model that considers a stationary vehicle on the track.

The discrete supports of the track actually introduces a quasi-periodic irregularity in the track system. Researchers have been debating whether or not the discrete feature of track should be introduced in the track model [92]. It has been clear that the dynamic force due to a rail corrugation may be quite different at the midspan and over the tie at some speeds. It seems to be appropriate to take into account this feature if the high frequency responses are of concern.

Ideally, it is the best to represent the track as an infinite system if the vehicle is considered to be traveling on the irregularities. If the discrete feature of track is ignored, it is relatively easy to do so. However, so far it has been impossible to directly take into account an infinite track in a FE model if a time-step integration technique is employed to calculate the vehicle-track interaction.

For most practical problems, a finite length of track is sufficient to represent the track system interactions. The deflections of track far from the loading point are actually small and they have little effect on the wheel/track interactions. Different track lengths have been used in the models. For example, 12 tie spans was used by Tunna [152], 35 tie spans by Nielsen et al. [109], and 40 tie spans by Cai et al. [18].

The main problem with a finite track model is that boundaries may introduce undesirable effects in the response to a moving load. This should be take into

account in the modeling of such a system. If the length of the track is taken long enough and the vehicle can always be kept in the center part of the finite track, such a problem may be satisfactorily resolved. A 'ring' model has been proposed to represent the infinite track [92], in which the length of the track is physically finite but the two ends are connected to form an imaginary circle. In such a way, the vehicle traveling on the track indefinitely can be simulated. A disadvantage of such a model is that the size of dynamic equations may be significantly increased if the FE method is employed in the modeling.

1.2.6 FREQUENCY-DOMAIN SOLUTION METHODS

The diversity of modeling is largely because many different techniques and arithmetic are used in the calculations. Knothe and Grassie [92] have classified them as the frequency-domain solution methods and time-domain solution methods.

Frequency-domain methods for a stationary point load

One of the major purposes to investigate the response due to a stationary oscillating point load is to find the receptance and use it to calculate the vehicle-track interaction. The displacement response at the point of excitation is usually called direct receptance (or receptance) and the response at any other point is called cross receptance.

The receptances for models represented by beams on distributed supports are usually easy to be obtained by using the integral transformation techniques. Receptance for a continuously supported Euler beam was first obtained by Timoshenko [92]. Receptance for an Euler beam on a separated layer of rigid

ties was first calculated by Sato [127]. A approach to calculate the receptances for a Timoshenko beam on a layer of rigid or elastic ties was proposed by Grassie et al. [67] and used later by some other researchers [147]. The track's lateral and longitudinal receptances has also been calculated by Grassie et al. [68,69]. Patial [113] investigated the response of a distributed supported track subjected a stationary vibrating mass, which may be regarded as the coupled wheel/track receptance.

An algorithm has been developed to calculate the receptance for a model represented by a rail on discrete supports and used by many researchers [67,106,133]. The first step in the algorithm is that finite-element matrices, or their equivalent, for a characteristic track section are formulated either analytically or numerically. Then Floquet's theorem is used to connect the displacements on different sections in the periodic system. By imposing the boundary conditions, the unknown eigenvalue can be determined and the harmonic displacement at any point can be calculated. In the case of a complex periodic structure, the transfer matrix method is usually employed in the algorithm for a numerical solution [149].

The receptance at around the so-called 'pinned-pinned' frequency (about 750 Hz on the conventional track) in the discrete support model is quite different from that in the distribute support model [67,92]. There is, however, no significant difference at other frequency ranges. In the pinned-pinned eigenmode, the rail vibrates with a wavelength equal to two tie spans with nodes located above the ties. This mode may be excited in the impact response due to wheel flats and railjoints. As a general model, the discrete feature of the track should be included in the modeling.

The receptance on vehicle may also be obtained theoretically [67,149] or experimentally [147]. After obtaining the receptances, the interaction between the vehicle and track is obtained by coupling the receptances (including the contact receptance) to form appropriate transfer functions between input and output. The transfer function may be the required final solution, e.g. in the noise study [149], or it may be transferred to the time domain, e.g. for dynamic force due to wheel and rail irregularities [62]. If the irregularity is sinusoidal, the response is found directly from the transfer functions. To calculate the response to non-sinusoidal irregularities, their Fourier transform must first be found. The waveforms with their wavelengths smaller than the contact patch can also be effectively filtered in this procedure [62,149]. The above approach for the calculation of the vehicle-track interaction is called the receptance method. It is an efficient tool and has been widely used in the investigations of corrugations [53,67,93,147], wheel/rail noises [123,123,127], dynamic forces due to wheel and rail irregularities [62].

Frequency-domain methods for a moving point load

Fourier and Laplace-Carson integral transformation techniques have been widely used to find the response of a beam on a continuous support subjected to a moving constant or oscillating (prescribed) load. A coordinate system moving with the load is usually introduced in the system and a steady-state response can be obtained. This type of solution techniques have been used in many studies to solve the "moving load problem". According to [92], the first in this field is Hovey, who gave a solution of a moving constant load on a continually supported Bernoulli beam in 1933. The same problem was solved again by Dorr in 1945 [92] and by Kenney [87] in 1954. Mathews [92] (1958) was the first who investigated an oscillating load moving on a Bernoulli beam. A constant load

moving on a Timoshenko beam was first considered by Achenbach and Sun [2] in 1965. The influence of an additional axial force was investigated by Kerr [88] in 1972. Weitsman [154] (1970) and Torby [151] (1975) took account of the fact that the ballast reacts in compression only. The solution to the problem of an oscillating load moving on a Timoshenko beam was contained in Ref. [67] (1982), and was later also solved in detail by Bogacz et al. [92] (1983). The work on the moving load problem was reviewed by Fryba [55] in 1972 and by Kerr [90] in 1981. A few years ago, Duffy [41] investigated the steady-state response of an Bernoulli beam subjected to a moving mass.

The stability of a load moving along a beam is a major concern in the moving load problem. There exists a "critical speed" at which the speed of the moving load would be equal to that of wave propagation in the beam. The critical speed is usually much larger than the present or even foreseen train speed and therefore has only academic interest to railway researchers.

The dynamic response of a moving load on a discretely supported Euler beam was first obtained by Mead [104,105], who gave a wave type solution that utilizes Floquet's theorem. Similar technique was used by Smith and Wormley [139], and Bogacz et al. [92]. Jezequel [81] has also proposed another solution approach for this problem. In his approach, the differential equation of the rail (Euler beam) is formulated in a coordinate system which moves with the load. The combined reaction forces acting on the rail through the pad are developed into Fourier series and thus are transformed into continuous (but non-uniform) distributed forces. This technique has also been used by Kisilowski et al., Ilias et al. and Sibaei according to Ref. [92]. Sibaei has considered the problem of excitation by two wheelset in a bogie, which required enormous computational

effort. The third method of calculating the response of discretely supported track to a moving wheelset (represented as a rigid body) has been used by Grassie et al. [67]. In this the response is assumed to comprise a steady-state component whose amplitude varies symmetrically about the sleeper (which is essentially the response to a moving irregularity), plus a transient component which varies with position in the span of track between ties. The latter is found by a root-locus technique. The discrete feature of track supports can be easily incorporated in a FE track model.

1.2.7 TIME-DOMAIN METHODS AND FE MODELING

Whereas there is a long history of frequency-domain solutions, the time-domain solutions have become common only in the last 20 years. This is largely because of the lack of sufficient computational power. Also for this reason, at the early stage, the vehicle and track models with time-domain solutions were usually relatively simple [80,103]. In the last few years, there is a greater interest in employing the finite element method and numerical time-step integral techniques to simulate the vehicle-track interaction.

Several numerical methods have been used in the modeling of vehicle-track or vehicle-bridge interactions. For example, Ting et al. [150] have proposed an algorithm based on finite differences to calculate the dynamic response of a finite elastic beam supporting a moving mass. Blejwas et al. [15] have used Lagrange multipliers to impose kinematics constraints between vehicle and structure. Dahlberg [29] has proposed an approach to calculate the vehicle/bridge interaction. The reciprocity method has also been used by Dahlberg [28] to predict the track response due to a moving force.

With the versatile FE method, detailed models of vehicles and tracks may be formulated in a rational manner. Several good commercial FE packages, such as ANSYS, NASTRAN, ADINA and ABAQUS, are available. However, so far, it is still difficult to use these software to simulate the interaction between a moving vehicle system and a stationary track. A special FE software is needed to deal with the interaction problems.

FE analysis in conjunction with moving loads has been reviewed by Filho [50]. Direct use of the FE method and a numerical time-step integration has been made by Shah et al [135], Lin and Trethewey [96], Cifuentes [22], Nielsen et al. [110]. Olsson [111] derived a structure/vehicle finite element by eliminating the contact degrees-of-freedom of the vehicle. Solution of moving load problems with a commercial computer code has been described by Schneider et al [132]. Fryba et al. [56] have adopted a so-called stochastic finite element for the investigation of an infinitely long beam subjected to a moving constant force, in which the foundation stiffness and the damping along the beam are represented as random variables. Lin and Trethewey [97] implemented an active vibration control technique on beam structures subjected to a moving force.

Modal superposition technique is often attractive in the dynamic analysis of structures exhibiting a linear time-invariant behavior. Once a structure has been modeled as modal components, a considerable reduction in integration time may be obtained. Because of this, modal superposition technique has been employed in most of the vehicle-track system models. In the case of wheel flat problem, frequencies up to 2 kHz may be involved in the response and a large number of modals have to be considered in the calculation. For example,

Newton and Clark [107] used 125 modals and Neilsen [109] used 200 modals in his modeling. A major disadvantage of the modal superposition technique is that it is difficult to deal with the non-linear factors in the track and vehicle structures.

The modal equations used in the time-step integral technique may be obtained by using an analytical method. Because of this, such an approach is often called semi-analytical or combined analytical-numerical technique. At one extreme of this type of solution technique is the work of Cai et al. [17], who undertook an exact modal analysis of an infinite Bernoulli beam on rigid rollers. This solution is elegant but it is difficult to extend it to more complex models of the beam and supports. Semi-analytical approaches have been used by Lyon [98], El-Sibaie and Klauser [46] for a Bernoulli-Euler beam on Winkler or damped Winkler foundation. Newton and Clark [107] have also proposed a semi-analytical solution for a Timoshenko beam on Winkler foundation. A semi-analytical approach that takes advantage of the receptance method was used by Fingberg [51] to investigate wheel-rail squealing noise. A disadvantage of these semi-analytical methods is that it is relatively difficult to study structural irregularities such as variations in tie spacing, hard spots and voids.

Several numerical methods have been used to obtain the modal parameters (eigenvalues, eigenvectors and normalized constant) for the modal analysis, e.g. [19,155,156]. The techniques used in the modal superposition are also different. A real-valued modal superposition technique for the track has been used by e.g. Clark et al. [25], Tunna [152], and Cai and Raymond [18]. Huang and Shah [78] modeled both vehicle and track as real-valued modal components. In [111], the structure in the structure/vehicle finite element is modeled by its real-valued

modal parameters. Decoupling of equations of motion by use of complex-valued normal modes is used by Nielsen [110].

1.3 SCOPE OF THE INVESTIGATION

From the literature survey of past experiences, it is evident that there is a need for a comprehensive vehicle/track interaction model which must be general enough to simulate a wide range of wheel/rail defects and irregularity. The track model must be sufficiently detail as it plays a strong role in the wheel/track interaction specially at high speeds under high frequency of vibration. It appears to be satisfactory to consider the rail as a Timoshenko beam for most problems listed in Table 1.1. As reported, for vertical dynamic studies, it is fairly good to model the wheel/rail relationship as a one dimensional spring in the calculation of dynamic contact force due to irregularities with wavelength several times larger than the wheel/rail contact length. However, an adaptive contact model is needed to automatically take into account all the possible wavelengths in the simulation.

For high speed simulation of vehicle/track interaction, FE approach has been found to be practical and useful. One of the major difficulty has been in the representation of infinite track. For most practical problems, however, a finite length of track is sufficient to represent the track system interactions. On the other hand, it is quite possible that in using finite track model, the boundaries may introduce undesirable effects in the response to moving loads. Ideally, it is better to represent the track as an infinite system if the vehicle is considered to be traveling on the irregularities. However, so far it has not been possible to

directly take an infinite long track in FE model if a time-step integration technique is employed to calculate the vehicle-track interactions. There is clearly a need for further research in this area.

The scope of this study is therefore, aimed at developing a comprehensive general purpose dynamic model of railway vehicle/track system. Such a validated model is essential to investigate the vertical dynamic forces due to wheel and rail tread defects and parametric excitation of the track in high frequency range. The important contributing feature of the present modeling are as follows:

- A FE model of Timoshenko beam is extended and employed to represent the rail so that the strains in the rail can be directly evaluated with high accuracy, which are essential for the model validation and track design;
- An adaptive multi-point wheel/rail contact model is proposed and used to calculate the normal and geometrical longitudinal forces due to irregularities in the wheel/rail contact region. The model can automatically take into account all possible wavelength of irregularities, the nonlinear wheel/rail contact stiffness and the loss of wheel/rail contact, in the simulation.
- The rail-pad and ballast are modeled as distributed spring-damper elements which account for the non-linear factors such as rail lift-off from the tie and tie lift-off from the ballast;

- The standard FE approach is applied in conjunction with Newmark's direct integration technique. A simple cutting and merging method and a set of special boundary conditions are proposed to extend finite length of the track to infinitely long track so that a vehicle can be modeled to travel on the track indefinitely with a time-dependent speed.

The developed FE model is validated against available experimental data obtained from British Rail and Canadian Pacific (CP) Rail. Such a validated model can be used to study almost any aspect of vehicle/track vertical dynamics. As specified in the literature review, some of the important concerns in recent years have been on the effect of wheel and rail irregularities such as wheel flats, wheel shells, rail joints and rail corrugations. This study, therefore, focuses on prediction and understanding of the dynamic forces due to the above defects by utilizing the developed FE model. On each aspect of the investigation, an extensive parametric study is carried out to evaluate the influence of parameters and to obtain an in-depth understanding of related dynamics.

Details of the FE modeling of railway vehicle/track system is presented in Chapter 2. The vehicle system models employed in this investigation are presented along with their equations of motion. Various elements of the track system model are described along with their FE representation. The extension of finite length of track to infinite track is also presented in this chapter. Finally, the proposed adaptive wheel/rail contact model used in this investigation is outlined.

A new approach to calculate the natural frequencies of a singular system such as a free-free concrete tie and wheelset is proposed and presented in the first part of Chapter 3. The chapter further presents the calculated natural frequencies of concrete ties, wheelsets and the vehicle/track system. Some available experimental data of concrete tie frequencies are available and they are used to validate the mathematical models of the concrete ties. The features of the important coupled vehicle-track frequencies and their mode shapes are also discussed in this chapter.

In Chapter 4, the background of wheel tread defects is first described. The calculated impact forces and rail strains due to wheel tread defects such as wheel flats and wheel shells are compared with the experimental data from British Rail and CP Rail to validate the FE model. Finally, the influences of system parameters on the impact loads are investigated extensively using the validated FE model.

The developed model is applied to investigate the dynamic forces due to rail joints as presented in Chapter 5. The characteristics of the dynamic forces due to a freight car traveling over a dipped rail joint are evaluated and discussed in this chapter.

The steady-state interaction between the vehicle and track, in which the wheel and rail are assumed to be perfect, is presented in Chapter 6. The results cover the responses of vehicle-track system in the speed range of 0-400 m/s. A parametric study on the resonant force due to the effect of tie spacing is presented. As an example of the FE model application, the dynamic forces due

to void (un-supported tie) and hard spot (over-supported spot) are also presented in this chapter.

The background of rail corrugations is briefly described at the beginning of Chapter 7. The dynamic forces due to rail corrugations are evaluated, presented and discussed. The mechanism of dynamic interaction between two wheels is also explored and presented in this chapter.

Finally, Chapter 8 presents important conclusions drawn from this study, and a list of recommendation for further studies in this area.

CHAPTER 2

MODELING OF RAILWAY VEHICLE-TRACK SYSTEM

2.1 INTRODUCTION

The vertical dynamic behaviors of railway vehicle/track system in high speed operation is primarily dominated by wheel/rail interaction and the dynamic behaviors of wheelset and track system. The track system model for realistic representation of its characteristics, irregularities and defects are the most important aspects in the modeling. The vehicle model on the other hand can be simplified to a great extent without the loss of realism as long as wheel/rail contact interaction is modeled with care.

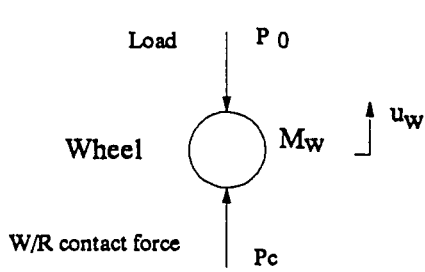
A major assumption made in the present modeling is that the vehicle is traveling on a straight track without losing its lateral stability. This assumption is justified if only the characteristics of vertical dynamic forces in the vehicle-track system are of interest. In such a case, the lateral and longitudinal relative motions between the wheel and rail are small and the creep forces at the wheel/rail contact interface have little effect on the vertical high frequency dynamic responses of the system. Therefore, they are ignored in this investigation to simplify the modeling, and focus on vertical dynamic aspects. However, the wear process of rail and wheel treads and the formation of rail and wheel corrugations may involve dynamic responses in all the three directions. They should be considered in the further studies, as recommended at the end of the thesis.

As discussed in the pervious chapter, a general model of vehicle-track system is composed of four parts, namely: vehicle model; track system model; wheel/rail contact model; and representation of wheel/rail irregularities. A "building block" approach to the development of vehicle-track system is adopted, where each component is modeled separately and then combined to form the final system. The following subsections present the details of the modeling carried out for this investigation.

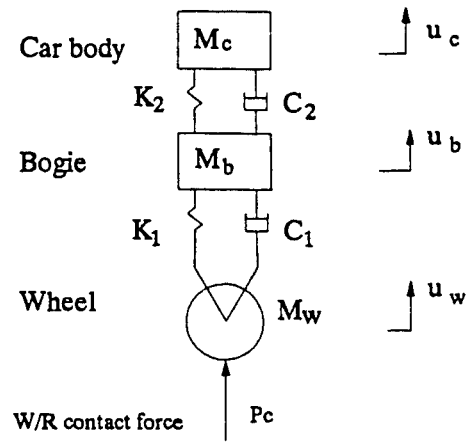
2.2 VEHICLE SYSTEM MODELS

A very wide range of vehicle models have been employed in studies dealing with vehicle-track interactions. During the modeling stage, it is usually desirable to develop a simple and credible model such that the motion of a dynamic system is fully described. The simplicity of a model, in general can be determined by the number of Degrees-of -Freedom (DOF) selected to simulate a given physical system. Often increased complexity of the model may lead to difficulties in interpretations of the system behavior. The credibility of a model is determined in part by its capability to simulate the system behavior realistically within the desired accuracy.

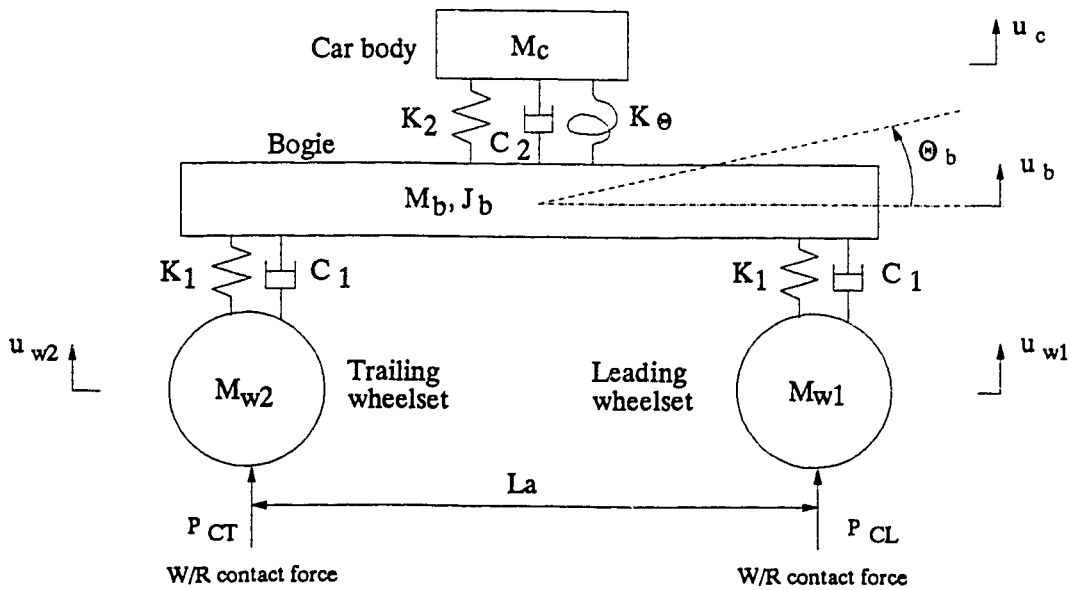
Some of the simple models for vehicle representation that can be adapted in this study are presented in Fig. 2.1. The simplest representation is a 1-DOF single wheel model rolling on the track, as shown in Fig. 2.1a. The wheel in this case represents the unsprung mass carrying a constant load. A 3-DOF model representing wheel, bogie and car-body in the vertical mode is presented in Fig. 2.1b. In this case, the wheelset and bogie is connected by primary suspension,



(a) Model I: 1-DOF vehicle model



(b) Model II: 3-DOF vehicle model



c) Model III: 5-DOF vehicle model

Figure 2.1 Vehicle models employed in the FE system model

and the car-body is supported on the bogie via secondary suspension. A more realistic model of the vehicle incorporating two wheelsets, a bogie and half car-body is represented as a 5-DOF model is shown in Fig. 2.1c. In this case, each wheelset has vertical DOF (u_{w1} and u_{w2}). The bogie has vertical (u_b) and pitch (θ_b) DOF, and the car-body has vertical (u_c) DOF. The primary suspension in this case is represented by spring and damping elements (K_1 and C_1) and secondary suspension is represented by spring and damping elements (K_2 , C_2 and K_θ). K_θ in this case represents the pitch stiffness between car and bogie. The wheel/rail contact forces for the leading and trailing wheel are represented by P_{CT} and P_{CL} , respectively.

The equations of motion for the three models of the vehicle (Model I, II and III in Fig. 2.1) can easily be expressed as presented by equations 2.1 to 2.3.

For Model I,

$$M_w \ddot{u}_w = P_0 - P_c \quad (2.1)$$

For Model II,

$$\begin{bmatrix} M_w & 0 & 0 \\ 0 & M_b & 0 \\ 0 & 0 & M_c \end{bmatrix} \begin{Bmatrix} \ddot{u}_w \\ \ddot{u}_b \\ \ddot{u}_c \end{Bmatrix} + \begin{bmatrix} C_1 & -C_1 & 0 \\ -C_1 & C_1 + C_2 & -C_2 \\ 0 & -C_2 & C_2 \end{bmatrix} \begin{Bmatrix} \dot{u}_w \\ \dot{u}_b \\ \dot{u}_c \end{Bmatrix} + \begin{bmatrix} K_1 & -K_1 & 0 \\ -K_1 & K_1 + K_2 & -K_2 \\ 0 & -K_2 & K_2 \end{bmatrix} \begin{Bmatrix} u_w \\ u_b \\ u_c \end{Bmatrix} = \begin{Bmatrix} p_c - M_w g \\ -M_b g \\ -M_c g \end{Bmatrix} \quad (2.2)$$

For Model III,

$$\begin{bmatrix} M_{w1} & & & & \\ & M_{w2} & & & \\ & & M_b & & \\ & & & J_b & \\ & 0 & & & M_c \end{bmatrix} \begin{Bmatrix} \ddot{u}_{w1} \\ \ddot{u}_{w2} \\ \ddot{u}_b \\ \ddot{\theta}_b \\ \ddot{u}_c \end{Bmatrix} + \begin{bmatrix} C_1 & 0 & -C_1 & -L_a C_1 / 2 & 0 \\ & C_1 & -C_1 & L_a C_1 / 2 & 0 \\ & & 2C_1 + C_2 & 0 & -C_2 \\ & & & L_a C_{L1} & 0 \\ & & & & C_2 \end{bmatrix} \begin{Bmatrix} \dot{u}_{w1} \\ \dot{u}_{w2} \\ \dot{u}_b \\ \dot{\theta}_b \\ \dot{u}_c \end{Bmatrix} \\
 + \begin{bmatrix} K_1 & 0 & -K_1 & -L_a K_1 / 2 & 0 \\ & K_1 & -K_1 & L_a K_1 / 2 & 0 \\ & & 2K_1 + K_3 & 0 & -K_2 \\ & & & K_\theta + L_a K_1 & 0 \\ & & & & K_2 \end{bmatrix} \begin{Bmatrix} u_{w1} \\ u_{w2} \\ u_b \\ \theta_b \\ u_c \end{Bmatrix} = \begin{Bmatrix} P_{cL} - M_{w1}g \\ P_{cT} - M_{w2}g \\ -M_b g \\ 0 \\ -M_c g \end{Bmatrix} \quad (2.3)$$

In the present investigation, each of the above three models are needed depending on the objective of the study. As indicated by Knothe and Grassie [92], for frequencies of over 20 Hz, car-body modes have negligible effect on the vehicle/track interaction. When dynamic response due to irregularities such as wheel flats and rail joints are of interest, the most active component of the vehicle is the wheelset or unsprung mass. It has been demonstrated [107] that in such studies dealing with impact load, it is adequate to consider the simple 1-DOF loaded wheel. In order to evaluate bearing forces and the influence of primary damping, it is prudent to consider the 3-DOF vehicle model representation.

In order to evaluate the interaction between the two wheelsets within a bogie, this study considers the 5-DOF model. This model can adequately represent the in-plane motion of vehicle system under high frequency excitations. In this model, it is assumed that the car-body has vertical mode and that there is no

interaction between the leading and trailing bogies and their wheelsets. In order to avoid further complication to the present model, the wheelset and bogie roll motion is neglected at this stage and is recommended under further studies at the end of this thesis.

2.3 FINITE ELEMENTS OF TRACK COMPONENTS

As discussed in the previous section, the track components include the rail, ties, rail-pad, ballast and subgrade, and fasteners. The finite elements and their formulation for each of these components are described in this section.

2.3.1 Finite element for rail

The most important component in the model is the mathematical representation of the rail. For this purpose, a Timoshenko beam element model is used in the finite element analysis. This FE beam model was originally developed by Thomas and Abbas [148] for a uniform Timoshenko beam to study its natural frequencies. In this study, this model is extended to a non-uniform Timoshenko beam. The changes of geometry along the length of beam and the foundation stiffness are taken into account in this extended model. The longitudinal force in the rail due to temperature changes is also considered. The bending and shear strains on the rail are continuous at every point with this FE beam model.

The Timoshenko beam element presented in Fig. 2.2 is a two-node element with four degrees of freedom for each node. The nodal coordinates of the element may be described in vector representation as:

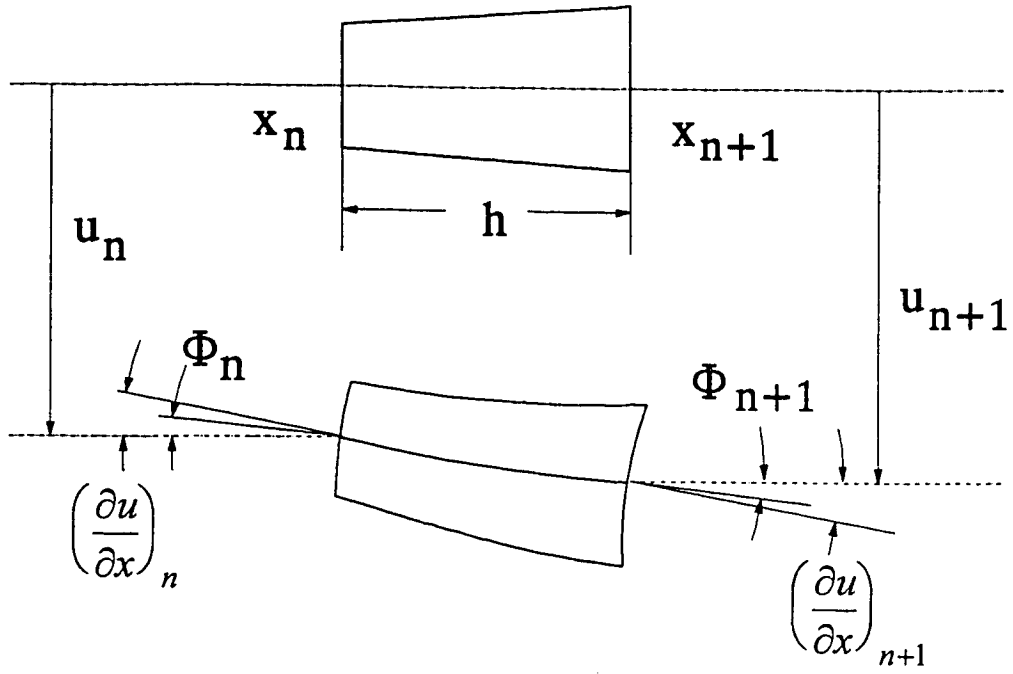


Fig. 2.2 A Timoshenko FE beam model

$$\{\eta^e\} = \{u_n^e, \phi_n^e, (\frac{\partial u}{\partial x})_n^e, (\frac{\partial \phi}{\partial x})_n^e, u_{n+1}^e, \phi_{n+1}^e, (\frac{\partial u}{\partial x})_{n+1}^e, (\frac{\partial \phi}{\partial x})_{n+1}^e\}^T \quad (2.4)$$

where u is the vertical displacement, ϕ is the rotational angle, e is the element number, n and $n+1$ are the global node numbers at each side of the element. It is assumed that u and ϕ can be represented by the polynomial expressions of the form:

$$u = \sum_i^8 \alpha_i \eta_i^e, \quad \phi = \sum_i^8 \beta_i \eta_i^e, \quad (2.5)$$

where $\alpha_i(\xi)$ and $\beta_i(\xi)$ are cubic polynomial shape functions expressed as:

$$\begin{aligned} \alpha_1 = \beta_2 &= (2 - 3\xi + \xi^3)/4, & \alpha_3 = \beta_4 &= h(1 - \xi)(1 - \xi^2)/8, \\ \alpha_5 = \beta_6 &= (2 + 3\xi - \xi^3)/4, & \alpha_7 = \beta_8 &= -h(1 + \xi)(1 - \xi^2)/8, \\ \alpha_2 = \alpha_4 = \alpha_6 = \alpha_8 &= \beta_1 = \beta_3 = \beta_5 = \beta_7 = 0, \end{aligned} \quad (2.6)$$

where h is the length of the beam element and ξ is non-dimensionalized coordinate expressed as:

$$\xi = (2x - h)/h \quad (2.7)$$

where x is the coordinate along the element length.

By using the energy method, the mass, stiffness and damping matrices and the force vector for the beam element are derived and they are presented as follows:

Mass matrix

The kinetic energy, U , of an elemental length, h , of a Timoshenko beam includes the rotational energy, U_r , and the vertical deflection energy, U_d .

$$\begin{aligned}
U &= U_r + U_d \\
&= \frac{\rho}{2} \left[\int_0^h I_r \left(\frac{\partial \phi}{\partial t} \right)^2 dx + \int_0^h A_r \left(\frac{\partial u}{\partial t} \right)^2 dx \right]
\end{aligned} \tag{2.8}$$

Non-dimensionalization of the kinetic energy yields:

$$U = \frac{\rho h}{4} \left[\int_{-1}^1 I_r \left(\frac{\partial \phi}{\partial t} \right)^2 d\xi + \int_{-1}^1 A_r \left(\frac{\partial u}{\partial t} \right)^2 d\xi \right] \tag{2.9}$$

Upon substituting for ϕ and u from Eq. (2.5) and for α and β from Eq. (2.6), the kinetic energy may be expressed as:

$$U = \frac{1}{2} \{ \eta^* \}^T [M^*] \{ \eta^* \} \tag{2.10}$$

where $[M^*]$ is a 8×8 mass matrix or inertia matrix and its elements are calculated by:

$$m_{ij} = \frac{\rho h}{2} \left(\int_{-1}^1 A_r \alpha_i \alpha_j d\xi + \int_{-1}^1 I_r \beta_i \beta_j d\xi \right) \quad (i, j = 1, 2, \dots, 8) \tag{2.11}$$

In this formulation, the first integration represents the vertical deflection inertia and the second one represents the rotational inertia.

Stiffness matrix

The potential energy, V , of an elemental length, h , of a Timoshenko beam includes the bending energy, V_b , the shear strain energy, V_s , and the support potential energy (for beam on elastic foundation only), V_f .

$$\begin{aligned}
V &= V_b + V_s + V_r \\
&= \frac{E_r}{2} \int_0^h I_r \left(\frac{\partial \phi}{\partial x} \right)^2 dx + \frac{T_r G}{2} \int_0^h A_r \left(\frac{\partial u}{\partial x} - \phi \right)^2 dx + \frac{1}{2} \int_0^h k_f u^2 dx
\end{aligned} \tag{2.12}$$

Non-dimensionalization of the potential energy yields:

$$V = \frac{E_r}{h} \int_{-1}^1 I_r \left(\frac{\partial \phi}{\partial \xi} \right)^2 d\xi + \frac{T_r G h}{4} \int_{-1}^1 A_r \left(\frac{2}{h} \frac{\partial u}{\partial \xi} - \phi \right)^2 d\xi + \frac{h}{4} \int_{-1}^1 k_f u^2 d\xi \tag{2.13}$$

Upon substituting for ϕ and u from Eq. (2.5) and for α and β from Eq. (2.6), the potential energy may be expressed as:

$$V = \frac{1}{2} \{ \eta^e \}^T [K^e] \{ \eta^e \} \tag{2.14}$$

where $[K^e]$ is a 8×8 stiffness matrix and its elements are calculated by:

$$\begin{aligned}
k_{ij} = \frac{2E_r}{h} \int_{-1}^1 I_r \frac{d\beta_i}{d\xi} \frac{d\beta_j}{d\xi} d\xi + \frac{T_r G h}{2} \int_{-1}^1 A_r \left(\frac{4}{h^2} \frac{d\alpha_i}{d\xi} \frac{d\alpha_j}{d\xi} + \beta_i \beta_j - \frac{2}{h} \beta_i \frac{d\alpha_j}{d\xi} - \frac{2}{h} \beta_j \frac{d\alpha_i}{d\xi} \right) d\xi + \frac{h}{2} \int_{-1}^1 k_f \alpha_i \alpha_j d\xi \\
(i, j = 1, 2, \dots, 8)
\end{aligned} \tag{2.15}$$

In this formula, the first integration represents the bending stiffness, the second one represents the shear stiffness and the third one represents the support stiffness.

Damping matrix

For a unit length of the beam, the viscous damping coefficient is c_r . Similar to the foundation stiffness matrix, the elements of damping matrix, c_{ij} are calculated from:

$$c_{ij} = \frac{h}{2} \int_{-1}^1 c_r \alpha_i \alpha_j d\xi \quad (i, j = 1, 2, \dots, 8) \quad (2.16)$$

Force vector

By using the virtual work method, the element equivalent nodal forces $\{F^e\}$, are derived and for arbitrary distributed load, $p(\xi, t)$, they are expressed as:

$$F_i^D(t) = \frac{h}{2} \int_{-1}^1 p(\xi, t) \alpha_i d\xi \quad (i, j = 1, 2, \dots, 8) \quad (2.17)$$

for concentrated force, $P(t)$, the expressions are:

$$F_i^C(t) = P(t) \alpha_i(\xi_p) \quad (i, j = 1, 2, \dots, 8) \quad (2.18)$$

Geometric stiffness

The matrix resulting from the axial force (N_a) is usually called geometric stiffness matrix [116]. The axial force, N_a , may be caused by the temperature changes in the rail. It may be estimated using the expression:

$$N_a = \alpha_t E_r A_r (T - T_0) \quad (2.19)$$

where α_t is temperature coefficient, T is actual temperature of rail and T_0 is the rail neutral temperature at which there is no longitudinal temperature force in the rail. From the geometric relationship and virtual work method, the geometric stiffness matrix is derived and its elements are calculated by:

$$k_{Gij} = \frac{2}{h} \int_{-1}^1 N_a \frac{d\alpha_i}{d\xi} \frac{d\alpha_j}{d\xi} d\xi \quad (i, j = 1, 2, \dots, 8) \quad (2.20)$$

Strains on rail

The strains that are of concern in the study are the normal and shear strains on the cross-section of straight rail. The normal strain is mainly composed of bending and temperature strains, and can be calculated from:

$$\varepsilon_y = \frac{2Y}{h} \sum_{i=1}^8 (d\beta_i / d\xi) \eta_i^e + \frac{N_s}{E_r A_r} \quad (2.21)$$

where Y is the vertical position coordinate on the cross-section of rail, measured from the neutral plane. The shear strain on the neutral plane is calculated from:

$$\gamma_{xy} = \frac{2}{h} \sum_{i=1}^8 (d\alpha_i / d\xi) \eta_i^e - \sum_{i=1}^8 \beta_i \eta_i^e \quad (2.22)$$

By taking a very large shear modulus (say $G = 2.0 \times 10^{13} N / m^2$) in the calculation of stiffness matrix and dropping the rail rotational inertia in the mass matrix, the Timoshenko beam model can actually be switched to an Euler beam model. This makes it easy to compare results from different beam theories.

2.3.2 Finite elements for ties

Wooden and concrete tie have been considered as either rigid bodies (or lumped masses) or Euler beams or Timoshenko beams in this study, depending on the objective. If only the dynamic contact force and strains in the rail are of concern, it is not necessary to model the ties as the sophisticated Timoshenko beams, which will increase the size of the equations of motion. To reduce the time required for the computation, a well-known two-node Euler beam element with 2-DOF for each node [122], is employed to model the ties. However, the natural frequencies of a tie may be overestimated by using Euler beam theory.

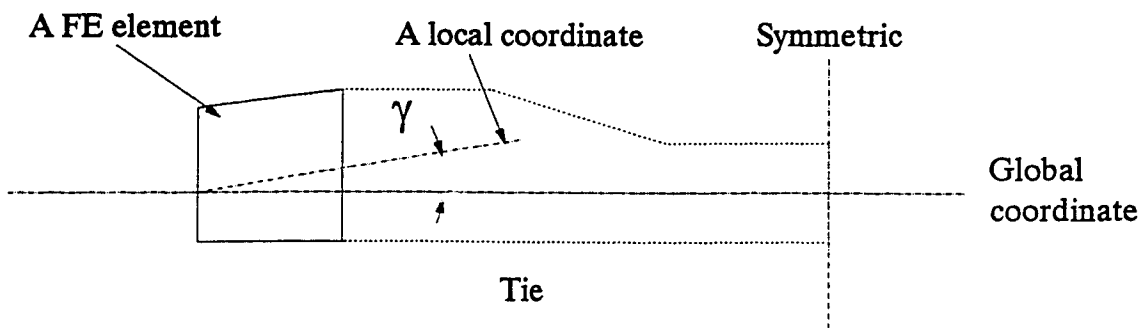


Figure 2.3 The relationship between local and global coordinates for non-uniform ties

rail-pad can either be a single spring-damper element or a distributed spring-damper element inserted between the rail and tie. It also makes it possible to take into account the rotational motion of the tie if the rail-pad and ballast are modeled as distributed spring-damper elements.

The stiffness matrix for the distributed rail-pad layer is derived from the deflection of the track, as shown in Fig. 2.4. To establish the stiffness matrix for Element 1, an infinitesimal force experienced in the pad due to the deflection is considered and it may be expressed as:

$$dF = k_p(x) \cdot (u_r - u_t) dx \quad (2.24)$$

where $k_p(x)$ is the pad stiffness per unit length along its width and

$$u_r = \sum_i^8 \alpha_i \eta_i \quad \text{and} \quad u_t = U_T + x\theta \quad (2.25)$$

where U_T is the vertical displacement of the tie at the tie center and θ is the rotational angle of the tie. The equivalent forces on the rail element nodes resulting from the pad force can be calculated from:

$$F_i^e = \int_{-L_p/2}^0 \alpha_i dF = \int_{-L_p/2}^0 \alpha_i k_p (u_r - u_t) dx \quad i=1, 3, 5, 7 \quad (2.26)$$

where L_p is the pad width along the rail. The equivalent forces on the tie can be calculated from:

$$F_T = \int_{-L_p/2}^0 dF = \int_{-L_p/2}^0 k_p (u_r - u_t) dx,$$

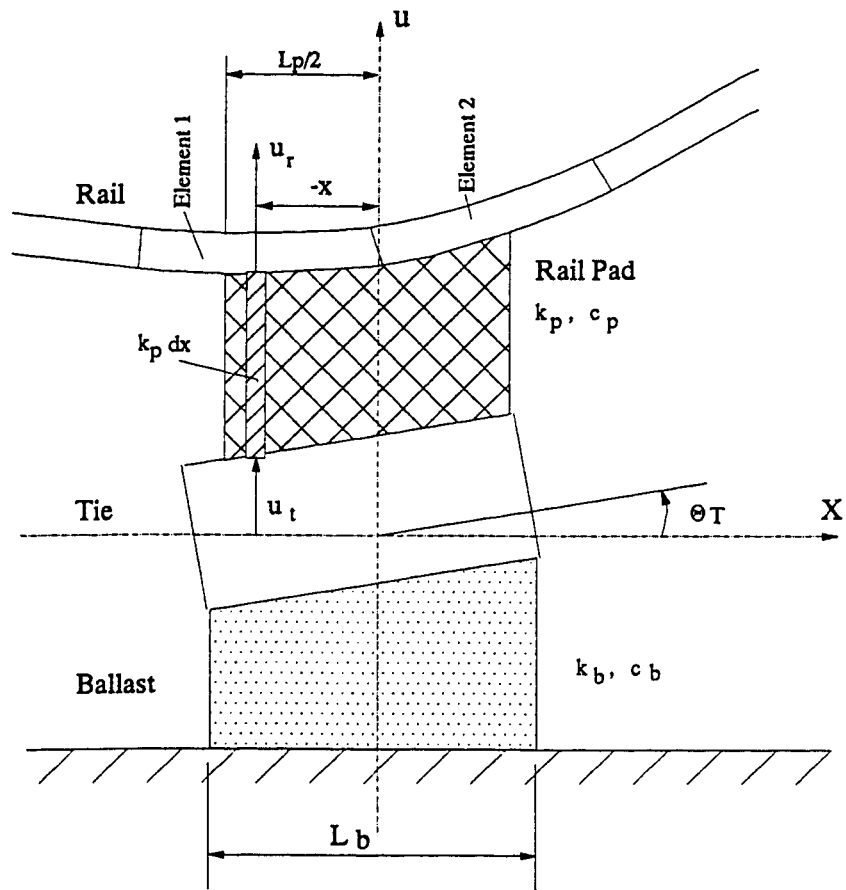


Figure 2.4 Rail-pad, tie and ballast finite elements

$$F_{\theta} = \int_{-L_p/2}^0 x dF = \int_{-L_p/2}^0 x k_p (u_r - u_t) dx \quad (2.27)$$

By substituting Eq. (2.25) into Eqs. (2.26) and (2.27), the relationship between the force and displacement vectors can be expressed as:

$$\begin{Bmatrix} \{F^e\} \\ \{F^t\} \end{Bmatrix} = \begin{bmatrix} [K_R] & [K_{RT}] \\ [K_{TR}] & [K_T] \end{bmatrix} \begin{Bmatrix} \{\eta^e\} \\ \{\eta^t\} \end{Bmatrix} \quad (2.28)$$

where $\{\eta^e\}$ is the same as in Eq. (2.5) and $\{F^e\}$ is its corresponding force vector for the rail element, $\{\eta^t\}$ and $\{F^t\}$ are force and displacement vectors of the tie and they may expressed as:

$$\{\eta^t\} = [U_T \quad \theta]^T \quad \{F^t\} = [F_T \quad F_{\theta}]^T \quad (2.29)$$

The stiffness matrices in Eq. (2.28) can be calculated as following:

For elements of matrix $[K_R]$,

$$k_{ij}^R = \int_{-L_p/2}^0 k_p \alpha_i \alpha_j dx \quad i, j = 1, 3, 5, 7. \quad (2.30)$$

For elements of matrix $[K_{RT}]$,

$$k_{i\theta} = -\int_{-L_p/2}^0 k_p \alpha_i dx, \quad k_{\theta\theta} = -\int_{-L_p/2}^0 k_p \alpha_i x dx \quad i=1, 3, 5, 7. \quad (2.31)$$

For elements of matrix $[K_T]$,

$$k_{TT} = \int_{-L_p/2}^0 k_p dx, \quad k_{T\theta} = \int_{-L_p/2}^0 k_p x dx, \quad k_{\theta\theta} = \int_{-L_p/2}^0 k_p x^2 dx \quad (2.32)$$

Similarly, the stiffness matrix for element 2 can be derived. Its stiffness elements can be calculated following the same steps as described as in Eqs. (2.30 to 2.32) except that the integration limit in this case is from 0 to $L_p/2$.

In a similar manner, the damping matrix due to distributed pad damping can be derived from the force established by the relative velocity of the rail and tie. Because the damping is assumed to be viscous damping, the damping matrix has the same form as the stiffness matrix. The elements in the damping matrix can be calculated by simply replacing the k_p with c_p , where c_p is the pad damping per unit length along the pad width. In this study, the pad stiffness and damping per unit length are taken as constant along the rail and they are equal to K_p/L_p and C_p/L_p , respectively.

2.3.4 Finite element for ballast and subgrade

The ballast and subgrade are modeled as a massless distributed spring-damper element in the FE system model developed in this study. The tie is assumed to be a rigid body as far as its rotational motion is concerned. Hence, it is straightforward to obtain the ballast stiffness and damping matrices. The ballast stiffness in the vertical (K_{bT}) and rotational (K_b) modes may be calculated from:

$$K_{bT} = \int_{-L_s/2}^{L_s/2} k_b dx \quad K_b = \int_{-L_s/2}^{L_s/2} k_b x^2 dx \quad (2.33)$$

where k_b is the distributed ballast stiffness per unit length along the rail and it is assumed to be constant and equal to K_b/L_s . The damping in the ballast is also

assumed to be viscous and the expressions for ballast damping coefficients are similar to those in Eq. (2.33).

2.3.5 Finite element for fastening

A fastener can be modeled as a spring element with vertical and rotational stiffnesses. The pre-load on the fastening is also considered in the system model. Actually, the fastening stiffness is usually significantly smaller than that of rail-pad stiffness and in general has little effect on the dynamic wheel/rail contact force and strains in the rail. However, modeling the fastening separately may be useful to analyze the dynamic forces on the fastener.

2.4 TRACK SYSTEM MODEL

The track system model for this study is developed in two stages. The track is first modeled as a basic FE structure of finite length. Secondly, the procedure proposed for extending the finite track to infinite track is outlined.

2.4.1 Basic track system model

In modeling the track, a section of single straight track is considered. The track is represented by a Timoshenko beam on discrete supports as shown in Fig. 2.5. The length of track selected depends on the vehicle model used. The experience obtained from this study suggests that a length of 20 tie-spacing is adequate even if the 5-DOF vehicle model (Model III) is chosen in the interaction simulation.

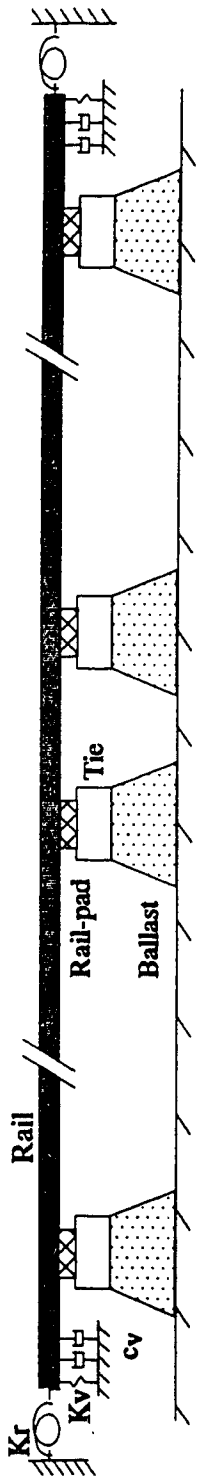


Figure 2.5 Physical track system in the FE system model

By properly expanding and assembling the matrices of rail element and the matrices of discrete components, the track dynamic equations may be expressed as:

$$[M]\{\ddot{\eta}\} + [C]\{\dot{\eta}\} + [K]\{\eta\} = \{F\} \quad (2.34)$$

where [M], [C], and [K] are global mass, damping and stiffness matrices, respectively, and {F} and {η} are global force and coordinate vectors, respectively. The expressions for elements of each of these matrices and vectors are derived and presented in section 2.3.

In some cases, especially on a wooden-tie track, it is possible for the rail to lift off from the tie and/or the tie to lift-off from the ballast. This nonlinear factor is taken into consideration in this model. The distributed gravity force on the system is considered in the system modeling to properly take into account this non-linear factor. In the cases of rail lift-off from tie and/or tie lift-off from ballast, the pad stiffness and/or ballast stiffness is taken as zero. The condition for rail lift-off from tie is:

$$u_r - u_t > 0, \quad (2.35)$$

and tie lift-off from ballast is:

$$u_t > 0 \quad (2.36)$$

where u_r is rail vertical displacement and u_t is tie vertical displacement. The coordinate is positive for the upward displacements and forces. These

relationships are checked at every time step and the system matrices are modified according to the rail and tie displacements.

2.4.2 Extension of finite length of track to infinite track

One might take a very long portion of track in the model and calculate the dynamic response of the system. This is not economical because the size of system matrices would be significantly increased and a lot of time would be required for the computation. The effect of a track far from the location of a vehicle on the wheel-rail interaction is actually small and the track in those areas can be cut-off so that only a short portion of the track may be used for the physical FE model. However, a moving vehicle would quickly reach one end of the track in such a model. To overcome this problem, a "ring" model has been proposed [92] to represent the track, in which the length of the track is physically finite but the two ends are connected to form an imaginary circle. A major drawback of such a model is that the size of dynamic equations may be significantly increased if the FE method is employed in the modeling. Alternatively, a simple approach of "cutting and merging" is proposed and adopted in this investigation to realize infinite track length. In this method, a short section at the rear end is simply cut-off and a new section is merged to the front end after the vehicle has traveled over the distance equal to the length of the cut away section (say, a tie-spacing), as shown in Fig. 2.6. In this way, the track becomes infinitely long and the vehicle could run on it forever. It should be noted that the vehicle is always located in the center part of the track and hence limits any significant influences that the spring-connected end conditions may introduce.

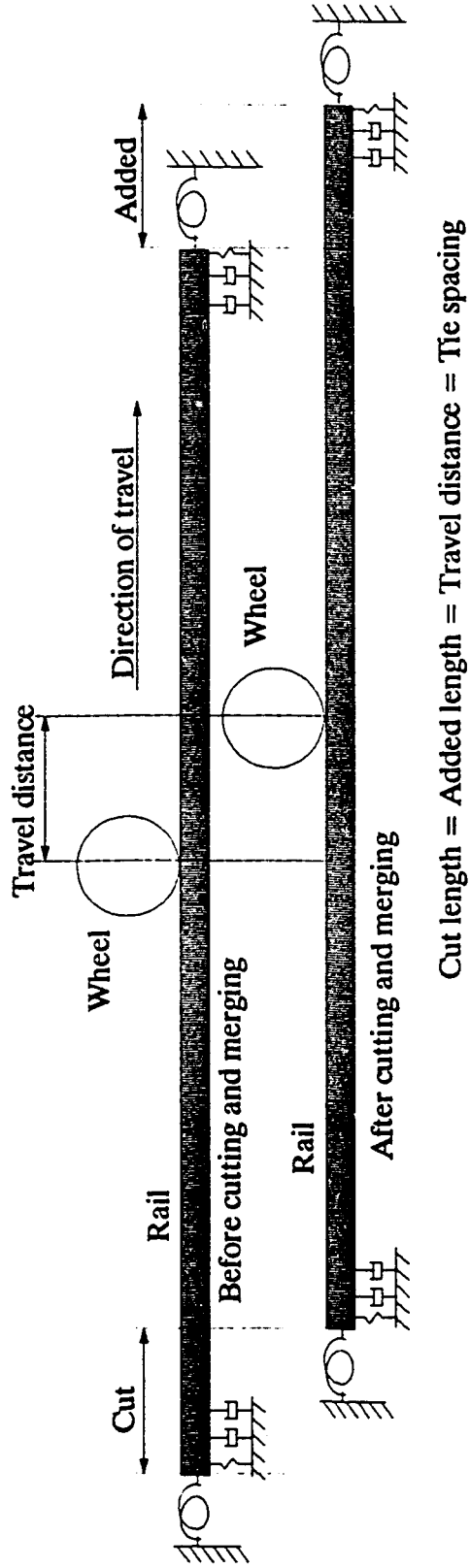


Figure 2.6 Extension of finite length of track to infinite track

The boundary condition at the two ends of the rail is primarily treated as a combination of vertical and rotational equivalent springs. Such boundary conditions can be conveniently imposed in the FE modeling by simply adding stiffness values of each spring to the corresponding elements in the system stiffness matrix. The influence of the boundary element stiffness on the system response will depend on the length of the track considered. If the track in the model is taken long enough and the vehicle is always located at the center part of the track model, the effect of boundary stiffness parameter may be negligible. On the other hand, if the track length required is to be minimized an approximately selected boundary spring stiffness will be required.

For the case of impact response, it is possible that vibration waves resulting from the impact are reflected from the ends, and the response after the first strike is affected by these waves. The rail actually serves as a medium for the propagation of vibration waves. In reality, the waves are supposed to travel away along an infinite rail and gradually be damped out by the damping in the track. To facilitate such behavior of the track model, artificial damping is added on the end elements as shown in Fig. 2.6. The damping added near the ends can not change the nature of the original track system but they can absorb the wave energy transmitted to the ends. This is equivalent to letting the waves travel away along the rail. The added extra damping at the ends can also damp out most of the disturbances caused by the cutting and merging process. Part of the disturbance waves may also be damped out by the track damping as they propagate on the way to the wheel/rail contact point. The influence of the boundary spring stiffness and damping parameter on the dynamic response of the track will be investigated as a part of this study.

2.5 REPRESENTATION OF WHEEL/RAIL CONTACT FORCES

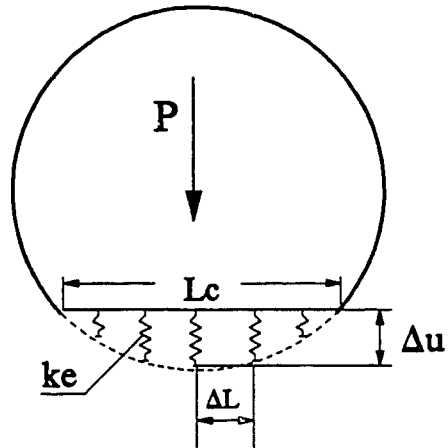
To overcome the limitations of the single point contact models as discussed in Chapter 1, an adaptive contact model is proposed in this study, which can be used to calculate the vertical dynamic contact force and longitudinal force due to geometric relationship between the wheel and rail.

The most realistic representation of any irregularity in the modeling is to let the vehicle travel over the irregularity. This is the irregularity representation employed in this investigation.

2.5.1 Calculation of vertical contact force

Fig. 2.7 shows the proposed wheel-rail contact model in this study. This model is similar to the adaptive tire model [20] used to represent the road-tire relationship in road vehicle modeling. The wheel/rail relationship is represented by a set of element springs which are uniformly distributed in the vertical plane and have the same stiffnesses. This allows the springs to adapt to any irregularity in the contact patch. For this reason, it is called adaptive contact model. A multi-point contact at a rail joint may be easily simulated by using this contact model in the calculation. Unlike the road-tire system, in which the contact stiffness is mainly determined by the tire itself, the stiffness of the element spring in the wheel-rail system depends on the material and geometric shapes of both wheel and rail. A simple approach is proposed to estimate the element spring stiffness.

First, the total static load, P_0 , is applied to the wheel and the deformation, Δu , is calculated from Hertzian contact model described in Eq. (1.1). That is,



k_e : element spring stiffness

Δu : deformation under static load

L_c : contact length

m : number of element springs for stiffness calculation

P : static load

ΔL : distance between two spring elements

Figure 2.7 An adaptive contact model

$$\Delta u = (P_0 / C_H)^{2/3} \quad (2.37)$$

It is then assumed that the contact length in the longitudinal direction (L_c) is equal to the chord length that has the height equal to the deformation, as shown in Fig. 2.8. From the known contact length, the distance between two neighboring element springs is calculated as:

$$\Delta L = L_c / (m - 1) \quad (2.38)$$

where m is the number of element springs in effect under the static load. The stiffness of the element spring is then calculated as:

$$k_e = P / \sum_{i=1}^m \Delta u_i \quad (2.39)$$

where Δu_i is the deformation of element springs and they are calculated by assuming that the wheel has a perfect principal rolling circle. In the dynamic force calculation, the element deformations or overlaps are calculated by:

$$\Delta u_{di} = u_{ri} - u_{wi} - f_i \quad (2.40)$$

where i corresponds to the i -th element spring, f is the irregularity function and u_r is the rail displacement, and u_w is the wheel displacement which is calculated by assuming that the principal rolling circle of wheel is perfect. The force on the element spring can therefore be calculated as:

$$P_i = k_e \Delta u_{di} \quad (2.41)$$

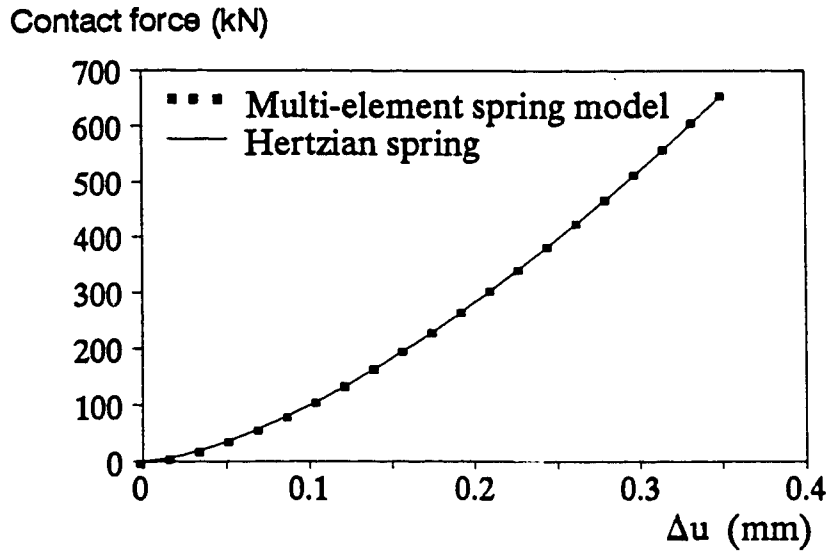
Each element force is then transferred as nodal equivalent forces using Eq.(2.18). The total vertical force is summed as:

$$P = \sum P_i \quad (2.42)$$

which is applied to the wheel to calculate the vehicle response. The relationship between the total vertical force and the total deformation for the proposed contact model is equivalent to that of the Hertzian spring represented by Eq.(2.37), as shown in Fig. 2.8.

2.5.2 Calculation of geometric longitudinal force

The contact between the wheel and rail may not always happen on the centerline of the wheel [40,152]. This may be affected by the motion of the wheel and the irregularities on the wheel and rail. An off-centered contact may generate a longitudinal component of the contact force, which may serve as a resistive or driving force, depending on the actual contact position. This force is due to the geometric contact relationship between the wheel and rail. To identify this force from the longitudinal force caused by the creep of the wheel over the rail, it will be referred to as "geometrical longitudinal force", in this study. This force may be small if the wheel and rail are smooth for a possible train speed and it has often been ignored in the study of dynamic contact forces. However, this force may become significant due to the wheel and rail irregularities such as wheel flats and rail corrugations. It may increase the energy consumption of the vehicle and accelerate the deterioration of wheel and rail treads.



Static load: 82 kN

Contact length (L_c): 18.8 mm

Number of elements used (m): 20

Stiffness of single element spring (k_e): 70.4 kN/mm

Figure 2.8 The relationship between W/R overlap and vertical static force

The adaptive contact model mentioned before is extended to predict the geometric longitudinal force. In this extension, it is assumed that the curvature at a given contact point remains unchanged after the deformation of the wheel and rail materials under the contact force. Based on the relationship shown in Fig. 2.9, the longitudinal force on a element contact spring, F_{xi} , is calculated by

$$F_{xi} = p_i \tan(\alpha_{gi}) \quad (2.43)$$

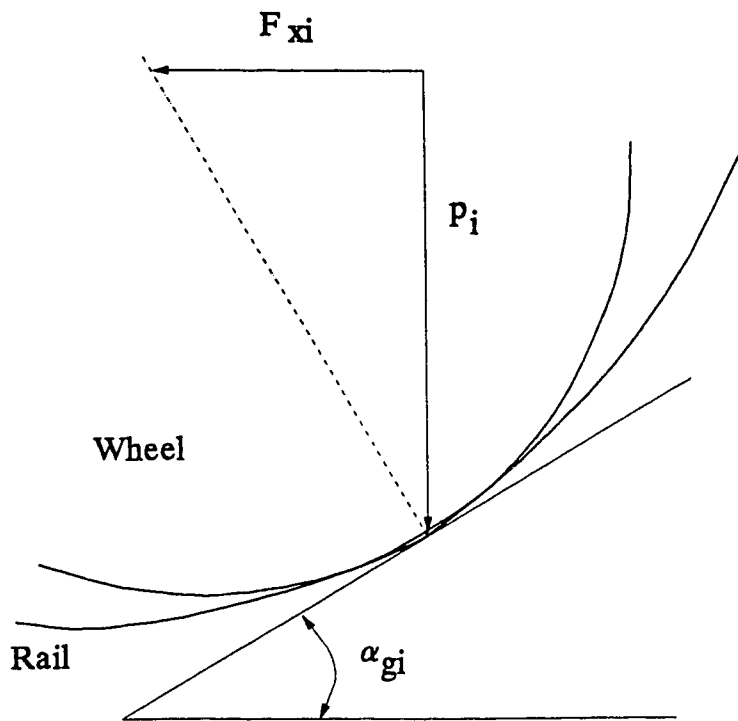
where p_i is the vertical force on the i -th element spring, and α_{gi} is the contact angle at the location of the i -th element spring.

Besides the adaptive contact model, the linearized Hertzian, non-linear Hertzian and Tunna's contact models described under literature review have all been incorporated in the computer program for the FE model developed in this study.

2.6 PROCEDURES OF VEHICLE-TRACK INTERACTION CALCULATION

The overall vehicle-track system is divided into two systems separated at the wheel-rail interface in the calculation of their interaction. They are related by the contact force calculated from the contact model, as shown in Fig. 1.3. An iteration procedure is used to obtain the response in the time domain. This is convenient to make any modification on both the vehicle and track systems.

The calculation is started from the static deformation of the whole system. Then, the vehicle is assumed to travel at a specified forward speed and a solution of time history is obtained. This can avoid introduction of some undesired motions



P_i : Normal force on element spring (from Eq. 2.41)

F_{xi} : Geometric longitudinal force

α_{gi} : Wheel/rail contact angle along longitudinal direction

Figure 2.9 Geometric longitudinal force

in the system so that a steady-state interaction can usually be obtained after the vehicle has traveled about 4 or 5 tie-spacings.

2.7 SUMMARY

A general FE model of railway vehicle-track system is developed. The assumptions of this model are:

- The vehicle is traveling on a straight track;
- The track is symmetric with respect to its center line so that only a single rail is considered in the track modeling;
- The creep forces between the wheel and rail are small and their effects on the vertical motion of vehicle-track can be ignored;
- Hertzian contact coefficient is constant.

The components of the vehicle-track system modeled are as follows:

- A vehicle is modeled as a lumped parameter system which consists of a body, bogies, primary and secondary suspension and rigid wheels;
- Wheel/rail contact is modeled as distributed springs in the contact patch in the normal direction;
- The rail is modeled as infinite, discretely-supported Timoshenko beam;
- The rail-pad is modeled as a distributed a spring-damper element;
- The fastener is modeled as a vertical and a rotational springs;
- The tie is represented by either a rigid body or a non-uniform Euler beam;

- The ballast and substrate are considered together and modeled as a distributed spring-damper element.

The basic features of this model are summarized as follows:

- A vehicle traveling on an infinite track indefinitely with a time dependent speed can be simulated;
- The adaptive contact model can adapt any irregularities on the wheel and rail treads and multi-point contact along the longitudinal direction can be simulated; the actually measured rail and wheel profiles can be directly input in the model for calculation without first filtered any high frequency irregularity; the geometric longitudinal force can also be estimated from this contact model;
- The problems arising from the vehicle/track interaction for frequency range up to 2.5 kHz can be investigated on this model;
- Irregularities in the track support, such as irregular tie spacing, voids and hard spots under the ties and missing rail-pads, can be taken into account;
- This model is valid for all present and foreseen train speeds;
- The dynamic forces in the system and rail strains can be directly obtained from this FE model, where the rail strains are continuous anywhere.

The major limitations of this model are:

- Asymmetric motions of vehicle and track system can not be simulated;

- The bending motions of wheelset have not been included in this model and their effect on the vertical dynamic force can not be studied using this model;
- The strains in the ballast and subgrade can not be predicted;
- The calculated strains in the rail near the wheel/rail contact region are not valid because the rail is modeled as a beam and the influence of contact force on the strains is not considered;
- The wheel and rail tread irregularities in the lateral direction are not considered, and their influence on vertical dynamic force can not be evaluated.

CHAPTER 3

NATURAL FREQUENCIES OF VEHICLE-TRACK SYSTEM

3.1 INTRODUCTION

Natural frequencies are important properties of a structure. They can provide useful information to understand the basic dynamic behaviors of the vehicle-track system. There is a relative motion between the vehicle and track and this may affect the coupled wheel/track frequencies to some extent. However, this influence should be small for the possible speeds of present trains because the lowest wave propagation speed in the rail is about 1900 km/h [107]. Hence, the vehicle and track can be considered to be stationary to analyze the system frequencies.

The natural frequencies of the vehicle-track system can be basically divided as frequencies of structure components and frequencies of coupled system. For the present study, concrete ties, wheelsets and coupled wheel-track system are the major components of the model. The natural frequencies for each of these components are investigated and compared with experimental data whenever possible.

3.2 NATURAL FREQUENCIES OF CONCRETE TIES AND WHEELSETS

The concrete ties and wheelsets are assumed to be beams and the Timoshenko beam element model described in Chapter 2 is used to calculate their natural

frequencies. The boundary conditions for them at their two ends are assumed to be:

$$\begin{aligned} \Phi' &= 0, & \text{for } x=0, L \\ u' - \Phi &= 0, & \text{for } x=0, L \end{aligned} \quad (3.1)$$

where u is the tie vertical displacement, Φ is the rotational angle of cross-section, and L is the total length of beam. After imposing the boundary conditions, the dynamic equations of the beam may be expressed as:

$$[M]\{\ddot{\eta}\} + [K]\{\eta\} = 0 \quad (3.2)$$

This is the dynamic equation used to compute the natural frequencies of a concrete tie and a wheelset. There is no essential boundary condition in the free tie and wheelset systems and this equation is singular. Not all the existed methods for the calculation of eigenvalues can be directly used on this system because some of them may involve in the inverse of stiffness matrix, such as the Rayleigh-Ritz subspace iteration method [120]. It is found that the simplest approach to overcome this problem is to impose a pair of soft springs to the free beam, as shown in Fig. 3.1, so that the free-free beam becomes non-singular. The effects of the springs on the bending frequencies are negligible if the spring stiffness is much smaller than that of the beam, as indicated in Fig. 3.2. This figure further shows that the springs have little effect on the frequency value of a particular vibration mode if the springs are located near the node points of this mode. With such modification, any existing method can be used to calculate the frequencies. Rayleigh-Ritz subspace iteration method [120] is employed to calculate the natural frequencies of concrete ties and wheelsets in this study.

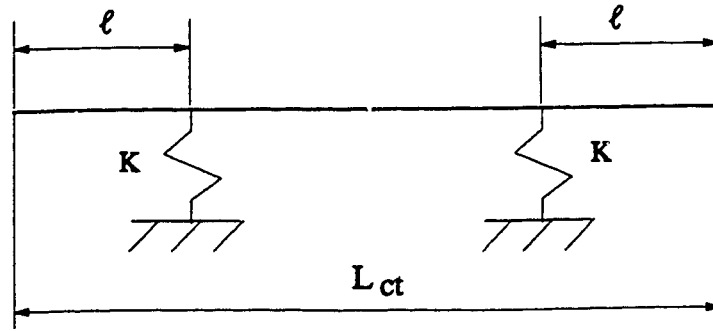


Figure 3.1 Imposing a pair of springs to a free-free beam

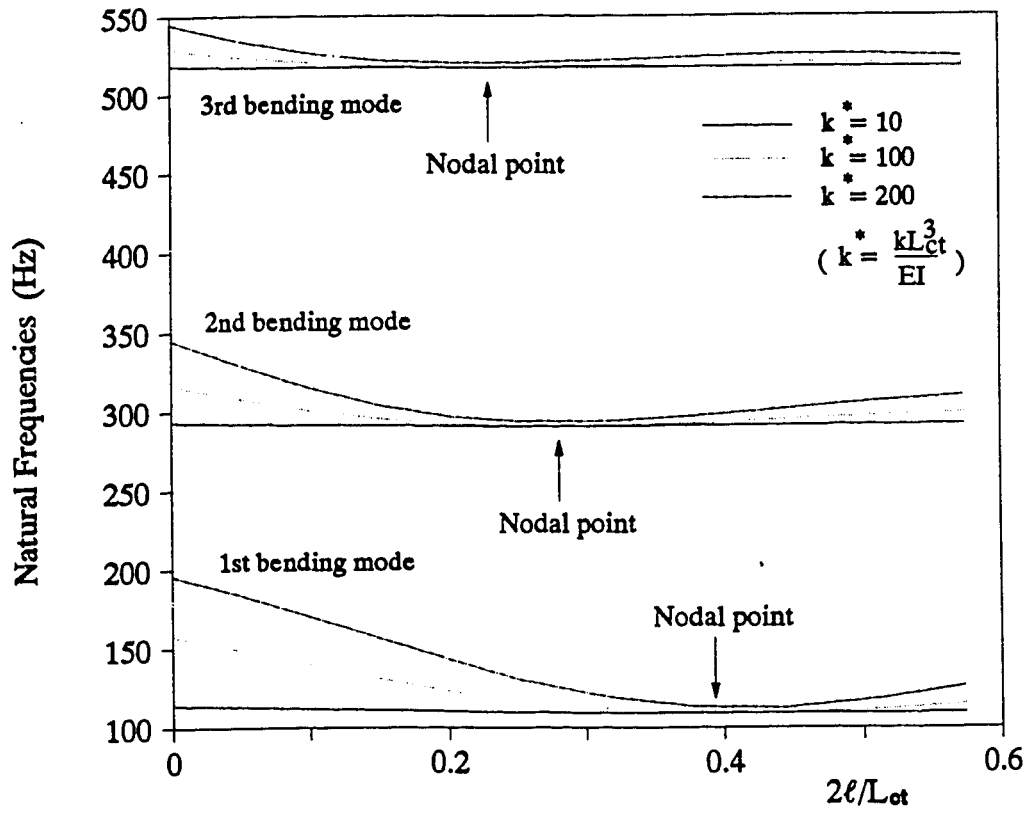


Figure 3.2 Effects of spring stiffness and support locations on frequencies (CT-3 track concrete tie, TBS model)

3.2.1 CN Type-A bridge concrete tie

CN Type-A concrete bridge tie (Fig. 3.3) has an approximately uniform cross section along its length. The first seven natural frequencies and modes of the concrete tie were measured by Igwemezie [79] and they are used for model validation in this study. The calculated results based on Euler beam theory and Timoshenko beam theory together with the experimental data are all presented in Table 3.1. The Error or the percentage of difference in the table is defined as

$$\text{Error} = \frac{\text{theoretical value} - \text{experimental value}}{\text{experimental value}} 100\% \quad (3.3)$$

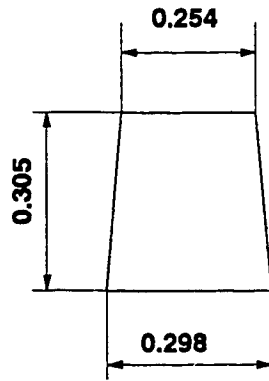
The parameters used in this part of the study is basically adopted from [79] and are as following:

$$\begin{aligned} E_{ct} &= 3.214 \times 10^{10} \text{ N/m (4662 ksi)} & G_{ct} &= 1.340 \times 10^{10} \text{ N/m (1943 ksi)} \\ \rho_{ct} &= 2458 \text{ kg/m}^3 \text{ (} 2.3 \times 10^{-4} \text{ lb-s}^2/\text{in}^4 \text{)} & m_{ct} &= 206.8 \text{ kg/m (} 3 \times 10^{-5} \text{ kip-s}^2/\text{in}^2 \text{)} \\ I_{ct} &= 6.4936 \text{ m}^4 \text{ (1560 in}^4\text{)}, & \nu_{ct} &= 0.2, & T_{ct} &= 0.845 \end{aligned}$$

Timoshenko coefficient (T_{ct}) of the concrete tie is calculated from the formulas proposed in [26], which is expressed as:

$$T_{ct} = \frac{10(1 + \nu_{ct})}{12 + 11\nu_{ct}} \quad (3.4)$$

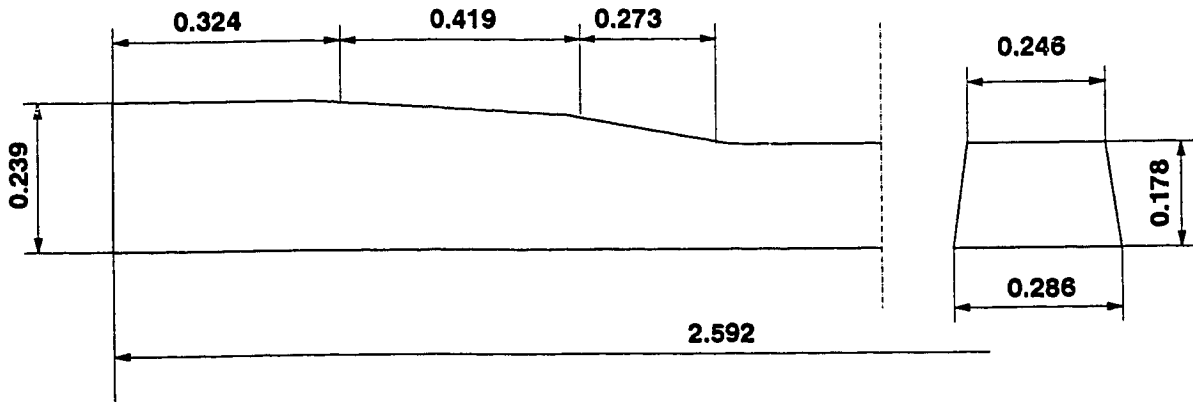
As shown in Table 3.1, the frequencies calculated with the Timoshenko beam theory are very close to the experimental results. The difference between the experimental results and the theoretical results calculated with the Euler beam



Length of the tie:
Lct = 3.658 m

Unit: m



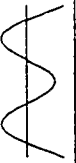


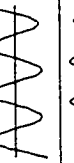
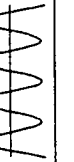
Figure 3.3 Dimension of CN Type-A bridge concrete tie



Unit: m

Figure 3.4 Dimension of CT-3 concrete track tie

Table 3.1 Natural Frequencies of CN Type A Concrete Bridge Tie

Mode No.	Bending Shapes	* Measured Frequencies (Hz)	Euler Theory Frequencies (Hz)	Euler Theory % Errors	Timoshenko theory Frequencies (Hz)	Timoshenko theory % Errors
1		81.25	83.92	3.3	82.6	1.7
2		214	233	8.9	219	2.3
3		417	457	9.6	407	2.4
4		634	755	19.1	634	0.0
5		930	1128	21.3	888	4.5
6		1223	1576	28.9	1161	5.1
7		1576	2098	33.1	1448	8.1

* The experimental data are from Ref.[79].

theory becomes larger with the mode increasing. This is because the Euler beam theory ignores the shear deformation and the inertia of rotation and makes the beam stiffer than it really is. This results in overestimation of the calculated frequency. This effect on the first two bending modes of the concrete tie is small and it may be neglected. However, it is much better to use the Timoshenko beam theory for the concrete tie if the higher modes are concerned in the investigation.

3.2.2 CT-3 concrete track tie

The CT-3 concrete (Fig. 3.4) tie was installed in the test site for an impact load investigation carried out by CP Rail System [36]. Its natural frequencies were obtained in the in-situ field tests [36] and they are used to further validate the theoretical tie model in this study.

In order to justify the theoretical tie model used in the FE model of the vehicle-track system, four different models for the CT-3 concrete tie are considered in the calculation. They are the free-free non-uniform Timoshenko beam (FTB), the free-free non-uniform Timoshenko beam on elastic foundation (TBEF), the non-uniform Timoshenko beam supported on two springs (TBS), the equivalent free-free uniform Euler beam (EUEB) and the equivalent non-uniform Euler beam on elastic foundation (ENEB). The parameters used in the calculation are:

$$\begin{aligned}
 E_{ct} &= 3.214 \times 10^{10} \text{ N/m (4662 ksi)} & G_{ct} &= 1.340 \times 10^{10} \text{ N/m (1943 ksi)} \\
 \rho_{ct} &= 2458 \text{ kg/m}^3 (2.3 \times 10^{-4} \text{ lb-s}^2/\text{in}^4) & k_f &= 2.977 \times 10^8 \text{ N/m (4318 lb/in}^2\text{)} \\
 K_v &= 8.268 \text{ MN/m (210 kip/in)}, & \nu_{ct} &= 0.2, & T_{ct} &= 0.845
 \end{aligned}$$

The Timoshenko shear coefficient is calculated from Eq. (3.4). The equivalent uniform beam is calculated from the following criteria:

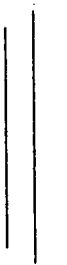




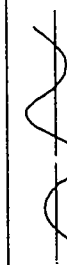
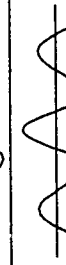

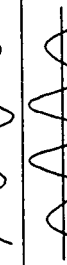
- (a) the total length of the tie remains unchanged;
- (b) the width of the tie bottom remains unchanged;
- (c) the total amount of mass remains unchanged;
- (d) the angle between the bottom and the side remains unchanged;
- (e) all the physical parameters remain unchanged.

Table 3.2 shows the calculated natural frequencies, together with the experimental data. As shown in this table, the calculated frequencies from the TBEF model generally have very good correlation with the experimental data. The measured first bending frequency was originally recognized as 73 Hz in the preliminary analysis reported in [36], which should in fact be for the near rigid-body translation or/and rotation modes (01 and 02 in Table 3.2). This erroneous observation is probably because the nodal points of the first bending mode (about 130 Hz) are very close to the rail seats and hence this mode may not have been excited effectively to be detected during testing.

The results in this table show that the continuous foundation stiffness strongly affects the first bending frequency but it has little effect on the higher modes. This may also be explained qualitatively using the following expression for the natural frequency (f_n) derived for an Euler beam on elastic foundation [60]:

$$f_n = \frac{1}{2\pi} \left\{ \frac{EI}{mL} [\pi(n+0.5)]^4 + \frac{k_f}{m} \right\}^{\frac{1}{2}}, \quad n = 1, 2, 3, \dots \quad (3.5)$$

Table 3.2 Natural Frequencies of CT-3 Concrete Track Tie

Mode No.	Mode shape	FTB Model Hz	TBEF Model Hz	Experimental data * Hz	TBS Model Hz	EUEB Model Hz	ENEB Model Hz
1		0.0	70	73	51.3	0.0	73
2		0.0	72		53.1	0.0	83
3		109	131		109	121	123
4		291	299	300	293	336	285
5		518	522	525	520	658	538
6		868	871		868	1088	874
7		1282	1283		1281	1625	1379
8		1602	1603		1602	2270	
9		1994	1995		1994	3023	

* Experimental data are from Ref. [36]

where E is Young's modulus for the beam material, I is the second moment of area of beam cross-section, m is beam mass per unit length and k_f is the stiffness of elastic foundation. With the parameters used in this study, this expression for the concrete tie becomes:

$$f_n = 35.12 \times [2.34 \times (n + 0.5)^4 + 4.145]^{\frac{1}{2}}, \quad n = 1, 2, 3, \dots \quad (3.6)$$

The second term (4.145) in the bracket represents the influence of foundation stiffness on the frequencies. Its effect on the first frequency is large but it will quickly disappear with the increase of the mode order (n) and the frequency then become approximately proportional to the square of mode order.

Similar to the continuous support discussed above, there is no significant difference among frequencies for different discrete support conditions, except for the first frequency, as shown in Table 3.2. If the support stiffness is small, the effect of support conditions can even be ignored, as was shown in Fig. 3.2. In the tests carried out by Dean et al. [34], the influences of support conditions on the bending frequencies were not observed, even on the first bending mode. This is probably because the ties were not tightly restricted on the supports in the tests and the tie behaved basically like a free-free beam.

The geometric changes along the length of the tie have some effect on the frequency values, as indicated in Table 3.2. It is a general case that the concrete tie has a thinner part in the middle and a thicker part at the two ends or at the rail seats. This makes the tie frequencies smaller than those of its equivalent uniform beam. It is difficult to give a general conclusion for this

factor. As the results indicated, the method developed in this study can be used to predict the frequencies and mode shapes accurately.

Based on above discussions, it is clear that it is appropriate to model the concrete tie as a non-uniform Timoshenko beam laying on elastic foundation (TBEF) in a track model. However, this may increase the size of the governing equations of the track system. On the other hand, only the first few frequency values and vibration modes of the tie have some effects on the response of the dynamic wheel/rail contact force and strains in the rail. Hence, to reduce the computing time, the tie modeled as an ENEB is used in the system model described in Chapter 2 and its natural frequencies are also listed in Table 3.2 for comparison. As the results show ENEB model of the tie is as good as that of TBEF for the first 6 modes.

3.2.3 Natural frequencies of a wheelset

The natural frequencies of wheel rim in the vertical plane may be estimated from the following expression [67]:

$$f_n = \frac{1}{2\pi R_w} (1+n^2)^{1/2} (E_w / \rho_w)^{1/2} \quad n = 1, 2, 3 \dots \quad (3.7)$$

where ρ_w is the mass density of wheel rim, E_w is the Young's modulus for rim steel and R_w is wheel rim effective radius. For a AAR 36" diameter freight car wheel, the free rim frequencies are 2754 Hz, 4355 Hz, and et al. [67]. The wheel plate can further stiffen the wheel rim considerably and increase the frequencies.

Hence, the frequencies of the rim are too high to be of concern in this study. The axle/wheel mass is therefore modeled as a lumped mass in this investigation.

To bring into the geometric shape and the shear flexibility of the wheelset along the axle, the wheelset is modeled as a non-uniform Timoshenko beam with lumped masses and free-free end boundary conditions, as shown in Figs. 3.5 and 3.6. The mass and second moment of the wheel rim and web are assumed to be concentrated at the locations of rolling center. The wheel hubs are considered to be clamped on the beam. The wheelset is assumed to be supported on the springs at the locations of bearings, as shown in Fig. 3.6. The wheelset modeled as Timoshenko beam on spring supports is referred to as TBS model. The free-free Timoshenko beam model (FTB) and the free-free Euler beam model (FEB) are also employed in this investigation for comparison. The results of the free-free Euler beam model are also obtained by properly modifying the developed computer program.

The dynamic equation of the wheelset is the same as Eq. (3.2) developed to calculate the natural frequencies of concrete ties, except that the lumped masses (M_w) and inertia moments (J_w) of the wheels have to be added to mass matrix. The model parameters for an AAR Axle Type C wheelset are taken as:

$$\begin{aligned}
 E_w &= 2.1 \times 10^{11} \text{ N/m (30459 ksi)} & G_w &= 8.077 \times 10^{10} \text{ N/m (11715 ksi)} \\
 \rho_w &= 7757 \text{ kg/m}^3 (7.259 \times 10^{-4} \text{ lb-s}^2/\text{in}^4) & M_w &= 350 \text{ kg/m (1.9987 kip-s}^2/\text{in)} \\
 J_w &= 25 \text{ kg-m (221 lb-s-in)}, & \nu_w &= 0.3, & T_w &= 0.886, & K_v &= 2.2 \text{ MN/m.}
 \end{aligned}$$

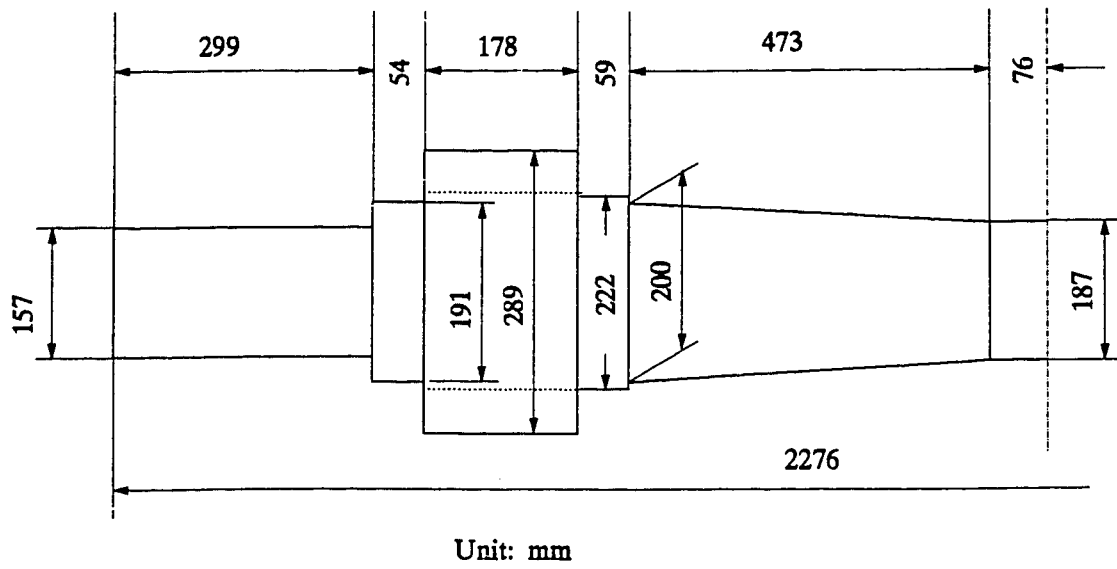


Figure 3.5 Dimension of wheelset axle system

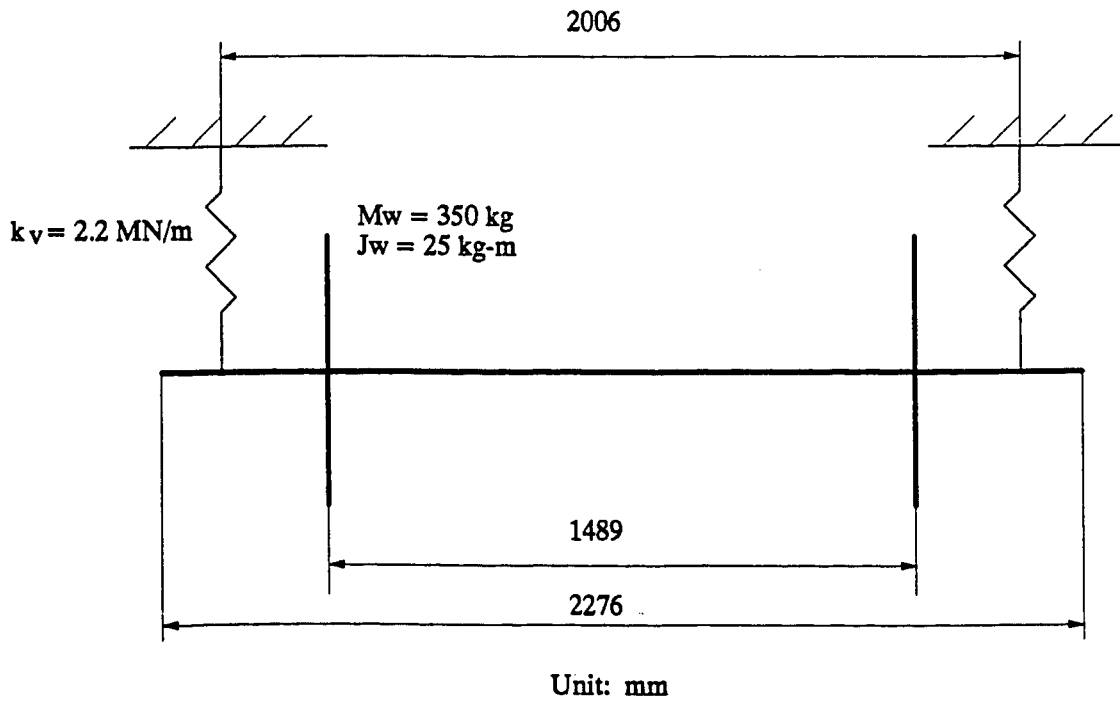


Figure 3.6 Wheelset Model

The Timoshenko shear coefficient (T_w) for the wheelset axle is calculated from the following expression [26]:

$$T_w = \frac{6(1 + \nu_w)}{7 + 6\nu_w} \quad (3.8)$$

The evaluated results along with percentage difference from the FTB model are shown in Table 3.3. A comparison of results obtained using FTB and TBS models indicate that the influence of primary suspension stiffness on the wheelset natural frequencies is negligible. This is due to the fact that the wheelset axle stiffness is significantly larger than that of primary suspension. The mass and inertia moment of the wheels are significant and they strongly affect the frequency values and mode shapes. The test method used to measure the frequencies of concrete ties should also be good for wheelsets.

3.3 NATURAL FREQUENCIES OF VEHICLE-TRACK SYSTEM

The natural frequencies of vehicle-track system is evaluated in two stages. First a detailed wheel/track model is considered to identify the coupled wheel/track frequencies. A simplified car-wheel-track system is then considered to estimate its natural frequencies.

3.3.1 Wheel-track system

One of the coupled wheel/track natural frequencies is the wheel/rail contact resonant frequency. The wheel/rail contact stiffness is usually very large under a quasi-static loaded condition. For example, it is about 1.8×10^9 for a 36' AAR

Table 3.3 Natural Frequencies of Wheelset

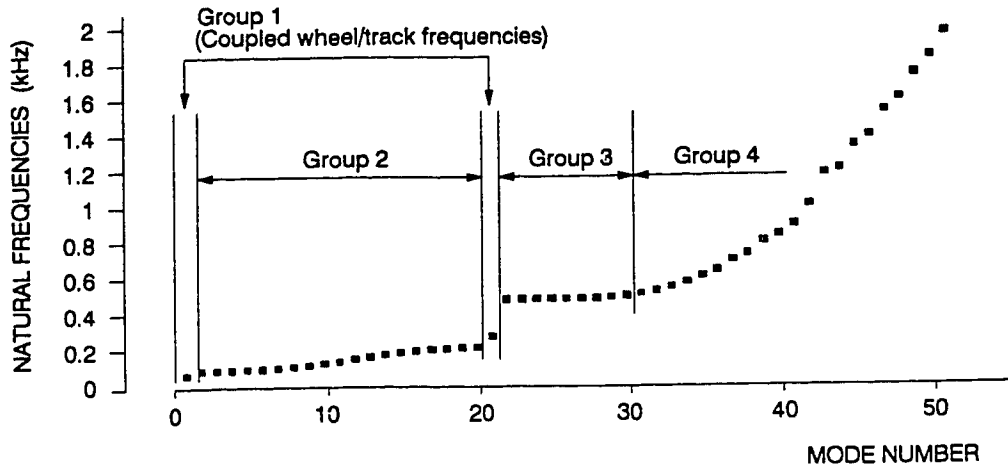
Mode No.	Mode shape	FTB Model Hz	TBS Model Hz	% difference $\frac{ FTB - TBS }{FTB} \%$	FEB Model Hz	% difference $\frac{ FTB - FEB }{FTB} \%$
1		0.0	9.3		0.0	
2		0.0	12.9		0.0	
3		115	116	0.9	116	0.9
4		287	287	0.0	295	2.8
5		679	679	0.0	746	9.9
6		1027	1028	0.0	1126	9.6
7		1032	1030	0.0	1132	9.7
8		1327	1327	0.0	1593	20.0
9		2112	2112	0.0	2723	28.9

FTB Model: Free-free Timoshenko beam model
 TBS Model: Timoshenko beam on spring supports
 FEB Model: Free-free Euler beam model

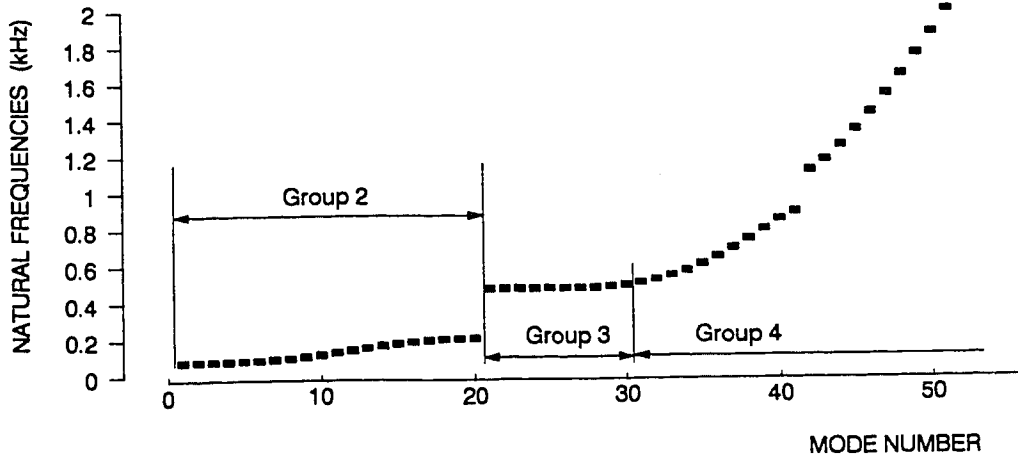
wheel on a R136 rail under a static load of 147 kN (33 kips). The rail-pad stiffness are usually several times smaller than this stiffness and its effect on this contact resonant frequency can be ignored. Furthermore, the rail equivalent mass is usually much smaller than the wheel mass and the displacement of wheel may be ignored for estimation of wheel/rail contact resonance. Hence, the resonant frequency due to this contact spring can be evaluated by only taking into account the rail equivalent mass and contact stiffness, which forms a 1-DOF system. In doing so, the wheel/rail contact resonant frequency is estimated to be in the range of about 800-1000 Hz.

In the following discussions, in order to identify other coupled wheel-track frequencies and simplify the FE modeling, the wheel/rail contact stiffness is assumed to be infinitely large and the wheel mass is rigidly attached to the rail at the contact point. The model of the track system is the same as that described in Chapter 2. The ties are considered rigid bodies in this case. The natural frequencies of the wheel-track system vs. their mode number are plotted in Fig. 3.7a. To identify the effects of the wheel on the frequencies, the track frequencies are also calculated and plotted in Fig. 3.7b.

From these two figures, it can be seen that only a few frequencies are significantly affected by the participation of the wheel on the track. Two of them are important for the vehicle-track interactions. The first one is the fundamental track frequency (80 Hz) and it is replaced by the first coupled wheel-track frequency (54 Hz). The second is the fundamental rail/tie anti-phase frequency (474 Hz) and it is replaced by the wheel-rail/tie anti-phase frequency (266 Hz). The presence of wheel does not significantly change the basic distribution of the frequencies.



(a) Wheel-track system



(b) Track system

Figure 3.7 Dispersion relations for a wheel-track system

The frequencies of the wheel-track system may roughly be divided into four groups, as indicated in Fig. 3.7. The first group includes the two coupled wheel-track frequencies. The wheel, rail and tie move in phase as the system is vibrating at the first coupled frequency (54 Hz). The mode shape of this frequency is very close to the deflection shape of the track as shown in Fig. 3.8 for various configuration. Hence, it is an important frequency in the vehicle-track system. Mair [99-102] indicated that this frequency may have a relationship to long-wave corrugations. A possible source causing the resonance is the effect of tie spacing. The tie spacing is usually in the range of 0.55 to 0.8 meter in the present tracks. The first coupled wheel/track frequency is usually in the range of 30 to 60 Hz. The corresponding resonant speed due to tie spacing will be in the range of 16.5 to 48 m/s (60 to 173 km/h). This range covers most of conventional railway speeds. A further discussion on this problem will be presented in Chapter 6.

The first coupled wheel/track frequency mainly depends on the unsprung mass (M_w), track equivalent mass (M_{TR}) and track effective stiffness (K_e). The track effective stiffness is composed of the rail stiffness and the foundation stiffness. The equivalent mass and stiffness may be estimated from the formulae proposed in [10]:

$$K_e = 2(4EI k_f^3)^{0.25} \quad \text{and} \quad M_{TR} = 3m_{TR}(EI / K_e)^{1/3} \quad (3.9)$$

where EI is rail stiffness, m_{TR} is track equivalent mass per unit length and k_f is track equivalent stiffness per unit length. In this study, the track equivalent mass per unit length is taken as:

$$m_{TR} = m_r + M_t / L_t \quad (3.10)$$

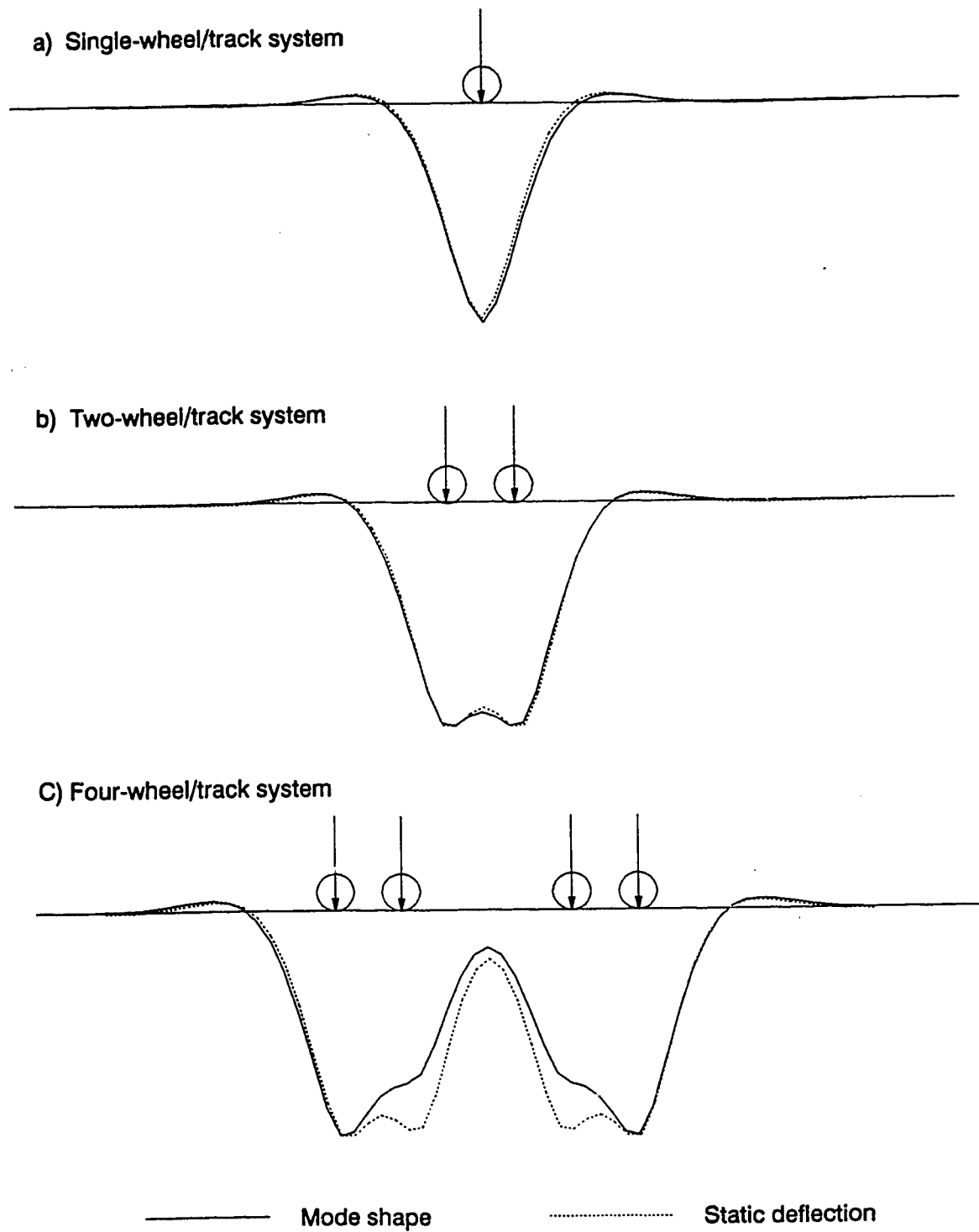


Figure 3.8 Comparison of the mode shape of the fundamental wheel/track frequency with the deflection shape of track

The track equivalent stiffness is taken as:

$$k_f = K_s / L_t \quad (3.11)$$

where K_s is the equivalent stiffness on each support and it is calculated from:

$$K_s = \frac{k_p k_b L_p L_s}{k_p L_p + k_b L_s} \quad (3.12)$$

The first coupled frequency can then be calculated as:

$$f_{W/T} = \frac{1}{2\pi} \sqrt{\frac{K_e}{M_w + M_{TR}}} \quad (3.13)$$

The coupled frequency may also be calculated from the formulae proposed in [100]:

$$f_{W/T} = \frac{1}{2\pi} \left(\frac{k_f}{m_e} \right)^{1/2} \quad \text{where} \quad m_e = m_{TR} + \frac{M_w}{1.89} \left(\frac{k_f}{4EI} \right)^{1/4} \quad (3.14)$$

The frequency calculated from above Eq. 3.14 is about 49 Hz and it is lower than the results obtained from the FE model and the expression given in Eq. (3.13).

The second coupled wheel/track frequency (266 Hz) represents the anti-phase motion between the wheel (plus the rail equivalent mass) and the tie. Because the wheel mass is usually several times larger than the tie mass, the anti-phase frequency mainly depends on the tie mass, rail-pad stiffness and ballast stiffness.

The frequencies in the rest of the three groups are mainly determined by the properties of the track system. The frequencies in the second group (80 to 203 Hz) is characterized by their mode shapes in which the rail and tie basically move in phase. The frequency values are closely spaced in this group but their mode shapes are individually distinct from each other. Physically, this is because a long rail is a slender structure and the energy in each mode in the low frequency range is close to each other. Mathematically, this can be explained from Eq. 3.5. For a reasonable length (L) of track used in the calculation, the first term in the formulas is not significant until the mode number (n) increases to some point. Below this point, the second term, which is constant, dominates the values of the frequencies. Therefore, the frequency values can be very close to each other, even though their mode shapes are orthogonal.

The frequencies in the third group (474 to 478 Hz) are also close to each other but for a different reason. In this group, the rail and tie basically vibrate in anti-phase manner. The feature of discrete tie supports contributes to a number of closely spaced frequencies.

As the frequency increases (larger than about 478 Hz), the influences of supports become smaller and the properties of the rail gradually dominate the behaviors of the system. This may also be explained from Eq. 3.5. As the mode order increases to some point, the constant term, which represents the support condition, is no longer significant in determining the frequency values. This suggests that the rail vibrations at very high frequencies are relatively independent to the support conditions.

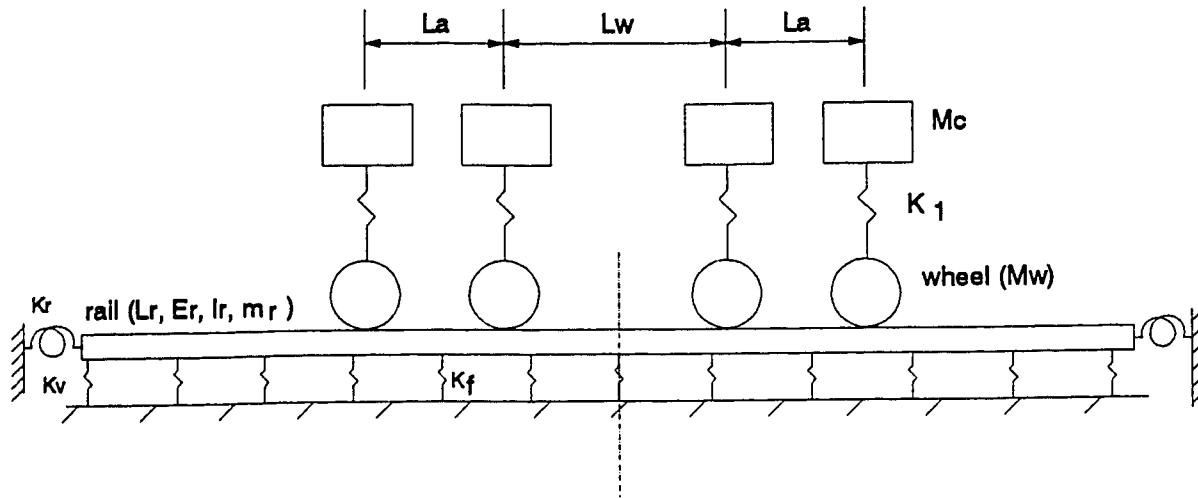
3.3.2 Car(body)-wheel-track system

To estimate the natural frequencies of car-wheel-track system, a simplified model as shown in Fig. 3.9 is considered. The evaluated natural frequencies presented in Table 3.4 can be basically divided into three groups,. The first group (2.69-2.70 Hz) belongs to the vehicle sprung system. Usually, the primary stiffness is designed to assure the isolation of vibrations from the exciting sources and the fundament frequency of sprung system is less than 10 Hz. The second one is for the coupled wheel-track frequencies (about 54 Hz) and the third group is for the track system. The frequencies in the first group can actually be calculated fairly accurately by only taking into account the sprung mass and primary stiffness. In spite that the positions of the four lumped mass-wheel units are quite different, the frequency for each unit is almost the same, as shown in Table 3.4. These mean that the properties of the wheel-track system have little effect on the fundamental frequency of the vehicle sprung system. Also because of the isolation provided by the primary suspension, the frequencies of the wheel-track system are relatively independent of the sprung system.

The results of this section clearly indicate that for evaluation of track frequency, and wheel/track coupled frequency, it is sufficient to only consider the wheel-track system.

3.4 SUMMARY

The natural frequencies of the major components of the model namely track system, wheelset system and car body system are evaluated. The frequencies



- La** : Wheelset axle spacing (1.74 m)
- Lw** : Wheelset distance between two vehicles (2.9 m)
- Lr** : Total length of track used in the calculation (16.24 m)
- Er** : Young's modulus for rail steel (2.07×10^{11} Pa)
- Ir** : Rail second moment of area (2.35×10^{-5} m⁴)
- mr** : rail mass per unit length (56 kg/m)
- Kv** : Boundary verticle effective stiffness (33.4 MN/m)
- Kr** : Boundary rotational effective stiffness (11.69 MN/Rad)
- Kf** : Foundation stiffness per unit length (40 M/m/m)
- Mw** : Wheel mass (500 kg)
- Mc** : Sprung vehicle mass (10000 kg)
- K1** : Vehicle primary suspension stiffness (3.0 MN/m)

Figure 3.9 Car-wheel-track system

TABLE 3.4 NATURAL FREQUENCIES OF A CAR-WHEEL-TRACK SYSTEM

MODE No.	FREQUENCIES (Hz)
1	2.69
2	2.69
3	2.70
4	2.70
5	53.60
6	54.50
7	56.92
8	57.92
9	138.31
10	138.39
11	156.22
12	158.80
13	162.96
14	201.08
15	203.33
16	244.12
17	265.08
18	292.23
19	311.70
20	353.09

The diagram shows three groups of frequencies indicated by arrows pointing from the table to the right:

- Group 1 Sprung vehicle frequencies:** Modes 1 through 4.
- Group 2 Coupled wheel/track frequencies:** Modes 5 through 8.
- Group 3 Track frequencies:** Modes 9 through 20.

are also evaluated for wheel-track and car-wheel-track system to identify coupled natural frequencies.

A first stage validation of the model is carried out by comparing the FE results with those available from field testing. The calculated natural frequencies for concrete ties from the FE model showed good correlation with those obtained experimentally by CN and CP Rail. The results further show that the support conditions strongly affect the fundamental frequencies, but can safely be ignored for higher frequencies.

The results of wheelset natural frequency indicate that due to relatively large axle stiffness, the influence primary suspension is negligible.

Simulation of vehicle-track system show that for evaluation of track frequency and wheel-track coupled frequency, it is sufficient to only consider the wheel-track system. On the other hand, the sprung mass frequencies can be evaluated effectively from the sprung mass and primary suspension.

From this part of the investigation, the vehicle-track (wheel-track) coupled frequencies were identified as 54 Hz for in-phase motion and 266 Hz for out of phase motion between the wheel (with rail) and the tie. The frequencies corresponding to other modes are dictated by the properties of track system alone.

CHAPTER 4

IMPACT LOADS DUE TO WHEEL FLATS AND SHELLS

4.1 INTRODUCTION

The most common wheel tread defects encountered by railway industry are wheel flats (Fig. 4.1) and shells (Fig. 4.2). It is estimated that the railway industry in North America is currently spending approximately \$90 millions annually to replace 125,000 wheels due to wheel tread defects [1]. Since vehicles may operate with wheel tread defects before they are replaced, it is very important to evaluate their influence on the impact load experienced by vehicle and track components.

Wheel flats and wheel shells are known to cause abnormally high forces and stresses in the track and on the vehicle components. Depending on the size and shape of defect, axle load and speed, the stresses may be sufficient to initiate fatigue cracks, or cause final failure, which may lead to derailment of vehicles. Severe wheel flat and shell are clearly safety hazard. Smaller ones, on the other hand, contribute to track deterioration and increased cost of maintenance. In addition to safety and economic considerations, these defects reduce passenger comfort and significantly increase annoying noise. A quantitative definition of the impact loads and dynamic stresses in both wheel and rail are therefore important in predicting safe operating limits.

The mechanism for the initiation of wheel flats is not well documented. It is generally believed that wheel flats are mainly caused by braking. Once the

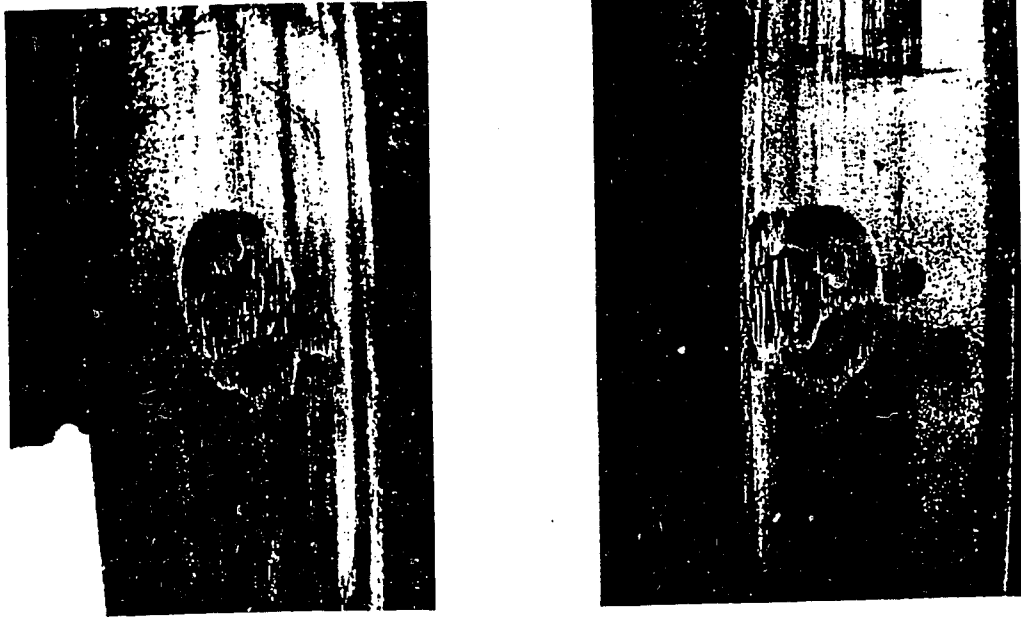


Figure 4.1 Wheel flats at the same "o'clock" position on a single wheelset



Figure 4.2 A fully shelled wheel

wheels of a vehicle become locked during braking, they slide along the track. The friction created by this adhesively wears a flat spot on the wheel. The flat spot, possibly starting as a chord of the wheel circumference, tends to get longer and rounded after a few cycles of wheel rotation. Then, the basic flat shape may stay on the wheel tread for a long time and repeatedly generate large impact forces. Sometimes, this type of wheel flat is referred to as skid flats or short wavelength flats (2.5 to 7.6 cm, in length) or traditionally flats by some researchers [9].

US. Federal Railroad Administration [6,9,35] and Canadian National Railways [134] have reported another type of wheel flat that has a longer wavelength (30 to 41 cm, in length). It has been called runout profile error in some articles since 'flat' may be no longer a proper definition for such a profile shape. The initiating process of runout profile is also uncertain either. Perhaps it starts from the traditional flat, where the car is moved without proper release of brakes. This process may induce a heat-affected zone on the tread and rim, with some reduction of hardness. A thin, hard layer of martensitic material may also be formed in this process from quick surface quench, but this layer should spall off rather quickly under impact loading. Slight differences in effective lubrication between the two wheels may result in long-term differences in profile shapes on the two wheels. The vertical dynamic force may favor the development of flat in some cases.

Wheel shells are mainly developed from micro-cracks initiated by high strains in wheel/rail contact region due to high axle load and creep forces. Even though the appearances of wheel shells are different from those of wheel flats, the measured irregularity functions are quite similar for both cases [36]. Hence,

their basic characteristics of the impact loads should also be analogous.

As an attempt to restrict the damage due to wheel tread defects, most railway administrations has placed limits, such as the AAR Interchange Rule 41 [11], on the length and depth of flats and shells that may stay in service. Experimental results [36] have shown that some non-condemnable wheel tread defects may cause higher impact loads than some of condemnable wheel tread defects [36]. Often the wheels with long wavelength runout profiles do not exceed the condemning limits of the AAR Interchange Rule 41 but they may also result in peak wheel/rail forces over 445 KN [157].

To replace the wheelsets with large flats, they have to be first detected. Many railways still carry out the detection manually, which are costly and difficult in the winter season. Devices for automatically detecting wheel-flats and wheel-shells have been studied for many year [153] and some detectors, such as 'Salient' wheel impact detector have been put into service [36]. Further improvements of the automatically detectors are needed to increase their reliability.

The problem of wheel/rail impact loads due to wheel tread defects have become an important concern with increase speed. The first successful investigation was carried out experimentally by researchers at AAR in 1950's [83]. Researchers at British Rail [24, 25, 80, 152] undertook excellent work in this area in 1970's. Ahlbeck and his colleagues [4-10, 72-73] and Grassie [62] have endeavored to measure the loads caused by actual wheel irregularities and compare these with calculated values in 1980's. Both short and long wheel flats have been considered in their investigations. CP Rail System has carried out a series of field tests on impact loads due to wheel tread defects in 1988 and 1989

[36, 37]. The Salient wheel impact detector was used to measure the impact loads. In recent years, more computer models of railway vehicle-track system have been developed and they have been applied to the impact load problem [18, 40, 49].

However, some aspects of the wheel tread defects remain unclear. In some cases, the observations reported by different researchers seem to be conflicting. For example, it has been reported by Fermer and Nielsen [49] that the dynamic component of impact load is not affected by the axle load but the experimental data obtained by CP Rail System [36] show that the dynamic loads on loaded cars are larger than those on empty cars. Further studies are therefore needed to examine all possible factors that may affect the impact load.

The objective of this section of the study is to carry out a thorough investigation of impact load characteristics due to wheel flats and shells. For this, the developed FE model is first validated against the available experimental data from British Rail and CP Rail. The validated model is then used to carry out an extensive parametric study to identify all possible factors that may affect the impact load. Finally, the model is used to examine the interaction between two wheels due to wheel tread defects. The validated FE model may provide an important tool for the design and development of reliable wheel impact load detector.

4.2 DESCRIPTION OF WHEEL DEFECTS

A fresh flat can be expressed as [4]:

$$f = \begin{cases} -R_w(1 - \cos \varphi) & 0 < \varphi < \varphi_f \\ 0 & \varphi > \varphi_f \end{cases} \quad (4.1)$$

and

$$\varphi = \begin{cases} \sin^{-1}(x/R_w) & 0 \leq x < L_f/2 \\ \sin^{-1}[(L_f - x)/R_w] & L_f/2 \leq x < L_f \end{cases} \quad (4.2)$$

where x is longitudinal coordinate, L_f is flat length and R_w is wheel tread radius.

After a few cycles of wheel rotation, a fresh wheel flat may get rounded under the impact load generated by this flat. Hence, Lyon [98] has suggested a haversine function as more realistic representation of a service-worn flat profile. It may be expressed by

$$f = 0.5D_f[1 - \cos(2\pi x / L_f)] \quad (4.3)$$

where L_f is the length of flat and D_f is the effective flat depth that may be calculated by

$$D_f = L_f^2 / (16R_w) \quad (4.4)$$

Unlike the fresh and rounded flats, it is difficult to use a simple function to express the wheel tread runout profiles and wheel shells. Device such as the profilometer developed by Salient system is available to measure the actual irregularities on wheel treads [36].

The haversine flat function expressed in Eq. 4.3 and the actually measured wheel flats and shells are considered in this study.

4.3 VALIDATIONS OF FE MODEL

As specified in the previous section, useful experimental results are available on the wheel/rail impact which can be used to validate the present FE model. Validation can be carried out either in frequency or time domain. It is easier to correlate few theoretical results to experimental data in the frequency domain. However, in problem such as wheel/rail impact a large range of vibration modes could be excited, and due to large contact stiffness, the force is very sensitive to wheel/rail response. It is therefore, crucial that the model for the proposed study is validated in time domain. A time history validation will further give added confidence on the model for its validity in other applications.

In the following subsection, the developed FE model is validated against experimental data from British Rail and CP Rail. The proposed adaptive contact model is also verified with other well established models and the result are discussed.

4.3.1 Validation against BR's experimental data

Newton and Clark [107] at British Rail carried out a field test to investigate the impact loads and validate their theoretical model in 1979. This experiment is one of a few excellent experiments in the studies of impact loads [92]. Even

though it was carried out about 15 years ago, the experimental data are still valuable for the studies of vehicle/track interaction.

Their experimental work was carried out with an ideal haversine approximation to a wheel flat which was ground into the rail, as shown in Fig. 4.3, thereby avoiding the difficulties of measuring the effects of an irregularity on a wheel which might strike at any point along the track. This also minimizes the influence of lateral position of wheel on the impact load. The haversine function for the wheel flat has been previously described in Eq. 4.3.

The parameters corresponding to the experimental setup presented in Table 4.1 is adopted in the FE model to duplicate the BR's test conditions. In this case, the vehicle is modeled as a unsprung mass carrying a constant load (Model I for vehicle in Fig. 2.1a). The tie is represented by a rigid body or a lumped mass. The element length of rail is half of tie spacing. Various rail models utilized in the simulation include: Timoshenko beam on discrete support model (TBDS), Euler beam on discrete support model (EBDS), the Timoshenko beam on elastic foundation model (TBEF) and the Euler beam on elastic foundation model (EBEF).

The simulated time history contact forces for each of the above rail models along with BR's experimental data are presented in Fig. 4.4. As the results indicate, the basic shapes of the contact forces from all the models are similar to each other, but the first peak values (maximum impact load) for different models are quite different. The lowest peak value resulting from the TBDS model is the closest to the experimental data.

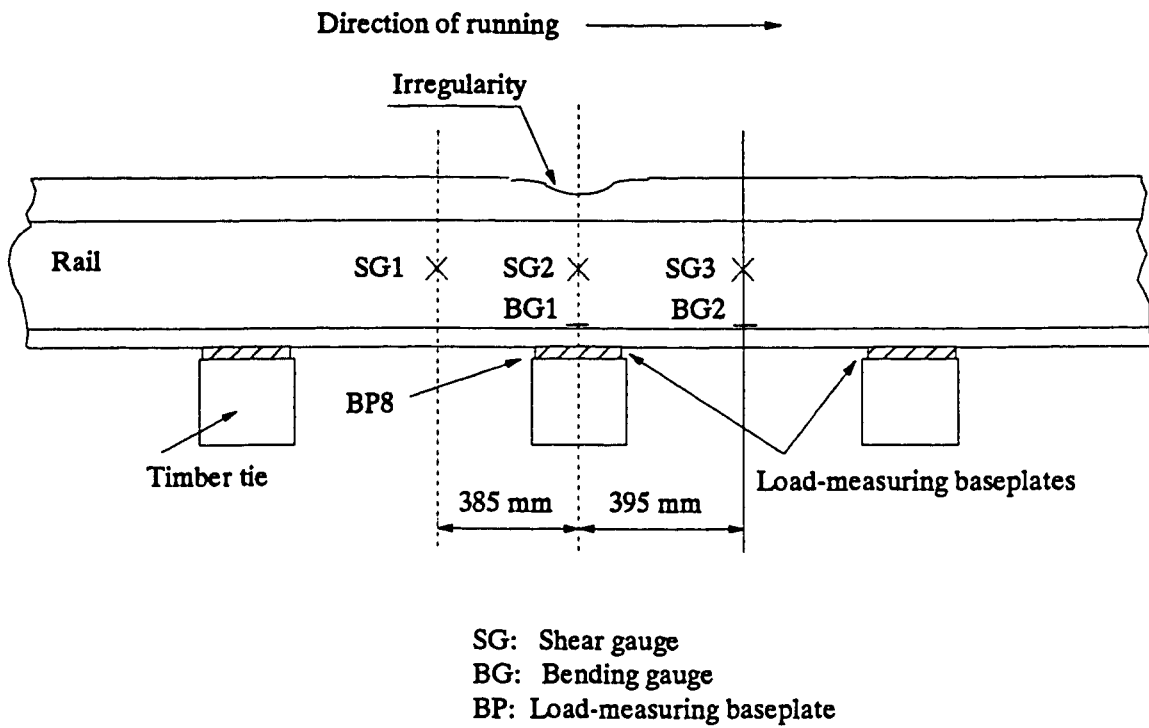


Figure 4.3 Configuration used in British Rail experiment

TABLE 4.1
NOMINAL PARAMETER VALUES
FOR BRITISH RAIL'S EXPERIMENTAL SYSTEM
(BASED ON REF. [107])

E_r	Young's modulus for rail steel, 2.07×10^{11} N/m ²
G_r	Shear modulus for rail steel, 8.1×10^{10} N/m ²
I_r	Rail second moment of area, 2.35×10^{-5} m ⁴
m_r	Rail mass per unit length, 56 kg/m
m_{TR}	Track mass per unit length for beam on elastic foundation models, 119 kg/m
c_f	Foundation damping per unit length for beam on elastic foundation models, 2.76×10^4 N•s/m ²
k_f	Foundation stiffness per unit length for beam on elastic foundation models, 4×10^7 N/m ²
K_p	Railpad stiffness, 2.0×10^8 N/m
K_b	Ballast spring stiffness, 3.16×10^7 N/m
L_t	Tie spacing, 0.79 m
A_r	Cross-sectional area of rail, 7.17×10^{-3} m ²
T_r	Timoshenko shear coefficient, 0.34
C_H	Hertz spring constant, $.0 \times 10^{11}$ N/m ^{3/2}
D_f	Depth of haversine wheel flat, 2.15 mm
L_f	Length of haversine wheel flat, 2.15 mm
M_w	Wheel mass, 500 kg
P_0	Static load, 82 kN

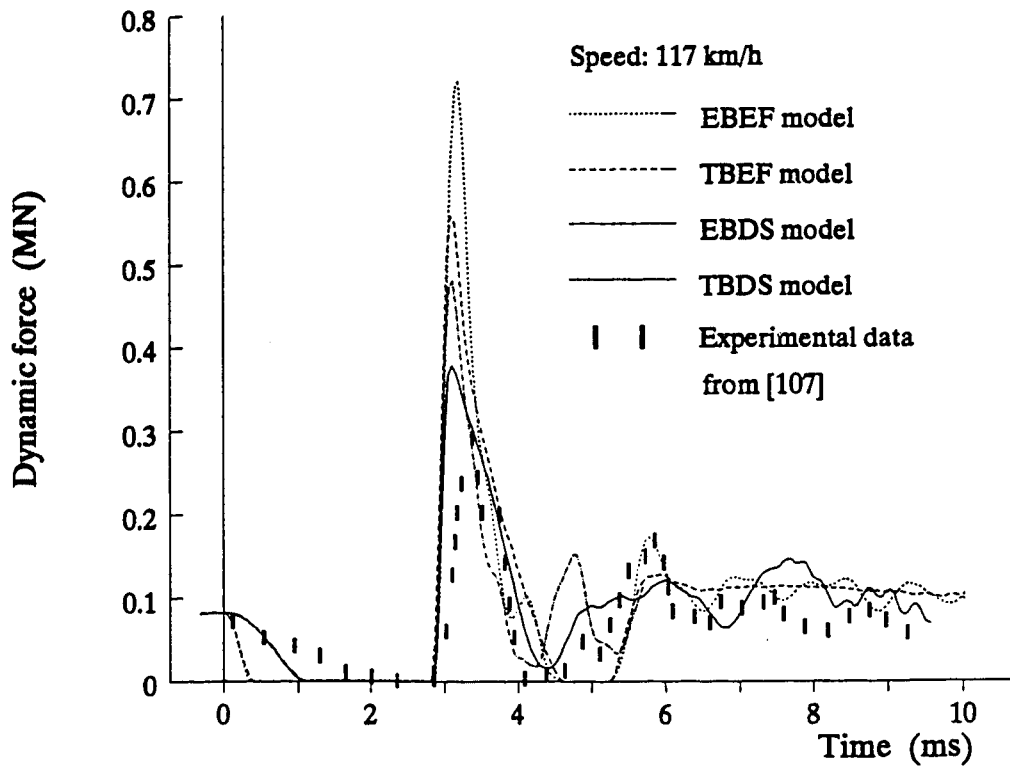


Figure 4.4 Wheel/rail contact force due to wheel flat

The reason for the large discrepancy in the peak dynamic force to some extents can be attributed to excessive mass being lumped to the rail in the distributed support models used in the calculation. Fig. 4.5 shows the effect of increasing equivalent track mass on the impact load calculated from the distributed support TBEF model. It can be seen that the first impact peak (usually called P_1 [80]) is very sensitive to the track equivalent mass. For the given speed (117 km/h), the major frequency involved in the first peak is about 1 kHz (the first peak lasts only about 1 ms, as shown in Fig. 4.4) and it is reasonable to expect that only a small amount of tie mass could take part during impact at such high frequencies. Hence by simply lumping the tie mass to the rail largely overestimates the impact load. This suggests that the equivalent track mass on the EBEF and TBEF models should be taken as a function of frequencies involved in the response. This is one of the major drawbacks of all models in which the track is represented as a beam on a single-layer elastic support.

Another reason for the large variation in the peak dynamic force predicted from different models is the difference between the two beam theories. Euler beam theory ignores the rotational inertia and the shear stiffness of the rail. This makes the rail stiffer than what it really is. This significantly changes the rail dynamic behavior at high frequencies. For this reason, the impact loads calculated from Euler beam theory are again overestimated for a given vehicle speed.

The dynamic force on the pad (pad force) under the rail irregularity that represent the wheel flat [107] is calculated from TBDS model and presented in Fig. 4.6. This figure also presents the experimental data in terms of dynamic force factor (dynamic force divided by static load). It can be seen that the force

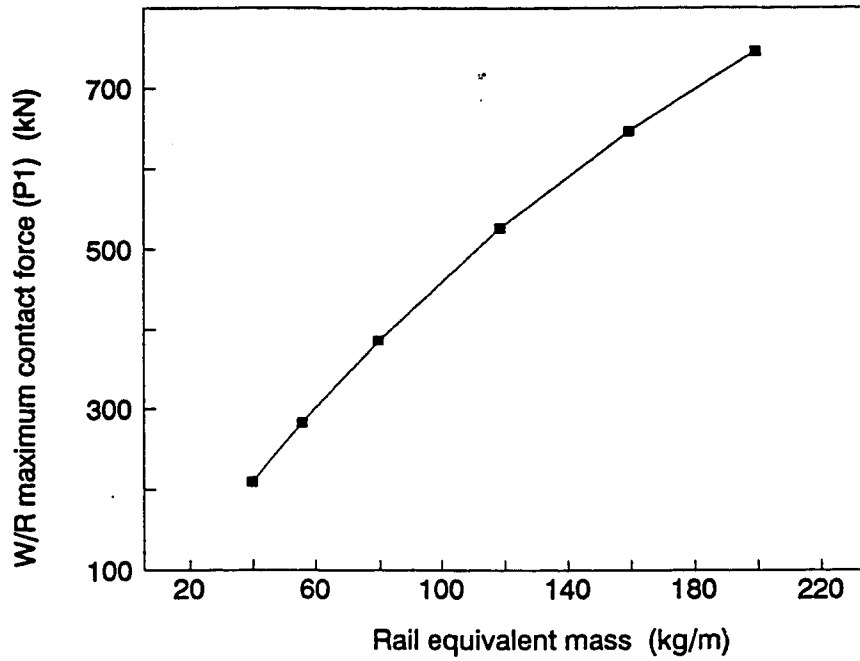


Figure 4.5 Effect of rail equivalent mass on impact load
(Calculated from the TBEF track model)

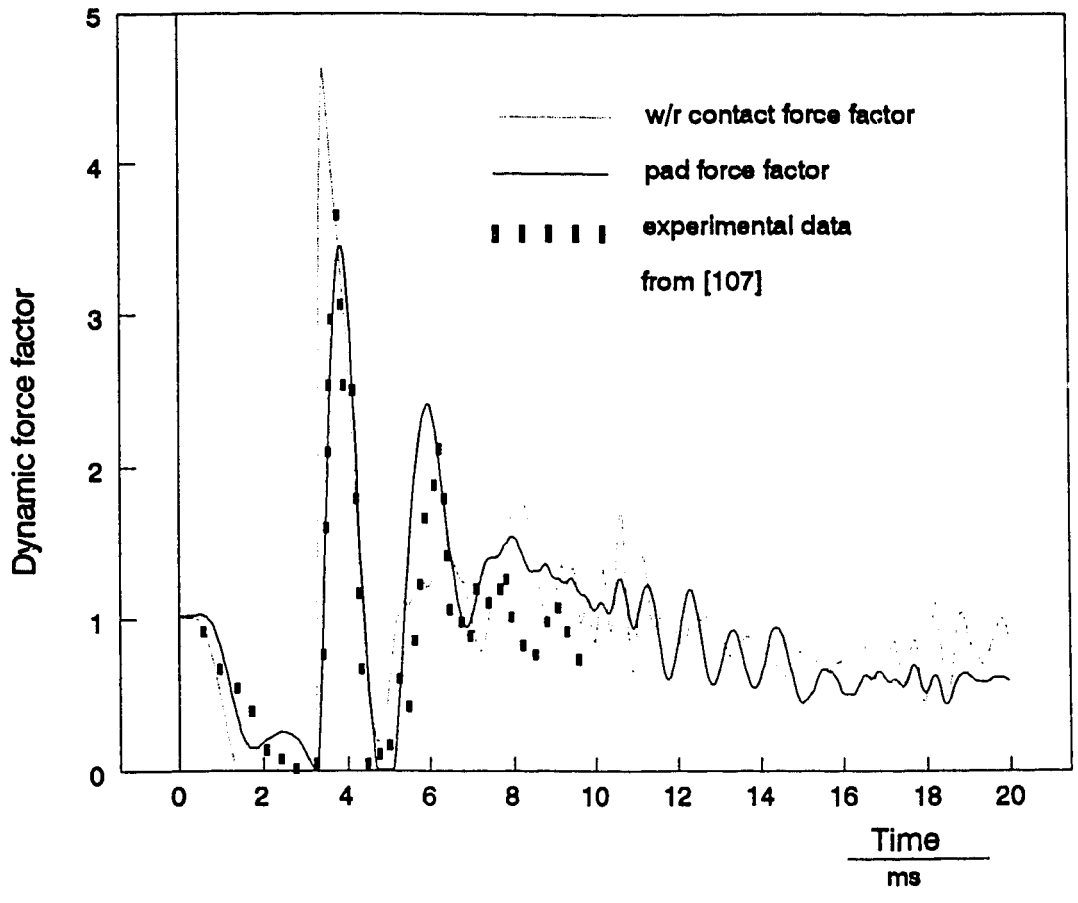


Figure 4.6 Dynamic wheel/rail and pad force factors due to a wheel flat

on the pad has a better correlation with the experimental data than the wheel/rail contact force. This is because the force data for both the rail and the rail-pad in [107] were inferred from a load-measuring baseplate that was located at the position of rail pad and hence the experimental data should represent accurately the force on the rail pad.

The model is next validated by simulating the time history of strains developed at the rail against those obtained experimentally. The calculation of strains in the rail further involve deterioration of the rail displacement using (Eqs. 2.20 and 2.21). Simulation and experimental results corresponding to rail foot bending strains at BG1 and BG2 (Fig. 4.3) are shown in Fig. 4.7. Similarly shear strains obtained at SG1, SG2 and SG3 (Fig. 4.3) are presented in Fig. 4.8. These results are obtained using FE model with element length equal to half tie spacing and lumped mass for tie. In general the results show very good agreement for the first peak with some deviation for others.

The model is then further refined by: using element length equal to quarter of tie spacing; adding extra damping near the rail ends to absorb the transmitted waves; and modeling the tie as a beam. The above simulation is then repeated and compared with experimental data as shown in Fig. 4.9 for rail foot bending strains and in Fig. 4.10 for shear strains.

By comparing the results shown in Figs. 4.7-4.8 and Figs. 4.9-4.10, it can be seen that these modifications to the model do not significantly change the first peak values, which are the main concern in the cases of wheel flats and shells. However, some improvements can be seen in these results. For example, these modifications make the reflected waves from the rail ends disappear, and the

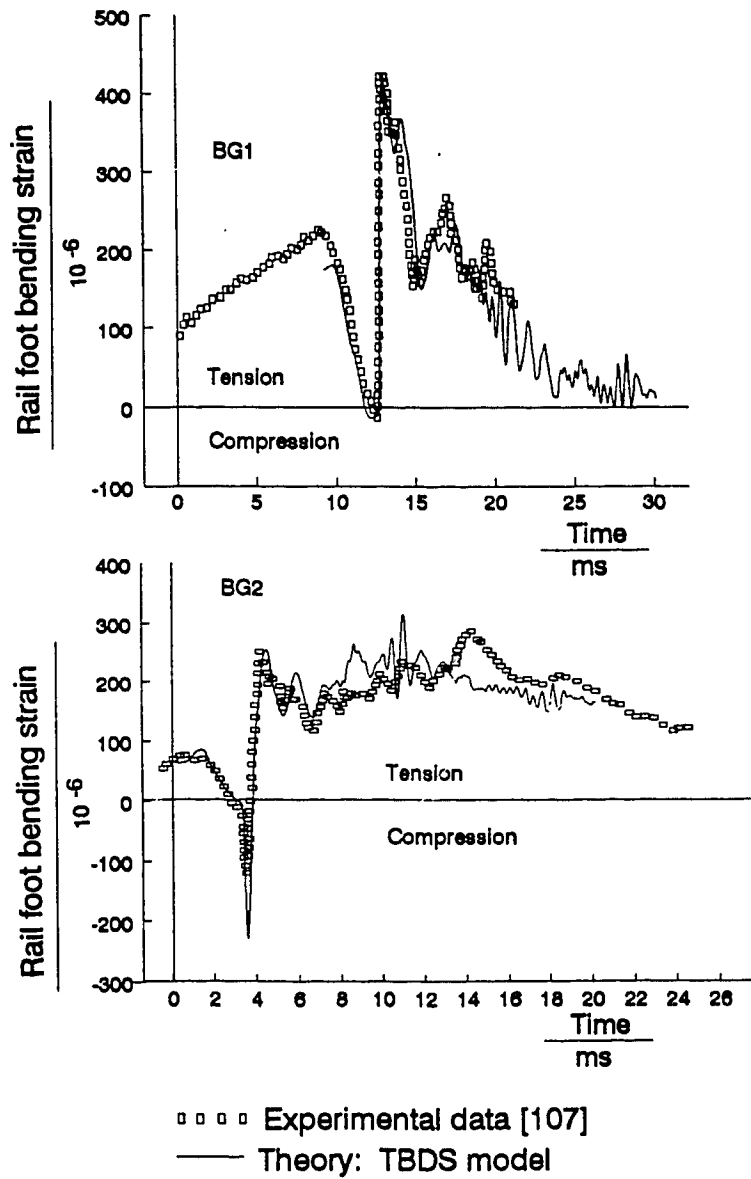


Figure 4.7 Rail foot bending strains

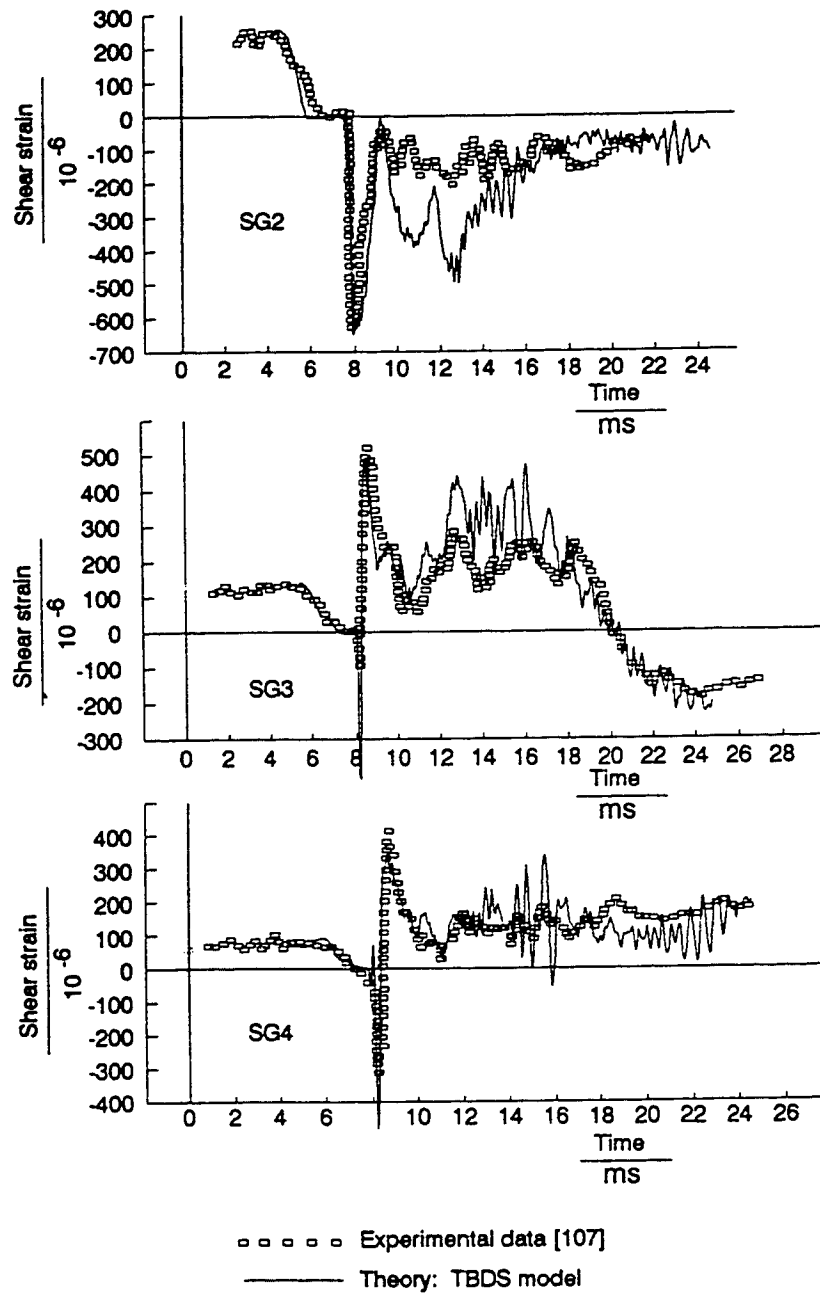


Figure 4.8 Rail shear strains

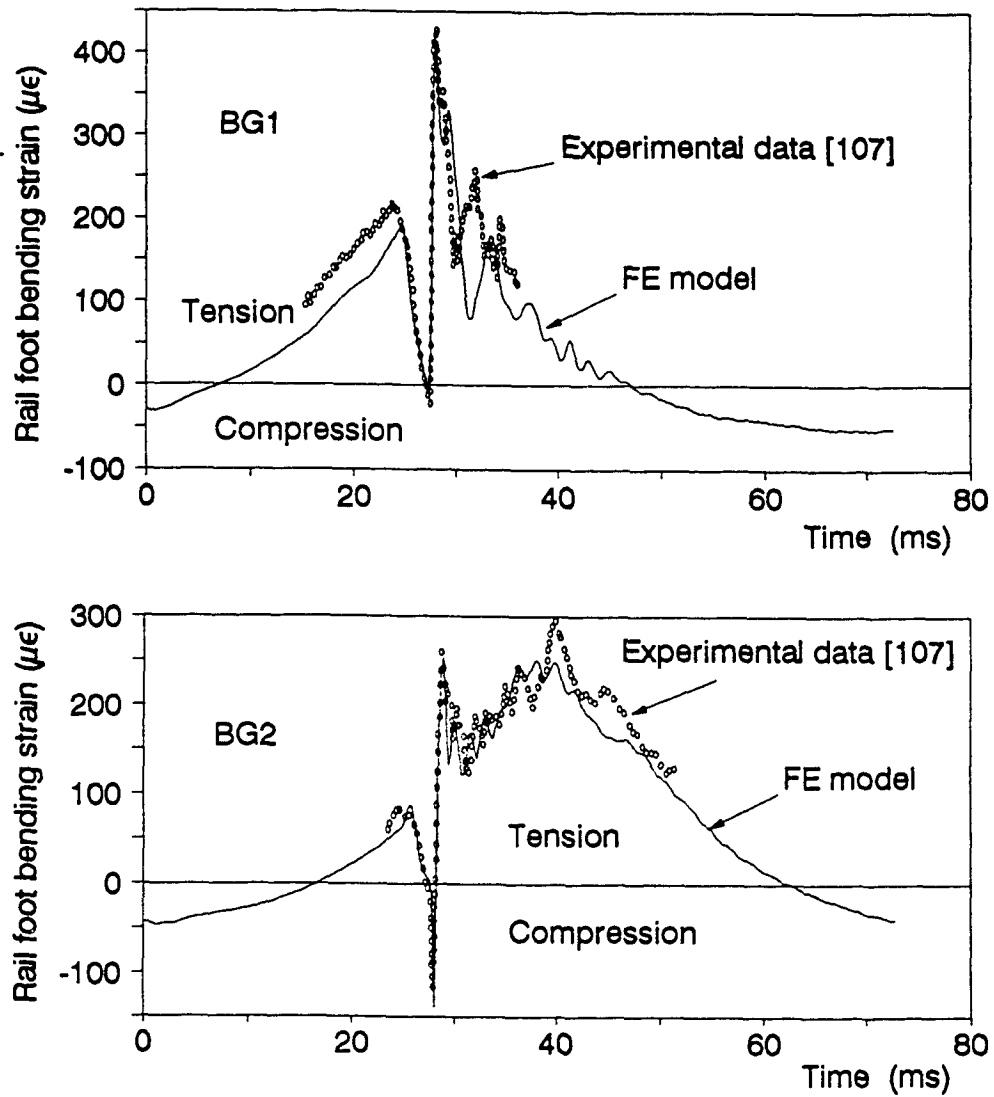


Figure 4.9 Rail foot bending strains calculated from refined FE model

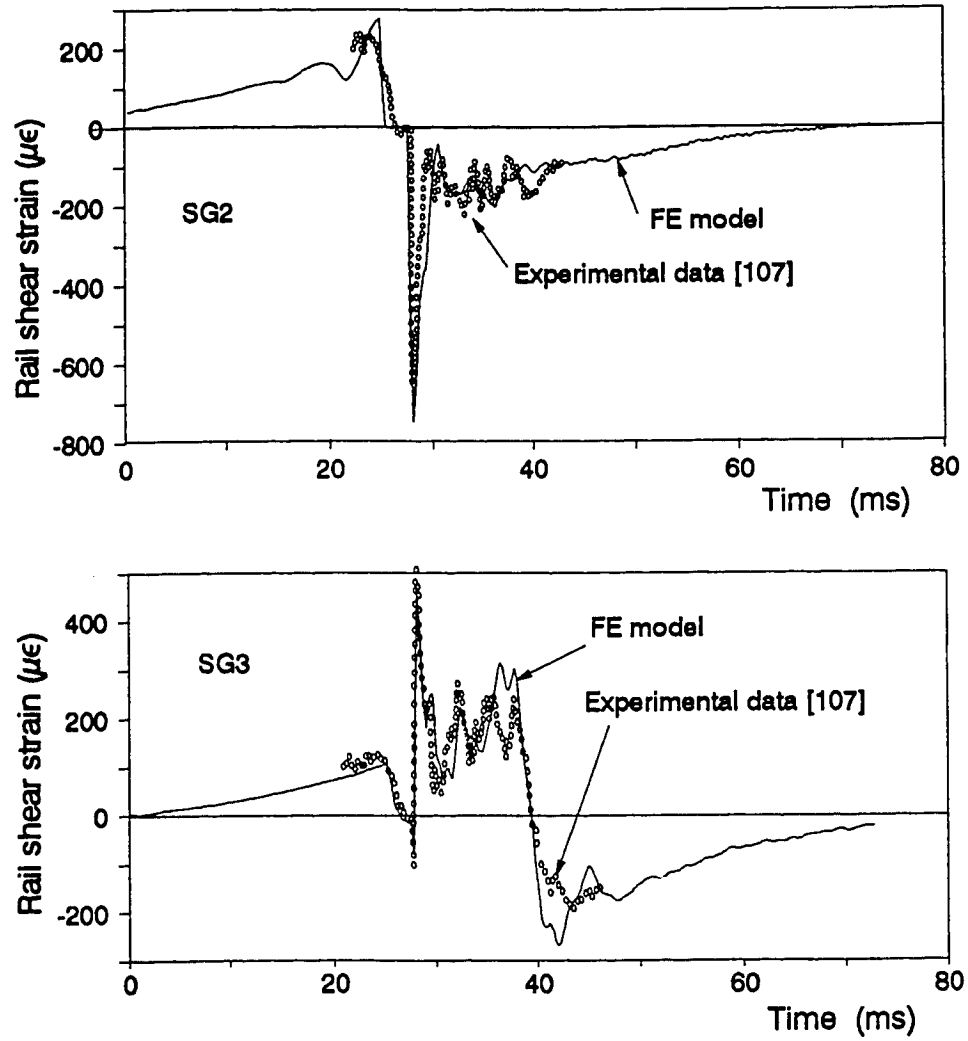


Figure 4.10 Rail shear strains calculated from refined FE model

strains in the rail after their first peaks are significantly improved when compared with the experimental data.

To examine the effect of extra damping near each end of rail and the boundary spring stiffness, wheel/rail contact force is calculated for various values of damping and boundary spring stiffness, and the results are presented in Fig. 4.11. As it can be seen from this figure, there is no significant difference between the two responses for the quite different two sets of stiffness values: (i) $K_v=10^8$ MN/m, $K_r=10^8$ MN/m; (ii) $K_v=0$, $K_r=0$. This indicates that the stiffness of the boundary spring has little effect on the impact response. This means that it is not necessary to impose any restriction at the rail ends if the track in the model is taken long enough and the vehicle is always located in the center part of the track model.

On the other hand, Fig. 4.11 shows that the reflected waves from the ends are satisfactorily absorbed when some viscous damping ($c_v=20$ kN-s/m²) is added on the last two finite elements at each rail end. The added extra damping at the ends can also damped out most of the disturbances caused by the cutting and merging process in extension of finite length of track to infinite track in the FE modeling. These suggest that adding damping near each end is very useful to improve a long term response in the dynamic modeling of vehicle/track interaction.

Dynamic response of the model in term of peak force factor, rail acceleration and rail strain as a function of forward speed is presented in Fig. 4.12. Experimental data [107], wherever available is superimposed for comparison. The dynamic force factor for the pad again shows a better correlation with the experimental

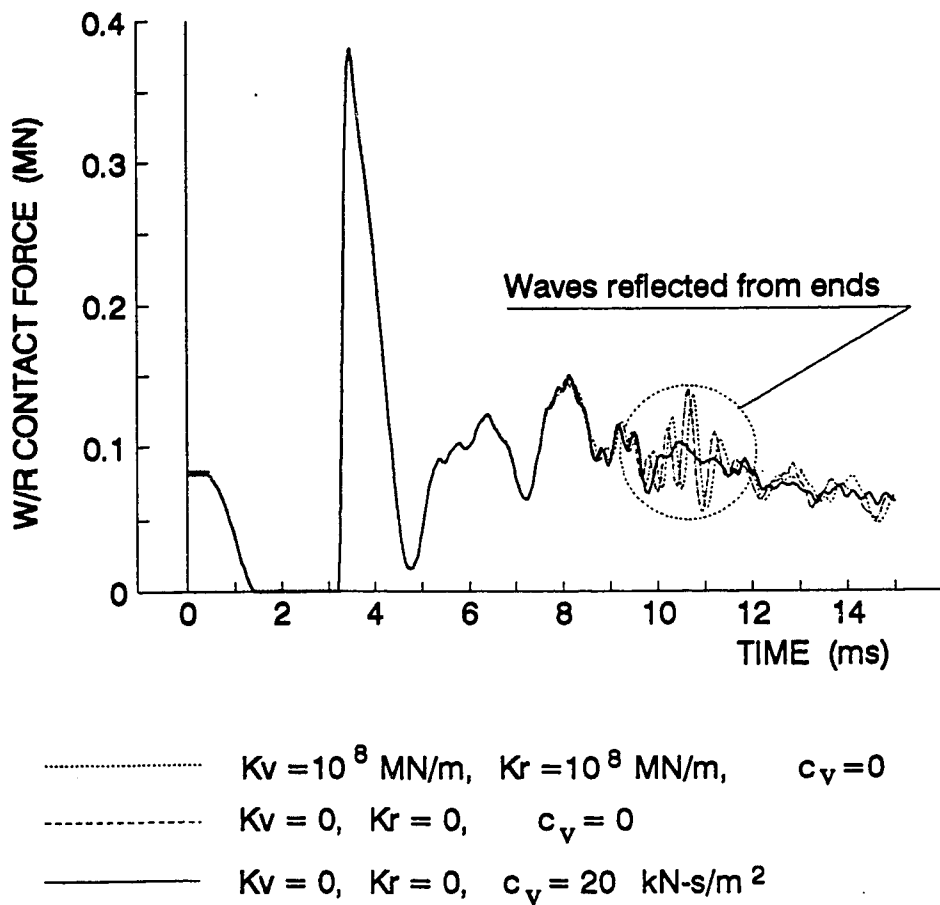


Figure 4.11 Effect of boundary conditions on the impact response due to a haversine wheel flat

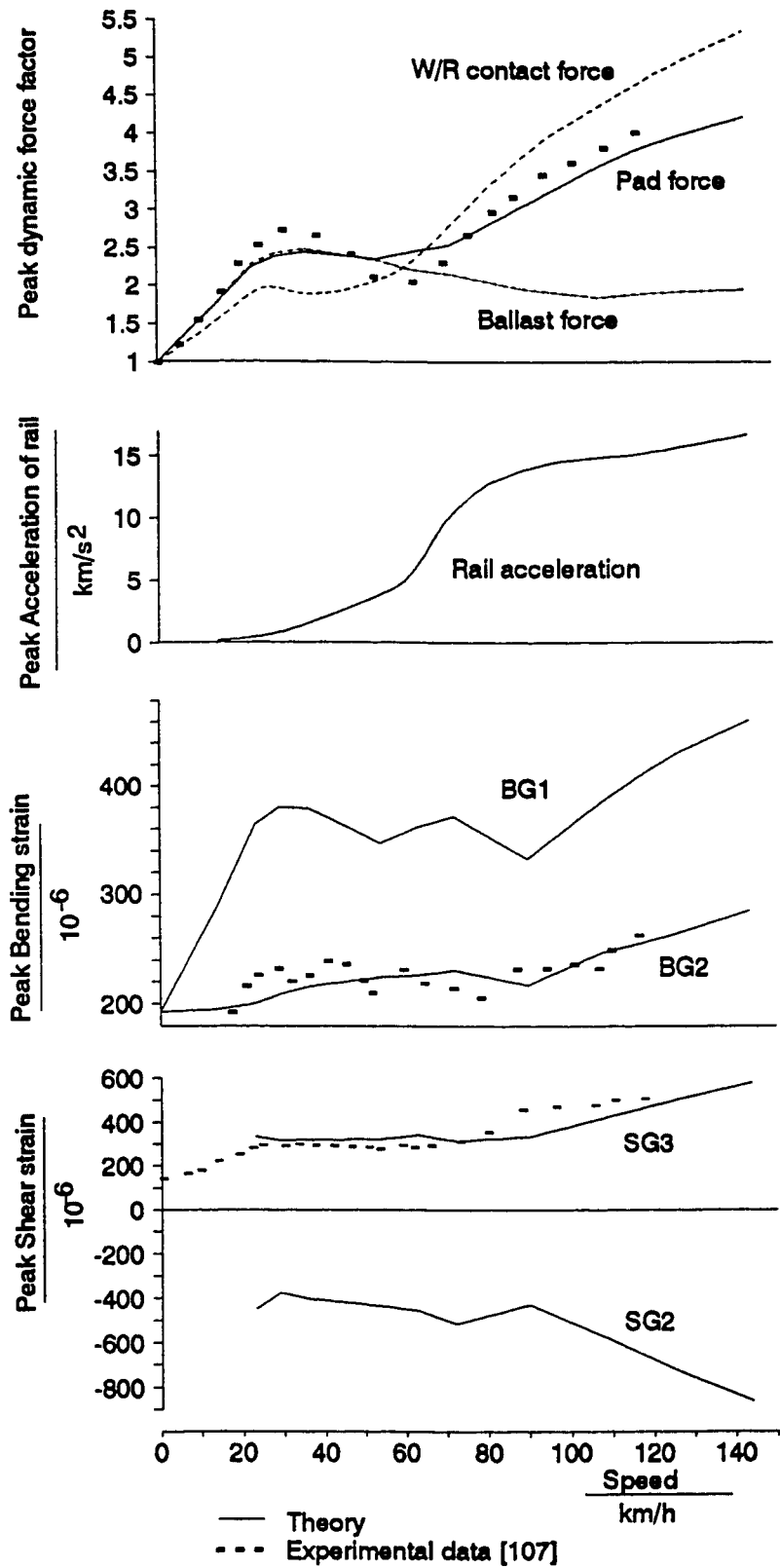


Figure 4.12 Effect of speed on dynamic response

data than the W/R contact force. At low vehicle speeds, both wheel/rail contact and pad forces have the same order of magnitude. However, for higher vehicle speeds they differ significantly.

4.3.2 Validations against CP Rail experimental data

A Salient Wheel Impact Load Detector was installed on CP Rail Systems' main line tangent track at Mile 47.8, Mountain Subdivision in the province of British Columbia, Canada, to measure and report wheel impact loads. CP Rail Research and Operations Development Department (CPRS) conducted a series of field tests in April 1988 [36] and early February 1989 [37]. The main test objectives were: to study the integration of the system into the inspection procedure of empty coal trains; to compare impact load values from different types and sizes of tread defects; to establish a wheel load distribution for coal trains; to determine projected wheel removal rates for different alarm level settings; and to assess the effect of frozen track structure on impact loads.

The detector was installed on 136 RE rail with CP Rail CT-3 concrete ties, with 30.48 m (100 feet) of concrete ties on the approaches [36]. The ties were spaced 0.6096 m (24") apart, and Portec Polyurethane 4.76 mm (3/16") rail-pads were installed. These pads were reduced from 0.1905 m (7-1/2") to 0.127 m (5") in length to ensure more circumference wheel coverage. A motion detector was used to sense approaching eastbound and westbound trains and activate the Salient detector. The detector was calibrated with a vertical loading fixture developed by the Centre for Surface Transportation Technology, National Research Council of Canada [36]. Two concrete ties were also strain gauged to

measure their dynamic behavior under impact loads.

Fig. 4.13 shows one of the consists used in the tests, in which twenty wheelsets with tread defects were selected and installed under five coal cars. These defects were shells, flats and built-up treads, both condemnable and not condemnable by AAR Rule 41. Wheel circumferential profiles were measured with a special profilometer developed by Salient Systems [36]. Several examples of the profiles are shown in Fig. 4.14. In these tests, the cars were both empty and fully loaded. Some of the wheels used in Summer tests [36] were also used in Winter test [37] for comparison of the impact loads on frozen and unfrozen tracks. Test data from these series of tests reported by CPRS [36, 37] are employed to validate the FE model. The major parameters used in this simulation are same as those corresponding to CP rail's experimental system as presented in Table 4.2.

One of the methods used to measure the impact load, such as that employed in the Salient Wheel Impact Load Detector, is shown in Fig. 4.15a. The net shear strain differential is measured from the rail web and it is simply multiplied by a calibration constant to obtain the wheel/rail contact force or impact load. A trace of the actual vertical contact force measured from the detector, together with the FE theoretical curve, is shown in Fig. 4.15b. In the detecting (or linear) range (about 280 mm in this case), the shear strain differential is more or less constant and its value is approximately proportional to the contact force, as calibrated in [136]. The theoretical result is derived from the shear strain differential (Fig. 4.15c) calculated from the FE model in a steady-state vehicle-track interaction, in which the wheel and rail treads are assumed to be perfect and the vehicle is traveling on the track at a constant speed. The contact force calculated from the

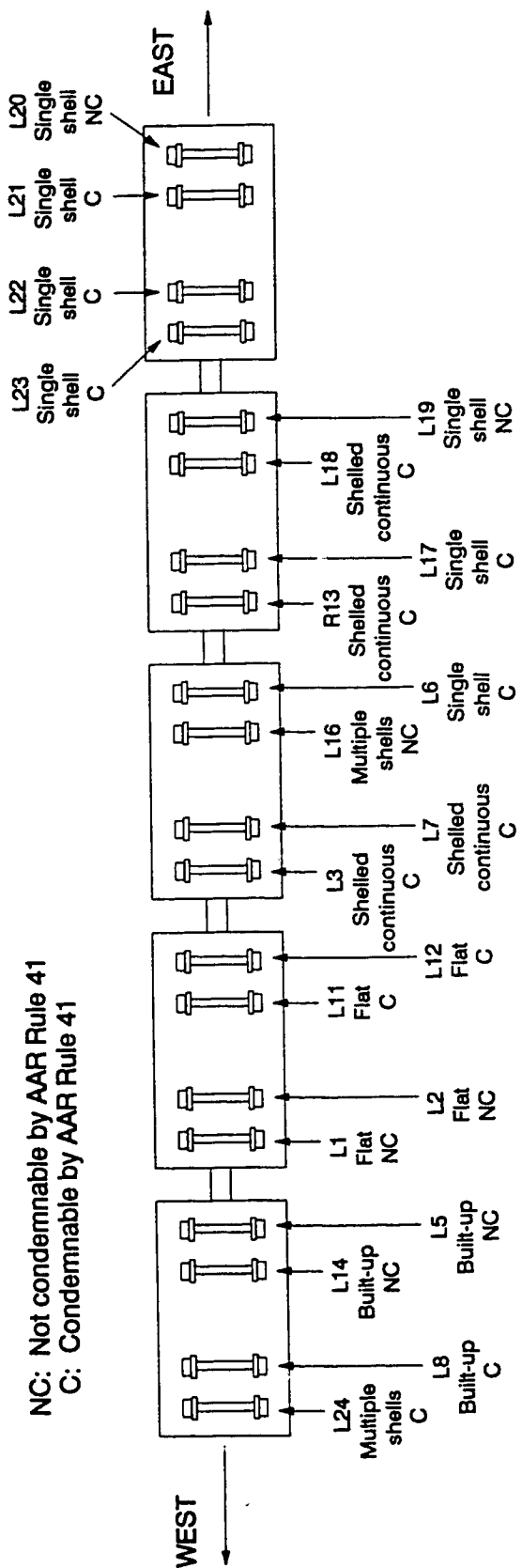


Figure 4.13 Location of defective wheels on the consist

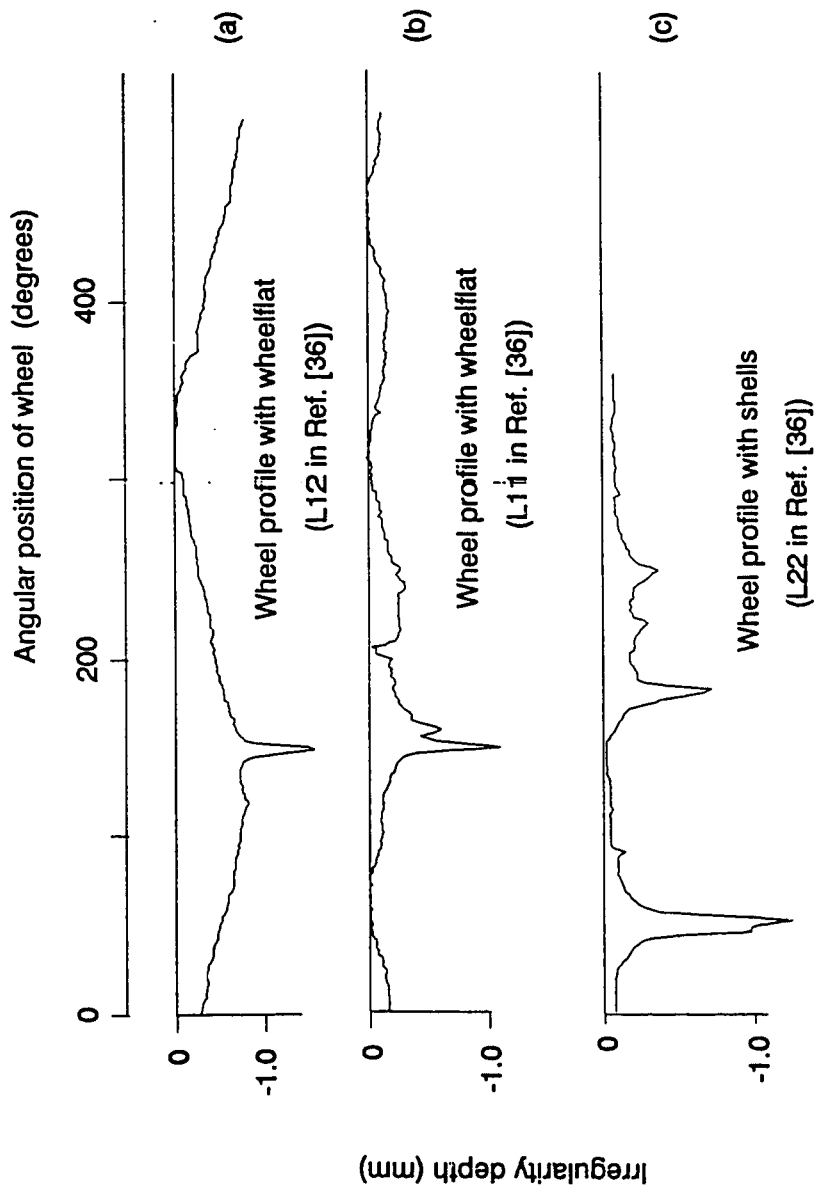


Figure 4.14 Changes in effective rolling radius of wheel with defects

TABLE 4.2
NOMINAL PARAMETER VALUES
FOR CP RAIL'S EXPERIMENTAL SYSTEM
ASED ON REF. [36])

<u>Track system</u>		C_p	Railpad damping, 30 kN•s/m
E_r	Young's modulus for rail steel, 2.07×10^{11} N/m ²	C_b	Ballast damping, 50 kN•s/m
G_r	Shear modulus for rail steel, 8.1×10^{10} N/m ²	<u>Vehicle system</u>	
T_r	Timoshenko shear coefficient for rail, 0.34	P_0	Static load per wheel, 146.8 kN (loaded car), 3.11 kN(empty car)
A_r	Cross-sectional area of rail, 8.61×10^{-3} m ²	M_b	Sideframe mass, 500 kg
I_r	Rail second moment of area, 3.95×10^{-5} m ⁴	M_w	Wheel mass, 650 kg
m_r	Rail mass per unit length, 67.57 kg/m	J_b	Sideframe pitch inertial, 176 kg m ²
L_{ct}	Total length of concrete tie, 2.591 m	M_b	Bolster and part of car body mass
E_{ct}	Young's modulus for concrete tie, 3.214×10^{10} N/m ²	K_1, K_2 :	Primary spring stiffness, 788 MN/m
G_{ct}	Shear modulus for concrete tie, $.340 \times 10^{10}$ N/m ²	C_1, C_2 :	Primary damping, 3.5 kN•s/m
T_{ct}	Timoshenko shear coefficient for concrete tie, 0.845	K_3	Secondary spring stiffness, 6.11 MN/m
ρ_{ct}	Mass density of concrete tie, 2458 kg/m ³	C_3	Secondary damping, 158 kN s/m
K_p	Pad stiffness, 200 MN/m	R_w	Wheel rolling radius, 0.4572 m (18 in)
K_b	Ballast spring stiffness, 4.0×10^7 N/m	L_a	Wheelset axle spacing, 1.78m
		C_h	Hertz spring constant, $.15 \times 10^{11}$ N/m ^{3/2}

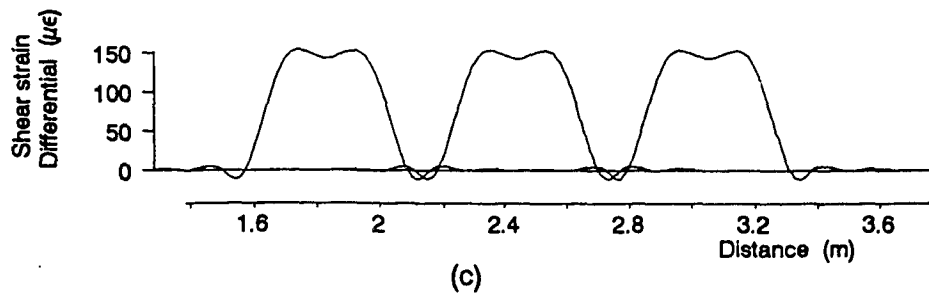
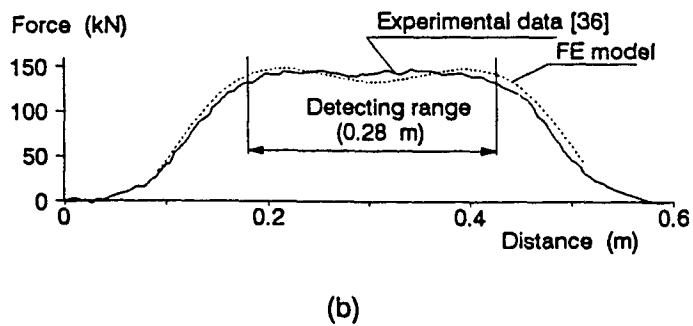
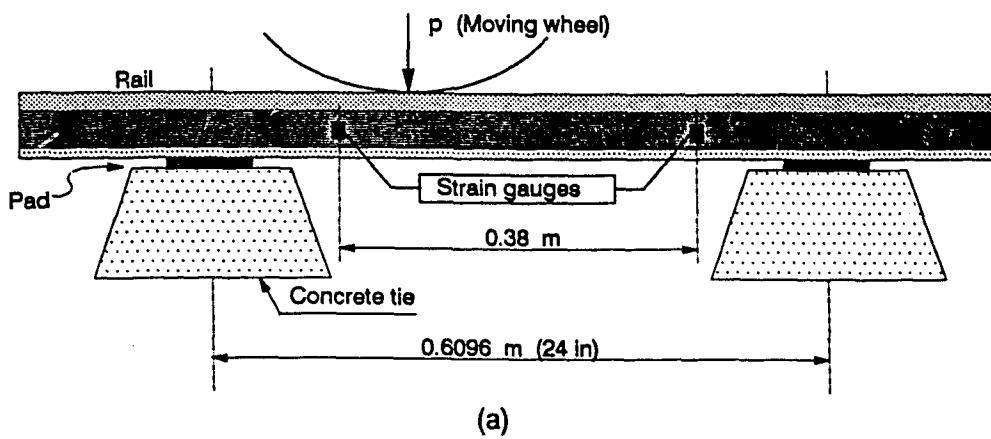


Figure 4.15 Simulation of a wheel impact detector

FE model is basically consistent with the measured trace except that the theoretical curve is slightly lower in the center part of the detecting range than those at the two shoulders. The error is less than 5% in this case if the average value of the differential is chosen to determine the theoretical calibration constant.

Wheel dropping response

Some wheel drop tests have been carried out on a wooden tie track by CP Rail System to correlate the force measured on an instrumented wheel plate and the force measured on instrumented rail [136]. The load detector installed on the rail is similar to Salient impact detector. In the tests, one wheelset in-situ was raised and dropped from various heights to impact the rail using a quick release jack. The impact force was measured simultaneously by detectors both on the wheelset and the rail. These drop tests are also simulated using the FE model. An example of the predicted drop impact response, together with the corresponding experimental trace, is shown in Fig. 4.16. As evident, the theoretical prediction has a good correlation with the experimental data. It is interesting to note that the dynamic force measured from the net shear strain differential is almost exactly the same as the contact force directly calculated using the FE model.

Comparisons of impact loads due to wheel tread defects

Extensive validation of impact load prediction by the FE model has been presented in the previous section. In this section the scope of validating the model where the vehicle is represented by a track with two wheelsets and a car body is utilized. As shown in Fig. 4.13, CP rail experimental train consisted of several cars where each axle had defective wheels.

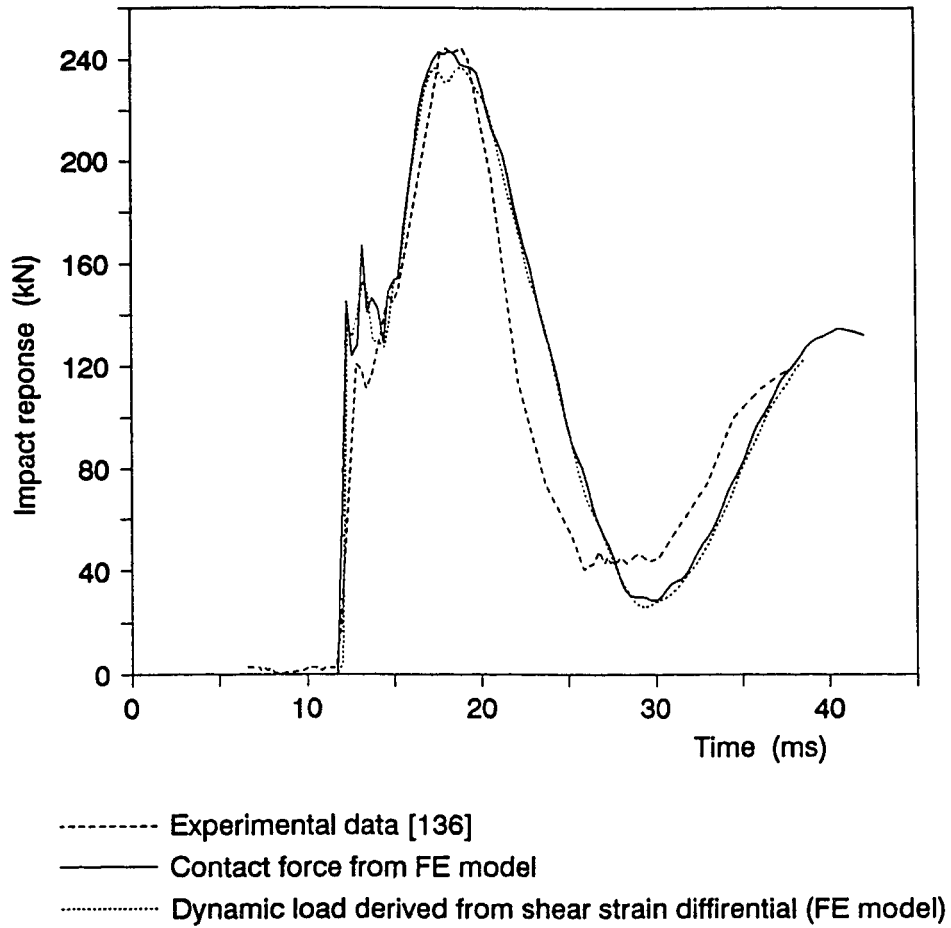


Figure 4.16 Wheel/rail contact force in a drop test

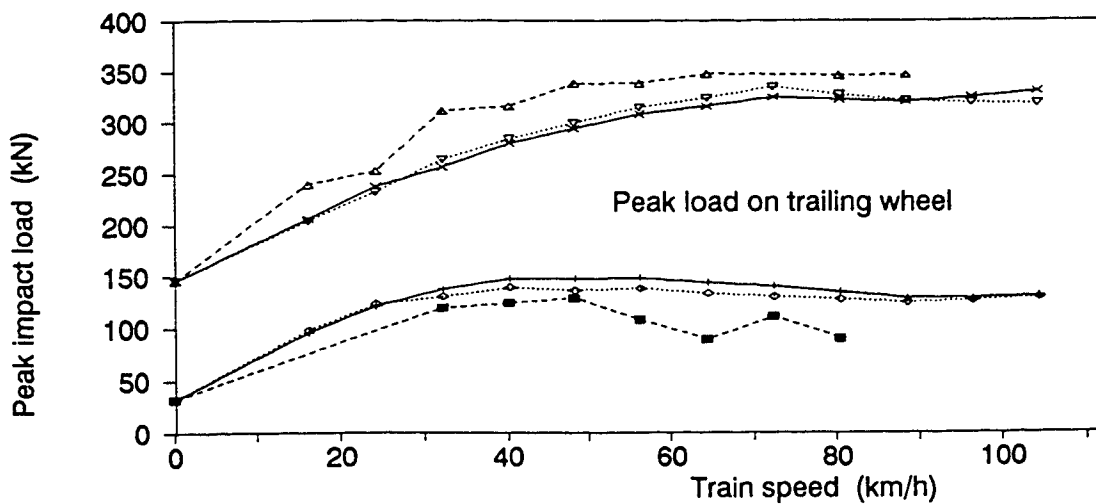
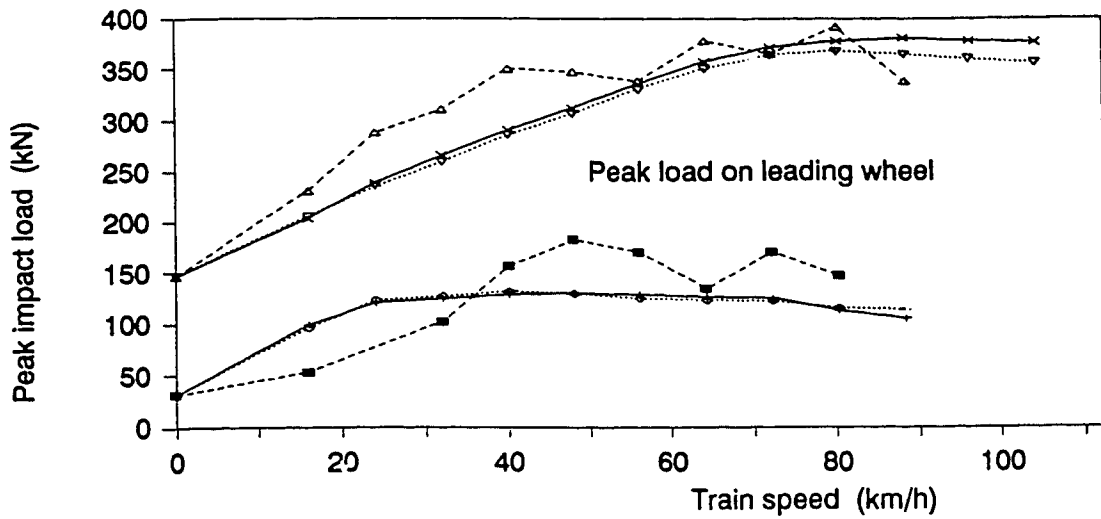
The FE model with 5-DOF vehicle representation is simulated using wheel tread profile L12 for the leading wheel and L11 profile for the trailing wheel. The characteristics of wheel profile L11 and L12 are shown in Fig. 4.14

The peak impact loads computed from shear strain differential and contact force directly from FE model as a function of speed is presented in Fig. 4.17 for empty as well as loaded cars. The experimental data for corresponding wheel defects within a track is superimposed on the results for comparison, as shown in Fig. 4.17. As the results show the correlation of the theoretical results with the experimental data is quite acceptable. The dynamic forces derived from the calculated shear strain differentials are also found consistent to the contact forces directly calculated in the FE model.

The predicted peak impact loads due to the wheel shell in Fig. 4.14c (L22 in [36]), together with the experimental data, are plotted in Fig. 4.18. Elastomeric shear pads were installed on the truck pedestals to simulate a radial truck in the tests and to investigate its effects on the impact loads [36]. This pad is modeled by reducing the primary spring stiffness (K_1 and K_2 on the vehicle model in Fig. 2.1c). The theoretical predictions show reasonably good agreement with the experimental data, and both results indicate that minimal isolation is provided by the shear-pads.

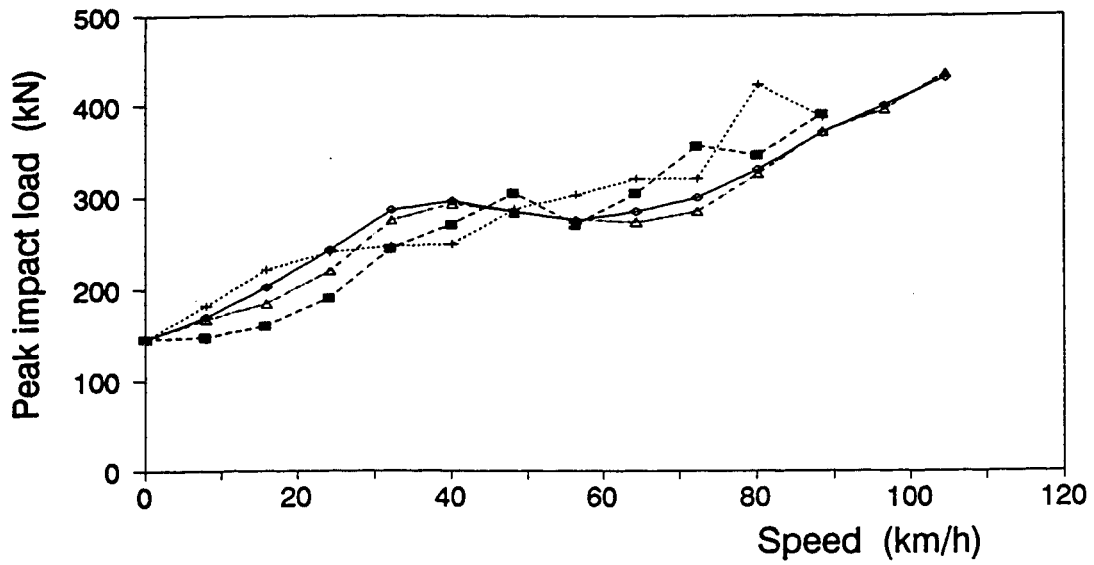
4.3.3 Verifications of the adaptive contact model

Frequency-domain techniques have been used by many researchers to study



- △---△--- Measured (loaded car) [36]
- Measured (empty car) [36]
- ×---×--- Directly calculated from FE model (loaded car)
- +---+--- Directly calculated from FE model (empty car)
- ▽---▽--- Derived from shear strain differential (loaded car)
- ◇---◇--- Derived from shear strain differential (empty car)

Figure 4.17 Impact loads due to wheel flats (L11 and L12 in [36])



- +---+--- Experimental data (without pads) [36]
- Experimental data (with pads) [36]
- ◇---◇--- FE model (K1=788 MN/m)
- △---△--- FE model (K1=200 MN/m)

Figure 4.18 Impact loads due to a wheel shell (L22 in [36])

the vehicle-track interactions, e.g. [62,75,130,149]. The major advantage of these techniques is that a solution can be obtained efficiently. However, all the calculations using these techniques tacitly assume that the whole system model is completely linear, as indicated in [107]. The contact stiffness also has to be linearized. A linear Hertzian contact spring, as expressed in Eq. 1.2, is often used in these calculations. If the variation of the overlap is small, this simplicity is reasonable. However, if the variation is large, especially if there is a loss of wheel/rail contact, the predicted contact force with the linear model may be quite different from a non-linear model, as shown in Fig. 4.19. The dynamic force shown in this figure is caused by a haversine wheel flat (Eq. 4.3) ($D_f = 1.5$ mm and $L_f = 100$ mm).

Fig. 4.20 shows the W/R contact force and the shear strain at SG2 (Fig.4.3) calculated with Hertzian contact model, Tunna's contact model [152] and the proposed adaptive contact model. A haversine wheel flat (Eq. 4.3) ($D_f = 2.15$, $L_f = 150$ mm) is also assumed in this case. It can be seen that the loss of contact occurs earlier and disappears later for Hertzian model than that calculated using Tunna's model or the proposed model. The first peak value of the contact force is also smaller for Hertzian model than those for other models. Similar behavior can be seen for time history of shear strain presented in Fig. 4.20. The time and position of impact predicted from Tunna's model and the proposed model are very similar to each other. The experimental results corresponding to the present simulation were shown in Fig. 4.8, which indicate peak strain to be approximately $640 \mu\epsilon$. As the results in Fig. 4.20 show, the proposed adaptive contact model is in best agreement. Tunna's model therefore overestimates the contact force, and hence the shear strain. This is because the contact stiffness is overestimated at the corner of the flat by Tunna's model.

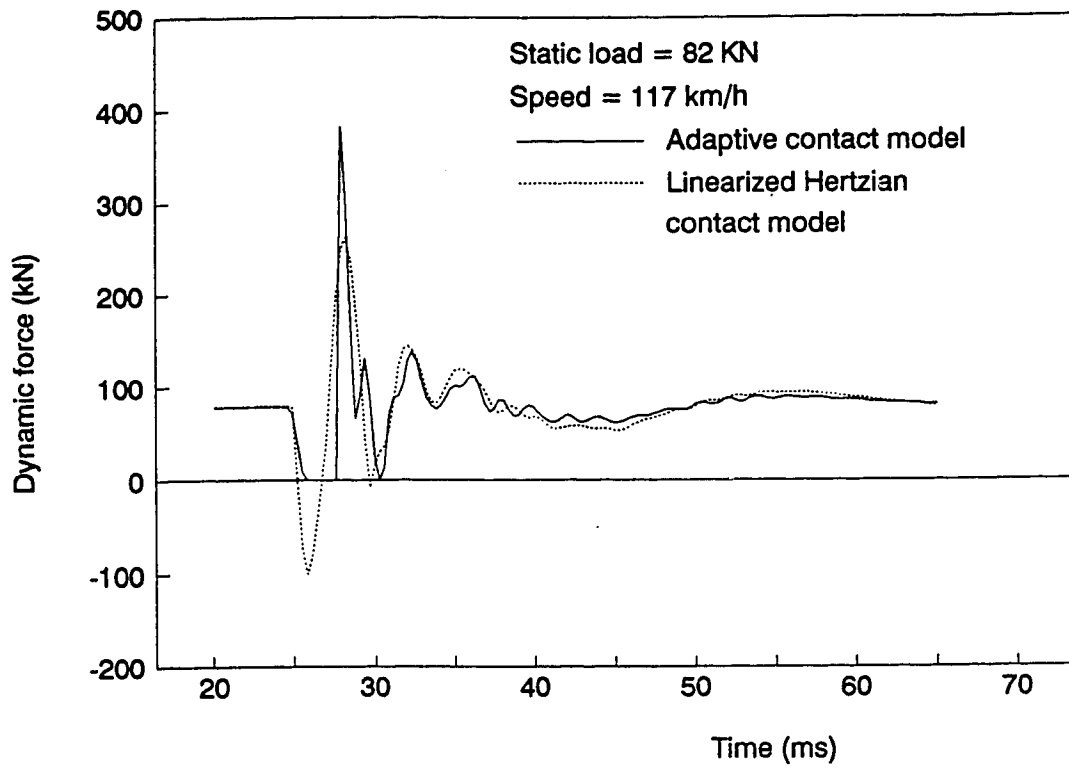


Figure 4.19 Wheel/rail contact force due to a haversine flat

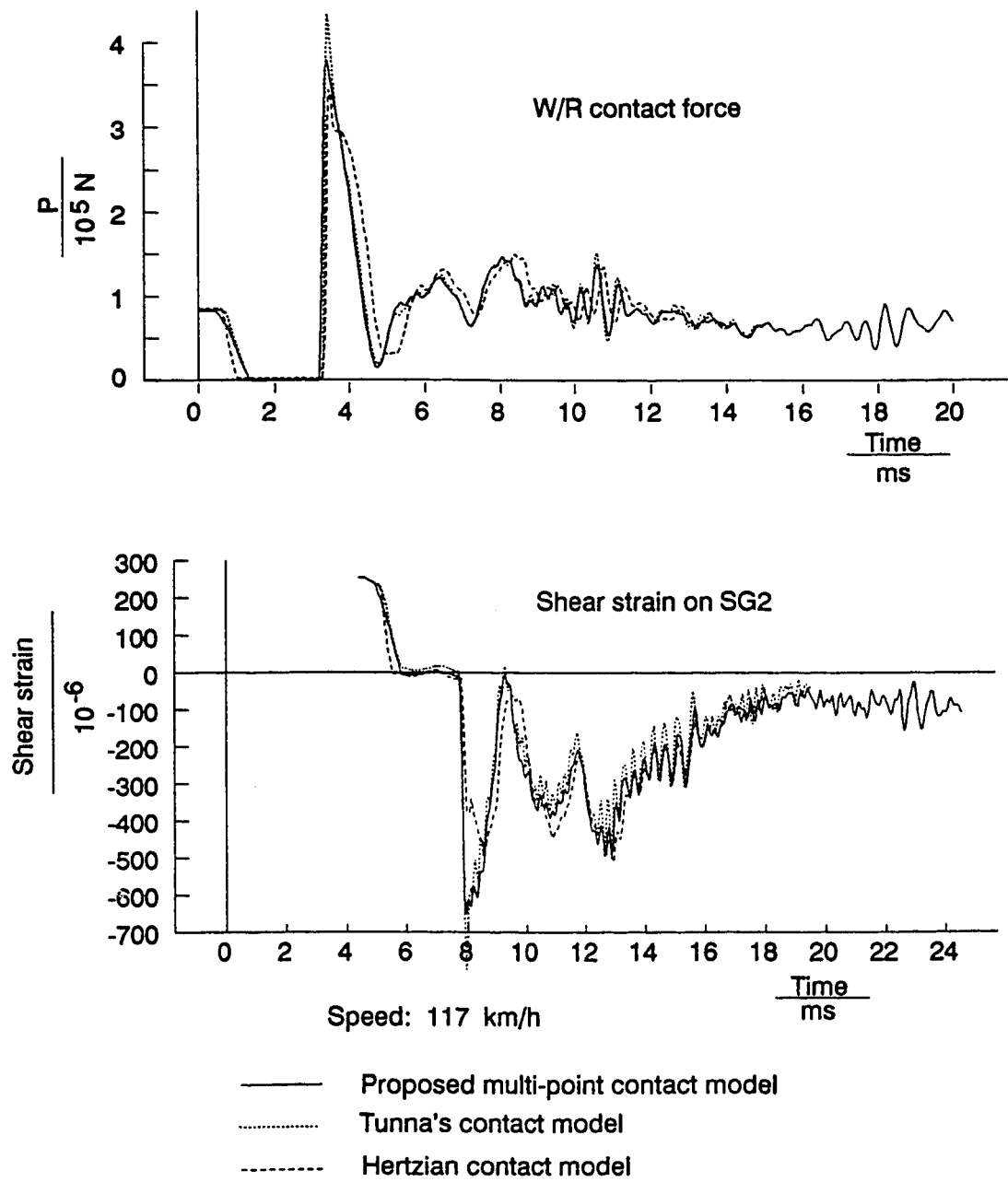


Fig. 4.20 Dynamic forces and strains calculated from different contact models

Some more comparisons of the dynamic forces calculated from Hertzian, Tunna's and the proposed contact models are shown in Figs. 4.21 and 4.22 for different wheel flat profiles. They show that the dynamic forces from the adaptive contact model at some locations are significantly lower than those from Hertzian and Tunna's models. These locations are usually corresponding to high frequency irregularities. This indicates that the single point contact models may overestimate the dynamic force in these situations. The adaptive contact model assumes a set of springs in effect in the contact patch so that it can adapt any irregularities in the contact region. It seems to be able to give a better representation of the actual contact situation. It can automatically deal with the two-point contact that may happen at a bolted rail joint. It may also be used to predict the distribution of the contact force in the contact patch.

4.4 DYNAMIC RESPONSE CHARACTERISTIC DUE TO WHEEL DEFECT

The validated FE model is subjected to irregularity function representing a wheel flat. The model parameters are same as those presented in Table 4.1 and the input irregularity is represented by Eq. 4.3. The input irregularity function along with system time history responses in term of: wheel/rail contact force; rail, wheel and tie displacements; pad and ballast forces; and rail acceleration are shown in Fig. 4.23. After the irregularity appears, the contact force does not drop quickly to zero but falls gradually. The wheel moves down and the rail rises up. The wheel loses contact with the rail for a while and then impacts the rail. The wheel does not hit the rail at the wheel vertical centerline but a little bit ahead of the centerline. This is shown by the vertical overlap (Δu^c) on the wheel vertical

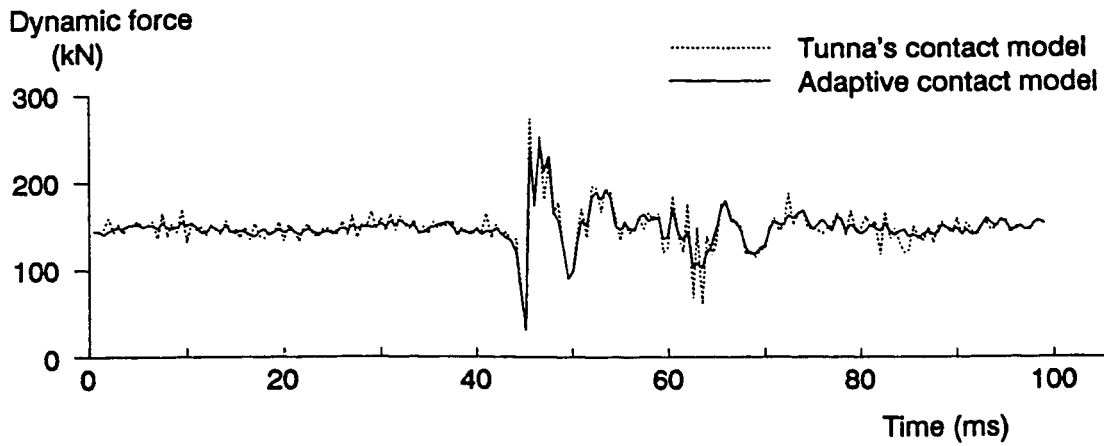


Figure 4.21 Dynamic forces calculated from different contact models due to a wheel tread defect (L11 in Ref. [36])

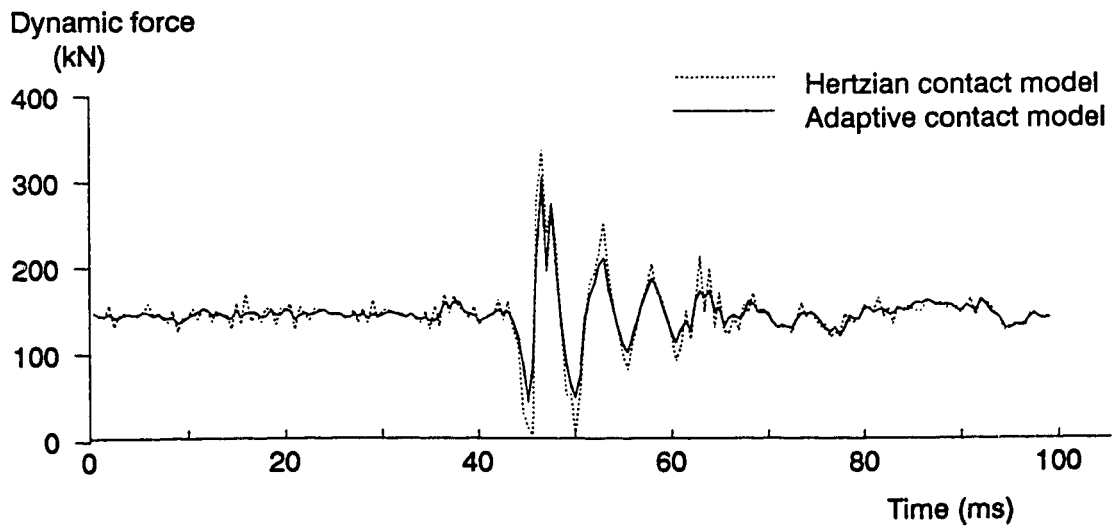


Figure 4.22 Dynamic forces calculated from different contact models due to a wheel tread defect (L12 in Ref. [36])

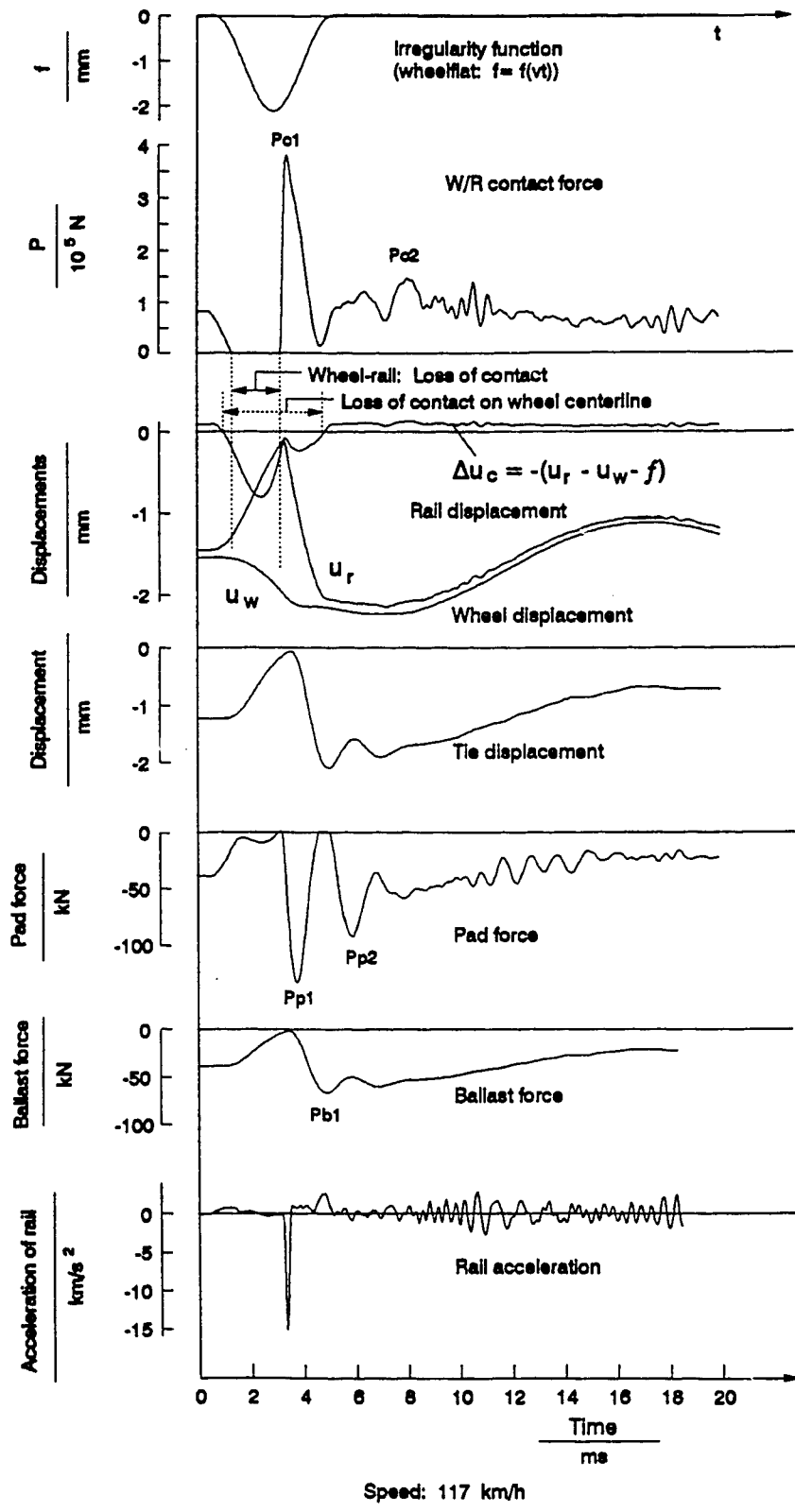


Figure 4.23 Response of forces and displacements

centerline in Fig. 4.23. The negative overlap indicates that the wheel is separated from rail on the wheel centerline.

The characteristic of rail acceleration is unique in comparison to other variables, as shown in Fig. 4.23. There is a very sharp and large peak in its time history, which happens at the moment when the wheel hits the rail after its free flight. Because the rail mass is very small compared with the wheel, the rail acceleration is the most sensitive variable in the impact response due to wheel or rail irregularities. This demonstrates the attraction of monitoring the rail acceleration to detect bad wheels; this principle is used in commercial wheel impact detection devices.

4.5 A PARAMETRIC STUDY ON IMPACT LOAD

The validated FE model of the vehicle track system considered here serves as a base line model for a detailed parametric study. The objective here is to examine the influence of important model parameters on the peak dynamic force and the maximum strain. As shown in Fig 4.14, there is no significant difference in the shape between wheel flat and shell. Hence the basic characteristic of these impact load should be similar, and it is not necessary to study them separately.

The results of the parametric study are discussed under the following sub-headings, where only one system parameter is varied at a time, while the others are kept constant and equal to their nominal values.

Two different cases have been considered in this parametric study. In the first

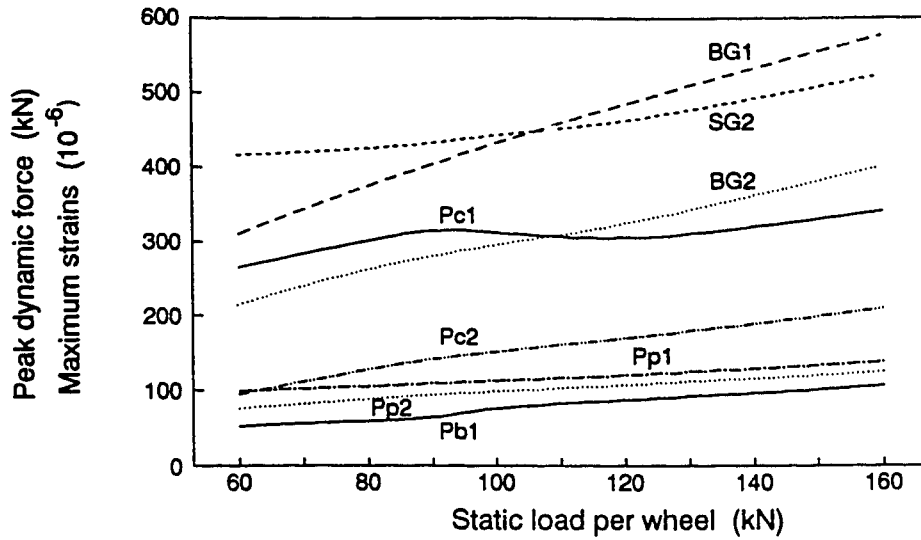
case, the vehicle is represented as a single wheel mass and the tie is modeled as a rigid body. The haversine wheel flat used by Newton and Clark [107] is utilized. The system parameters used are same as those listed in Table 4.1, which correspond to British Rail's test track and vehicle. The base vehicle speed is assumed to be 90 km/h in this case.

In the second case, the 5-DOF vehicle model is used and the tie is modeled as a non-uniform beam. If not specified, the irregularity function in Fig. 4.14a (L12 in [36]) is assumed for the leading wheel and the one in Fig. 4.14b (L11 in [36]) is for the trailing wheel. The basic system parameters are the same as those in Table 4.2, which corresponded to CP Rail's experimental track and vehicle. The vehicle speed used for this confirmation is 88.5 km/h (55 mph) if not specified.

As it will be presented below, the basic tendencies of the characteristics of impact loads due to wheel tread defects are the same in these two cases even though there are some differences between them in the system models, parameters and flat shapes.

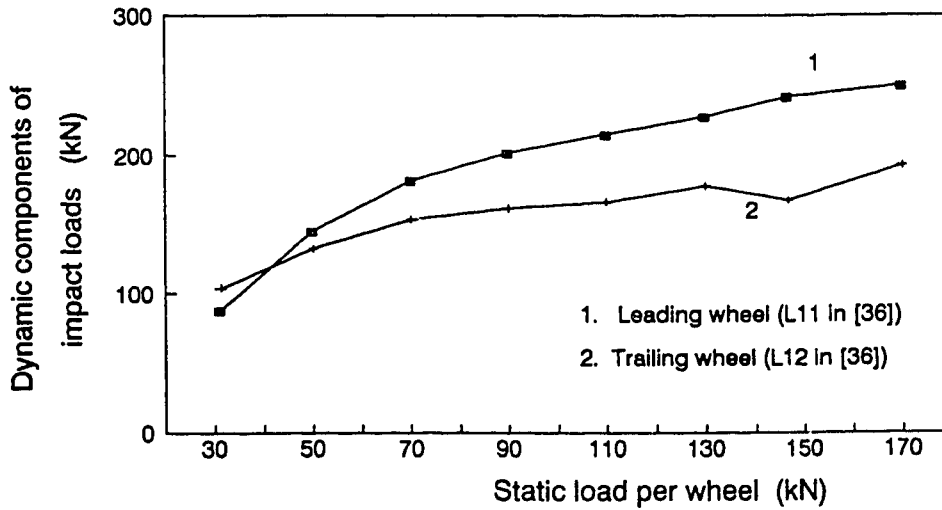
4.5.1 Effect of axle load

Fig. 4.24a shows the dynamic forces and strains for different axle loads due to a haversine wheel flat calculated for the BR parameters. Fig. 4.24b shows the dynamic components of impact loads at different axle loads for different wheel flats. Both figures indicate that increasing the axle load generally increases the impact load. This has also been observed in the experiments [36,107]. In most cases reported in [36], the dynamic component of contact force ($P_c - P_0$) on a loaded car is higher than those on an empty car.



BG1, BG2: Bending strains defined in Ref. [107] Pp1 : The first peak pad force
 SG2: Shear strain defined in Ref. [107] Pp2 : The second peak pad force
 Pc1 : The first peak W/R contact force Pb1 : The first peak ballast force
 Pc2 : The second peak W/R contact force

(a) From BR parameters



(b) From CPR parameters

Figure 4.24 Effect of static load on impact load

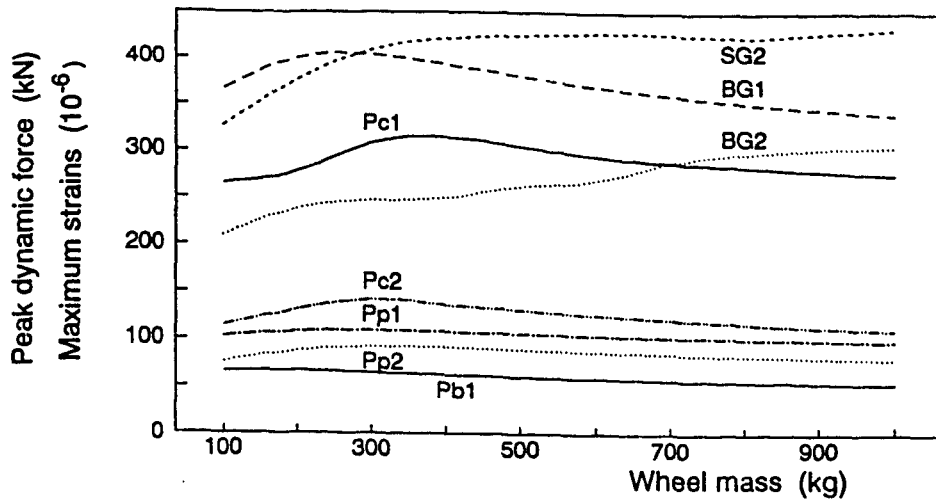
4.5.2 Effects of unsprung mass and vehicle primary stiffness

The impact force depends on both the mass and velocity of impacting objects. However, increasing wheel mass (unsprung mass) also reduces the instantaneous wheel vertical speed at the moment the wheel strikes the rail for a given load. For this reason, the impact load is not significantly changed by increasing wheel mass in the range analyzed in this study, as shown in Fig. 4.25.

Adding elastomeric shear pads on the wheelset bearing is equivalent to reducing the primary stiffness on the vehicle and therefore changing the equivalent unsprung mass. However, as indicated above, this has no significant effect on the impact load. This has been confirmed by both experimental data and theoretical predictions shown in Fig. 4.18. More experimental data about this can also be found in [36]. However, it is easy to understand that reducing the primary spring stiffness at the wheelset bearings can certainly reduce the dynamic forces on the bearings.

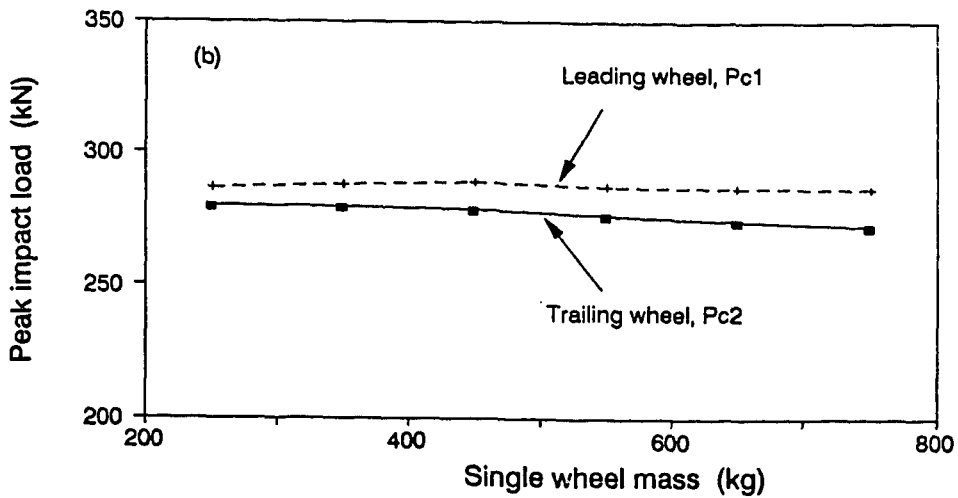
4.5.3 Effect of vehicle speed

In the case of haversine flat, both experimental and theoretical results show that there is a peak value in the dynamic force factor around 30 km/h (Fig. 4.26). This peak value is probably related to the coupled wheel-track natural frequency. The excitation frequency due to the wheel flat is 55.5 Hz, which is very close to the coupled wheel-track natural frequency. At low speeds, the wheel, rail and tie move together without separation during the impact process. However, for a higher operating speed (say larger than 60 km/h), the wheel/rail separation occurs and the peak force increases with speed. The peak impact force may probably reach a maximum value and then reduce since the wheel would fly over the flat at a very high speed. This speed is beyond the practical



BG1, BG2: Bending strains defined in Ref.[107] Pp1 : The first peak pad force
 SG2: Shear strain defined in Ref.[107] Pp2 : The second peak pad force
 Pc1 : The first peak W/R contact force Pb1 : The first peak ballast force
 Pc2 : The second peak W/R contact force

(a) Calculated with BR parameters



(b) Calculated with CPR parameters

Figure 4.25 Effect of unsprung mass on impact load

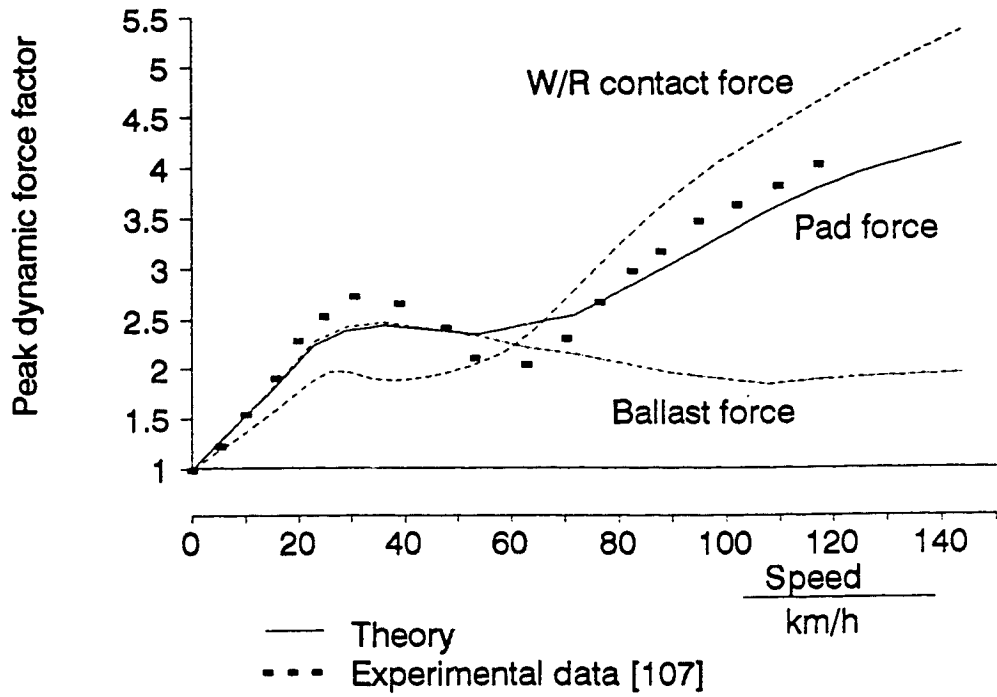


Figure 4.26 Effect of speed on dynamic force

operating speed for this particular wheel flat.

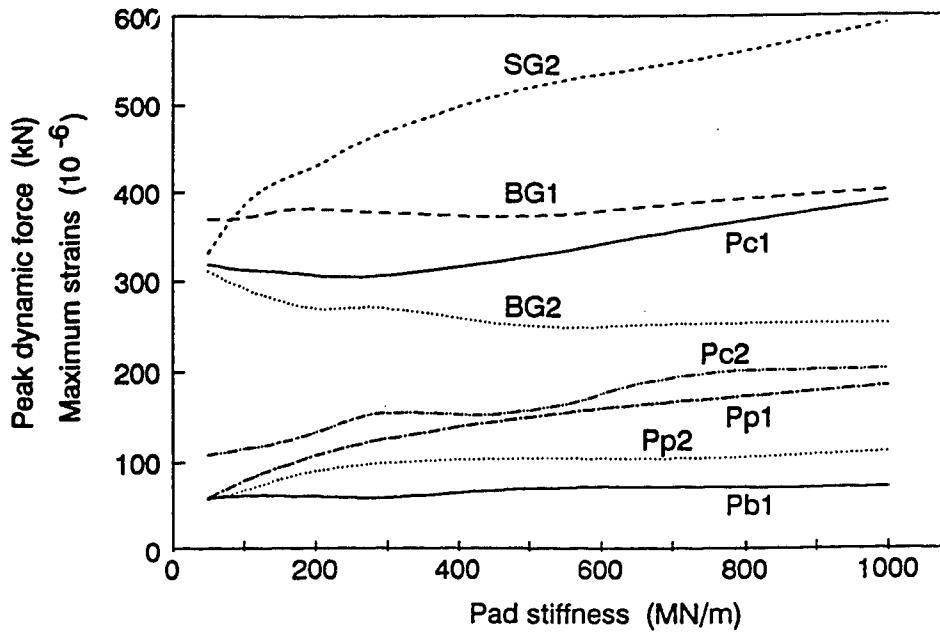
In the case of light axle load (empty car), the impact load increases with the vehicle speed before it reaches a certain point and then remains more or less constant for a large speed range, as shown in Fig. 4.17. This tendency is also shown in most cases presented in [36].

4.5.4 Effect of rail-pad stiffness

Increasing the rail-pad stiffness enhances the tie-rail connection and increases the track effective mass. This contributes in increasing the impact load, the shear strain in the rail and the force transmitted to the tie, as shown in Fig. 4.27. Fig. 4.28 shows the contact force in drop responses. It indicates that reducing the rail-pad stiffness can isolate some vibration motions of a concrete tie from the rail and it may benefit both the rail and the concrete tie. These observations show that reducing the rail-pad stiffness to a certain level (say 200~300 MN/m) is a practical and effective method to reduce the impact load and to protect the rails and concrete ties. This is basically consistent to the experimental results in [32] and [64].

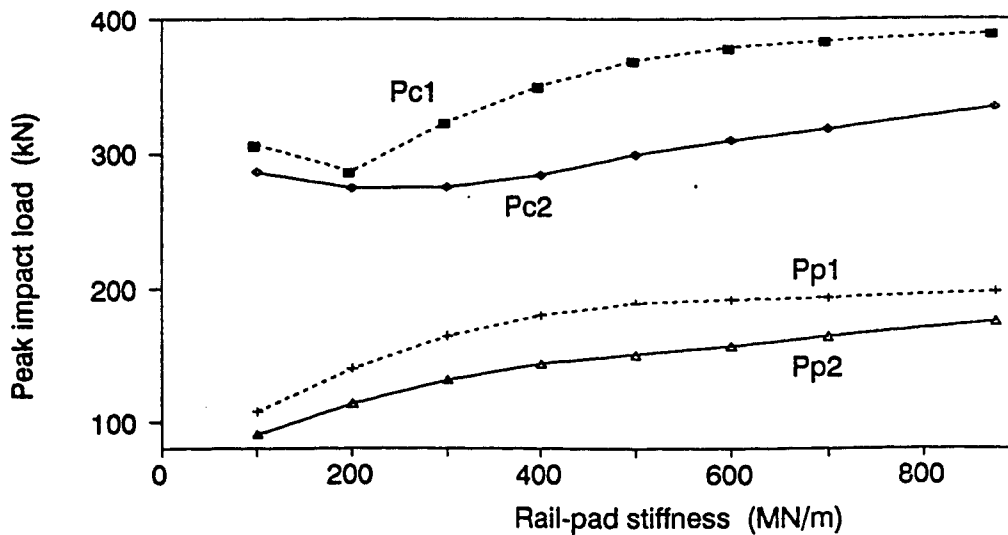
4.5.5 Effect of ballast stiffness

Increasing ballast stiffness increases the track stiffness and reduces the rail deflection. The rail bending strain is significantly reduced as the ballast stiffness increases, as shown in Fig. 4.29. However, the peak ballast force, the second peak contact force and the second peak pad force increase almost proportionally to the ballast stiffness as shown in Fig. 4.29a. Hence increasing ballast stiffness transfers more impact energy to the track substructure system.



BG1, BG2: Bending strains defined in Ref. [107]
 SG2: Shear strain defined in Ref. [107]
 Pc1 : The first peak W/R contact force
 Pc2 : The second peak W/R contact force
 Pp1 : The first peak pad force
 Pp2 : The second peak pad force
 Pb1 : The first peak ballast force
 Speed = 90 km/h (if not specified)

(a) Calculated with BR parameters



(b) Calculated with CPR parameters

Figure 4.27 Effect of rail-pad stiffness on impact force

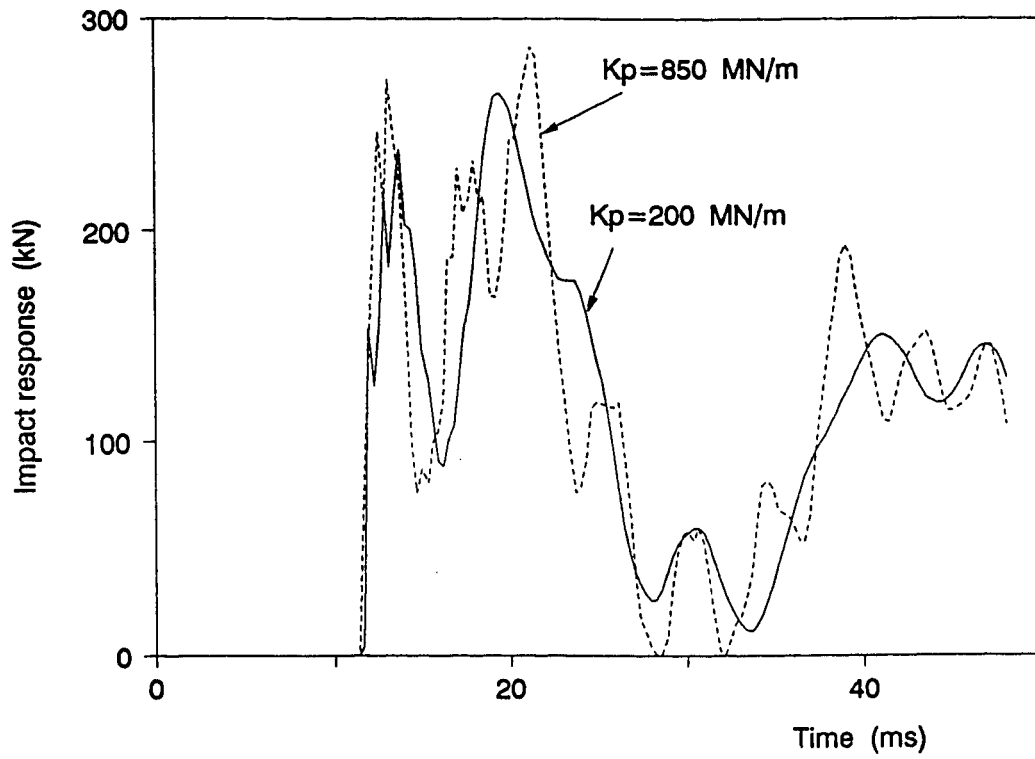
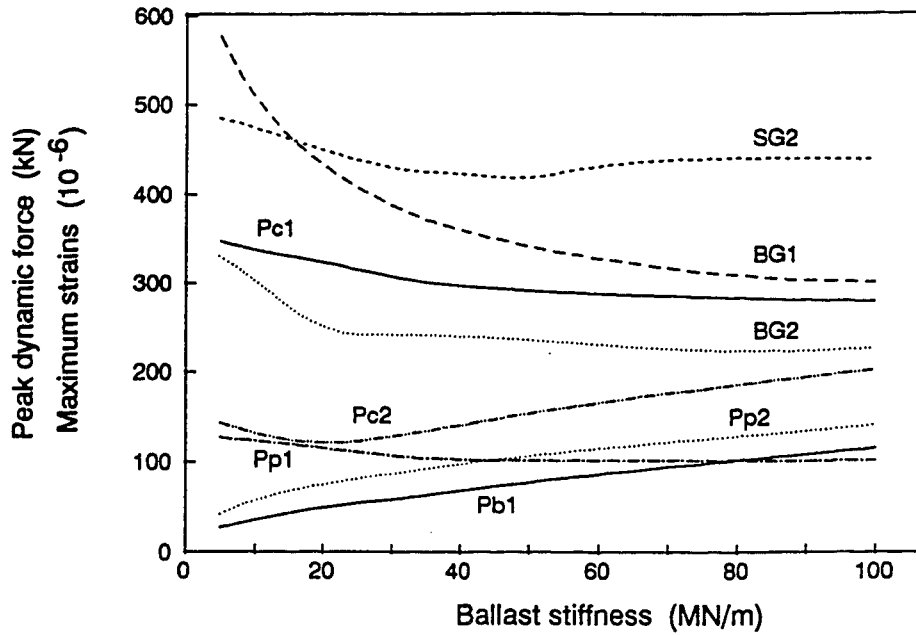
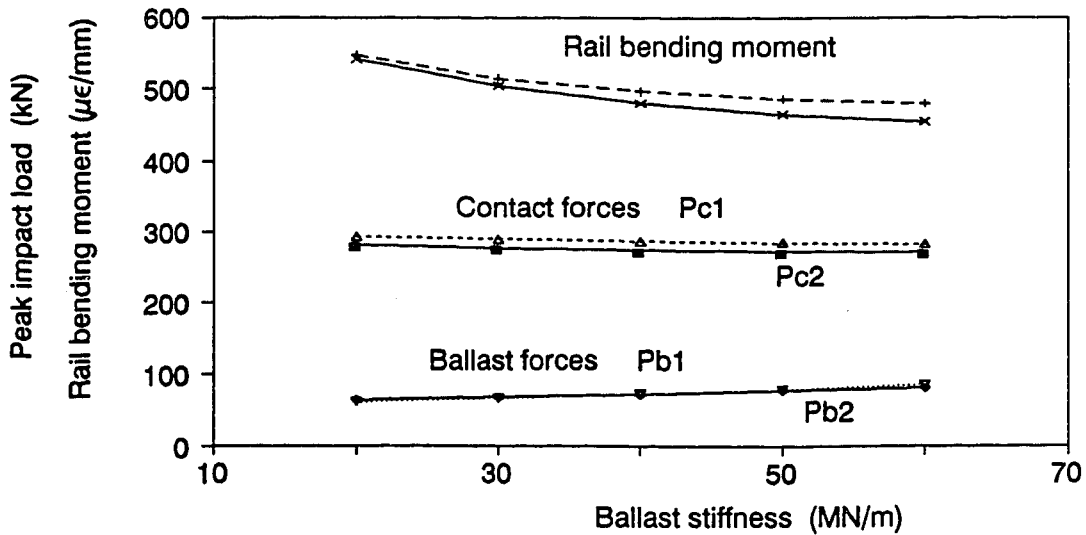


Figure 4.28 Dropping response on a concrete-tie track
(Calculated with CPR parameters)



BG1, BG2: Bending strains defined in Ref. [107] Pp1 : The first peak pad force
 SG2: Shear strain defined in Ref. [107] Pp2 : The second peak pad force
 Pc1 : The first peak W/R contact force Pb1 : The first peak ballast force
 Pc2 : The second peak W/R contact force

(a) Calculated with BR parameters



(b) Calculated with CPR parameters

Figure 4.29 Effect of ballast stiffness on impact force

4.5.6 Equivalent tie mass

Fig. 4.30 shows the effect of equivalent tie mass on the impact forces and strains. Increasing the tie mass increases marginally the pad force. It does not have much effect on the first peak (P_{c1}) of the contact force but it has large effect on the second peak (P_{c2}). Increasing the tie mass increases the discrete mass in the track system. This causes a significant increase in rail shear strain (see SG2 in the figure).

4.5.7 Effect of rail type

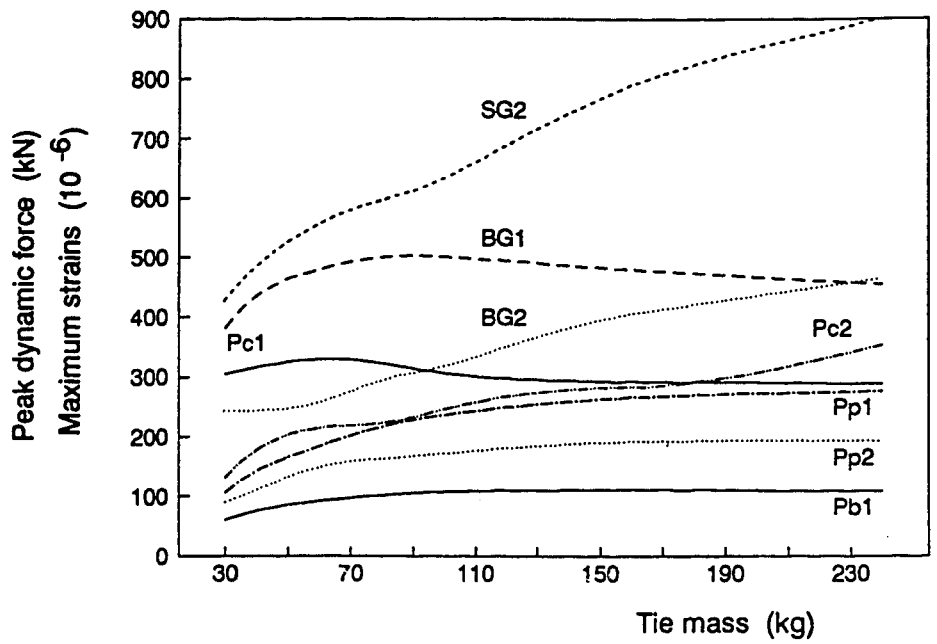
Increasing rail weight per unit length increases the rail effective mass and rail stiffness. This gives only marginal difference of the impact load among the rail types commonly used at present time, as shown in Fig. 4.31.

4.5.8 Impact position

To investigate the effect of impact position on the impact load, only one wheel is assumed to have the flat as in Fig. 4.14a (L12 in [36]) and the other wheel to be perfect. A total length of 60 tie spacings is continuously traveled by the vehicle in the calculation and every peak load vs. its location relative to the tie center is plotted in Fig. 4.32. It shows a clear distribution pattern and indicates that the impact load over the tie is about 10% larger than that at the midspan between two ties. This is because the rail effective mass and stiffness over the tie are larger than those at the midspan. There is no significant difference if the rail-pad is modeled as a single spring-damper discrete or layered element, as also shown in this figure.

4.5.9 Effect of flat size

By varying the size of the haversine flat (L_f and D_f in Eq. 4.3), different impact



BG1,BG2: Bending strains defined in Ref.[107] Pp1 : The first peak pad force
 SG2: Shear strain defined in Ref.[107] Pp2 : The second peak pad force
 Pc1 : The first peak W/R contact force Pb1 : The first peak ballast force
 Pc2 : The second peak W/R contact force

Figure 4.30 Effect of equivalent tie mass on impact load
 (Calculated with BR parameters)

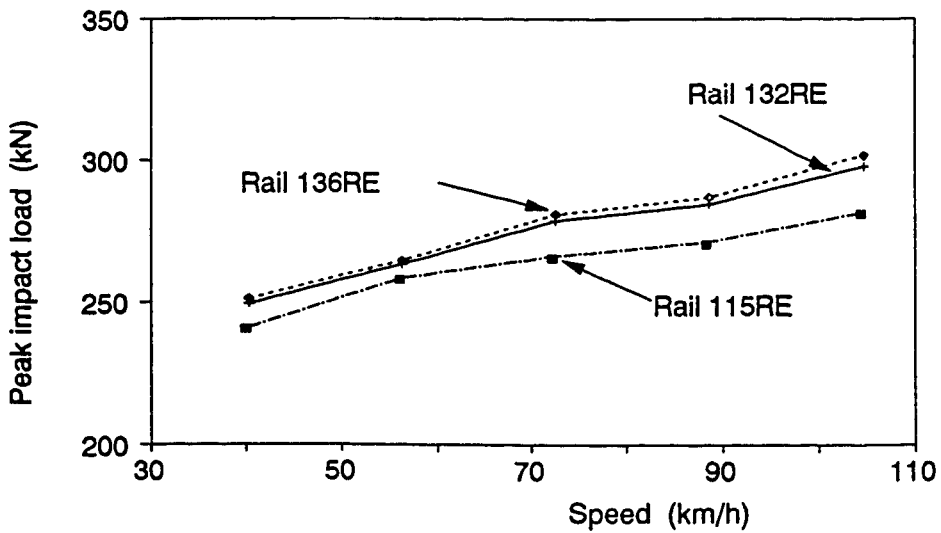
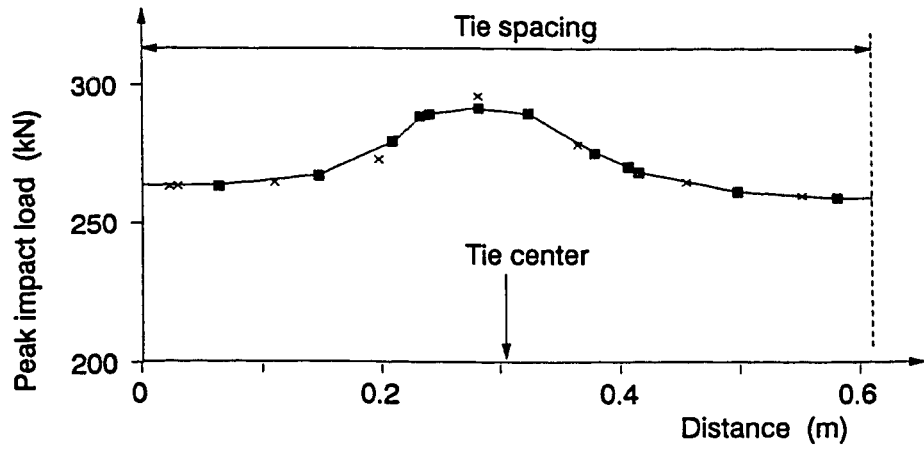


Figure 4.31 Effect of rail type on impact load
 (Calculated with CPR parameters)



- × Rail-pad modeled as a single spring-damper discrete element
- Rail-pad modeled as a spring-damper layered element

Figure 4.32 Effect of impact position on impact load (CPR parameters)

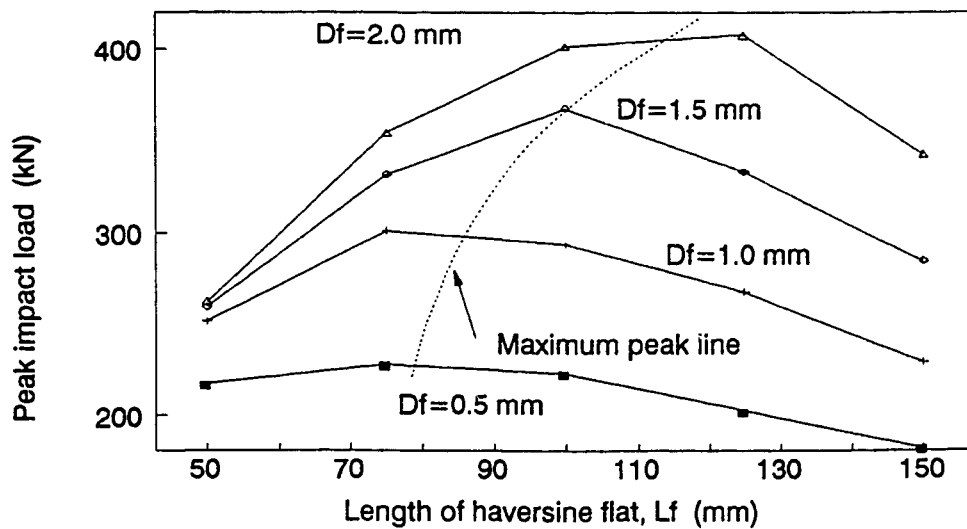


Figure 4.33 Effect of flat size on impact load (CPR parameters)

loads are predicted and plotted in Fig. 4.33. This figure indicates that for a given depth of flat, there is a critical flat length at which the impact load reaches its maximum value for a given speed. The deeper the flat is, the longer the critical flat length is. There is a maximum peak line that goes through particular combinations of flat length and depth for a given system and vehicle speed, as shown in Fig 4.33.

4.5.10 Effect of lift-offs of rail from tie and tie from ballast

The effect of lift-off of the rail from the tie and tie from the ballast on the wheel/rail contact force is also plotted in Fig. 4.34. It shows that the influence of lift-off on the first peak of the impact load is very little. Hence, it is not necessary to take this nonlinear factor into account if only the maximum impact load is of concern. However, changes in the time history after the first striking are significantly different, as shown in the figure. In the case of linear system (without lift-off), more vibration energy on the ties is transferred to the rail and a larger oscillation in the response is caused. This results in a higher second peak.

4.5.11 Effect of longitudinal force

The effect of longitudinal force is to increase (if in tension) or reduce (if in compression) the rail stiffness. However, its equivalent stiffness is not compatible with the rail stiffness until the longitudinal force is larger than 10^8 N in the case studied (Fig. 4.35). The rail temperature corresponding to this force is not practical. Therefore, the effect of longitudinal force on the impact load is usually very small and it can be ignored. However, the strains due to the variation in temperature plus the strains caused by the impact load may reach a very high level and result in damage to the rail in cold weather.

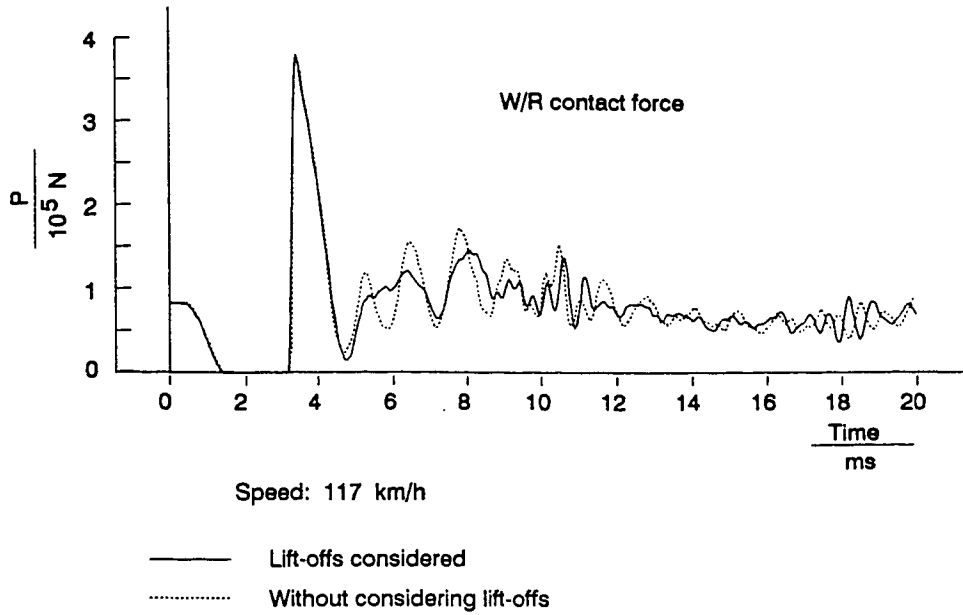


Figure 4.34 Effect of lift-offs on impact load

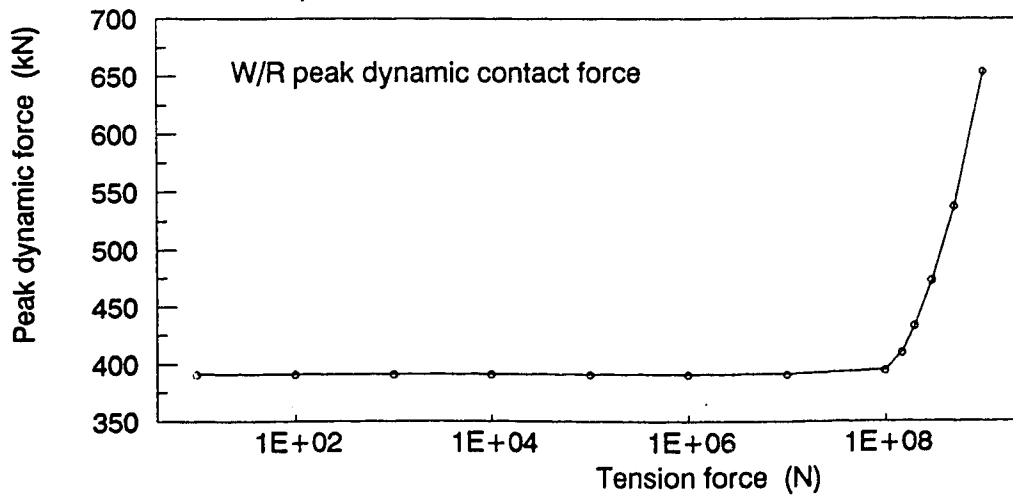


Figure 4.35 Effect of longitudinal force on impact load (BR parameters)

4.6 DYNAMIC INTERACTION BETWEEN TWO WHEELS DUE TO WHEEL TREAD DEFECTS

The wheel/rail dynamic contact force generated at one wheel may partially be transmitted to a neighboring wheel and cause the interaction between two wheels. The force at the neighboring wheel due to this interaction will be called "across-wheel force" in this study. To understand the mechanism of the interaction between two wheels, it is important to understand how the forces are transmitted. Some researchers believed that the across-wheel force is caused by the pitch motions of sideframes [18]. This may be partially true if the sideframe and wheelset are connected with a bearing assembly that has a very large stiffness, such as that on a three-piece truck.

However, this study shows that most part of the high frequency interaction forces are transmitted by the rail in a general case. To demonstrate this, Fig. 4.36 shows the time histories of the wheel/rail contact forces calculated with two different values of the primary stiffness (K_1) in the 5-DOF vehicle model. In this case, a haversine wheelflat (Eq. 4.3) ($D_f = 1$ mm and $L_f = 100$ mm) is assumed to be on the leading wheel tread. When K_1 is 1.5 MN/m, the high frequency dynamic forces are actually isolated by the suspension and it is unlikely for the wheel-bogie-wheel or wheel-sideframe-wheel chain to transmit the high frequency forces from one wheel to another wheel. Even though the stiffness values have a difference of two power orders, there is no significant difference between the contact forces. This indicates that the impact force is mainly transmitted through the track system, particularly through the rail because it has a relatively small equivalent mass and large stiffness. The wheels and bogie or sideframes are usually massive and they may serve as energy reservoirs like a

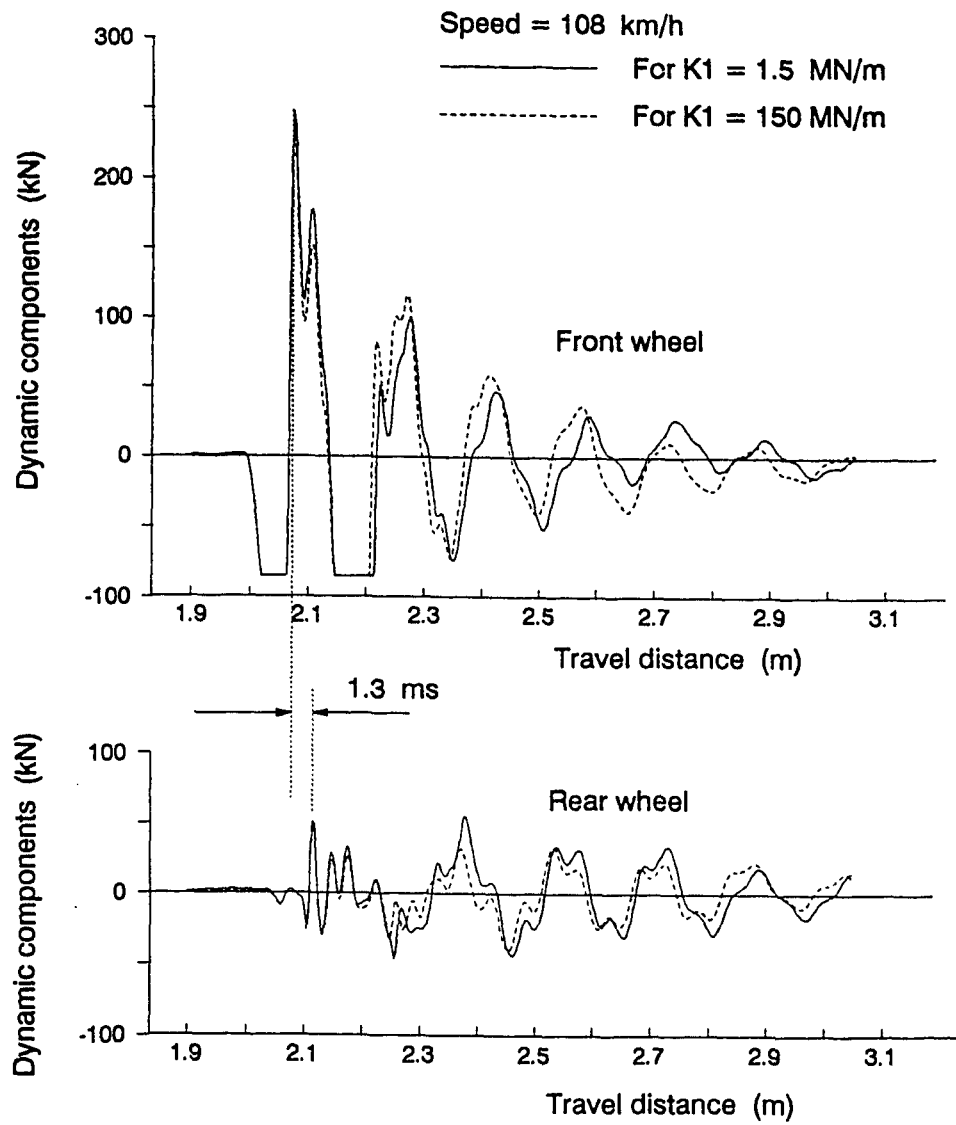


Figure 4.36 Across-wheel force due to a wheel flat

flywheel. They may only influence low frequency dynamic forces, which is not the case analyzed in this study. The results in Fig. 4.36 further indicate that the primary stiffness has little effect on the impact loads, which has been mentioned above and observed in the experimental data [36].

The phase (time) lag of the across-wheel force on the trailing wheel caused by the impact force on the leading wheel (Fig. 4.36) also indicates that the interaction force is mainly transmitted by the rail. The first peak of the cross-wheel force is delayed about 1.3 ms after the first peak of the leading wheel force occurs. The wheelset axle spacing used in the calculation is 2.4 m and thus the transmission speed is about 1850 m/s, only the wave propagation in the rail can reach such a speed in this case. Hence, it is the wave propagation in the rail that transmits the impact load mostly.

The basic mechanism that controls the interaction between any two wheels is the principle of superposition. To demonstrate this, the same wheelflat as used in the last section is first assumed to be on the leading wheel and then on the trailing wheel, respectively, and the contact forces are calculated separately. Then the forces are superposed for each wheel to obtain the dynamic forces that should be for the case of both wheels having the wheelflats. These forces are compared with the forces directly calculated for both wheels having the same wheelflats. As shown in Fig. 4.35, there is no significant difference between the forces calculated from both approaches, even though the non-linear contact model is used in the calculations.

Because of the superposition, the maximum dynamic force may be affected by the relative position of the wheelflats on the two wheels. Hence, if wheelflats

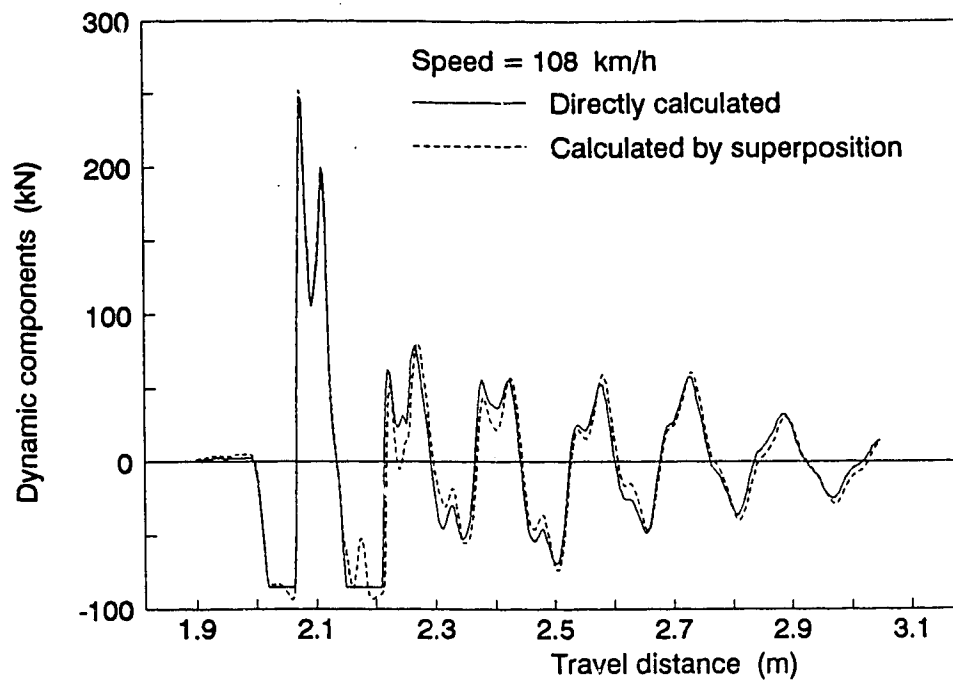


Figure 4.37 Dynamic force superposition

occur on neighboring wheels, the dynamic forces on them may be significantly different from a single flatted wheel. This should be taken into account in the experiments and data analysis.

4.7 SUMMARY

The FE model of vehicle-track system is employed to duplicate the experiments carried out by British Rail and CP Rail System. The theoretical results such as the wheel/rail contact forces, rail-pad forces and strains in the rail showed very good correlation to the experimental data. Extensive results are compared with experimental data in the time domain for through validation of the developed model.

A wheel impact detector that utilizes the net shear strain differential on rail to measure the dynamic force is also simulated on the FE model. The FE modeling shows that the dynamic force derived from the net shear strain differential is basically consistent with the wheel/rail contact force. This suggests that the basic principle used in the detector is sound.

The characteristics of the impact loads due to wheel flats and shells are investigated based on the validated FE model. This study shows that the impact loads are mainly affected by the shape and size of flat or shell, axle load, vehicle speed and rail-pad stiffness. The impact load of a wheel on the rail over a tie is larger than that at the midspan. Adding elastomeric shear pads on the wheelset bearing does not reduce the wheel/rail dynamic contact force but it may reduce the dynamic force on the bearing. Reducing rail-pad stiffness to a certain level

on a concrete-tie track may significantly reduce the dynamic load and the force transmitted to the concrete tie.

CHAPTER 5
THE DYNAMIC EFFECTS OF
CONVENTIONAL FREIGHT CAR RUNNING OVER A DIPPED-JOINT

5.1 INTRODUCTION

The FE model of vehicle-track system validated in the last chapter is applied in this section to evaluate dynamic responses over prescribed rail joints.

Even though the welded rail joints have been widely used on the railway track, there are still a large number of bolted rail joints in the field. The bolted rail joint could be a weak point of the track and large dynamic loads could be generated on the joints with increasing vehicle speed and axle load. The dynamic force could produce large stresses in track, fatigue cracks in rail and tie, geometric deformation of ballast, and damage the components of trucks, such as wheelset bearings. The track deterioration occurs giving rise to a progressive increase in forces. All those increase maintenance costs of track and bogie truck. It is therefore considered a useful application of the developed model to obtain better understanding of the nature and magnitude of the dynamic loads.

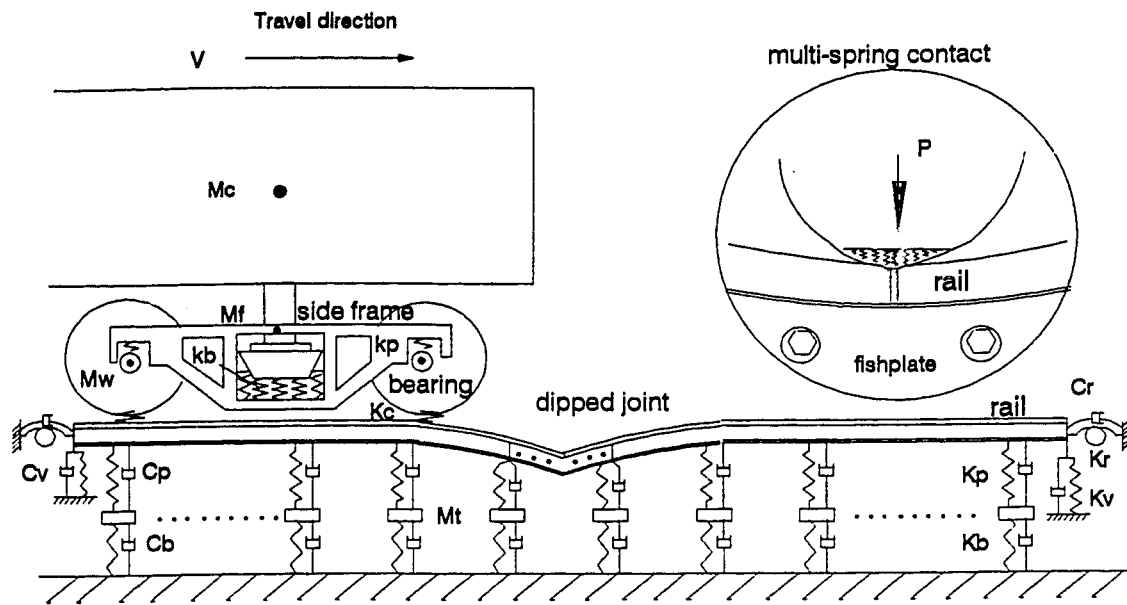
Several track models have been employed to study the dynamic loads due to wheel flats and rail joints. They can basically be classified as lumped parameter models [10,80,128], beam on distributed supports [56,98,127] and beam on discrete supports [18,25,108]. The validated FE model of vehicle-track system developed in this study is employed in this investigation. This model is extended to the bolted rail joint problem by including the fishplate and rail gap. By using this model, the effects of change in parameters of the vehicle-track system on

dynamic contact force are investigated. The effects of rubber bearing pad in freight cars with three piece truck on the bearing impact force are also studied.

5.2 VEHICLE-TRACK SYSTEM MODEL

Similar to the procedures used in Ref. [107], the vehicle and track are divided into two systems at the wheel/rail interface and modeled separately. The two systems are coupled by a Hertzian contact spring or an adaptive contact model presented in Chapter 2. The most sensitive component of the vehicle is the wheelset. To consider the dynamic force on the bearing, the sideframe has to be taken into account. For these reasons, the vehicle is represented by a half car model with five DOF, as shown in Fig. 5.1.

The track is represented by a Timoshenko beam on equally spaced pad-tie-ballast supports, as shown in Fig. 5.1. The most sensitive component in the track is the rail because of its proximity to the exciting sources and has small equivalent mass. The strains in the rail are usually important for the analysis and designs. Consequently, an accurate Timoshenko beam element is used to represent the rail. It is a two-node element with four degrees of freedom at each node. The details of the formulation have been presented in Chapter 2. The separated rails at a joint are physically connected by two pieces of fishplates. In this model, the fishplates are also modeled as Timoshenko beams and their mass and stiffness matrices are combined with the rail matrices. The rail gap is considered in the rail irregularity function. The length of track in the model is considered to be 39 tie spacing. The pad and ballast are considered to be massless spring-dashpot elements. The tie is considered to be a lumped mass.



K_p and C_p : stiffness and damping of pad of tie; K_b and C_b : stiffness and damping of ballast
 K_r, K_v, C_r and C_v : bending, vertical stiffness and damping of track at the end
 k_p : stiffness of pad or contact stiffness of side-frame/bearing
 k_b : stiffness of bolster on half truck
 K_c : contact stiffness of wheel/rail; M_w, M_f, M_c : mass of wheel, side-frame and one-fourth body

Fig. 5.1 Vehicle/track model at dipped rail joint

This model is referred to as FE model or Timoshenko beam on discrete supports (TBDS) model in this study.

By properly assembling the track elements, the dynamic equations may be expressed as

$$[M]\{\ddot{\eta}\} + [C]\{\dot{\eta}\} + [K]\{\eta\} = \{F\} \quad (5.1)$$

where $[M]$ is mass matrix, $[C]$ is damping matrix, $[K]$ is stiffness matrix and $\{F\}$ is force vector. Hertzian contact spring is usually used to represent the relationship between the wheel and the rail. Tunna [152] indicated that the centerline contact assumption may not be true in some cases and has proposed an approach to find the maximum overlap and to calculate the contact force. The maximum overlap used in his calculation may overestimate the dynamic force in some cases. In order to overcome this drawback and to simulate the multi-point contact on a rail joint, a multi-spring contact model presented in Chapter 2 (also shown in Fig. 5.1) is employed in this study.

5.3 DYNAMIC RESPONSE

Results are obtained as dynamic wheel/rail and bearing forces for a vehicle running over a dipped joint. A single wheel response is evaluated for different track models. A two wheel model is also considered to examine the impact forces at each wheel and bearings.

A simple set of formulae have been proposed by Jenkins et al. [80] to calculate the so-called peak forces, P_1 and P_2 due to a single wheel over a dipped rail joint, which are expressed as:

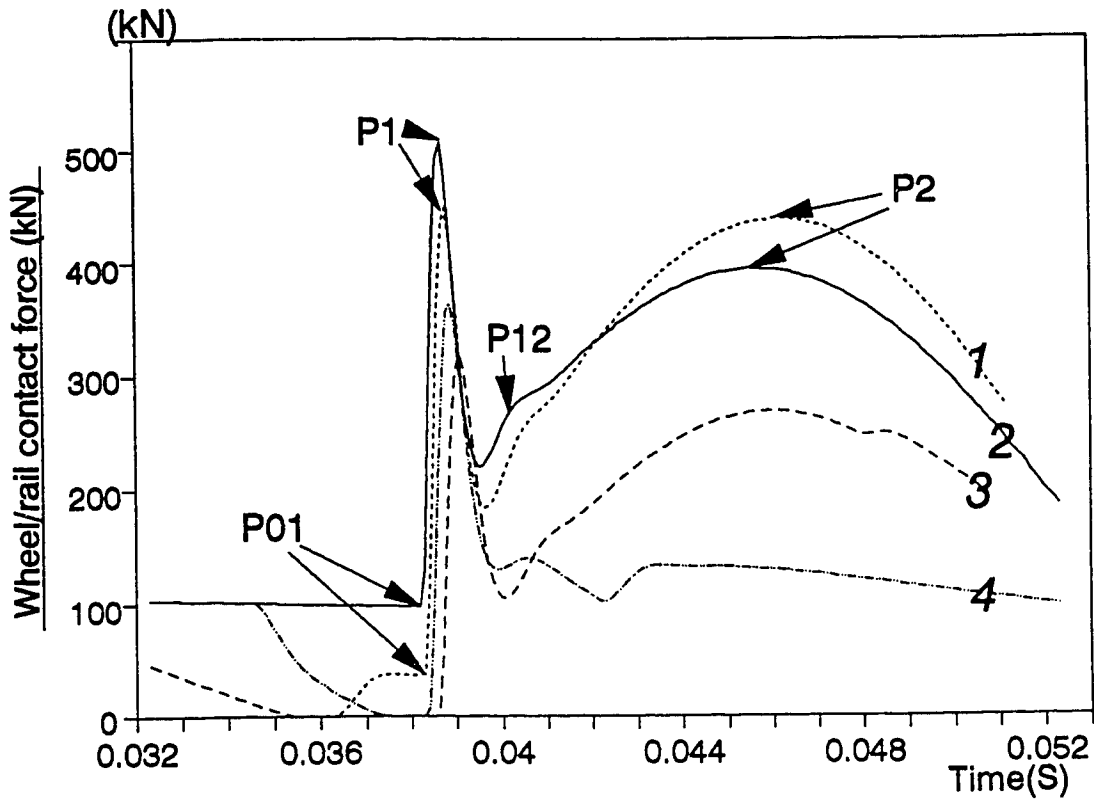
$$\begin{aligned} P_1 &= P_0 + 2\alpha V \sqrt{K_H m_e / (1 + m_e / m_u)} \\ P_2 &= P_0 + 2\alpha V \left(\frac{m_u}{m_u + m_t} \right)^{1/2} \left(1 - \frac{c_t \pi}{4k_t (m_u + m_t)} \right) \sqrt{k_t m_u} \end{aligned} \quad (5.2)$$

where P_0 is vehicle static wheel load, m_u is vehicle unsprung mass, K_H is linearized wheel/rail contact stiffness, V is vehicle speed, α is joint angle, and m_e , m_t , k_t and c_t are equivalent track system parameters defined in [80]. According to these formulae, P_1 depends on the product of V and α , if other parameters are fixed. To confirm this point, the track model (EBEF: Euler beam on elastic (damped Winkler) foundation) proposed in [46] is employed in this study and some examples are shown in Fig. 5.2. The irregularity function of dipped-joint used in the calculation is expressed by

$$f(x) = \begin{cases} D_1(1 - \cos(2\pi x / L_1)) & 0 \leq x \leq L_1 / 4 \\ D_1(1 + \cos(2\pi x / L_1)) & L_1 / 4 < x \leq L_1 / 2 \end{cases} \quad (5.3)$$

where D_1 and L_1 are the maximum depth and the affecting length of rail joint, respectively.

A sample results as wheel/rail impact load time history obtained for a fixed joint angle (α), but different wave length of dipped joint, are shown in Fig. 5.2. These responses calculated with this model are similar to those calculated from Lyon's model [80, 98]. Although the speed and α are kept to be the same in the calculation of the responses, the first impact load (P_1) is different for different



$$\alpha = 2\pi(D1/L1) = 0.01$$

$$V = 160 \text{ km/h}$$

$$1: D1 = 0.0055 \text{ m}, L1 = 3.4 \text{ m}$$

$$2: D1 = 0.022 \text{ m}, L1 = 13.6 \text{ m}$$

$$3: D1 = 0.00275 \text{ m}, L1 = 1.7 \text{ m}$$

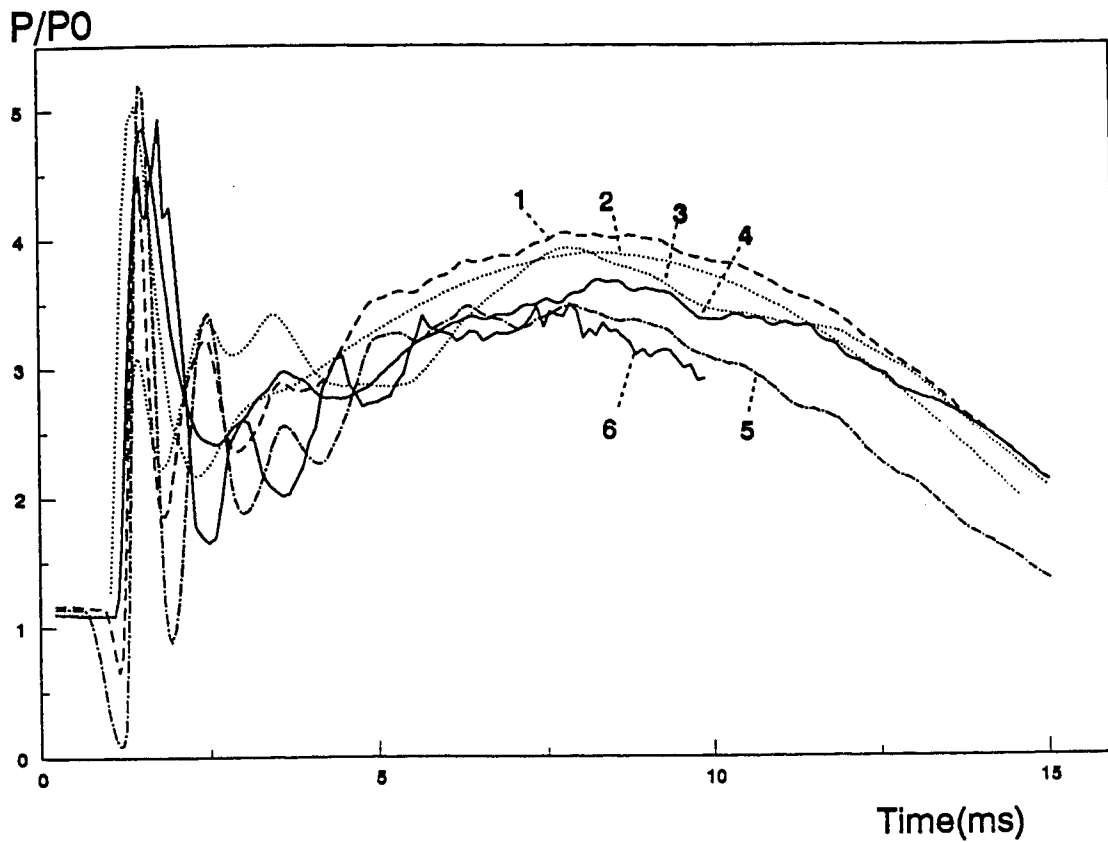
$$4: D1 = 0.0011 \text{ m}, L1 = 0.68 \text{ m}$$

Fig. 5.2 Impact Responses Calculated from an Euler Beam on Elastic (Damped Winkler) Foundation

wave lengths of dipped joints. Hence, the impact load is strongly dependent on the actual shape of an irregularity on the rail and the formulae in Eq. 5.2 may only give a rough estimation of the impact load on dipped rail joints.

The FE model described in section 2 can be easily converted to a Timoshenko beam on elastic (damped Winkler) foundation (TBEF) model. The response calculated with this TBEF model along with the predictions from other models (EBEF and TBDS) and the experimental data from [80] is shown in Fig. 5.3. It can be seen that the response is similar to the results calculated with the method in [46]. This indicates that a reasonable prediction can be achieved by using the FE method. The major advantage of the FE method is that detailed modeling of the track system can be taken into account to study the influences of track parameters on the impact loads. Further, the dynamic forces on the components such as fasteners, pads, ties and ballast can be analyzed.

In the simple track model such as in EBEF or TBEF models, the tie mass per unit length is usually simply added to the rail. It is noticed that if the tie mass is separated from the rail as in the FE model in this study, the impact response shows some significant changes, as shown in Fig. 5.3. The first change is a significant reduction in the first peak value. However, this peak does not match with the experimental data as shown in this figure. One of the possible reasons is that the irregularity function may not be accurately described in the calculation. For this reason, the irregularity function in Eq. 5.3 is modified and it is expressed as:



V=160km/h

1: TBDS (D1=0.022m,L1=13.6m,D2=0.002m,L2=0.04m)

2: EBEF model(D1=0.022m,L1=13.6m,D2=L2=0.0)

3: TBDS (D1=0.022m,L1=13.6m,D2=L2=0.0)

4: TBEF model (using FE solution method)
(D1=0.022m,L1=13.6m,D2=L2=0.0)

5: TBDS (D1=0.017m,L1=13.6m,D2=0.005m,L2=0.08m)

6: Experiment data from shear strain gages

Fig. 5.3 Impact response for different track models

$$f(x) = \begin{cases} D_1(1 - \cos(2\pi x / L_1)) & 0 < x \leq (L_1 - L_2) / 4 \\ D_1(1 - \cos(2\pi x / L_1)) + D_2(1 - \cos(2\pi(x - L_1 / 4 + L_2 / 4))) & (L_1 - L_2) / 4 \leq x \leq L_1 / 4 \\ D_1(1 + \cos(2\pi x / L_1)) + D_2(1 + \cos(2\pi(x - L_1 / 4 + L_2 / 4))) & L_1 / 4 \leq x \leq (L_1 + L_2) / 4 \\ D_1(1 + \cos(2\pi x / L_1)) & (L_1 + L_2) / 4 \leq x < L_1 / 2 \end{cases} \quad (5.4)$$

The response using this modified irregularity function is closer to the experimental data than other theoretical predictions, as shown in Fig. 5.3 (Curve 5).

For the study on two wheel vehicle system, the FE model is employed to investigate the impact load on a CN freight car (100 T) running on a typical dipped-joint ($D_1=0.01\text{m}$, $L_1= 3.654\text{m}$, $D_2=0.002\text{m}$, $L_2=0.04\text{m}$) of CN track (60 kg/m, 2640 ties/mile). The irregularity function in Eq. 5.4 is used in this investigation.

The phenomenon of the interaction between two wheels presented in Chapter 4 is also observed in the dynamic response due to the rail joint. The time history of wheel/rail and bearing forces at the leading and trailing wheels are shown in Fig. 5.4. The results show that some of the impact energy on the first wheel is transmitted to the second wheel. The high frequency peaks on the second wheel are transmitted through the rail and some of the low frequency waves are transferred through the truck. The impact force on one of the wheels may be affected by the dynamic force on another wheel.

Fig. 5.5 shows an example of the dynamic forces on the leading and trailing wheels. It indicates that the dynamic force magnification, $(P_{1r} - P_{01r})$ and $(P_{1f} - P_{01f})$ may be approximately the same but the total forces are different even though the

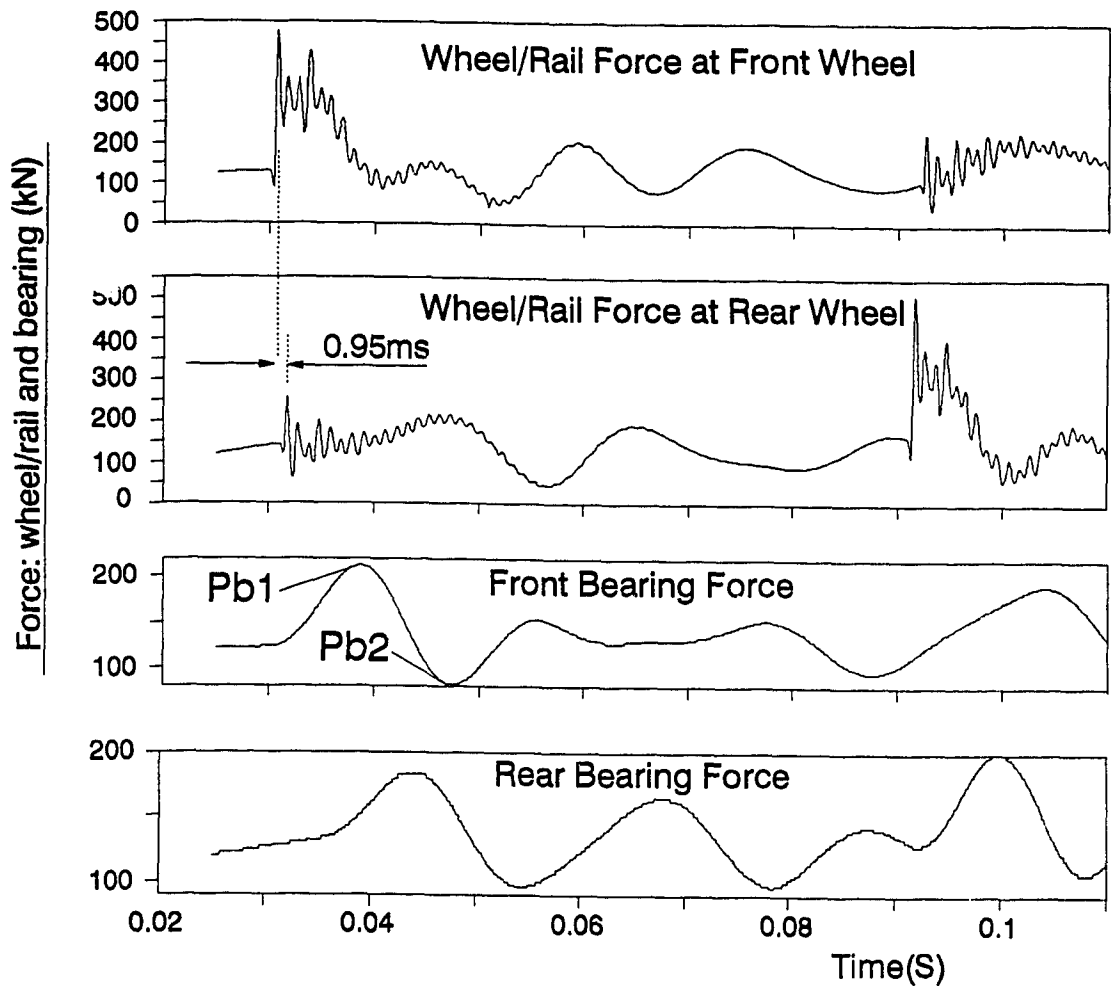


Fig. 5.4 Impact forces at two wheels

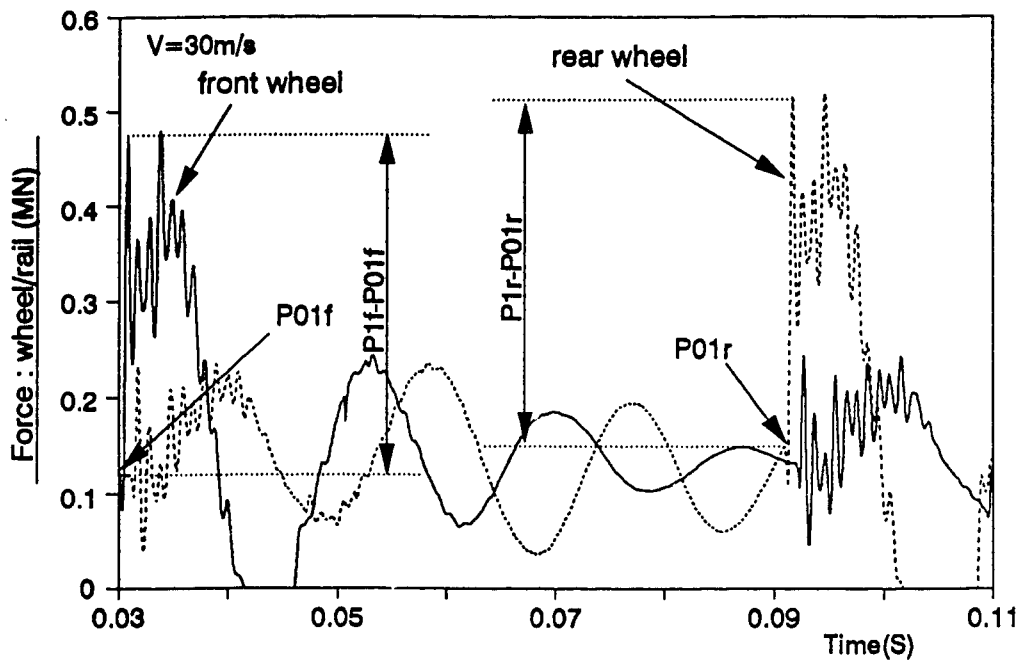


Fig. 5.5 Dynamic forces on leading and trailing wheels

axle loads on the two wheels are the same. The total force seems to depend on the force level (P_{01}) before the wheel begins to lose contact with the rail at the joint.

5.4 PARAMETRIC STUDY

Fig. 5.6 shows the effect of wheel mass on the dynamic forces at the contact point, rail pad and bearing. Comparing with the equivalent mass of rail, the unsprung mass of truck is usually very large. The change of wheelset mass has little influence on P_1 when the weight of wheelset is more than 600-800 kg. P_2 increases almost proportionally with the wheel mass. When the mass of wheelset is less than some value, the peak forces, P_1 and P_2 are transferred to the bearing and the impact force acting on the bearing is increased.

A rubber pad has been introduced as a suspension element for wheel bearings on the three-piece truck of the freight car considered in this study. Fig. 5.7 shows the stiffness of rubber pad on the impact load. It indicates that reducing the pad stiffness has little effect on the first peak load but it can reduce the dynamic force on the bearing. The second peak of the contact force can also be reduced when the bearing pad stiffness is reduced. Placing a rubber pad on the bearing is a beneficial choice from the point of view of vertical dynamic force. However, the lateral stability may be threatened by the introduction of the rubber pad. This problem should be studied in detail.

Axle load (P_0) has important effect on both P_1 and P_2 , as shown in Fig. 5.8. It shows that increasing axle load increases the total impact load. Fig. 5.9 shows

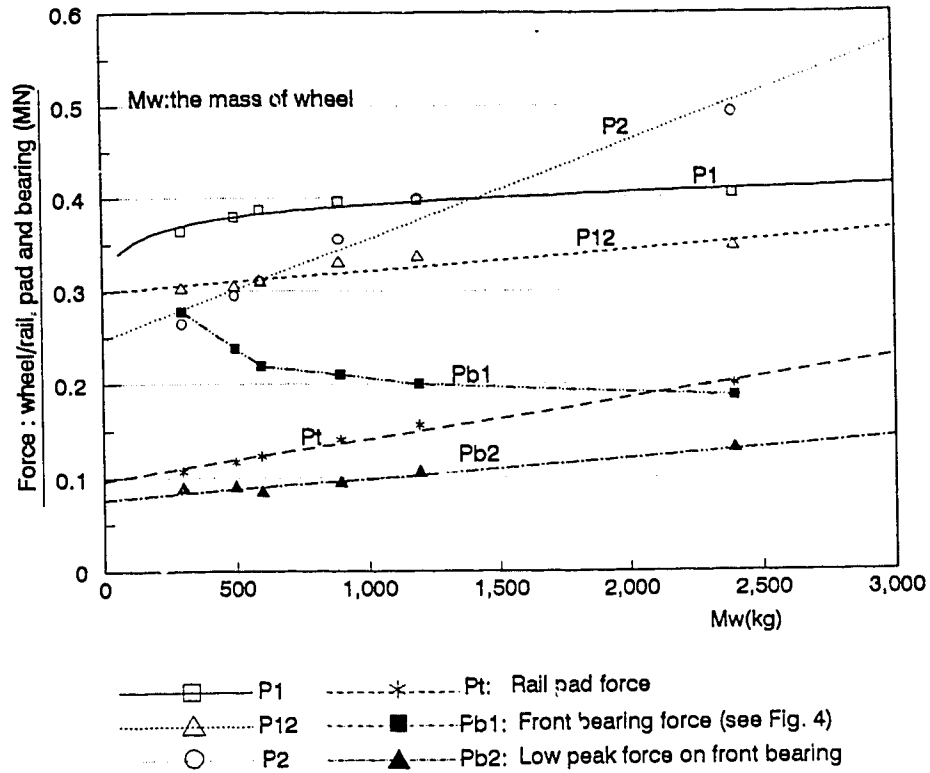


Fig. 5.6 Effect of Wheel Mass

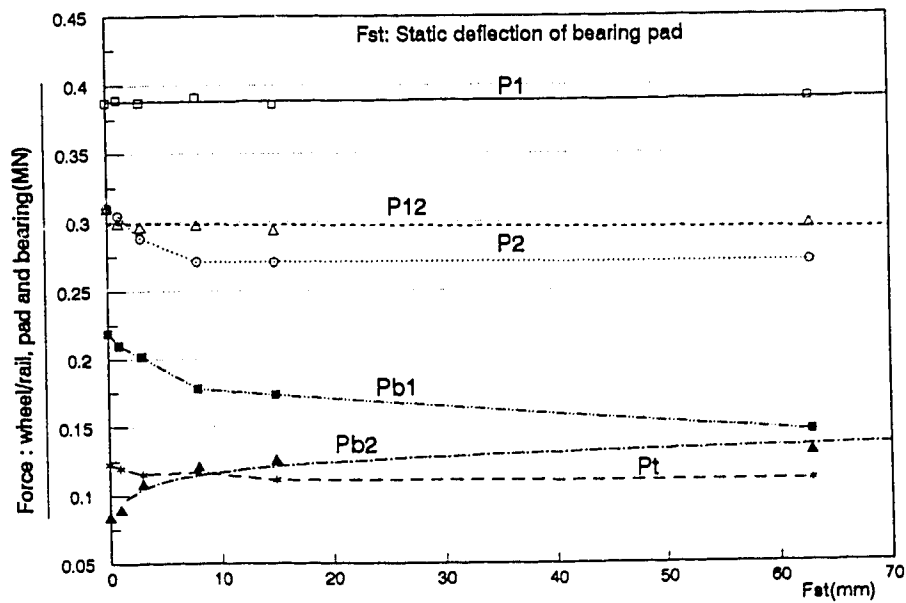


Fig. 5.7 Effect of Bearing Pad Stiffness

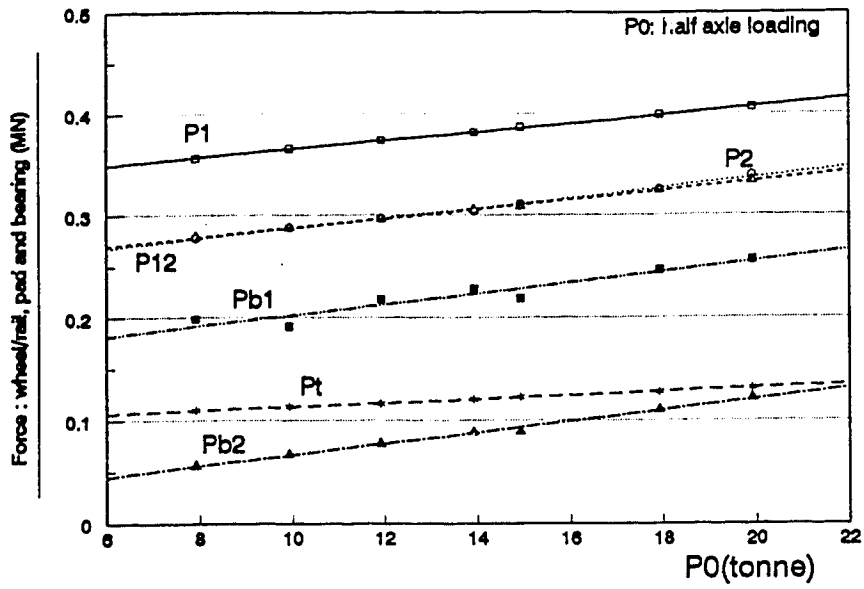


Fig. 5.8 Effect of Axle Load

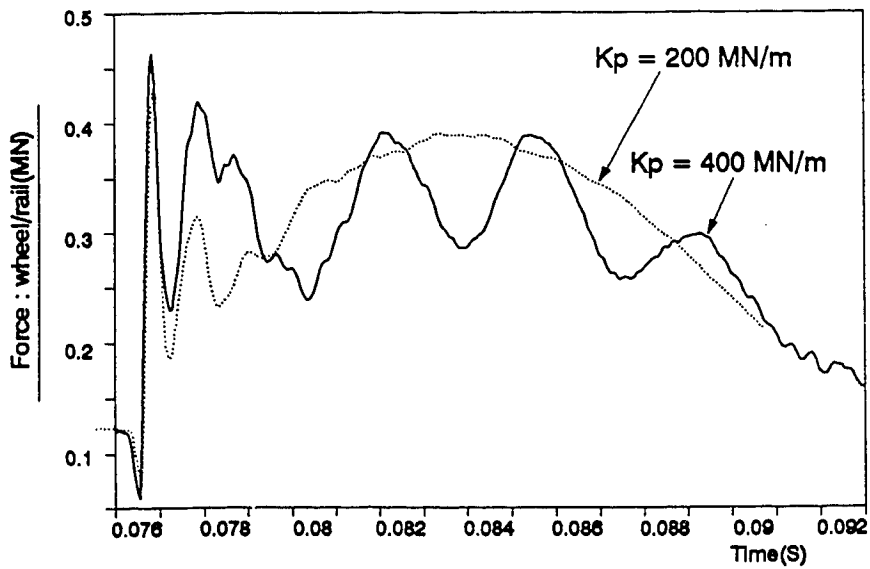


Fig. 5.9 Effects of Increasing Stiffness of Rail Pad

that increasing rail pad stiffness enhances the effect of tie in the impact process and increases the oscillations of dynamic contact force after the first impact. Fig. 5.10 shows that the rail mass has very large influence on P_1 and P_{b1} . Fig. 5.11 shows that decreasing the ballast stiffness has little effect on P_1 , but it can reduce P_2 .

Fig. 5.12 shows an example of the effect of bearing stiffness on the impact forces. The mass of side frame is often considered as unsprung mass in the dynamic studies since the bearing stiffness is usually very large on the three piece truck. This practice has little effect on P_1 but it may not give a proper prediction of P_2 because it is affected by the bearing stiffness, as shown in this figure.

Properly designing a profile near the rail joint may reduce the impact load. Fig. 5.13 gives a comparison of various responses at a dipped joint with different profiles. The calculation is carried out with the EBEF model. It shows that properly raising the position of rail near a joint can reduce the impact force. Practically, the ties at the two sides of the joint may be kept at a certain elevation to modify the joint profile. As calculated with the TBDS model, Fig. 5.14 shows that rising the position of the ties near the joint can reduce P_1 and P_2 . Another way to reduce P_1 and P_2 is to decrease the stiffness of the rail pads and to raise the positions of ties near the joint at the same time. Fig. 5.15 shows that this combined method can improve the dynamic behavior of wheel/rail at dipped joint significantly. Fig. 5.16 shows that this method can reduce the wheel/rail dynamic contact force, especially at high speeds.

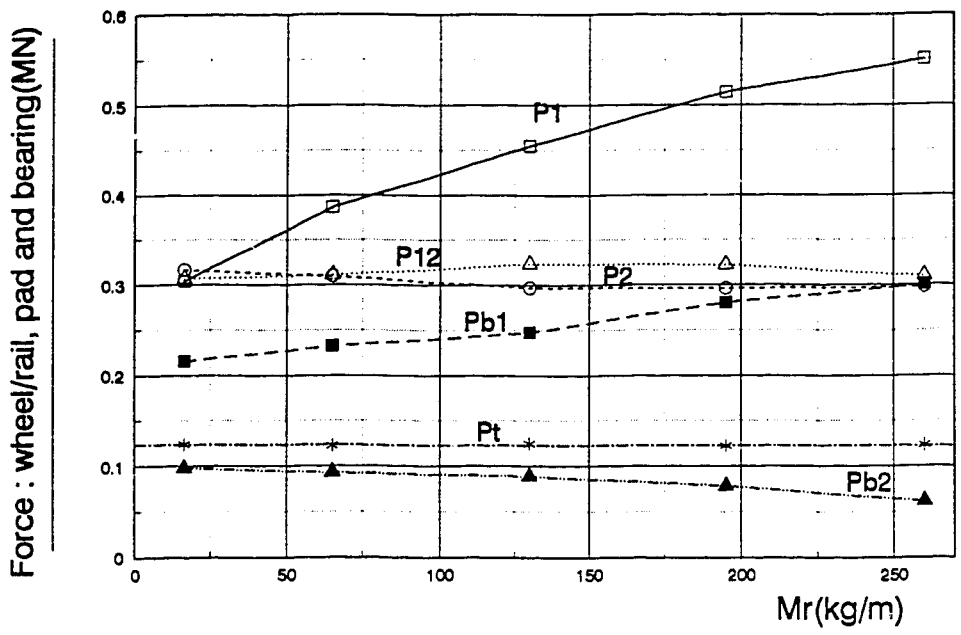


Fig. 5.10 Effect of Rail Mass

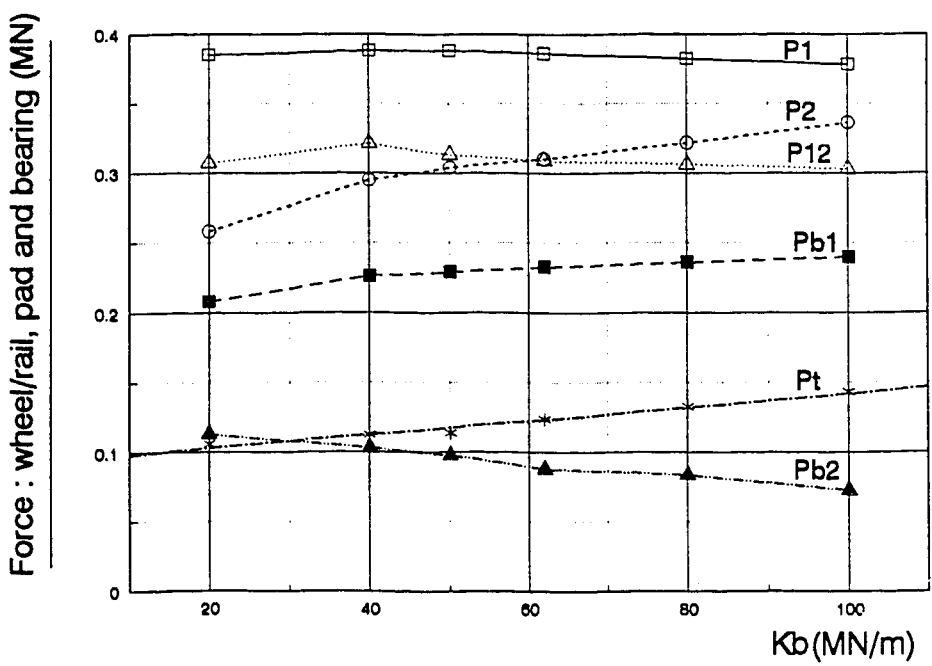


Fig. 5.11 Effect of Ballast Stiffness

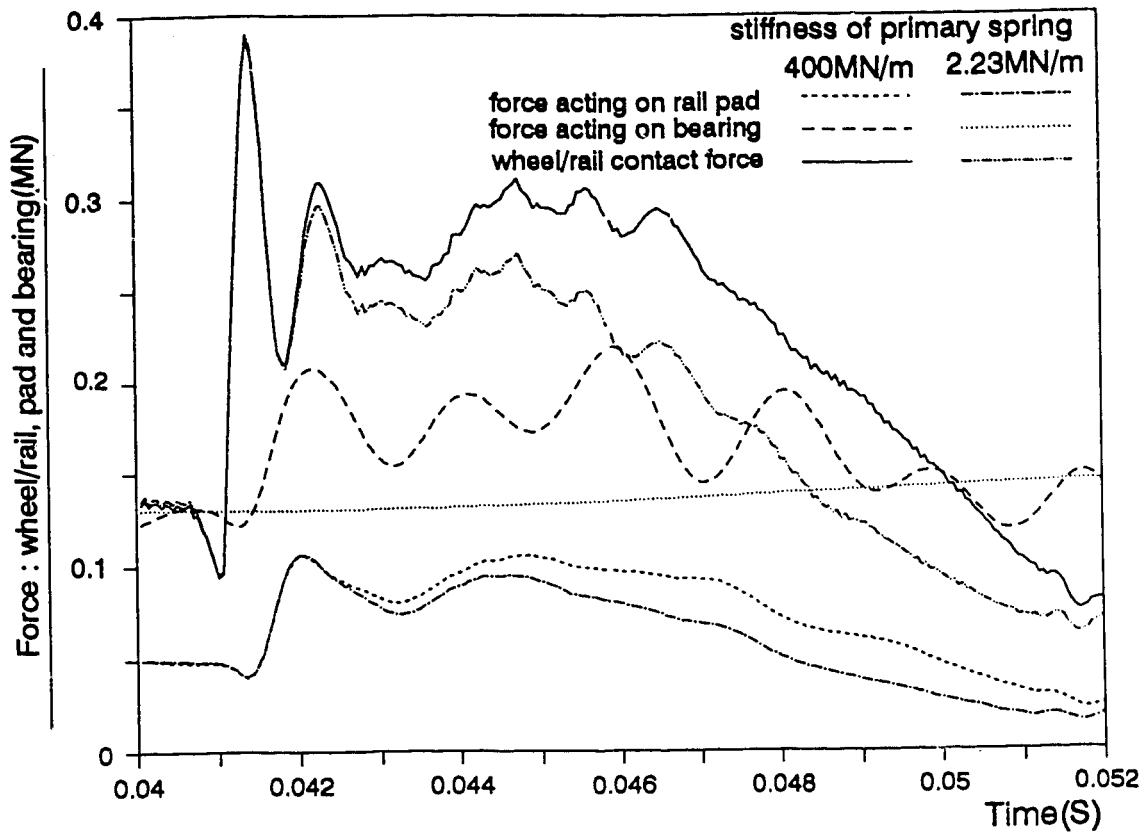
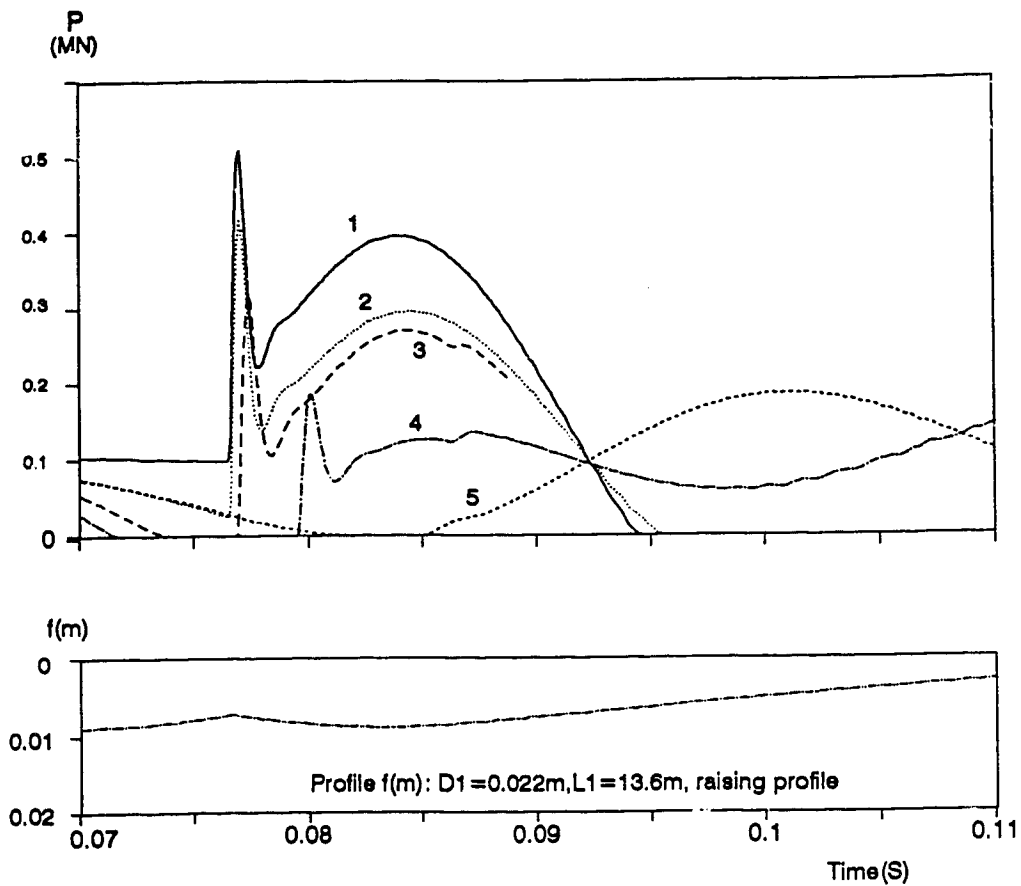
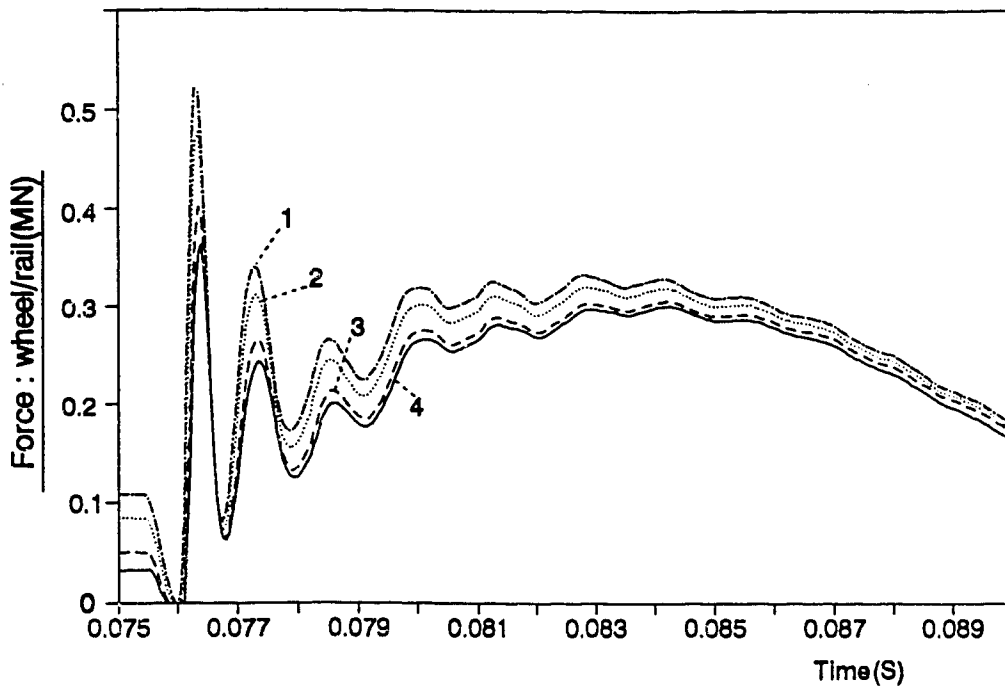


Fig.5.12 Effect of Bearing Pad Stiffness



- 1: $D1=0.022m, L1=13.6m, \text{no raising curve}$
- 2: $D1=0.022m, L1=13.6m, \text{raising profile}$
- 3: $D1=0.00275m, L1=1.7m, \text{no raising profile}$
- 4: $D1=0.00275m, L1=1.7m, \text{raising profile}$
- 5: $D1=0.0, \text{only raising profile}$

Fig. 5.13 Effect of Different Profiles



$d1=0.017m, L1=13.6m, d2=0.005m, L2=0.08m$

h_i : raising the height of the tie from joint point

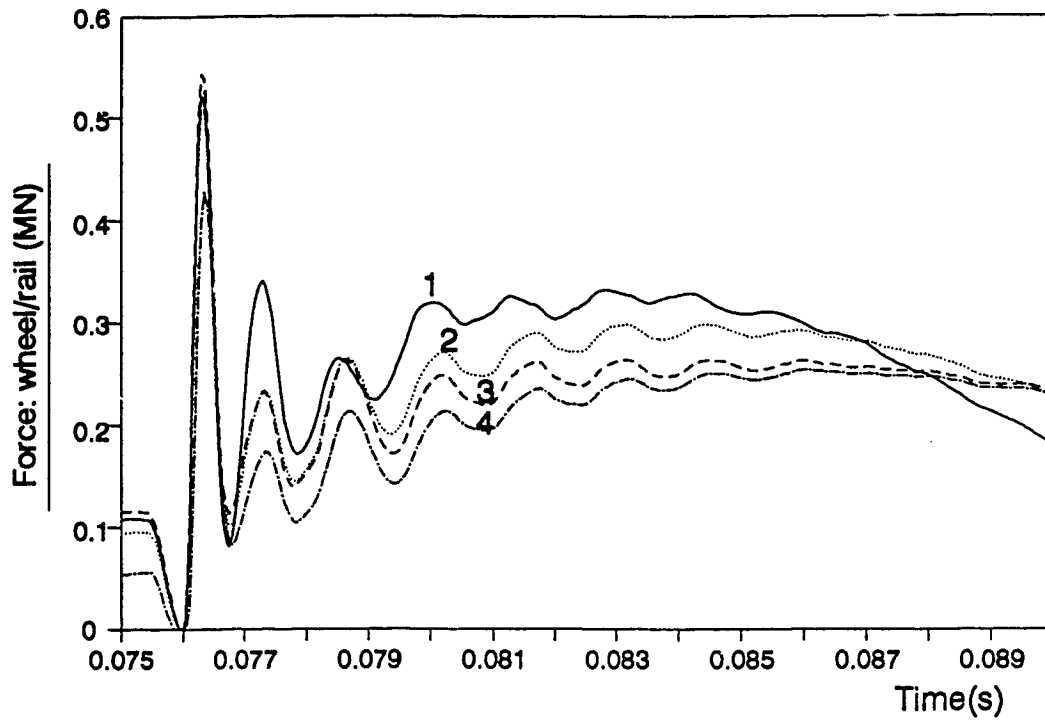
1: $h1-h4=0.0m$

2: $h1=0.004m, h2=0.001m$

3: $h1=0.01m, h2=0.003m, h3=0.001m$

4: $h1=0.016m, h2=0.006m, h3=0.002m, h4=0.001m$

Fig. 5.14 Effect of Raising the Tie Height



1: $K_p(\text{all})=200\text{MN/m}, h_1=h_2=0.0$

2: $K_{p1}=K_{p2}=40\text{MN/m}, K_p(\text{other})=200\text{MN/m}, h_1=0.01\text{m}, h_2=0.001\text{m}$

3: $K_{p1}=K_{p2}=20\text{MN/m}, K_p(\text{other})=200\text{MN/m}, h_1=h_2=0.0$

4: $K_{p1}=K_{p2}=20\text{MN/m}, K_p(\text{other})=200\text{MN/m}, h_1=0.01\text{m}, h_2=0.001\text{m}$

Fig. 5.15 Effect of Tie Height and Pad Stiffness

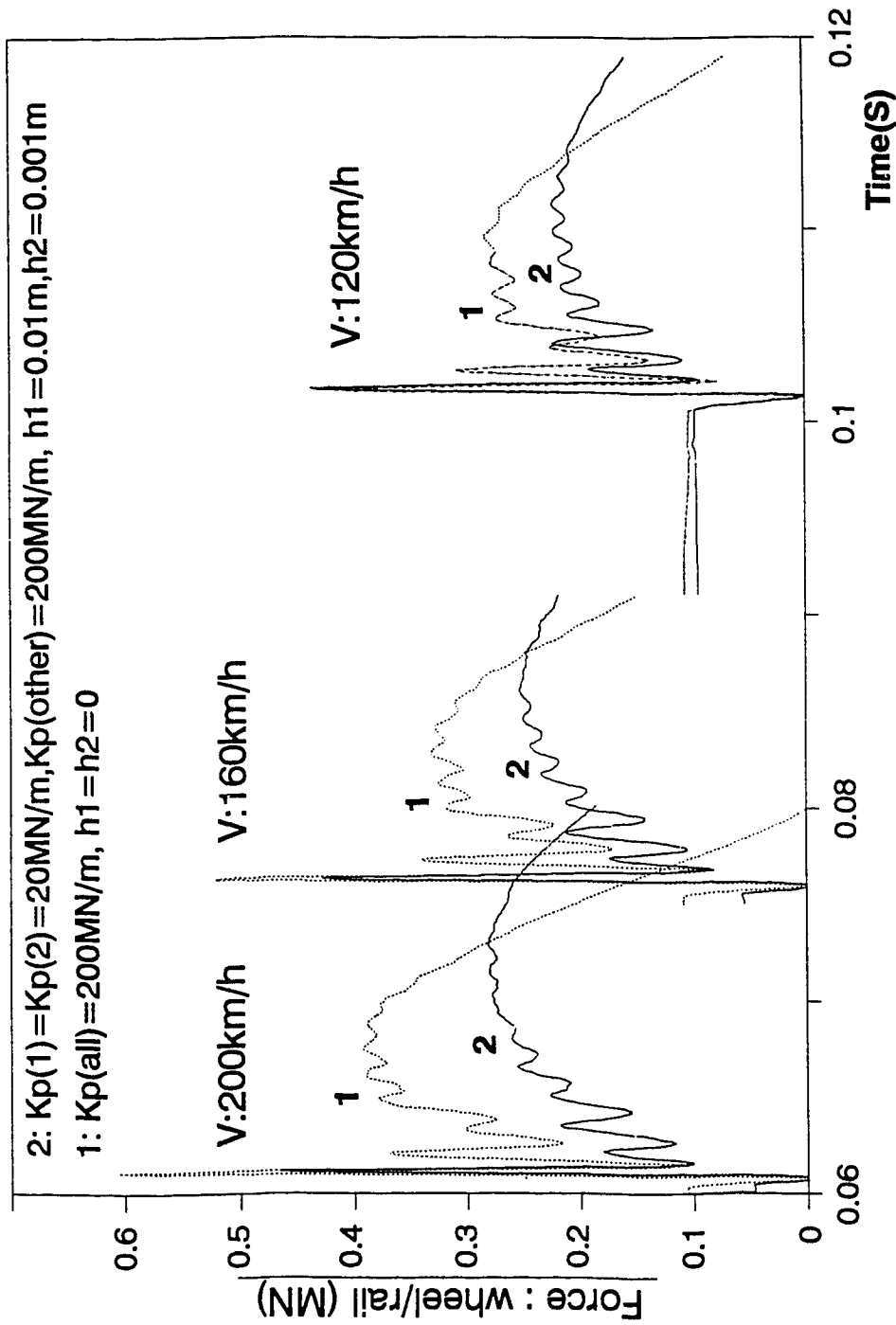


Fig. 5.16 Impact Response of High Speed Vehicle

5.5. SUMMARY

In this chapter, available experimental data of the dynamic force at a rail joint are used to further validate the FE model of vehicle-track system. The validated FE model is employed to investigate the characteristics of dynamic forces due to a dipped rail joint.

The results show that increasing axle load and rail equivalent mass significantly increase the first peak load (P_1). The wheel (unsprung) mass, stiffness of bearing rubber pad, and ballast stiffness mainly affect the second peak load (P_2). Properly designing a profile near the rail joint may reduce the dynamic load at the joint.

The results presented in this chapter also indicate that the dynamic load generated at one wheel can partially transmit to a neighboring wheel.

CHAPTER 6
STEADY-STATE INTERACTION
BETWEEN RAILWAY VEHICLE AND TRACK

6.1 INTRODUCTION

All the rails and wheels in service have some form of irregularities on their treads. It is an idealization to assume them to be perfect in the analytical formulation for steady-state response. The major purpose in such investigation is to evaluate the possible dynamic forces and track system responses when a vehicle is traveling on the track.

As a further simplification, the vehicle may be idealized as a constant moving load or a harmonically vibrating force. The problem then becomes the well-known "steady-state response due to moving forces" or "moving loads problem". The moving load problem has been studied by many researchers and it has been well documented for the track considered as an Euler beam or Timoshenko beam on Winkler or damped Winkler foundation. The beam response due to the moving forces can be easily solved analytically by first assuming its existence. Good reviews of such analyses have been given by Fryba [55] and Kerr [90]. A mass that is vibrating harmonically and moving at a constant speed has been included in the steady-state solution by Duffy [41] in the recent years. Fryba et al. [56] have recently employed the FE method to investigate the steady-state response of an Euler beam on damped Winkler foundation (with random stiffness and damping) subjected to a moving constant force. Several methods proposed by Jezequel [81], Mean [104,105] and Cai [17] may be used to solve

the steady-state response due to a moving force on a track model represented by a beam on discrete supports.

It remains unresolved that if the assumption of the existence of the steady-state solution is true or not [92] and that if there exists something like a stability limit similar to the critical speed for wheelset hunting. So far, the major finding in the investigations of the steady-state response has been the so-called "critical speed" at which the speed of the moving force would be equal to that of wave propagation in the beam. It is not clear if this critical speed correspond to an unstable situation, and if a system could travel on the beam at or larger than such a speed. This critical speed is usually greater than 1000 km/h for a general railway track and it is far beyond the speeds of present and foreseen trains. Hence, this critical speed may have only academic interest for railways.

It is obvious that the vehicle can not be considered as a constant moving load if dynamic wheel/rail contact force is present. The force generated in the steady-state interaction gives the lowest limit that could reach in the vehicle/track interaction. A quasi-steady-state interaction has been reported by Nielsen et al. [110] and a method for track design optimization based on the quasi-steady-state interaction has also been proposed by them [108]. Except this, no report has been found that investigates the steady-state interaction using a comprehensive vehicle-track system model.

For the speeds of present trains, it may make some sense to take into account the discrete feature of rail supports in the investigation of steady-state interaction. This is because the discrete supports may introduce dynamic force

and cause damage on the vehicle and track, even though this force is usually small [140].

The FE model developed in this study can be used to simulate the steady-state interaction for any speed (even beyond critical speed) without first assuming its existence. The validated FE model is employed in this chapter to explore the steady-state dynamic response of vehicle track system. This study may help to clarify some questions mentioned above. The steady state response simulated in this investigation is examined clearly in terms of forces on and deflection of wheel and rail. Since the model is capable of simulating rail and tie lift off, the track deflection in steady state interaction is examined in detail. A parametric study is also carried out to examine the effect of vehicle velocity and acceleration on the dynamic force, and the influence of system parameter on resonance force which has not been reported to date. The parameters used for the simulations in this chapter is presented in Table 6.1.

6.2 STEADY STATE DYNAMIC RESPONSE

For the simulation of steady-state interaction, the static deflection of the system for given parameter is first established. Then, the vehicle is given a constant speed and the steady-state solution can usually be obtained after the vehicle has traveled about 4~5 tie spacings in the conventional train speed range (say, less than 120 km/h). At a higher speed, it needs a longer distance to reach a steady-state solution. To reduce the time required for the system to get into a steady-state, the vehicle is kept on motion on the track model as the vehicle speed is switched from one speed to another one.

TABLE 6.1
NOMINAL PARAMETER VALUES

Track system

E_r	Young's modulus for rail steel, 2.07×10^{11} N/m ²
G_r	Shear modulus for rail steel, 8.1×10^{10} N/m ²
T_r	Timoshenko shear coefficient, 0.34
I_r	Rail second moment of area, 2.35×10^{-5} m ⁴
A_r	Cross-sectional area of rail, 7.17×10^{-3} m ²
m_r	Rail mass per unit length, 56 kg/m
m_{TR}	Track equivalent mass per unit length, $(m_r + M_t/L_t)$
M_t	Tie mass, 143 kg
J_t	Rotational inertia of tie, 1.2 kg-m ²
C_p	Pad damping, 30 kN•s/m
C_b	Ballast damping, 40 kN•s/m
c_v	Extra viscous damping added on the end elements of rail, 20.0 kN•s/m ²
k_f	Average foundation stiffness per unit length, (K_s/L_t)
K_p	Railpad stiffness, 280 MN/m
K_b	Ballast stiffness, 46.6 MN/m
K_s	Equivalent stiffness on each support, $K_p K_b / (K_p + K_b)$

E_{ct}	Young's modulus for concrete tie, 3.2×10^{10} N/m ²
I_{ct}	Tie second moment of area, 1.18×10^{-4} m ⁴
L_{ct}	Total length of tie, 2.36 m
L_t	Tie spacing, 0.6 or 0.7 m
L_p	Rail-pad width, 0.16 m
L_b	Tie bottom width, 0.3 m

Vehicle system

M_w	Wheel mass (unsprung mass), 500 kg
M_b	Bogie mass, 1500 kg for Model II, 3000 kg for Model III
J_b	Bogie rotational moment, 2800 kgm ²
K_1	The primary vehicle stiffness, 1.5 MN/m
K_2	The secondary vehicle stiffness, 0.6 MN/m
C_1	The primary vehicle damping, 10.0 kN•s/m
C_2	The secondary vehicle damping, 20.0 kN•s/m
L_a	Wheelset axle spacing, 1.75 or 2.6 m
C_H	Hertzian spring constant, 1.0×10^{11} N/m ^{3/2}
P_0	Static wheel/rail contact force, 85 kN

Fig. 6.1 shows the displacements and dynamic forces of several system components in a steady-state interaction. Generally, there are two distinct periodic waves in the time history of the dynamic wheel/rail contact force. The first one is mainly caused by the variation of overall track stiffness due to the effect of tie spacing and has a wavelength equal to the tie spacing. The dynamic peak always occurs in the second half of each tie span. This dynamic force may reach a local maximum when the tie-passing frequency of the wheel is equal to the coupled wheel-track resonant frequency or the loaded track frequency. For example, with the parameters specified in Table 6.1, the system resonance is excited when the wheel travels at about 41 m/s (148 km/h) and the tie passing frequency is about 52 Hz, which is approximately equal to the first coupled wheel-track natural frequency (51 Hz) calculated from Eq. 3.3 in Chapter 3. For this condition, the peak force occurs at a point of about a quarter of tie-spacing from the tie center, as shown in Fig. 6.2. A parametric study on this resonant force will be presented in Section 6.5 of this chapter.

SHORT WAVE FLUCTUATION IN STEADY-STATE INTERACTION

As found in Fig. 6.1, a second type of wave is superposed on the first one and it has a shorter wavelength in comparison to the first one. To assure that the short wave is real and not caused by the errors of the finite element modeling, different lengths of rail elements in the FE model are tested in the calculation. As shown in Fig. 6.3, the appearances of the waveforms have some differences for different element lengths, but the number of major waves in each tie span remains unchanged and the fundamental feature of the response is similar to each other. This means that although the short wave predicted by the FE

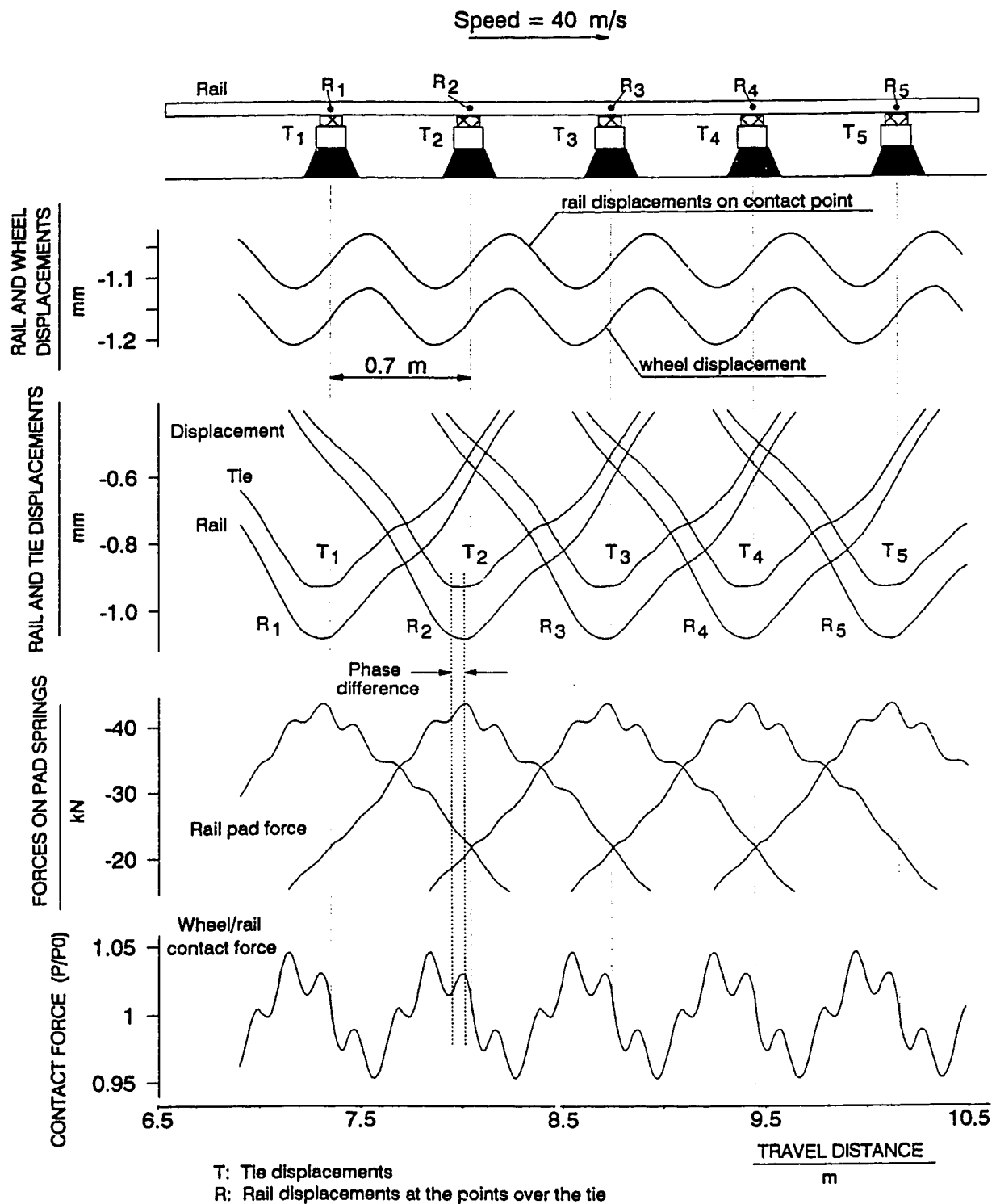
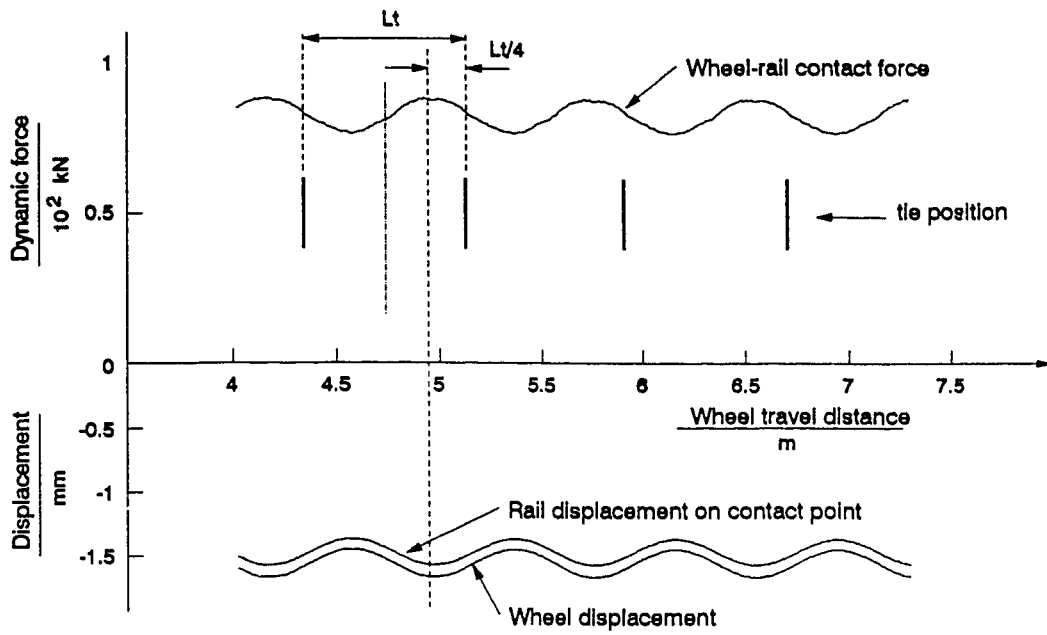


Figure 6.1 Wheel, rail and tie displacements, W/R contact force in a steady-state interaction



Wheel travel Speed: 41 m/s (148 km/h)
 Lt: Tie-spacing

Figure 6.2 A resonance in a steady-state interaction (parameters from Table 4.1)

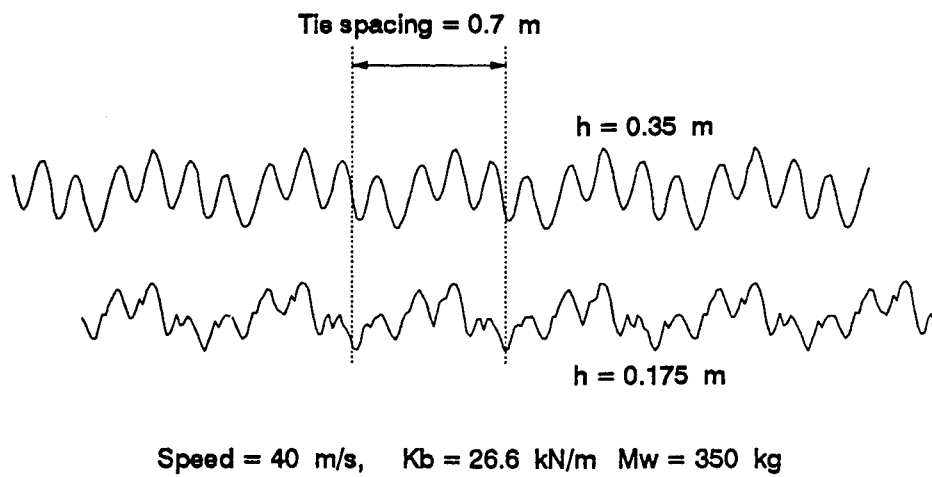


Figure 6.3 Effect of rail element length

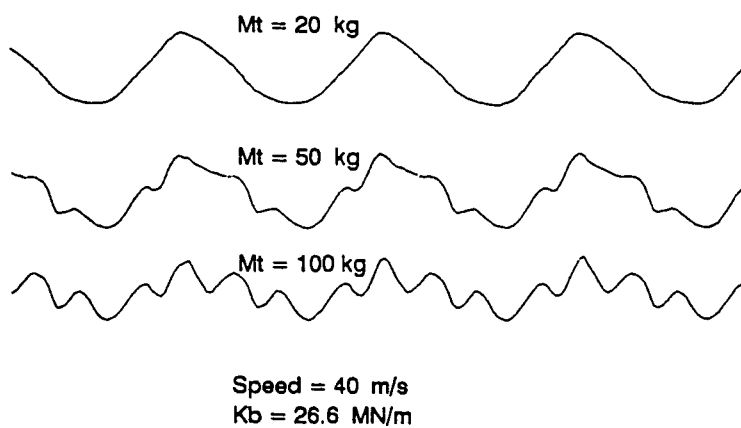


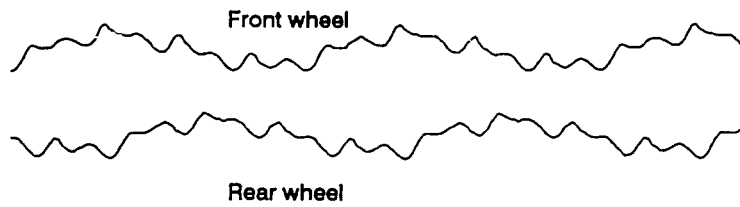
Figure 6.4 Effect of tie mass on short-wave fluctuation

model may vary depending on the element size, it reveals a phenomena in the vehicle-track interactions:

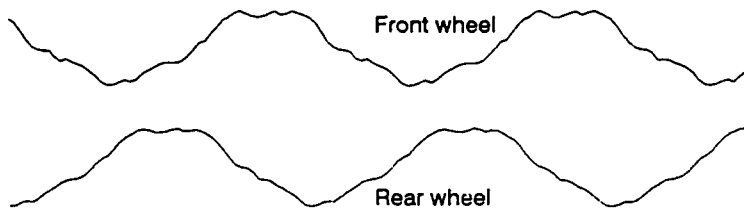
The short wave is caused by the traveling motion of the wheel and the oscillations of the discrete supports. This may be explained by the response shown in Fig. 6.1. The loading of a particular support due to a moving load is a transient process. As a wheel approaches a particular support, the moving load forces the tie to move downward through the rail and rail-pad. If the motion of the tie is not in phase with the motion of the rail over the tie, an oscillation of the support will occur and this may result in the fluctuation of the contact force. This may be seen clearly from the relationship between the rail and tie displacements shown in the figure. One may notice that each tie reaches its maximum displacement earlier than the rail over the tie and then tends to bounce back. This gives a resistive force to the rail that is still moving downward. It is hard to identify the short wave fluctuations in the rail and tie displacements but one can observe their presence clearly on the pad force. The number and position of the wave in the pad force are consistent with those on the contact force. The tie absorbs energy at first and then plays an active role in causing the short wave fluctuations in the contact force. It behaves like an absorber.

If the track bed is soft and the equivalent unsprung mass is small, the short wave may dominate the dynamic force profile at some speeds, as shown in Fig. 6.3. The short wave may disappear after the mass of tie is reduced to some level, as shown in Fig. 6.4. This is another evidence that the short wave is caused by the oscillation of the tie. As shown in Fig. 6.5, the steady-state force at the front wheel is similar to that at the rear wheel, except there is a phase

a) $L_a = 2.6$ m, $V = 20$ m/s, $L_t = 0.6$ m



b) $L_a = 2.6$ m, $V = 32$ m/s (resonance speed), $L_t = 0.6$ m



c) $L_a = 1.75$ m, Speed = 40 m/s, $L_t = 0.6$ m

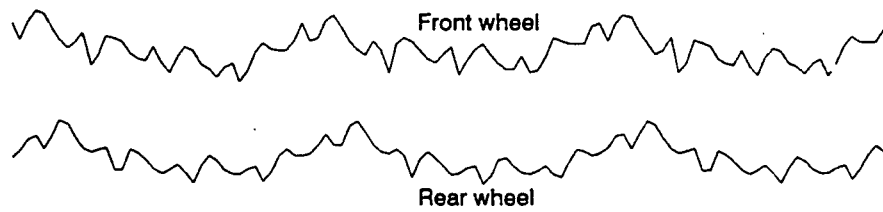
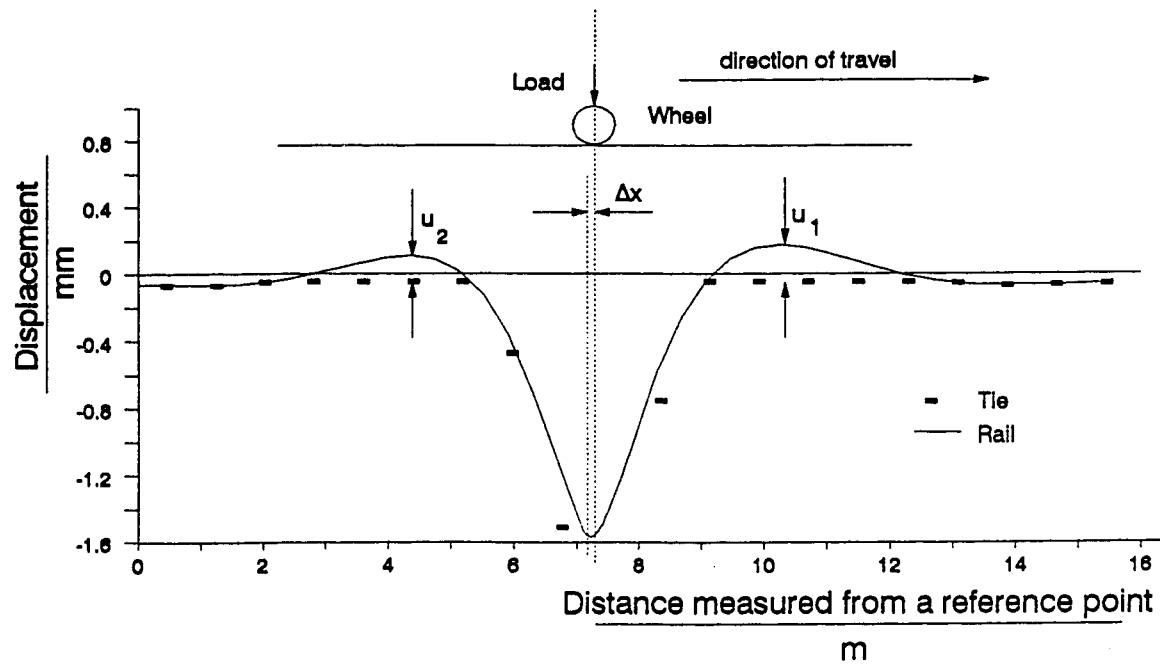


Figure 6.5 Steady-state dynamic forces on leading and trailing wheels

difference between them, which depends on the tie spacing and the wheel axle spacing. If the tie-passing frequency of the vehicle is equal to the coupled wheel/track resonant frequency, the wheel, rail and tie move in phase and the short wave may disappear, as shown in Figs. 6.2 and 6.5(b). The wavelength of the short wave is relatively independent to the vehicle speed as shown in Figs. 6.5(a) and 6.5(c). However, the dynamic feature of the supports may affect the wavelength. If the tie is modeled as a rigid body, only one vibration mode of a tie is introduced in the system and the major short wavelength is about a quarter of the tie spacing (Figs. 6.1 and 6.3). If the tie is modeled as a beam, more vibration modes of the supports are introduced in the system and the wavelength becomes shorter (Fig. 6.5). Based on the results obtained from this study, it is estimated that the short-wave dynamic force is usually less than 5% of the static load and it may be ignored in many practical problems.

6.3 TRACK DEFLECTION IN STEADY-STATE INTERACTION

In view of the models capability to simulate rail lift-off from the tie, and tie lift-off from the ballast, a closer examination of steady-state track deflected is presented in the section. Fig. 6.6 shows the dynamic deflection of track in a steady-state interaction at a conventional speed (117km/h). The deflection shape is asymmetric and it is caused by the motion of the load. The wheel centerline is slightly ahead of the maximum rail displacement. The rail lift-off from the tie in front of the wheel centerline (u_1) is larger than that behind the wheel (u_2). Such a phenomenon was also presented in [46], in which Euler beam on damped Winkler foundation model was used to calculate the dynamic response due to a moving load on an infinite track. The rail lift-off shown in Fig.



Wheel travel speed: 32.5 m/s (117 km/h)

u_1, u_2 : Rail lift-off from ties

Δx : Distance between the wheel centerline and the rail maximum deflection

Figure 6.6 Dynamic deflection of a non-linear track system
in a steady-state interaction (parameters from Table 4.1)

6.6 is larger than that was predicted in [46] because the track in this study is assumed to sustain compression only. A similar result was reported in [151], from experimental observation and from analytical results based on calculation of rail deflection when the rail lift-off from the foundation was taken into account. These comparisons indicate that the FE model can also work well for the non-linear track system.

Fig. 6.7 shows several examples of the dynamic deflections of the track at different speeds. It shows that the asymmetry increases with the vehicle speed. The higher the speed, the larger the distance between the maximum deflection of rail and the wheel center line. These phenomena are basically the same as those observed in the response of an infinite beam on damped Winkler foundation subjected to a moving constant load [55]. This confirms that track representation as a beam on damped Winkler foundation in the investigation of the steady-state response is quite acceptable, and the assumption of the steady-state solution is correct.

Fig. 6.8 shows the maximum deflection of the rail vs. the speed. The deflection increases with the speed until the vehicle reaches a critical speed. The critical speed observed in the case of 0.7m tie spacing is about 340 m/s. It is only marginally lower than the critical speed (358 m/s) calculated from the formulas derived from an Euler beam on elastic foundation [70]:

$$V_{cr} = \sqrt[4]{\frac{4k_f EI}{m_{TR}^2}} \quad (6.1)$$

where EI is the rail stiffness, k_f is track average stiffness per unit length and m_{TR} is equivalent track mass per unit length (including the rail and tie masses). The results obtained in this study show that the steady-state interactions are

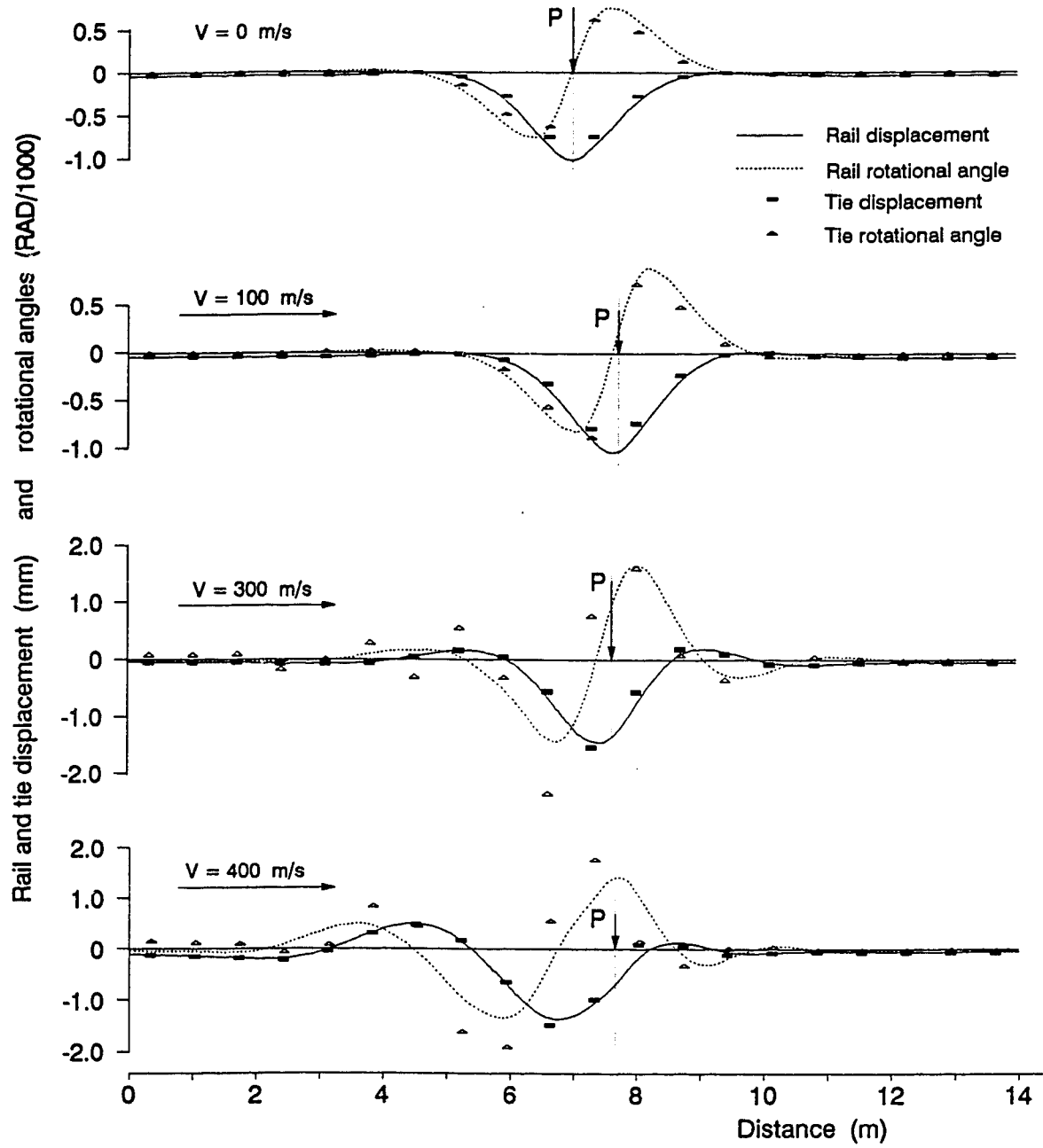


Figure 6.7 Track deflections at different speeds

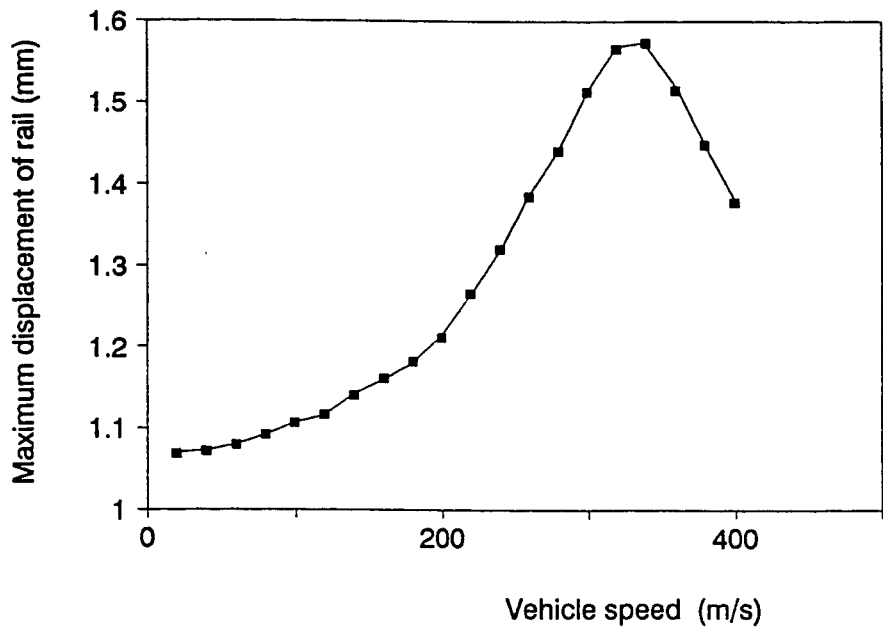


Figure 6.8 Effect of vehicle speed on maximum deflection of track

stable at the critical speed or even at a speeds greater than that, as demonstrated in Fig. 6.7.

6.4 EFFECTS OF VEHICLE SPEED AND ACCELERATION ON W/R CONTACT FORCE

To explore vehicle track system resonance, wheel rail contact forces are evaluated for very high speeds. Figs. 6.9 and 6.10 show several examples of the steady-state wheel/rail contact force at very high speeds. Fig. 6.11 shows the dynamic force vs. tie-passing frequency. In this figure, Curve 1 is calculated as the tie spacing is equal to 0.7m and Curve 2 is for 0.6m tie spacing. It shows that reducing tie spacing reduces the dynamic force due to the discrete supports. The dynamic force reaches its first peak as the tie-passing frequency (V/Lt) of the vehicle is equal to the fundamental coupled wheel/track natural frequency, which is about 54 Hz in this case. The second peak happens at about 145 m/s for 0.6 m tie spacing and 165 m/s for 0.7 m tie spacing. The tie-passing frequency for such speeds is about 240 Hz. This resonance is probably related to the second coupled wheel/track frequency (about 260 Hz in this case), in which the combined wheel-rail mass moves against the tie mass. The dynamic force increases with the speed after the speed is larger than about 300 m/s. This speed is much higher than the speeds of the present or even foreseen trains and it may have only academic interest.

As mentioned before, the steady-state interaction is calculated by assuming that the vehicle is traveling on the track continuously and the vehicle speed is changed by step to quickly obtain the response for different speeds. The responses of the whole system for all the speeds considered in this study are

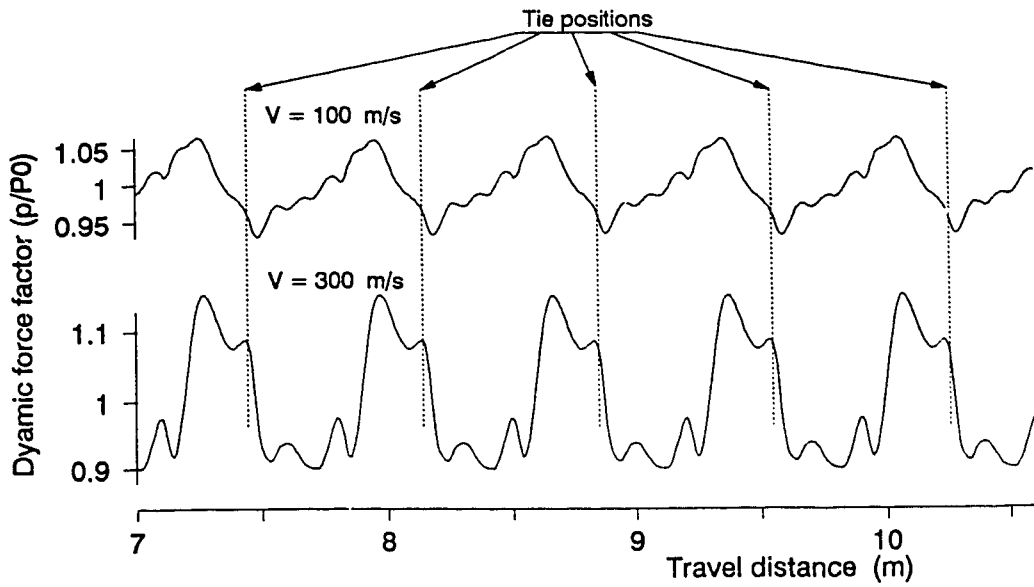


Figure 6.9 Steady-state dynamic W/R contact force (3-DOF vehicle model, 0.7 m tie spacing)

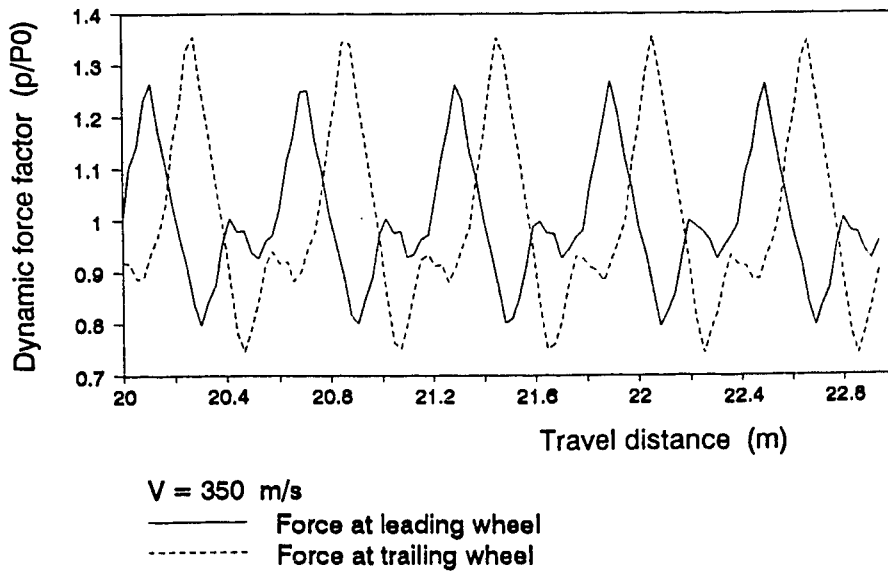


Figure 6.10 Steady-state dynamic W/R contact force (5-DOF vehicle model, 0.6096 m tie spacing)

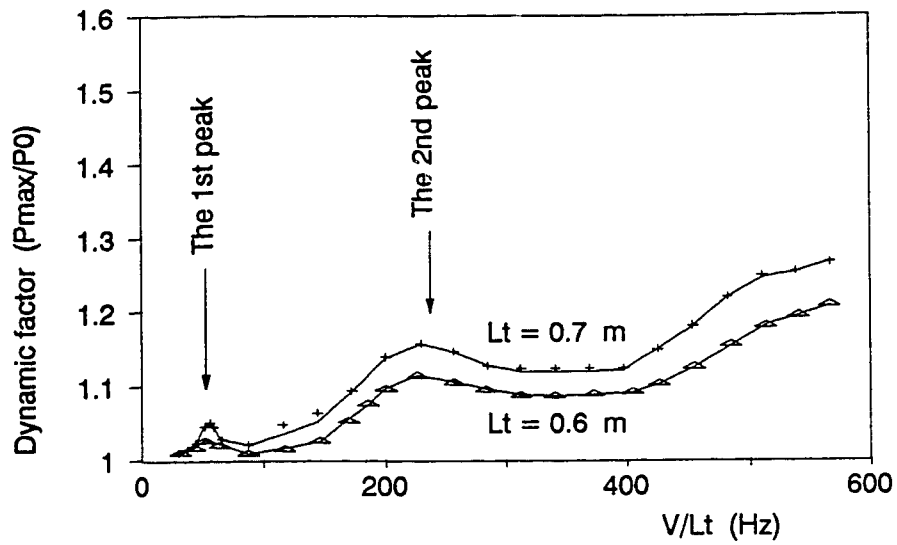


Figure 6.11 Effect of vehicle speed (tie passing frequency) on W/R contact force

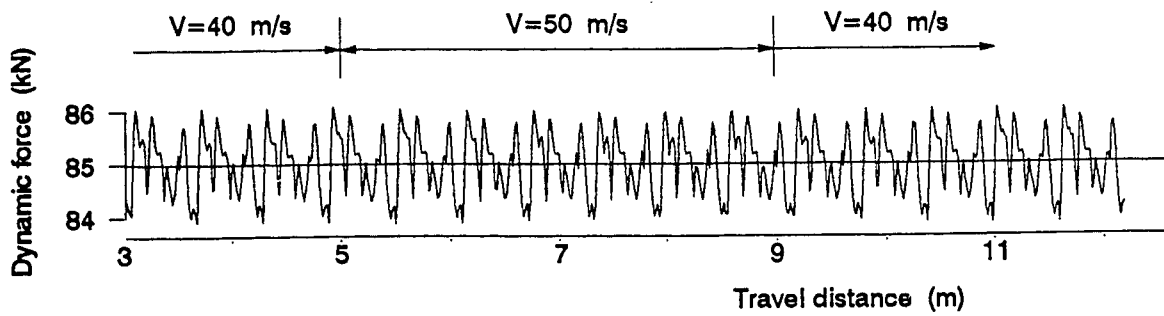


Figure 6.12 Effect of step-changed vehicle speed on W/R contact force

very stable no matter the speed is switched from a higher one to a lower one and vice versa. Fig. 6.12 shows a response in the speed switch. No significant dynamic force is observed in the switch. This demonstrates that any significant dynamic force in the wheel/track interaction should not be caused by any possible acceleration of the train.

6.5 INFLUENCE OF SYSTEM PARAMETER ON RESONANCE FORCE

The fundamental coupled wheel/track frequency is usually about 30~60 Hz for the tie spacing is in the range of 0.55~0.7 m, on the conventional tracks. The corresponding resonant speed due to the tie spacing is in the range of 16.5~42 m/s (60~150 km/h) and it is within many of the conventional train speeds. It is worth having a good understanding of the magnitude of the resonant force (the first peak in Fig. 6.11) caused by the effect of tie spacing. For this reason, the factors affecting the resonant force are investigated using the FE model. The 3-DOF vehicle model (Model II) is used in the calculation and the tie is considered as a rigid body in the track model. The base system parameters are the same as those listed in Table 6.1. The following results are obtained for variation of one parameter at a time.

Unsprung mass

The resonance force factor computed for different value of unsprung mass is presented in Fig. 6.13. It shows that increasing the unsprung mass (or wheel mass) increases the resonant force.

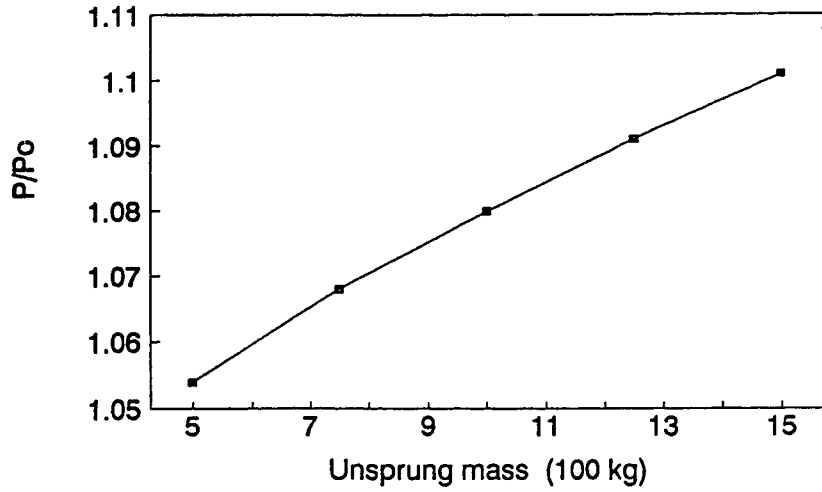


Figure 6.13 Effect of vehicle unprung mass

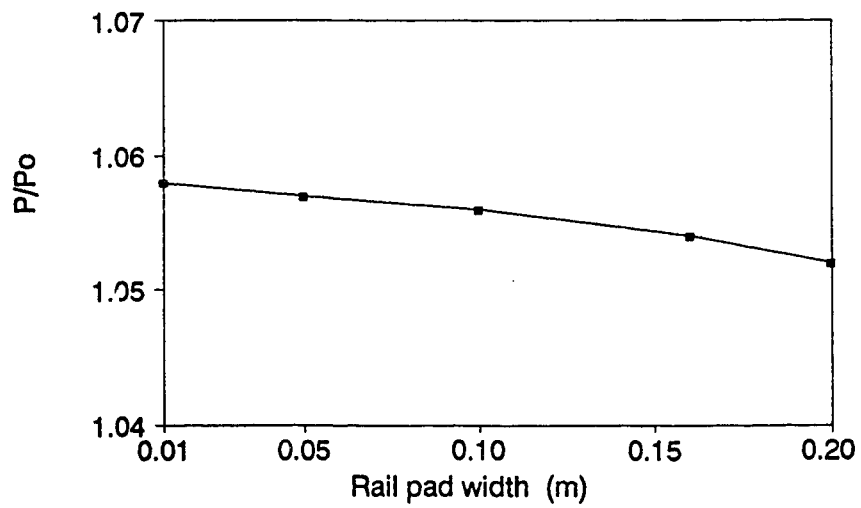


Figure 6.14 Effect of rail-pad width

Rail-pad width

In this case, the total stiffness (K_p) of the pad is kept unchanged but the pad width is changed in the calculation. Fig. 6.14 shows that increasing the pad width only marginally reduces the dynamic resonance force factor. This means that it is fairly well to represent the rail-pad as a point spring-damping element in the dynamic track model.

Damping

The influence of damping in the ballast, pad and primary suspension on the resonance force factor is presented in Fig. 6.15. As it can be seen from this figure, increasing damping in the ballast obviously reduces the resonant force while the damping on the pad has only a small effect. This is because the pad stiffness is several times larger than the ballast stiffness and the relative motion between the rail and tie is much smaller than that in the ballast so that vibration energy in the track is mostly absorbed in or radiated from the ballast. Increasing the primary suspension damping (C_1) on the vehicle also reduces the resonant force, as indicated in Fig. 6.15.

Equivalent tie mass

Increasing the equivalent tie mass increases the uneven distribution of the mass in the track but this does not increase the resonant force (Fig. 6.16). This suggests that the dynamic force due to tie spacing is not caused by the discrete masses of the supports. The variation of the contact force within a tie span is mainly caused by the variation of overall track stiffness over each spacing.

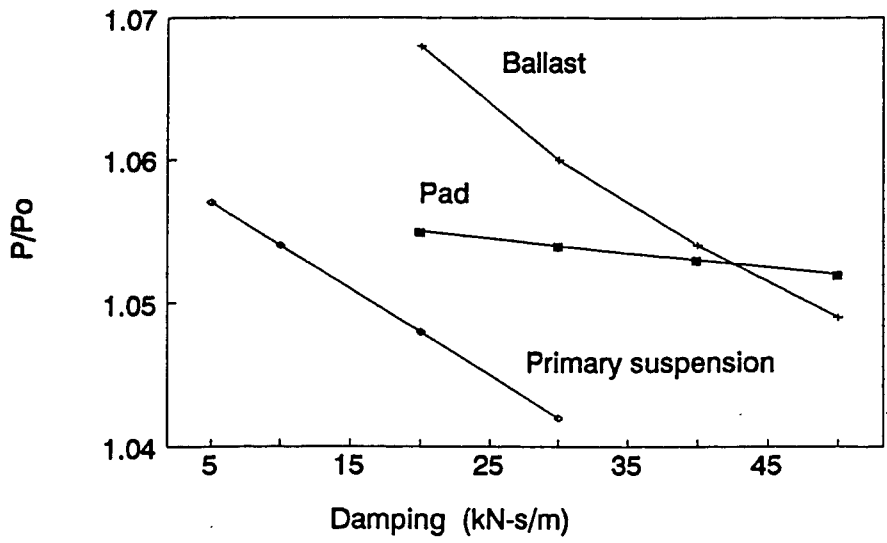


Figure 6.15 Effect of damping on primary suspension, pad and ballast

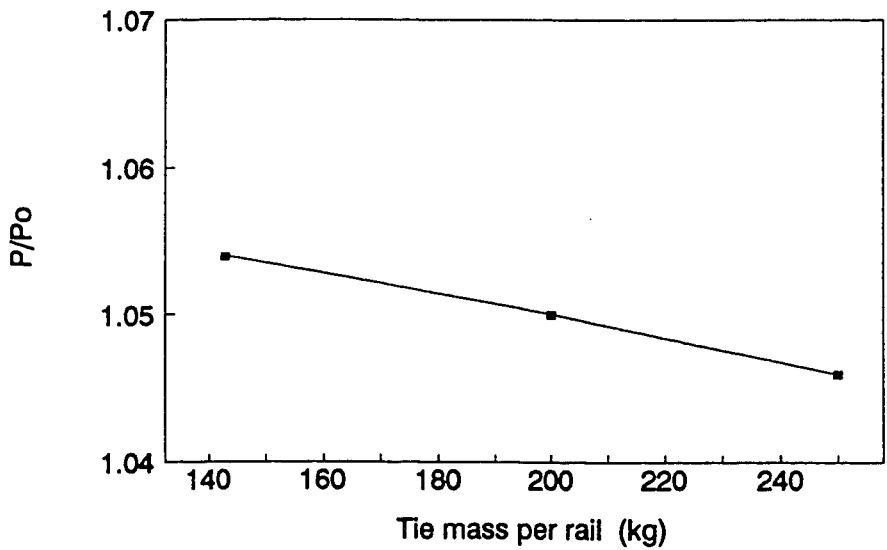


Figure 6.16 Effect of equivalent tie mass

Ballast stiffness and pad stiffness

Reducing the ballast stiffness reduces the dynamic force, as shown in Fig. 6.17. The change in pad stiffness only slightly influence the resonant force (Fig. 6.18). This demonstrates that the equivalent support stiffness (K_s) on each support is one of the major factors affecting the dynamic force. The support stiffness mainly depends on the ballast stiffness.

Tie spacing

Reducing tie spacing reduces the variation of the overall track stiffness and hence reduces the resonant force, as shown in Fig. 6.19.

Rail type

Increasing the rail size increases the rail stiffness ($E_r I_r$). This reduces the variation of the support stiffness in each spacing so that the resonant force is reduced by increasing the rail size, as shown in Fig. 6.20.

Based on the results presented above, it is estimated that the first wheel/track resonant force on a heavy haul track that has a small tie spacing (say, 0.61 m) and large size of rail (say, Rail 136RE) are small (less than 5%). Still, however, some attention should be paid to some special cases, in which some components may be excited by the effect of tie spacing, as reported in [140]. More attention should be paid to the coupled wheel/track resonance due to the discrete supports if the track has a large tie spacing, small rail size and stiff support. The second coupled wheel/track resonant force is larger than the first

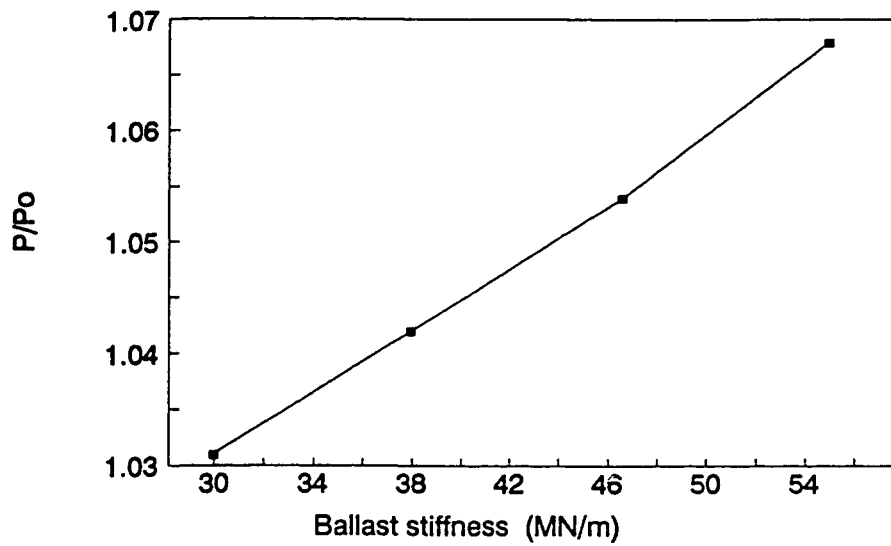


Figure 6.17 Effect of ballast stiffness

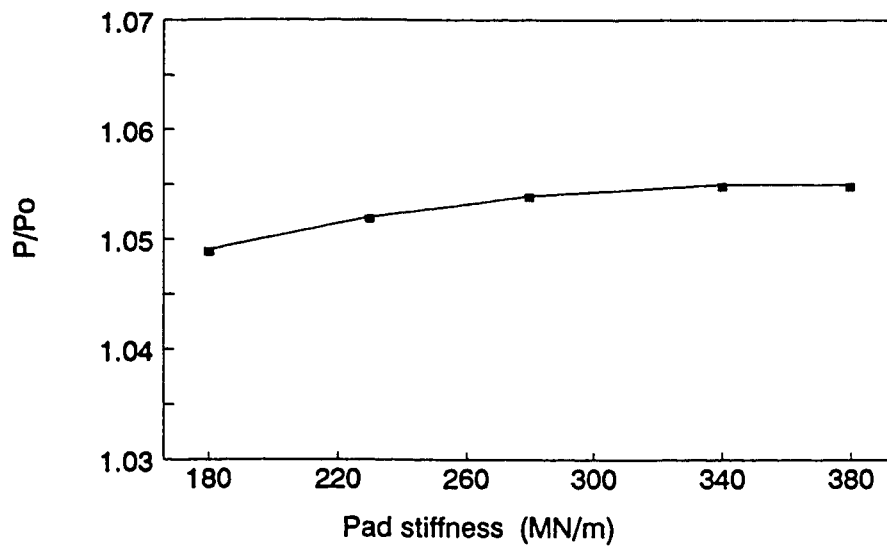


Figure 6.18 Effect of rail-pad stiffness

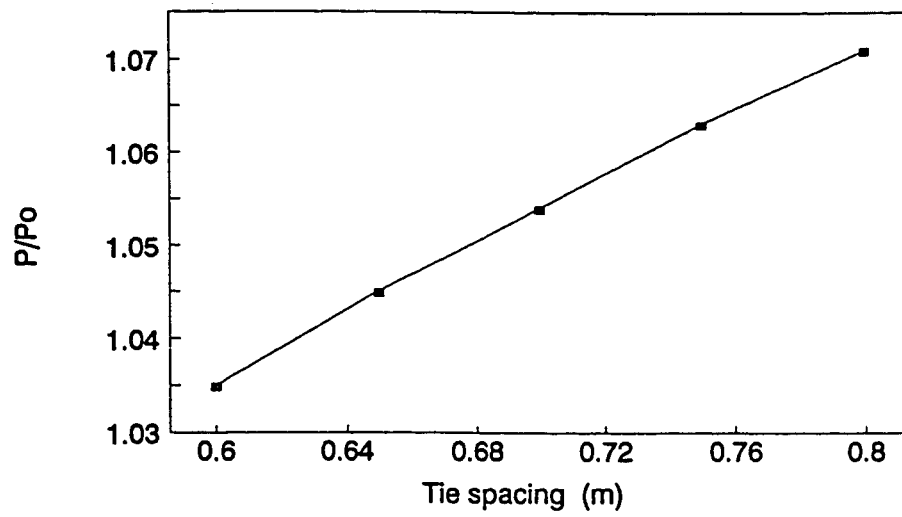


Figure 6.19 Effect of tie spacing

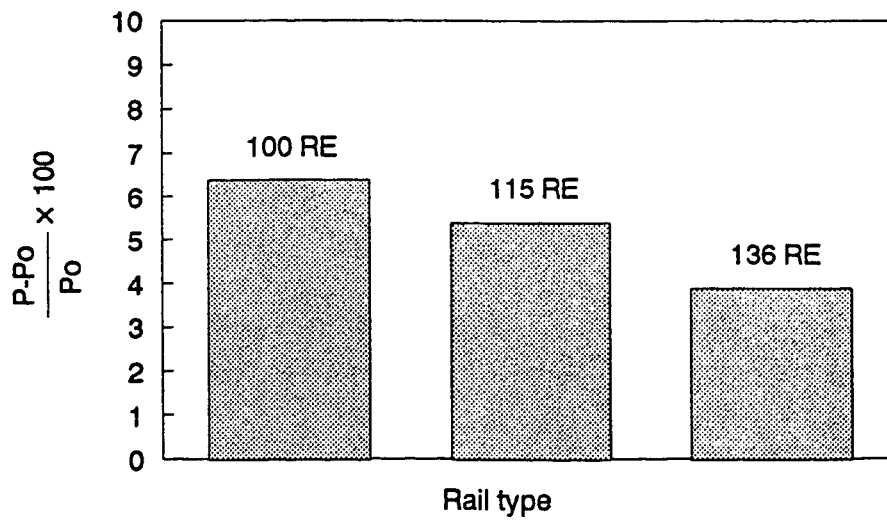


Figure 6.20 Effect of rail type

one but it usually occurs at a very high speed. It is expected that most of the factors affecting that resonance have similar characteristics to the first one.

6.6 AN APPLICATION OF THE FE MODEL TO HARD SPOT AND VOID

Dynamic forces may be caused by irregularities in track structure. The most significant irregularity is probably the variation of support height at ties. This irregularity is usually called hard spot for a over-supported tie location and void for an under-supported location.

The hard spot and void may be represented by a single parameter, Y_b , as shown in Fig. 6.21. It may be regarded as the difference between a particular support height and the average support height of ballast as the assembly of rails and ties is lift-off. If U_b is larger than zero, it forms a hard spot. Otherwise, it forms a void.

Grassie and Cox [66] has developed a sophisticated mathematical model to investigate the dynamic response due to a full void. The full void has also been investigated by Ferner and Nielsen [49] using a FE model of vehicle-track system. In these models, the track is assumed to be linear and it is difficult to use them to simulate a hard spot and a non-full void. This limitation has been overcome on the FE model developed in this study and the hard spot and void with any amplitude can be easily simulated. As an example, the dynamic force due to a hard spot and void at one tie is calculated and presented in this section.

Fig. 6.22 shows the dynamic forces vs. the ballast support height (Y_b) calculated from the FE model. In this case, the variation of the ballast support is assumed

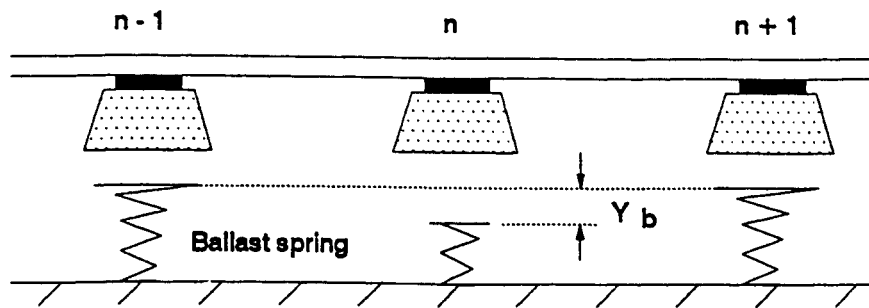
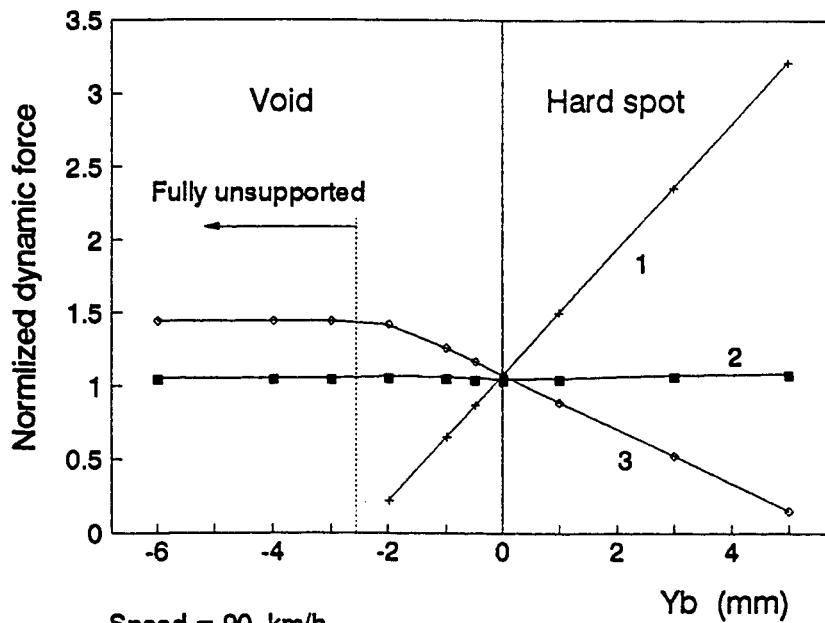


Figure 6.21 Representation of hard spot and void



Speed = 90 km/h

1. Ballast force at the tie (n) with a varying support height
2. W/R contact force
3. Ballast force under the tie (n+1) next to the varying support tie

Figure 6.22 Dynamic force due to hard spot and void

to happen under only one tie and all the ballast stiffness is assumed to be the same. As it can be seen in the figure, the wheel/rail dynamic contact force is not very sensitive to the variation of the ballast support height. This is because the variation in ballast support height can only cause a small variation of rail settlement with a long wavelength. It can not usually result in a very significant dynamic force. The effect of a void is actually similar to that of increasing the tie spacing in the steady-state interaction. If the vehicle speed is increased to some point at which the coupled wheel/track frequency is excited, the dynamic force may be increased to some extent. If a void involves in more ties, the unsupported spacing may be increased and hence the dynamic force may be increased. As shown in Fig. 6.22, the most significant effect due to the variation of ballast support height is the change of the load transferred from the rail to the ties. As expected, in the case of hard spot, the vertical load is concentrated on the over-supported tie. The neighboring ties share more load if a void happens.

6.7 SUMMARY

The steady-state interaction of a vehicle-track system in a very large speed range (0-400 m/s) is obtained with a time-step integration technique without first assuming its existence. The characteristics of the track dynamic deflection obtained from the comprehensive vehicle-track model are basically the same as those of an infinite beam on a damped Winkler foundation subjected to a moving constant load. This suggests that it is fairly well to use a beam on Winkler foundation to study the steady-state response of the track. This study also confirms that the steady-state response of track subjected to a moving force does exist.

The response of the whole system at the so-called 'critical speed' does not show a significant difference from those at other speeds, except that the track deflection reaches its maximum value. This critical speed does not mean an unstable situation in the vehicle/track interaction.

It is observed that there are two types of distinct periodic dynamic waves in the history of the wheel/rail contact force. The first one is caused by the variation of overall track stiffness due to the effect of tie spacing. The second one is caused by the traveling motion of wheel and the oscillations of discrete supports. In the present train speed range, the magnitudes of these dynamic forces are usually less than 5% of static load, except that the coupled wheel/track resonant frequencies are excited at some speeds.

The resonant forces due to discrete supports may be larger than 5% of static load in some cases. The magnitude of the resonant force mainly depends on the unsprung mass, tie spacing, vehicle primary and track ballast damping, rail stiffness and the stiffness on each support.

CHAPTER 7
WHEEL/RAIL DYNAMIC CONTACT FORCES
DUE TO RAIL CORRUGATIONS

7.1 INTRODUCTION

Rail corrugation may be defined as repetitive longitudinal wave formation on the rail tread. An example of rail corrugation is shown in Fig. 7.1. Rail corrugation was first mentioned in scientific literature in 1893 [141]. Since then it has been reported by many researchers [92]. The majority of the world's railways on both straight and curved track have the rail corrugation problem. Rail corrugation has quite a wide range of wavelength and depth. The corrugation with wavelength of 20 to 100 mm is often called short-pitch corrugation and it usually has a depth of up to 0.4 mm and primarily occurs on light axle load tracks and transit systems. The corrugation with longer wavelength (usually 150 to 1500 mm) may have a depth of up to 5 mm and is often called long-pitch corrugation. It is usually associated with heavy-haul freight railroads.

Rail corrugations cause dynamic forces and lead to the further damage to track and vehicle components, particularly to railclips, pads, fastenings and ties. The presence of corrugations gives rise to high noise-levels for passengers and people living near the railways. For this reason, corrugations are colloquially termed "roaring rails" by some people. The cost of corrugation to railways in North America alone was estimated as \$100 millions a year in 1985 [52]. In 1988, British Rail paid £5 millions for grinding and maintenance directly related to corrugation [124]. Hence, rail corrugation is not just a curious phenomenon but a serious problem.

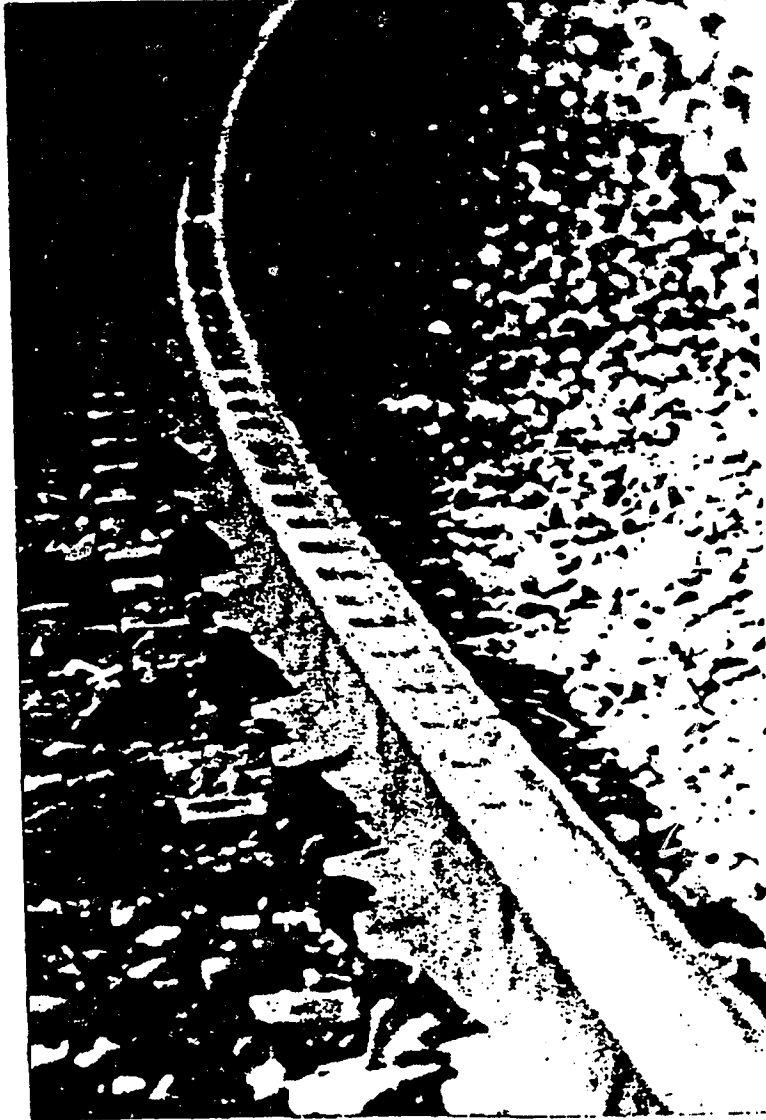


Figure 7.1 Rail corrugation

Because of this, researchers in different areas have concentrated their efforts to find the mechanisms of the corrugations that may lead to a certain cure of this problem. A large number of papers have been published on this subject. A historical review of corrugation problem has been presented under track maintenance in a text by Srinivasan [141], which covers the literature up to 1960s. Modern references (1968 through 1989) on rail corrugations have been cited in a literature review by Ahlbeck [8]. A article that surveys different types of corrugations has been written by Grassie [63].

Dynamic modeling has been successful in both revealing the cause and assessing the viability of treatments for some types of rail corrugations. Mair and his colleagues in Australia [99,100] have demonstrated that the coupled wheel-track resonance for iron ore wagons, excited particularly by rail welds and joints, give rise to corrugation at wavelengths of about 200 mm. It was also found that this resonance force was responsible for corrugation at wavelengths of 300-1500mm which occurred following bad welds on relatively light rail [61]. Similar reason was cited for some longer wavelength corrugation which occurs in the RATP in Paris [147]. Dynamic models of vehicle-track system can now be incorporated in design methods to prevent damage by this mechanism [62].

Several hypotheses have been proposed to explain the mechanisms of short-pitch corrugations [23, 75, 147]. However, a satisfactory theory has not be established. The growing understanding reveals that this type of corrugation is an enigma with variations. Like influenza, its appearance and cause exhibit great diversity. A well validated method that can prevent the formation of this corrugation has not been found. The major way to control the propagation of all types of rail corrugations is still carried out by grinding the rail.

The dynamic forces at the wheel/rail interface must play an important role in the formation and development of rail corrugations. The dynamic forces due to short-pitch rail corrugation are systematically investigated using the validated FE model developed in this study, which may help to understand this problem. In this investigation, a sinusoidal rail corrugation is assumed which consists of 60 mm wavelength and peak-to-peak depth of 0.2 mm. The basic parameters and symbols are listed in Table 7.1. The track modeled as Timoshenko beam on discrete supports (TBDS model) and the concrete ties in the track modeled as non-uniform Euler beam are employed in this study. For a constant vehicle speed, the vertical and geometrical longitudinal dynamic forces are evaluated. The dynamic interaction between two wheels is examined along with the phase relationship between the dynamic force and excitation. The nominal parameters used in this section of the study is presented in table 7.1.

7.2 VERTICAL AND GEOMETRICAL LONGITUDINAL DYNAMIC FORCES

The vehicle/track system with 3-DOF vehicle representation is used to evaluate the vertical and geometric longitudinal forces due to the rail corrugation, and its effect on energy consumption.

Time history of simulation results obtained for vertical and geometric longitudinal forces along with the defined corrugation input is presented in Fig. 7.2. Fig. 7.2 (b and c) presents the vertical contact force for forward speeds 117 and 252 km/h. In previous studies [24,70], it has been reported that the dynamic force over the tie is usually different from that at the midspan between two ties and the

TABLE 7.1
NOMINAL PARAMETER VALUES

<u>Track system</u>		<u>Vehicle system</u>	
E_r	Young's modulus for rail steel, $2.07 \times 10^{11} \text{ N/m}^2$	P_0	Static load per wheel, 85 kN
G_r	Shear modulus for rail steel, $8.1 \times 10^{10} \text{ N/m}^2$	M_w	Wheel mass, 650 kg
T_r	Timoshenko shear coefficient for rail, 0.34	M_b	Bogie mass, 2400 kg
A_r	Cross-sectional area of rail, $8.61 \times 10^{-3} \text{ m}^2$	J_b	Bogie pitch initial moment, 2000 kgm ²
I_r	Rail second moment of area, $3.95 \times 10^{-5} \text{ m}^4$	K_1	Primary spring stiffness, 1.5 MN/m
m_r	Rail mass per unit length, 67.57 kg/m	C_1	Primary damping, 4.5 kN·s/m
L_{ct}	Length of concrete tie, 2.58 m	K_2	Secondary spring stiffness, 0.6 MN/m
E_{ct}	Young's modulus for concrete tie, $3.214 \times 10^{10} \text{ N/m}^2$	C_2	Secondary damping, 15.0 kN s/m
ρ_{ct}	Mass density of concrete tie, 2458 kg/m ³	L_a	Wheelset axle spacing, 2.4 m
L_p	Railpad width, 0.18 m	R	Wheel radius, 0.4572 m
L_b	Tie bottom width, 0.28 m	C_H	Hertzian spring constant, $1.0 \times 10^{11} \text{ N/m}^{3/2}$
K_p	Rail-pad stiffness, $2.8 \times 10^8 \text{ N/m}$		
K_b	Ballast spring stiffness, $4.0 \times 10^7 \text{ N/m}$		
C_p	Railpad damping, 30 kN·s/m		
C_b	Ballast damping, 50 kN·s/m		
L_t	Tie spacing, 0.6096 m (24")		
μ	Peak-peak depth of rail corrugation, 0.2 mm		
λ	Corrugation wavelength, 60 mm		

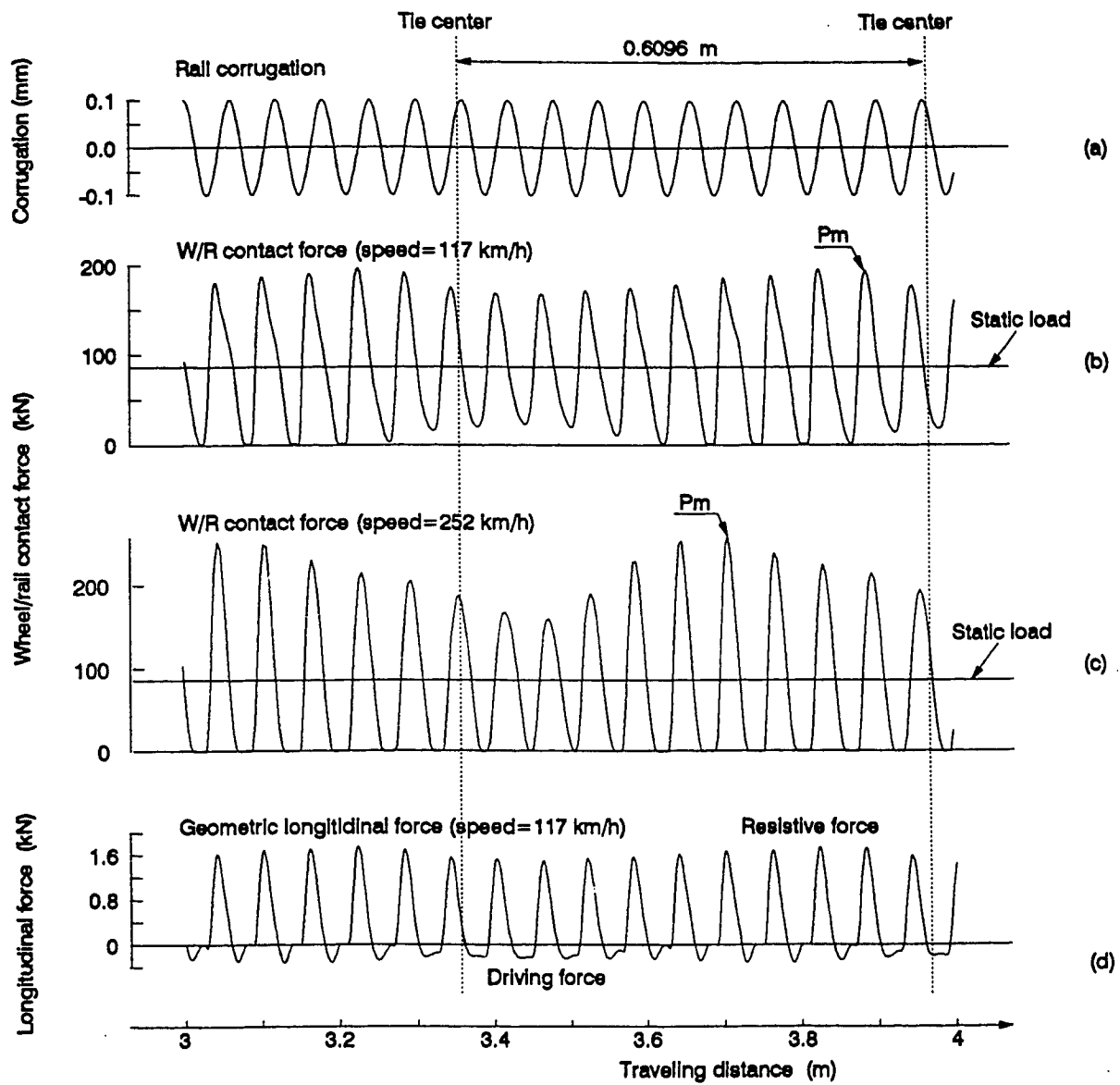


Figure 7.2 Dynamic responses due to rail corrugation

maximum peak contact force usually appears at the neighborhood of the tie center before the so-called pinned-pinned rail vibration modes are excited. This phenomenon is also observed in the FE model. The FE results show that if a system resonance is excited, the maximum peak may occurs in the second half of each tie spacing, as shown in Fig. 7.2(b). At a speed equal to 252 km/h, the first pinned-pinned mode is excited and the dynamic force reaches its maximum value. In this case, the peak is located around the midspan between two ties, as shown in Fig. 7.2(c). The same trend was also observed in [70],. however, the observed frequency (1167 Hz) of the pinned-pinned mode in this study is lower than that calculated from the formula proposed in [70], which may be expressed by:

$$f_{p-p} = \frac{1}{2\pi} (\pi / L_t)^2 \sqrt{E_r I_r / m_r} \quad (7.1)$$

which gives a value of 1470 Hz. The major reason for the discrepancy is that Eq. (7.1) is derived from Euler beam theory and it gives a higher value than that calculated from Timoshenko beam theory, which is used in this study.

The geometric longitudinal force due to the rail corrugation is shown in Fig. 7.2(d). The longitudinal force varies approximately in phase with the vertical dynamic force, which has a peak value on the up-hill side of the corrugation. The combination of these two forces may result in the forward flow of metal on the rail tread as corrugation is developed to some stage, which has been observed in the field [8]. The oscillation of the longitudinal force may also cause torsional vibration of the wheelset. The longitudinal force at the up-hill side is

always larger than that at the down-hill side of the corrugation. This generates a pure resistive force on the train and increases the energy consumption.

Fig. 7.3 shows the normalized vertical dynamic force vs. the vehicle speed. Several local maximum are shown in the figure and they correspond to various resonances in the vehicle-track system. The first resonance occurs at about 10 km/h and it is caused by the fundamental wheel/track frequency (47 Hz), in which the wheel, rail and tie move in phase. The second one is at about 45 km/h and it is caused by the second wheel/track frequency (210 Hz), in which the combined wheel-rail mass moves against the tie mass. The third one is at about 120 km/h at which the third bending mode (540 Hz) of tie is excited. The fourth one is at about (252 km/h) and it corresponds to the pinned-pinned mode (1167 Hz). Since the track system is considered to be symmetric, no asymmetric bending modes of the tie can be observed in the response. The first bending mode of the tie has its node point very close to the rail seat and it is not excited. The higher frequency modes of the tie do not show a strong effect on the dynamic force. This is probably because the vibration of rail at a very high frequency is relatively independent of the support conditions because of the isolation of the rail-pad. Comparing with the dynamic force due to the rail corrugation, the response due to the effect of tie spacing is small and it is difficult to be identified.

Fig. 7.4 shows the energy consumption due to the geometric longitudinal force on a corrugated rail at different speeds. It shows that the energy consumption is approximately proportional to the vertical dynamic force. The maximum energy consumption occurs as the pinned-pinned mode is excited. Fig. 7.5 shows how

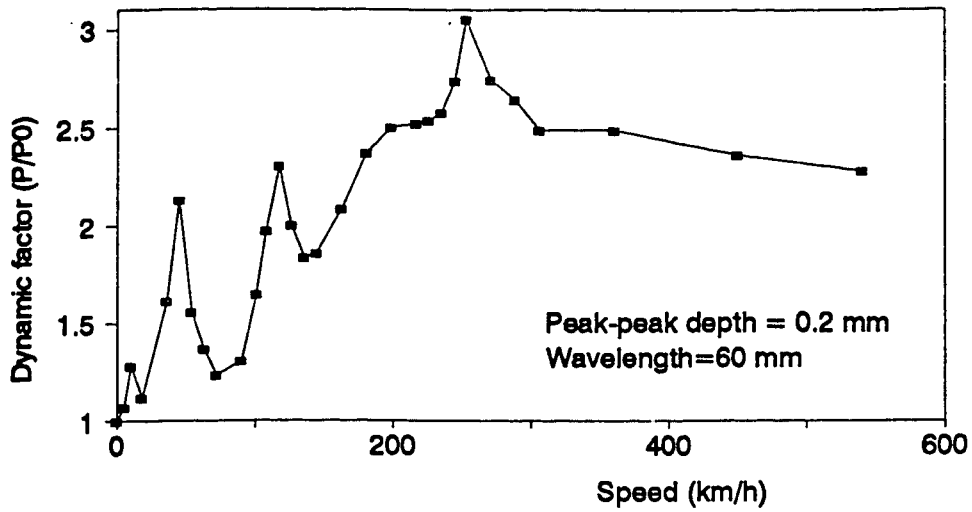


Figure 7.3 Dynamic force due to rail corrugation as a function of speed

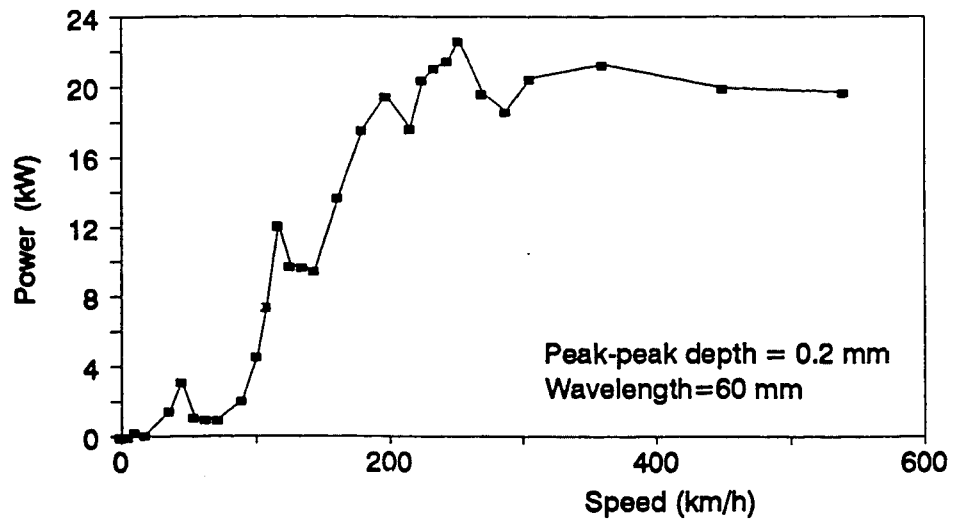


Figure 7.4 Work consumed per unit time on one wheel

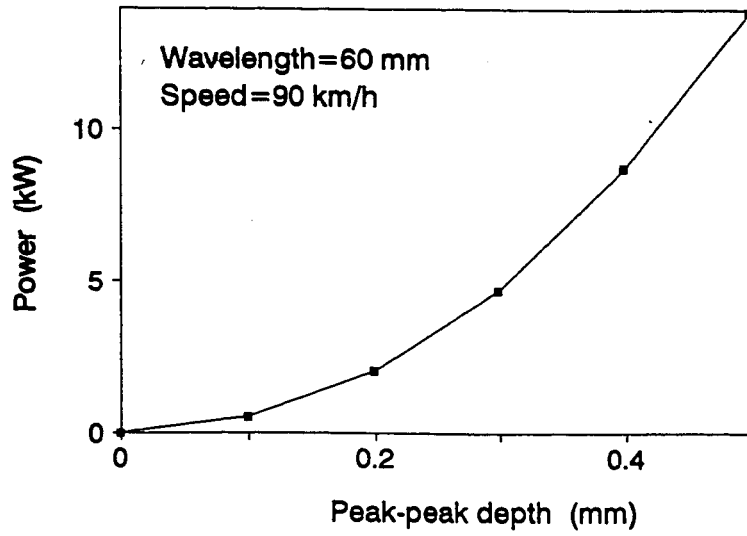


Figure 7.5 Effect of corrugation depth on energy consumption

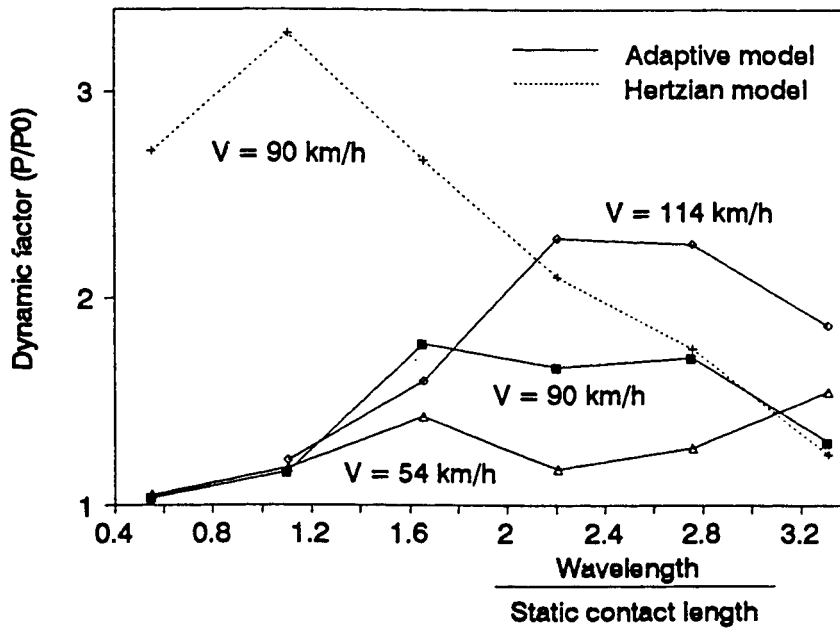
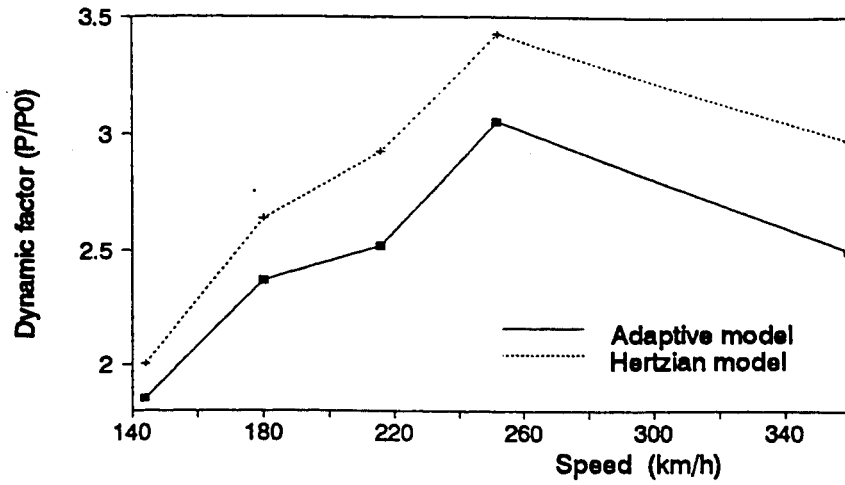


Figure 7.6 Effects of corrugation wavelength on dynamic force (Peak-peak depth=0.2 mm)

the energy consumption increases quadratically with the depth of the corrugation.

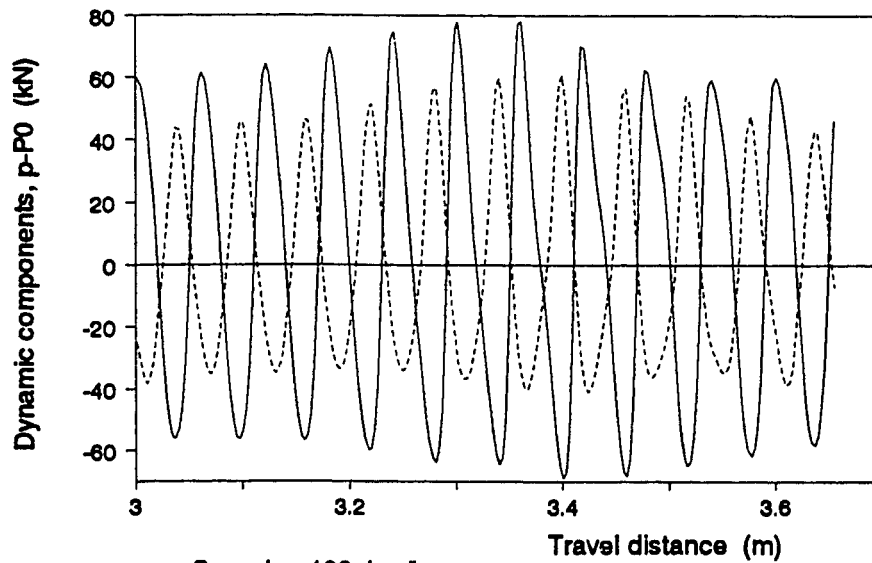
Fig. 7.6 shows the effect of corrugation wavelength on the dynamic wheel/rail contact force for a given depth of rail corrugation. The dynamic force is significantly suppressed by the contact patch as the corrugation wavelength is reduced to less than the static contact length. The contact force calculated with Hertzian contact model is significantly different from that obtained using the adaptive contact model as the corrugation wavelength is less than about 2.5 times of the contact length. The difference between the dynamic contact forces calculated from these two contact models generally increases with vehicle speed, as shown in Fig. 7.7. A single point contact spring can not take into account the effect of the contact patch and it may not be valid to predict the dynamic force due to a short wave irregularity.

The results presented in Fig. 7.6 also show that there is a local maximum for each speed for wavelength of corrugation in the range of 1.5-3 times of the contact length. This is resulting from the combination of two distinct factors. The first one is that the dynamic force generally increases with the reduction of the wavelength for a given wave depth, irrespective of the system resonant frequencies. This is because the slope of the input irregularity increases with the reduction of the wavelength for a given wave depth and vehicle speed. Secondly, when the wavelength is reduced to some stage, the overall slope of the wheel/rail overlap can no longer increase because of the effect of contact patch. Hence, the contact force reaches a local maximum before the wavelength is reduced to less than the static contact length. The position of this local maximum may be influenced by the system resonant frequencies. The actual



Wavelength=60 mm
 Peak-peak depth=0.2 mm

Figure 7.7 Effects of speed on dynamic force due to rail corrugation



Speed = 108 km/h
 — Initiating force
 - - - Across-wheel force
 Wavelength = 60 mm
 Peak-peak depth = 0.2 mm

Figure 7.8 Initiating and across-wheel forces due to a corrugation

wheel/rail contact length is usually in the range of 10-20 mm and hence the local maximum of the contact force should appear as the wavelength is about 15-60 mm. This range covers many of short-wave rail corrugations observed in the field [8,23,86]. Still, no corrugation with a dominated wavelength less than the static contact length has been observed in the field. Based on these observations, it is believed that the contact patch may influence in the formation and development of the short-wave rail corrugations.

7.3 DYNAMIC INTERACTION BETWEEN TWO WHEELS

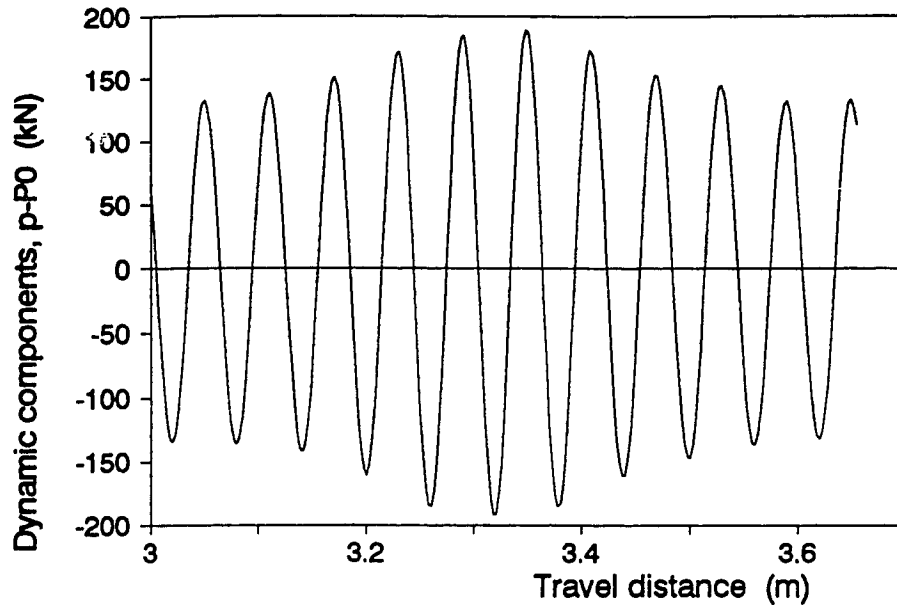
7.3.1 The mechanism of interaction

In this section, the 5-DOF vehicle model is employed to investigate the interaction between two wheels (on two wheelsets) caused by a sinusoidal rail corrugation. Fig. 7.8 shows the dynamic contact forces at two wheels purely due to the corrugation at the leading wheel. This figure clearly shows that the wheel/rail dynamic contact force generated at one wheel can partially be transmitted to a neighboring wheel in the adjacent wheelset and cause an interaction between them. In the following discussions, the force directly generated by an irregularity will be called "initiating force", and the force at the neighboring wheel caused by the initiating force will be called "across-wheel force".

The exciting frequencies of rail corrugations are usually in the high frequency range (larger than 20 Hz). Because the wheel and bogie (or sideframe) are usually massive, most part of the high frequency across-wheel force is not transmitted through the wheel-bogie-wheel chain but through the track system.

This is particularly true if a vehicle has a primary suspension system between the wheelset and bogie, which isolates high frequency vibrations of the wheel. The major component in the track system that transmits the across-wheel force is the rail because it has a relatively small equivalent mass and large stiffness. It is the wave propagation in the rail that mostly transmits the across-wheel force.

On the other hand, no matter how the across-wheel force is transmitted, the basic mechanism that controls the interaction between any two wheels is the principle of superposition. To show this, a corrugation is first assumed to be acting on the leading wheel and then on the trailing wheel, respectively, and the contact forces are calculated separately. Then the forces are superposed for each wheel to obtain the dynamic forces that should be for the case of both wheels excited by the corrugation. These forces are compared with the forces directly calculated when both wheels acted upon by the corrugation. As shown in Fig. 7.9, the forces calculated from both approaches are identical if the wheel/rail contact relationship is represented by a linearized contact spring. Fig. 7.10 is obtained by using the adaptive contact model in the calculations. Because of the non-linear wheel/rail contact, there is a difference between the peak values of the forces calculated from the two different approaches. This difference increases with the increase in the depth of corrugation because the variation of the wheel/rail overlap increases with the depth of corrugation, which increases the effect of non-linear factor in the wheel/rail contact. However, it is found that the non-linear contact relationship (adaptive contact model) has negligible effect on the phase relationship between the calculated responses from the method of superposition and direct approach, as shown in Fig. 7.10. Since the phase relationship among the initiating forces, across-wheel forces



Speed = 180 km/h

..... Calculated by superposition

———— Directly calculated

Wavelength = 60 mm, Peak-peak depth = 0.2 mm

Figure 7.9 Superposition of dynamic forces (linearized contact model)

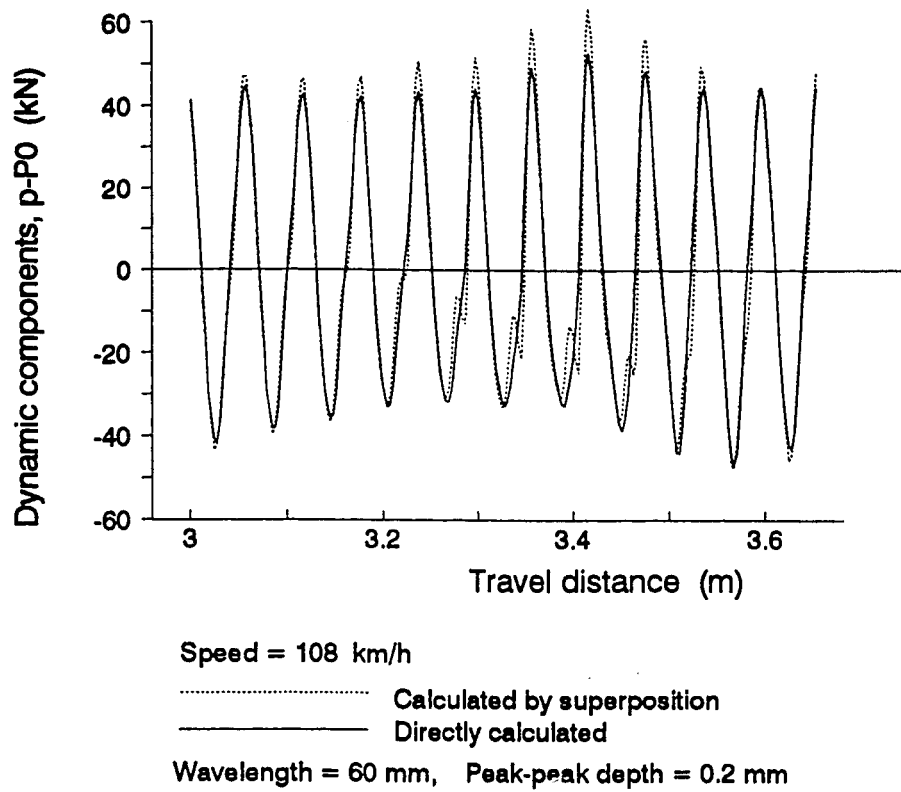


Figure 7.10 Superposition of dynamic forces (adaptive contact model)

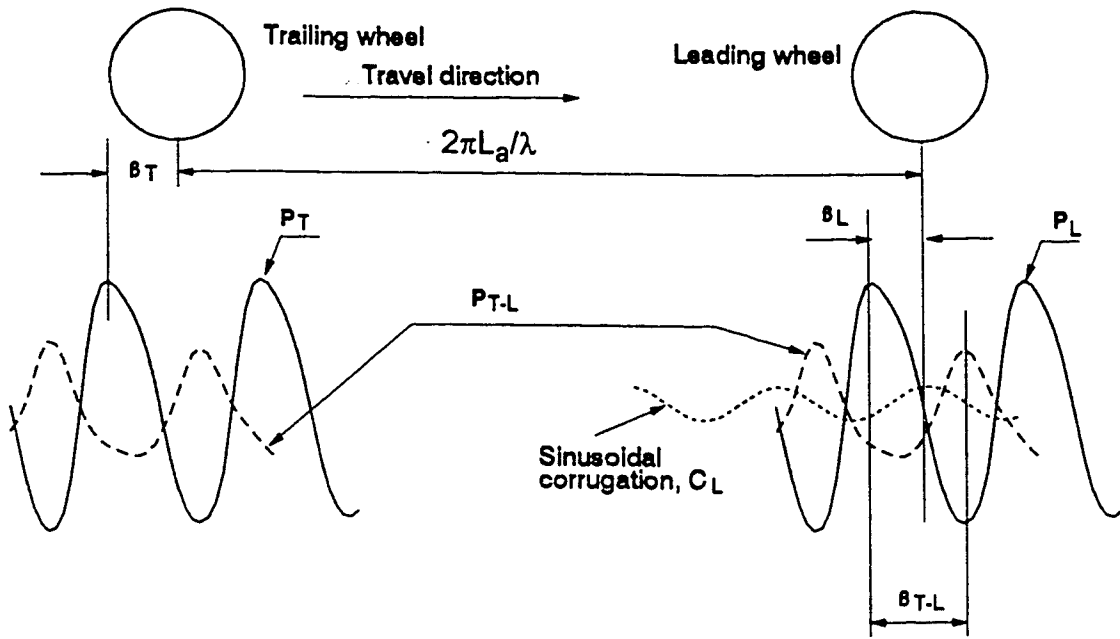
and exciting sources hold the key to understand the phenomena of the dynamic interaction between any two wheels on a corrugated track, the dynamic forces under corrugations calculated using the method of superposition is qualitatively valid.

7.3.2 Phase relationship between dynamic force and excitation

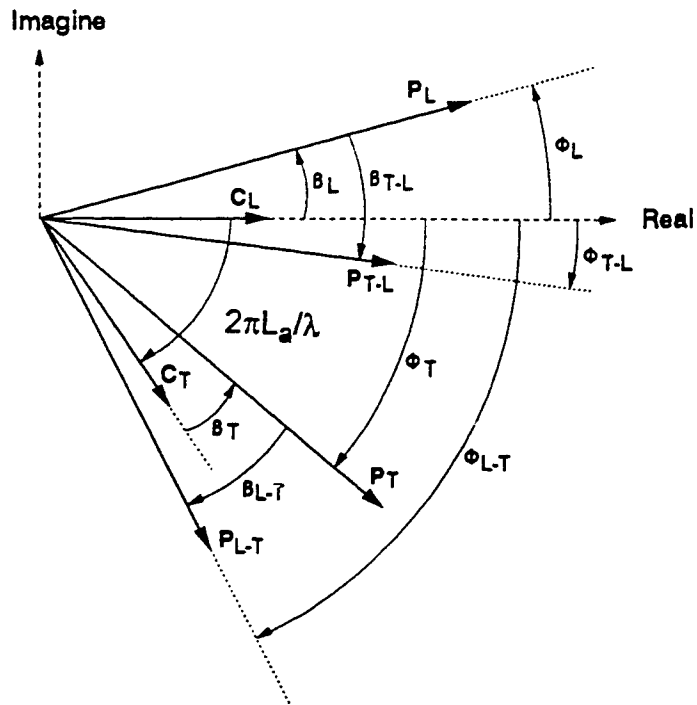
Figs. 7.11 shows phase relationship between the dynamic force and excitation source, which may be used to analyze the superposition of the total dynamic forces at the two wheels. In this figure, the phase of the exciting sinusoidal corrugation function at the leading wheel, C_L , is assumed to be zero and thus the corrugation vector at the trailing wheel, C_T , is $2\pi L_a/\lambda$. P_L and P_T are the initiating force vectors at the leading and trailing wheels, respectively. Their phase angles relative to the input corrugation at their respective wheels are β_L and β_T , respectively. P_{T-L} is the across-wheel force vector at the trailing wheel due to the initiating force at the leading wheel and it has a phase lag angle, β_{T-L} , relative to its initiating force. Similarly, P_{L-T} is the across-wheel force vector at the leading wheel due to the initiating force at the trailing wheel and it has a phase lag angle, β_{T-L} , relative to its initiating force. By taking the corrugation vector at the leading wheel as a reference, phase relationship among the force and excitation source may be expressed as following:

for the trailing wheel,

$$\Phi_T = \beta_T - 2\pi L_a/\lambda \quad \text{and} \quad \Phi_{T-L} = \beta_L - \beta_{T-L} \quad (7.2)$$



(a) Responses in time history



(b) Forces and exciting sources represented by vectors

Figure 7.1 Phase relationship among dynamic forces and exciting sources

and for the leading wheel,

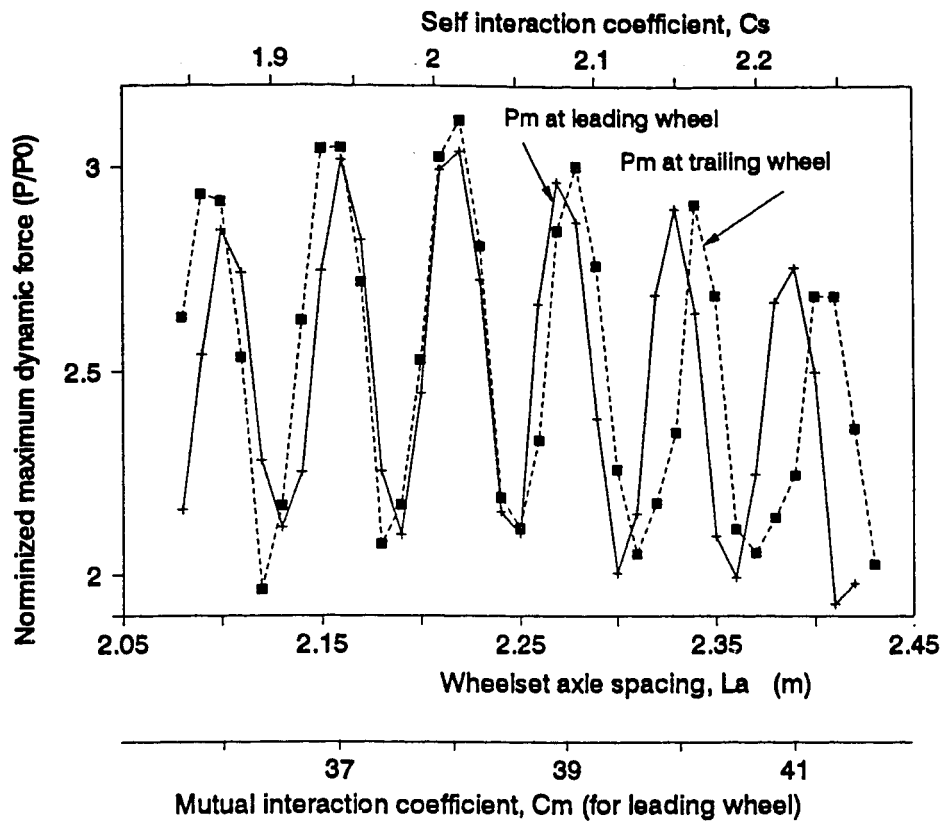
$$\Phi_L = \beta_L \quad \text{and} \quad \Phi_{L-T} = \beta_T - \beta_{L-T} - 2\pi L_a/\lambda \quad (7.3)$$

where L_a is the wheelset axle spacing, λ is the wavelength of corrugation. The total dynamic force at the each wheel depends on the phase difference between the initiating and across-wheel forces. This phase difference may be represented by a non-dimensional parameter, which will be called "mutual interaction coefficient". It is defined as:

$$C_m = |\Phi_i - \Phi_{i,j}|/2\pi \quad (7.4)$$

where i represents the wheel at which the total force is calculated, and j represents the wheel at which the across-wheel force is caused. If C_m is equal to an integer, the across-wheel force and the initiating force at the i -th wheel vary in phase and the total dynamic force reaches a resonant value, as shown in Fig. 7.12. This resonance is caused by the forces initiated at different wheels and thus it is called mutual interaction resonance in this study.

It is observed that the phase angles of initiating forces, β_L and β_T , mainly depend on the excitation frequency (V/λ) for a given depth of corrugation and they are approximately the same in a general case. Hence the difference between the phase angles of initiating and across-wheel forces, e.g., Φ_L and Φ_{L-T} , is mostly determined by β_{L-T} and the phase angle due to axle spacing ($2\pi L_a/\lambda$). It is observed that β_{T-L} (or β_{L-T}) is basically composed of two parts. The first part (ϕ_{f-d}) is due to the phase difference between the force and the displacement wave in the rail, or it may be regarded as the phase difference between the initiating



Speed = 180 km/h
 Corrugation wavelenth = 60 mm
 Peak-peak depth = 0.2 mm

Figure 7.12 Effect of wheelset axle spacing on maximum dynamic force due to a sinusoidal rail corrugation

force and the across-wheel force when wheelset axle spacing becomes zero, as shown in Fig. 7.13. The second part of β_{T-L} or β_{L-T} is due to the time delay for the rail displacement wave to travel from the one wheel to another wheel. Hence, β_{T-L} and β_{L-T} may be expressed as:

$$\beta_{T-L} = \phi_{f-d} - \frac{2\pi L_s V}{(V_w - V)\lambda} \quad (7.5)$$

$$\beta_{L-T} = \phi_{f-d} - \frac{2\pi L_s V}{(V_w + V)\lambda} \quad (7.6)$$

where V_w is the wave propagation speed in the rail and V is the train traveling speed.

As shown in Fig. 7.13, the values of β_{T-L} and β_{L-T} calculated from Eqs. (7.5) and (7.6), respectively, are consistent with the results directly calculated from the FE model. The wave propagation speed (V_w) estimated from the FE results is about 1369 m/s.

As shown in Fig. 7.14 or indicated in Eqs. (7.5) and (7.6), the across-wheel force at the trailing wheel has a different phase lag from that at the leading wheel. This is caused by the traveling motion of the vehicle. This difference increases with the vehicle speed. This demonstrates that it is appropriate to consider the vehicle as a moving system in the modeling of the vehicle-track interaction, especially for a high speed train. This phase difference also explains why the contact forces at the leading and trailing wheels are generally different even though the initiating forces on both wheels may be in phase (for the wheelset axle spacing equal to 2.28 m, 2.34 m, 2.4 m and et al.), as shown in Fig. 7.12.

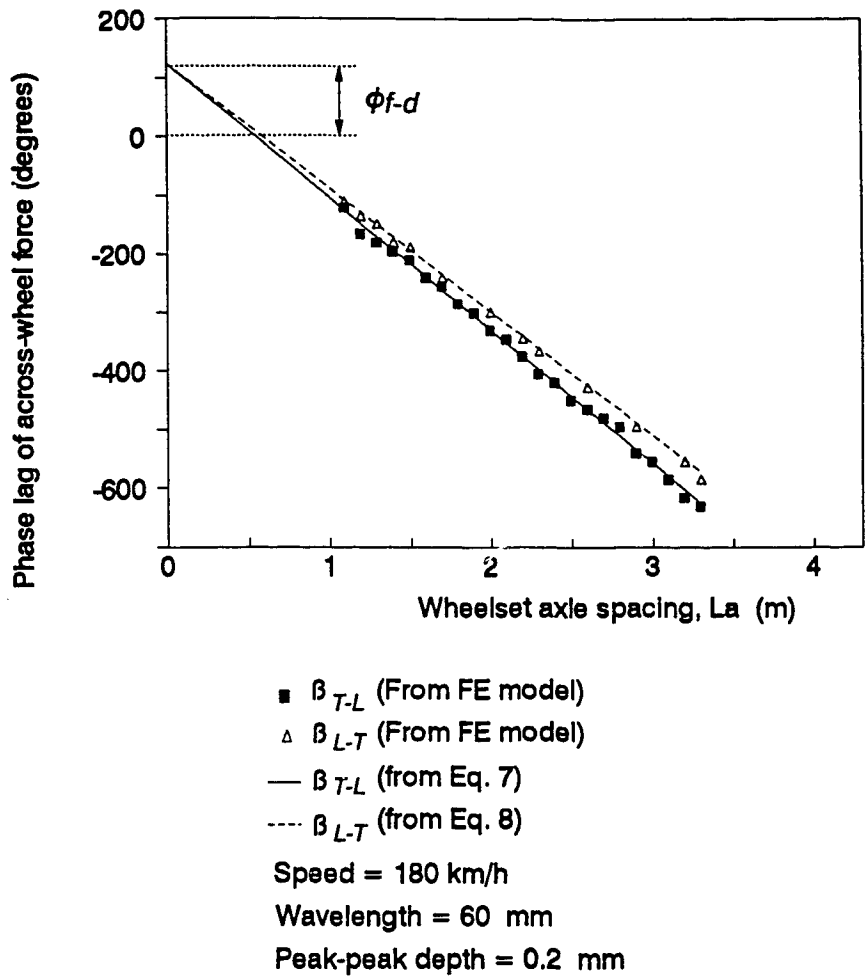
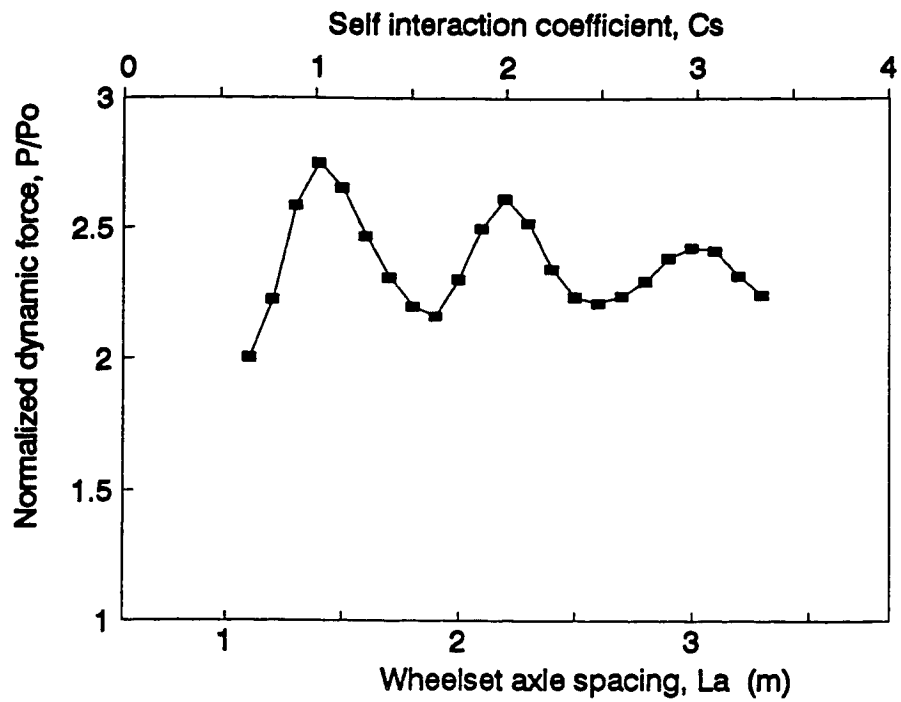


Figure 7.13 Effect of wheelset axle spacing on phase lag of across-wheel force due to a sinusoidal rail corrugation



Speed = 180 km/h
Wavelength = 60 mm
Peak-peak depth = 0.2 mm

Figure 7.14 The maximum peak dynamic force on trailing wheel purely due to a rail corrugation under trailing wheel

Fig. 7.12 also shows how the peak forces on the trailing and leading wheels are very sensitive to changes in the wheelset axle spacing (L_a) for a given speed (V) and corrugation wavelength (λ). This is because a small change in wheelset axle spacing, although does not change the phase angle of the across-wheel force significantly (mainly determined by Eq. 7.5 or 7.6), but causes a large change in the phase difference between the corrugation vectors at the trailing and leading wheels (C_T and C_L), represented by $2\pi L_a/\lambda$ (Fig. 7.11), and hence it is very sensitive to wheelset axle spacing. Another obvious phenomenon shown in Fig. 7.12 is that the total force at a wheel is approximately periodically changed with a wavelength equal to the corrugation wavelength. This is because the phase of the initiating force changes periodically with the wavelength of the corrugation.

Fig. 7.14 shows how the maximum dynamic force at the trailing wheel (purely due to the corrugation under this wheel or the corrugation on this wheel tread) is affected by the wheelset axle spacing. It is found that the across-wheel force itself can also generate another across-wheel force to affect the dynamic force at the original wheel at which the dynamic force is initiated. This demonstrates that the original force can be partially reflected back from a neighboring wheel. The phase relationship between the initiating force the reflected force may be represented by another interaction parameter, which will be called "self interaction coefficient". It is defined as:

$$C_s = |\beta_{L-T} + \beta_{T-L}|/2\pi \quad (7.7)$$

By substituting Eqs. (7.5) and (7.6) into Eq. (7.7), the self interaction coefficient may be expressed by:

$$C_s = |\varphi_{f-d}/\pi - 2L_a V / V_w / [(V_w^2 - V^2)\lambda]| \quad (7.8)$$

If C_s is equal to an integer, the initiating force and the reflected force are in phase and this causes the total force to reach a resonant value, as it can be seen in Fig. 7.14. This resonance is actually caused by the force generated at one wheel and thus it is called self interaction resonance in this study. Fig. 7.14 also shows that the dynamic force reduces with the increase of the axle spacing. This is because the dynamic wave dies down as it is traveling along the rail due to the energy consumption and dispersion in the track. As the self-interaction coefficient is equal to an even number, all the initiating and across-wheel forces on both wheels are approximately in phase. In this case, the mutual and self interaction resonances may happen simultaneously, as shown in Fig. 7.12.

The basic theory presented in this paper may be applied to analyze the interaction among the wheels for a whole train-track system. The dynamic forces on the two wheels within a wheelset may also be calculated using the principle of superposition. Based on the results presented above, it is expected that for some arrangements of wheelset axle spacings in a train, the dynamic forces at some wheels may be significantly different from those at other wheels as the train is traveling on a corrugated track.

7.4 SUMMARY

The vertical and geometric longitudinal dynamic forces due to a rail corrugation is calculated using the FE model. It is observed that the dynamic forces are

generally higher over a tie than that at the midspan between two ties but the location of the maximum force is reversed if the so-called 'pinned-pinned' modes are excited. A resonance may occur if the frequency of excitation due to a rail corrugation is equal to a natural frequency of the vehicle-track system, in which case the maximum peak contact force may occur in the second half of each tie spacing.

The energy consumption due to the geometric longitudinal force caused by a rail corrugation is evaluated. It is found that the energy consumption is approximately proportional to the amplitude of the vertical dynamic force and it reaches the maximum value when the so-called "pinned-pinned mode" is excited. The energy consumption increases quadratically with the depth of rail corrugation.

A local maximum of the dynamic force is observed as the excitation wavelength on the rail is about 1.5-3 times of the length of the wheel/rail static contact patch. It is further observed that the dynamic forces at two wheels are generally different from each other, even though all the conditions on the track and wheels are identical. Their difference may be significant in some cases and it is resulting from the interaction between the two wheels. The rail is the major transmission media in the interaction between two wheelsets. The basic mechanism that controls the interaction is the principle of superposition. The superposition of the initiating and across-wheel forces may cause a mutual interaction resonance and a self interaction resonance. The difference between the dynamic forces at two wheels due to a rail corrugation is strongly influenced by wheelset axle spacing.

CHAPTER 8

CONCLUSIONS AND RECOMMENDATIONS

8.1 HIGHLIGHT OF THE THESIS

The primary objective of this thesis is to investigate the characteristics of vertical dynamic forces due to wheel and rail irregularities through developing a comprehensive finite element model of vehicle-track system. The model for the rail is based on non-uniform Timoshenko beam. Care is taken in the modeling of track system to include realistic ties rail pads, ballast and subgrades. Four different track models, namely Timoshenko beam on discrete support model (TBDS); Euler beam on discrete support model (EBDS); Timoshenko beam on elastic foundation model (TBEF); and Euler beam on elastic foundation model (EBEF), are used with three different vehicle models. The three vehicle models are: 1-DOF carrying a constant load, 3-DOF single wheel with sprung and unsprung masses, and 5-DOF truck model with two axles and half car body.

A cutting and merging method along with a set of special boundary conditions is proposed to extend finite length of track to infinitely long track, which provides an approach to simulate a moving system on an infinite structure using the standard FE technique. This method is successfully used in the FE model developed in this investigation for the simulation of a vehicle traveling on the track model indefinitely with a time-dependent speed.

An adaptive wheel/rail contact model is developed to calculate the vehicle/track interaction forces in the vertical and longitudinal directions. This model can adapt to any irregularity on the wheel and rail tread in the vertical and

longitudinal direction. It can also be used to estimate the energy consumption due to geometric longitudinal contact force.

The developed model is capable of simulating wheel lift-off from the rail, rail lift-off from the tie and tie lift-off from the ballast. The model can further simulate the dynamic response under void and hard spot.

For all the various models developed in this study, considerable time and effort is devoted to validate them. The primary validation is achieved by comparing the results with the experimental data available in the literature (from British Rail and CP Rail Systems). The theoretical results calculated from the FE model, such as natural frequencies of concrete ties, the impact loads and dynamic strains on the rail, show good correlation with the experimental data. All validations are carried out in time domain to ensure that the model can simulate exact response behavior. Due to detailed FE modeling of the rail system a good quantitative correlation with experimental dynamic rail strain was possible giving added confidence in the model.

The validated FE model is employed to investigate the vertical dynamic response characteristics of the vehicle-track system, and the influences of system parameters on the dynamic response. The dynamic forces caused by the wheel flats and shells, rail joints and rail corrugations are currently a major concern to the railway industry and administrations. These are the major topics addressed and discussed in this study. This study also investigated the natural frequencies of concrete ties, wheelset and vehicle-track system, which are useful to understand the basic dynamic behaviors of the railway vehicle/track system.

For the first time, the rail-pad and ballast has been modeled as distributed spring-damping elements in the track mathematical model. However, this does not lead to a significant change in the wheel/rail contact force. This suggests that it is not necessary to consider these components in very detail if only the dynamic contact force and rail strains are of concern. Their detail models may be useful when the distributions of dynamic forces and strains in these components are required.

Specific conclusions drawn from each aspect of this study along with a list of recommendation for further work is presented in the following sections.

8.2 SPECIFIC CONCLUSIONS

8.2.1 Natural frequencies of vehicle-track system

- The mode shape of the fundamental coupled wheel/track natural frequency is very close to the deflection shape of the track under a constant load and hence it is an important vibration mode in the vehicle/track interaction.
- For evaluation of track frequency and wheel-track coupled frequency, it is sufficient to only consider the wheel-track system. On the other hand, the sprung mass frequencies can be evaluated effectively from the sprung mass and primary suspension.
- The foundation stiffness of track strongly affects the first bending frequency of a concrete tie but it has little influence on higher bending modes.

- Due to relatively large axle stiffness, the influences of primary suspension on the bending frequencies of wheelset are negligible.

8.2.2 Impact loads due to wheel flats and shells

- The impact loads are mainly affected by the shape and size of wheel and rail tread defects, axle load, vehicle speed and rail-pad stiffness.
- The impact load of a wheel on the rail over a tie is larger than that at the midspan.
- For a given set of system parameters and vehicle speed, there exists a special ratio (length/depth) of haversine wheel flat at which the impact load reach the maximum value.
- Reducing rail-pad stiffness to a certain level on a concrete-tie track may significantly reduce the dynamic load and the force transmitted to the concrete tie.
- Adding elastomeric shear pads on the wheelset bearing does not reduce the wheel/rail dynamic contact force but it may reduce the dynamic force on the bearing.
- The FE modeling shows that the dynamic force derived from the net shear strain differential is basically consistent with the wheel/rail contact force. This suggests that the basic principle used in the detector is sound.

- The dynamic force on one wheel is affected by those on its neighboring wheels. The major media that transmits the dynamic waves is the rail. The basic mechanism that control the interaction between two wheels is the superposition of the dynamic force directly generated at one wheel and the across-wheel force that is caused by the dynamic force at a neighboring wheel.

8.2.3 Dynamic force due to a dipped-rail joint

- Increasing axle load and rail equivalent mass significantly increase the first peak load (P_1). The wheel (unsprung) mass, stiffness of bearing rubber pad, and ballast stiffness mainly affect the second peak load (P_2).
- The dynamic force at one wheel at the joint is affected by those at its neighboring wheels. The basic mechanism that control the interaction between wheels is the same as that in the case of impact loads due to wheel flats and shells.

8.2.4 Steady-state interaction between vehicle and track

- The characteristics of the track dynamic deflection in the comprehensive vehicle-track model are basically the same as those of an infinitely beam on a damped Winkler foundation subjected to a moving constant load. This suggests that it is fairly well to use a beam on Winkler foundation to study the steady-state response of the track. This study also confirms that the steady-state response of track subjected to a moving force does exist.

- The response of the whole system at the so-called 'critical speed' does not show a significant difference from those at other speeds, except that the track deflection reaches its maximum value. This critical speed does not mean an unstable situation in the vehicle/track interaction.
- There are two types of distinct periodic dynamic waves in the history of the wheel/rail contact force. The first one is caused by the variation of overall track stiffness due to the effect of tie spacing. The second one is caused by the traveling motion of wheel and the oscillations of discrete supports. In the present train speed range, the magnitudes of these dynamic forces are usually less than 5% of static load, except that the coupled wheel/track resonant frequencies are excited at some speeds.
- The resonant forces due to discrete supports may be larger than 5% of static load in some cases. The magnitude of the resonant force mainly depends on the unsprung mass, tie spacing, vehicle primary and track ballast damping, rail stiffness and the stiffness on each support.
- The dynamic force due to a full void is similar to the case of increasing the tie spacing in a steady-state interaction. The force originally transmitted to the tie is shared by neighboring ties if a void happens. In the case of hard spot, more force is concentrated on a tie at the hard spot location.

8.2.5 Response to rail corrugation

- Dynamic force due to rail corrugation is higher over a tie than that at midspan. If corrugation frequency is equal to system response, the peak

force occur in the second half of tie spacing. The force is maximum with peak at the midspan of tie when so called "pinned-pinned" mode is excited.

- The energy consumption is approximately proportional to amplitude of vertical dynamic force that reaches a maximum value for "pinned-pinned" mode. The energy consumption increases quadratically with the depth of rail corrugation.
- Dynamic force at the two wheels are different due to interaction between them, where rail is the major transmission media. The force difference between the two wheels is strongly influence by the axle spacing.
- The influence of irregularities with wavelengths less than the wheel/rail contact length on the dynamic force is significantly suppressed. There is a local maximum of the dynamic force for the wavelength in the range of 1.5-3 times of the length of the wheel/rail static contact patch.

8.3 RECOMMENDATIONS FOR FUTURE STUDIES

- The present study provided a significant insight on the problems associated with wheel and track defects. For this, more attention is directed towards the track system modeling with simplified approach to vehicle model. Here no attempt is made in evaluating vehicle ride quality and suspension system. A list of further studies that can be carried out with the developed model along with recommendation for model improvement is presented in this section.

- The 5-DOF vehicle model can be used to evaluate vehicle ride quality and influence of primary and secondary suspension on the vehicle ride characteristics.
- In the vehicle/track system model developed, the vehicle and track is modeled separately. The in-plane vehicle model can easily be extended to include two trucks with four wheelsets and a complete carbody. Such model can be studied for vertical and rock motion.
- Similar to above, any number of trucks and wheelsets can be incorporated with FE track model to investigate wheel/rail interaction in a train. However, this will require an increase in the track length and computation time.
- The developed model is valid for majority of the problems in the vertical dynamics of vehicle-track system. Further studies can be carried out to study other aspects listed in Table 1.1, including noise studies.
- The FE model developed may be used to further investigate the influence of non-linear factors on the force measurement. This then can be incorporated in the measurement device for better accuracy.

Further model refinement of FE model

- An improvement on the present model should be aimed at increasing the computation efficiency and reducing the memories required. This may be achieved by using the matrix reduction technique and the FE-transfer matrix method.

- The ballast and subgrade mass may be included in FE model to investigate settlement of track bed.
- The model can be further refined by including bending vibration of wheelsets as it has been shown to have some influence in the dynamic force [4].
- Impact load in frozen track is greater than unfrozen track [37,107]. Hence attempts can be made to make provision for change in appropriate system parameter with temperature, in order to simulate frozen condition.
- For better understanding of rail corrugation formation, the model should be extended to include vertical, lateral, longitudinal and rotational motions of wheel and track. The non-linear characteristics of creep forces generated at the contact point should also be incorporated in the FE model.
- The model should be extended to 3-D representation to include two track, and complete wheelset to examine interaction between left and right wheels, and tracks.

REFERENCES

- 1 **Acharya, D.R. and Guins, T.S.,** "Economic analysis of high impact load wheels," *Technology Digest, TD93-013*, Dec. 1993.
- 2 **Achenbach, J.D. and Sun, C.T.,** "Moving load on a flexibly supported Timoshenko beam," *Int. J. Solids Structures*, 1965, **1**, 353-370.
- 3 **Ahlbeck, D.R.,** "*Program IMPWHL user's manual*," Battelle Columbus Laboratories, Columbus, Ohio, U.S.A, 1986.
- 4 **Ahlbeck, D.R.,** "A review of rail behavior under wheel/rail impact loading," *Report No. DOT-FRA-ORD-86-01*, U. S. Department of Transportation, Federal Railroad Administration, Washington DC, 20509, 1986.
- 5 **Ahlbeck, D.R.,** "The effects of railroad wheel profile roughness on impact loads and train resistance," *3rd International Heavy Haul Railway Conference*, October 1986, Paper No. IB-12.
- 6 **Ahlbeck, D.R. and Hadden, J.A.,** "Measurement and prediction of impact loads from worn railroad wheel and rail surface profiles," *ASME Trans. Journal of Engineering for Industry*, 1985, **107(2)**, 14-22.
- 7 **Ahlbeck, D.R.,** "An investigation of impact loads due to wheel flats and rail joints," *ASME Paper No. 80-WART-1*, 1980.
- 8 **Ahlbeck, D.R.,** "Investigation of rail corrugations on the Baltimore Metro - literature review," Interim Report, MTA-23-9002-2, Sept. 1989.
- 9 **Ahlbeck, D.R. and Harrison, H.D.,** "The effects of wheel/rail impact loading due to wheel tread runout profiles," *Proc. 9-th Int. Wheelset Congress*, Montreal, Paper 6-1, 1988.
- 10 **Ahlbeck, D.R., Meacham, H.C. and Prause, R.H.,** "The development of analytical models for railroad track dynamics," *Railroad Track Mechanics & Technology*, Edited by Arnold D. Kerr, 1975.
- 11 **Association of American Railroads,** Field manual of the interchange rules, Edition 1985.
- 12 **Ayabe, T., Sueoka, A. and Tamura, H.,** "Coupled vibrations between railway vehicle wheels and a rail," *JSME International Journal, Series III*, 1988, **31(1)**, 75-83.

- 13 **Birmann, F.**, "Track parameters, static and dynamic, interaction between vehicle and track," *Proc. I. Mech. E., Part 3F*, 1965-1966, **180**, 73-85.
- 14 **Björk, J.** "Dynamic loading at rail joints - effect of resilient wheels," *Railway Gazette*, 1970, 430-434.
- 15 **Blejwas, T.E., Feng, C.C. and Ayre, R.S.**, "Dynamic interaction of moving vehicles and structures," *J. Sound Vibr.*, 1979, **67**(4), 513-521.
- 16 **Bogacz, R. and Dzula, S.**, "Dynamics and stability of a wheelset in rolling contact motion on rails," *Proc. of International Symposium on Technological Innovation in Guided Transports*, Lille, France, Sept. 1993.
- 17 **Cai, C. W., Cheung, Y. K. and Chan, H. C.**, "Dynamic response of infinite continuous beams subjected to a moving force - an exact method," *Journal of Sound and Vibration*, 1988, **123**(3), 461-472.
- 18 **Cai, Z and Raymond, G. P.**, "Theoretical model for dynamic wheel/rail and track interaction," *Proceedings of Tenth International Wheelset Congress*, Sydney, Australia, Oct. 1992.
- 19 **Capron, M.D. and Williams, F.W.**, "Exact dynamic stiffnesses for an axially loaded uniform Timoshenko member embedded in an elastic medium," *J. Sound Vibr.*, 1988, **124**(3), 453-466.
- 20 **Captain, K. M., Boghani, A. B. and Wormley, D. N.**, "Analytical tire model for dynamic vehicle simulation," *Vehicle System Dynamics*, 1979, **8**, 1-32.
- 21 **Choros, J. and Adams, G. G.**, "A steadily moving load on an elastic beam resting on a tensionless Winkler foundation," *J. of Applied Mechanics*, 1979, **46**, 175-180.
- 22 **Cifuentes, A. O.**, "Dynamic response of a beam excited by a moving mass. *Finite Element in Analysis and Design*," *Transaction of the ASME*, 1989, **5**, 237-246.
- 23 **Clark, R.A.**, "*Slip-stick vibrations may hold the key to corrugation puzzle*," *Railway Gazette International*, July 1984, pp. 531-533.
- 24 **Clark, R.A., Dean, P.A., Elkins, J.A. and Newton, S.G.**, "An investigation into the dynamic effects of railway vehicles running on corrugated rails," *J. of Mech. Eng. Science*, 1982, **24**(2), 55-66.

- 25 **Clark, R.A. and Lowndes, V.P.,** "Discrete support track dynamics model - theory and program guide," *British Rail Research Technical Memorandum TMTS95*, May 1979.
- 26 **Cowper, G.R.,** "The shear coefficient in Timoshenko's beam theory," *J. of Applied Mechanics*, 1966, 335-340.
- 27 **Dahlberg, T.,** "Dynamic interaction between train and track: a literature survey," *Report F120*, Division of Solid Mechanics, Chalmers University of Technology, 1989.
- 28 **Dahlberg, T.,** "Structural responses to moving forces determined by reciprocity relations," *Vehicle System Dynamics*, 1990, 113-130.
- 29 **Dahlberg, T.,** "Vehicle-bridge interaction," *Vehicle System Dynamics*, 1984, 13(4), 187-206.
- 30 **Dahlberg, T., Fenander, A., Igeland, A. and Nielsen, J.,** "Railway vehicle on randomly profiled track," *Chalmers University of Technology, Solid Mechanics Report F137*, Gotheburg, 1991.
- 31 **Dahlberg, T. and Nielsen, J.,** "Dynamic behavior of free-free and in-situ concrete railway sleepers," *Chalmers University of Technology, Solid Mechanics Report F138*, Gotheburg. 1991.
- 32 **David, R.** "How resilient pads protect concrete sleepers," *Railway Gazette International*, 1988, pp. 85-87.
- 33 **Dawn, T.** "Ground vibrations from heavy freight trains," *J. Sound Vibr.*, 1983, 87, 351-356.
- 34 **Dean, F.E. and Harrison, A.D.,** "Laboratory study to determine the effects of tie pad stiffness on the attenuation of impact strain in concrete railway ties," *Report by Battelle Columbus Laboratories to the Federal Railroad Administration, Improved Track Structures Research Division*, Washington, June, 1981.
- 35 **Dean, F.E., Ahlbeck, D.R., Harrison, H.D., and Tuten, J.M.,** "Effect of tie pad stiffness on the impact loading of concrete ties," *2nd International Heavy Haul Railway Conference*, 1982, Paper No. 82-HH-41.
- 36 **de Jozes, B., Kendrik, A. and Pak, W.,** "Controlled tests and coal train monitoring with the Salient wheel impact detector," *Report No. T-993-88*, Research and Development, CP Rail System, November 1988.

- 37 **de Josez, B.**, "Controlled tests with the Salient wheel impact detector under frozen track conditions - Phase II," *Report No. T-1013-89*, Research and Development, CP Rail System, 1989.
- 38 **Delfpsse, P.**, "Very high speed train tests," *Vehicle System Dynamics*, 1992.
- 39 **Dhir, A.**, Ride dynamics of high mobility wheeled/tracked offroad vehicles: computer simulation with field validation, Ph.D thesis, Dept. of Mechanical Engineering, Concordia University, 1993.
- 40 **Dong, R.G., Sankar, S. and Dukkupati, R.V.**, "A finite element model of railway track and its application to wheelflat problem," *J. of Rail an Rapid Transit, Proc Inst. Mech Engrs*, 1994, (in press).
- 41 **Duffy, D.G.**, "The response of an infinite railroad track to a moving vibrating mass," *J. of Applied Mechanics, Transaction of the ASME*, 1990, 57, 66-73.
- 42 **Ehrenbeck, R., and Polcari, S.**, "Vehicle/track interaction assessment Techniques," *Report No. DOT-FRA-ORD-84/01.2*, U. S. Department of Transportation, Federal Railroad Administration, Washington DC, 20509, 1984.
- 43 **Eisenmann, J.**, "Railroad track structure for high-speed lines," *Contact Mechanics and Wear of Rail/Wheel Systems*, University of Waterloo Press, 1982.
- 44 **Elkins, J. A.**, "Prediction of wheel/rail interaction: the state-of-the-art," *Proc. 12th IAVSD Symposium* held in Lyon, France, 1991.
- 45 **El-Sibaie, M.A.**, "On the components of track damping measurements," *ASME Applied Mechanics / Rail Transportation symposium*, AMD Vol. 96, Rtd Vol. 2, 1988.
- 46 **El-Sibaie, M. and Klauser, P. E.**, "A beam on elastic foundation track model for use in a multi-body system simulation," *Transportation System 1990, Winter Annual Meeting of the ASME*, Dallas, U. S. A., Nov. 1990, 149-156.
- 47 **Fan, Q.H. and Zhao, J.J.**, "Analyses on mechanism of rail corrugation and studies with model tests - effect of the bending vibration of wheelset on rail corrugation," *AMD Symp, ASME Appl. Mech. Div. v96, Applied Mechanics Rail Transportation Symposium*, 1988, 141-148.

- 48 **Fastenrath, F.**, Railroad track theory and practice, English Edition by Frederick Ungar Co., Inc., New York, 1981.
- 49 **Fermer, M. and Nielsen, J.C.O.**, "Wheel/rail contact forces for flexible versus solid wheels due to tread irregularities," *Proc. of the 13th IAVSD Symposium on the Dynamics of Vehicle on Roads and on Tracks*, Chengdu, China, Aug. 1993.
- 50 **Filho, F.V.**, "Finite element analysis of structures under moving loads," *The Shock and Vibration Digest*, 1978, 10(8), 27-35.
- 51 **Fingberg, U.**, "A model of wheel-rail squealing noise," *J. Sound Vibr.* 1990, 143, 365-377.
- 52 "Focus on corrugations," *Progressive Railroading*, December 1985, pp42-46.
- 53 **Frederik, C. O.**, "A rail corrugation theory," *Proc. of the Second Symposium on Contact Mechanics and Wear of Wheel/Rail Systems*, Rhode Island, USA. 1986.
- 54 **Fryba, L.**, "Dynamic interaction of vehicles with tracks and roads," *Vehicle System Dynamics*, 1987, 16, 129-138.
- 55 **Fryba, L.**, Vibration of solids and structures under moving load, Noordhoff International Publishing, Groningen, The Netherlands, 1972.
- 56 **Fryba, L. Nakagiri, S. and Yoshikawa, N.**, "Stochastic finite elements for a beam on a random foundation with uncertain damping under a moving force," *J. of Sound and Vibration*, 1993, 163(1), 9-27.
- 57 **Ganesan, N. and Ramesh, T. C.**, "Free vibration analysis of composite railway wheels," *J. of Sound and Vibration*, 1992, 153(1), 113-124.
- 58 **Garg, V.K. and Dukkipati, R.V.**, Dynamics of railway vehicle systems, Academic Press, 1984.
- 59 **Gladwell, G. M. L.**, Contact problems in the classical theory of elasticity, Alphen aan den Rijn: Sijthoff and Noordhoff, 1980.
- 60 **Gorman, D. J.**, Free vibration analysis of beams and shafts, John Wiley & Sons, 1975.
- 61 **Grassie, S.L.**, "Corrugation on Australian National: cause, measurement and rectification," 4th Intl. Heavy Haul Conf., Brisbane, 1989.

- 62 **Grassie, S.L.**, "A contribution to dynamic design of railway track," Proc. 12th IAVSD Symposium held at Lyon, 1991.
- 63 **Grassie, S.L.**, "Corrugation: Variations on an enigma," *Railway Gazette International*, July 1990, 531-533.
- 64 **Grassie, S.L.**, "Behavior in track of concrete sleepers with resilient railpads," *J. of Rail an Rapid Transit, Proc Inst. Mech Engrs*, 1989, 203, 97-101.
- 65 **Grassie, S. L. and Cox, S. J.**, "The dynamic response of railway track with flexible sleepers to high frequency vertical excitation," *Proc Inst. Mech Engrs*, 1984, 189D(7), 117-124.
- 66 **Grassie, S. L. and Cox, S. J.**, "The dynamic response of railway track with unsupported sleepers," *Proceedings of Institution of Mechanical Engineers, Part D*, 1985, 199(2), 123-135.
- 67 **Grassie, S. L., Gregory, R. W., Harrison, D. and Johnson, K. L.**, "The dynamic response of railway track to high frequency vertical excitation," *Journal of Mechanical Engineering Science*, 1982, 24(2), 77-90.
- 68 **Grassie, S.L, Gregory, R.W. and Johnson, K.L.**, "The dynamic response of railway track to high frequency lateral excitation," *Journal of Mechanical Engineering Science*, 1982, 24(2), 91-95.
- 69 **Grassie, S.L, Gregory, R.W. and Johnson, K.L.**, "The dynamic response of railway track to high frequency Longitudinal Excitation," *Journal of Mechanical Engineering Science*, 1982, 24(2), 97-102.
- 70 **Grassie, S.L., Gregory, R.W. and Johnson, K.L.**, "The dynamic loading of rails at corrugation frequencies," *Contact Mechanics and Wear of Rail/Wheel Systems*, University of Waterloo Press, 1982.
- 71 **Harrison, H.D., Dean, F.E., Selig, E.T. and Stewart, H.E.**, "Correlation of concrete tie track performance in revenue service and at the Facility for Accelerated Service Testing," *Report, No. DOT/FRA/ORD-84/021*, U.S. Department of Transportation, Washington, August 1984.
- 72 **Harrison, H.D. and Ahlbeck, D.R.**, "Railroad track structure performance under wheel impact loading," *Transportation Research Board, 66th Annual Meeting*, Washington, D.C., Jan. 1987.

- 73 **Harrison, H.D., Bethune, A.E. and Ahlbeck, D.R.,** "Comparison of measured and predicted impact loads on 100 Ton coal Gondolas," *Proc. 4th Int. Heavy Haul Railway Conference*, Brisbane, 1989, 409-413.
- 74 **Hay, W.W.,** Railroad engineering, John Wiley & Sons, 1982.
- 75 **Hempelmann, K., Hiss, F., Knothe, K. and Ripke, B.,** "The formation of wear patterns on rail tread," *Wear*, 1991, **144**, 179-195.
- 76 **Hampton, R.D.,** "Rail corrugation - Experience of U.S. transit properties," *Transportation Research Record 1071*, 1988, 16-18.
- 77 **Hu, Y.S, Dong, R.G. and Sankar, S.,** "An investigation of dipped rail joints," *IVC'94*, Beijing, China, 1994.
- 78 **Huang, T. C. and Shah, V. N.,** "Elastic system moving on an elastically supported beam," *J. Vib. Acoustics Stress Reliability Des. ASME*, 1984, **106**, 292-297.
- 79 **Igwemezie, J.O. and Mirza, M.S.,** "Impact load distribution in concrete bridge ties," *Journal of Structural Engineering*, 1989, **115**(3).
- 80 **Jenkins, H. H., Stephenson, J. E., Clayton, G. A., Morland, J. W. and Lyon, D.** "The effect of track and vehicle parameters on wheel/rail vertical dynamic forces," *Railway Eng. J.*, 1974, 2-16.
- 81 **Jezequel, L.,** "Response of periodic systems to a moving load," *J. of Applied Mechanics*, 1981, **48**, 613-618.
- 82 **Johnson, K.L.,** Contact mechanics, Cambridge University Press, 1984.
- 83 **Joint Committee on Relation Between Track and Equipment of the Mechanical and Engineering Division, AAR,** "Effect of flat wheels on track and equipment," *AAR Report No. MR-113*, May 1951.
- 84 **Kalker, J. J.,** "Survey of wheel-rail rolling contact theory," *Vehicle System Dynamics*, 1979, **8**, 317-358.
- 85 **Kalker, J. J.,** "A simplified theory for Non-Hertzian contact," *Proceedings 8th IAVSD Symposium*, Cambridge, Massachusetts, USA, 1983.

- 86 Kalousek, J. and Johnson, K.L., "An investigation of short pitch wheel and rail corrugations on the Vancouver mass transit system," *J. of Rail and Rapid Transit, Proc Instn Mech Engrs*, 1992, 206F, pp. 127-135.**
- 87 Kenney, J.T., "Steady-state vibrations of beam on elastic foundation for moving load," *J. Appl. Mech.*, 1954, 76, 359-364.**
- 88 Kerr, A.D., "The continuously supported rail subjected to an axial force and a moving load," *Int. J. Mech. Sci.*, 1972, 14, 71-78.**
- 89 Kerr, A.D., "On the vertical modulus in the standard railway track analysis," *Rail International*, November 1987.**
- 90 Kerr, A.D., "Continuously supported beams and plates subjected to moving loads - a survey," *SM Archives*. 1981, 6(4), 401-449.**
- 91 Kaper, H.P., "Wheel corrugation on Netherlands railways (NS): origin and effects of 'polygonization' in particular," *Journal of Sound and Vibration*, 1988, 120(2), 267-274.**
- 92 Knothe, K. and Grassie, S.L., "Modeling of railway track and vehicle/track interaction at high frequencies," *Vehicle System Dynamics*, 1993, 22, 209-262.**
- 93 Knothe, K. and Ripke, B., "The effects of the parameters of wheelset, track and running conditions on the growth rate of rail corrugations," *Proceedings of 11th IAVSD Symposium*, Kingston, Canada, 1989, 345-356.**
- 94 Knothe, K., Willner, K. and Strzykowski, Z., "Rail vibrations in the high frequency range," *J. of Sound and Vibration*, 1993.**
- 95 Kuroda, S., "Dynamic variation of wheel load attributed to vertical deformation of rail end," *Q. Rep., JNR*, 1973, 14(3), 143-144.**
- 96 Lin, Y. H. and Trethewey, M.W., "Finite element analysis of elastic beams subjected to moving dynamic loads," *J. of Sound and Vibration*, 1990, 136, 323-342.**
- 97 Lin, Y.H. and Trethewey, M.W., "Active vibration suppression of beam structures subjected to moving loads: a feasibility study using finite elements," *J. of Sound and Vibration*, 1993, 166(3), 383-395.**

- 98 Lyon, D. "The calculation of track forces due to dipped rail joints, wheel flats and rail welds," Paper presented at the Second ORE Colloquium on *Technical Computer Programs*, May 1972.
- 99 Mair, R.I., "Natural frequency of rail track and its relationship to rail corrugation," *I.E.Aust., Civil Eng. Trans.*, CE19(1), 1977.
- 100 Mair, R.I. and et al., "The characteristics and control of long pitch rail corrugation at heavy axle loads," *Proceedings, Heavy Haul Conference*, Perth, Western Australia, Paper I.8, 1978.
- 101 Mair, R.I., "Aspects of railroad track dynamics (Part I: Vertical Response)," *BHP Melb. Res. Labs Rep. MRL 81/3 (BHPMNM/RDC/74/017)*, Feb. 1974.
- 102 Mair, R.I., "The rail as a beam on a stiffening elastic foundation," *Rail International*, August 1976.
- 103 Meacham, H.C. and Ahlbeck, D.R., "A computer study of dynamic loads caused by vehicle-track interaction," *ASME Paper No. 69-RR-1*, 1969.
- 104 Mead, D.J., "Free wave propagation in periodically supported infinite beams," *J. of Sound and Vibration*, 1970, 187-197.
- 105 Mead, D.J., "A new method of analyzing wave propagation in periodic structures: application to periodic Timoshenko beams and stiffened plates," *J. of Sound and Vibration*, 1986, 104, 9-27.
- 106 Munjal, M. L., and Hechl, M., "Vibrations of a periodic rail-sleeper system excited by an oscillating stationary transverse force," *J. of Sound and Vibration*, 1982, 81(4), 491-500.
- 107 Newton, S.G. and Clark, R.A., "An investigation into the dynamic effects on the track of wheel flats on railway vehicles," *J. of Mech. Eng. Science*, 1979, 21(4), 287-297.
- 108 Nielsen, J.C.O., "Dynamic interaction between wheel and track - a parametric search towards an optimal design of rail structures," *Vehicle System Dynamics*, 1993 (in press)
- 109 Nielsen, J.C.O. "Coupling of moving and stationary dynamic systems - theoretical and experimental analysis of railway structures considering wheel and track imperfections," *Dissertation*, Chalmers University of Technology, Goteborg, Sweden, Dec. 1993.

- 110 Nielsen, J.C.O. and Abrahamsson, T.J.S., "Coupling of physical and model components for analysis of moving nonlinear dynamic systems on general beam structures," *Int. J. Numer. Meth. Engng.*, 1992, **33**, 1843-1859.
- 111 Olsson, M., "Finite element, modal co-ordinate analysis of structures subjected to moving loads," *J. of Sound and Vibration*, 1985, **99**(1), 1-12.
- 112 Ono, K. and Yamada, M., "Analysis of railway track vibration," *J. of Sound and Vibration*, 1989, 269-297.
- 113 Patil, S.P., "Response of infinite railroad track to vibrating mass," *J. of Engineering Mechanics*, 1988, **114**, 688-703.
- 114 Patil, S.P., "Natural Frequencies of A Railroad Track," *J. of Applied Mechanics*, 1987, **54**, 299.
- 115 Paul, B., "Surface and subsurface stresses associated with non-Hertzian contact," *Proceedings Contact Mechanics and Wear of Rail/Wheel Systems*, Vancouver, Canada, 1982.
- 116 Paz, M., Structure dynamics, Van Nostrand Reinhold, New York, 3rd edition, 1991.
- 117 Prasad, B. and Garg, V. K. "Dynamic models of a railroad track system. *Applied Mathematical Modelling*," 1979, **3**, 359-366.
- 118 Private Conversation with Mr. Wilson Pak at Research and Development Dept. of PC Rail System.
- 119 Radford, R. W., "Wheel/rail vertical forces in high-speed railway operation," *J. of Engineering for Industry*, 1977, 849-858.
- 120 Rao, S.S., The finite element method in engineering, Pergumon Press, 1982.
- 121 Raymond, G.P., "Analysis of track support and determination of track modulus," *Transport. Research Record. No. 1022*, 1985, pp.80-90.
- 122 Reddy, J.N., An introduction to the finite element method, McGraw-Hill Book Company, 1988.

- 123 Remington, P.J.,** "Wheel/rail squeal and impact noise: what do we know? what don't we know? Where do we go from here?" *J. of Sound and Vibration*, 1985, **116**, 339-353.
- 124** "Roaring rails explained?" *Railway Engineering*, 1988/2, pp28-29.
- 125 Rucker, W.,** "Dynamic interaction of a railroad-bed with the subsoil," *Soil Dynamics & Earthquake Engineering Conf. Southampton*, 1982, 435-448.
- 126 Sankar, T. S. and Samaha, M.,** "Research in rail vehicle dynamics-state of the art," *Shock and Vibration Digest*, 1986, **18(2)**, 9-18.
- 127 Sato, Y.,** "Study on high frequency vibrations in track operated with high-speed trains," *JNR, Railway Technical Reviews, Quarterly Report*, 1977, **18**, 109-114.
- 128 Sato, Y.,** "Evaluation of rail head surface configuration viewed from wheel load variation," *JNR, Railway Technical Reviews, Quarterly Report*, 1983, **24(2)**, 68-71.
- 129 Suda, Y. and Iguchi, M.,** "Basic study of corrugation mechanism on rolling contact in order to control rail surfaces," *Proceedings of 11th IAVSD Symposium*, Kingston, Canada, 1989, 566-577.
- 130 Sato, Y., Odaka, T. and Takai, H.,** "Theoretical analyses on vibration of ballasted track," *JNR, Railway Technical Reviews, Quarterly Report*, 1988, **29(1)**, 30-32.
- 131 Schneider, E. and Popp, K.,** "Noise Generation in railway wheels due to rail-wheel contact forces," *J. of Sound and Vibration*, 1988, **120(2)**, 227-244.
- 132 Schneider, H-J., Elf, H.P. and Kollé, P.,** "Modelling of travelling-loads and time-dependent masses with ADINA," *Computers & Structures*, 1983, **17(5-6)**, 749-755.
- 133 Schwab, C. A., and Mauer, L.,** "An interactive track/train dynamics model for investigating system limits in high speed track," *Proceedings of 11th IAVSD Symposium*, Kingston, Canada, 1989, 502-514.
- 134 Scott, J.F.,** "Evaluation of concrete turnout ties and bridge ties," *AREA Bulletin 706*, Vol. 87, May 1986, pp. 216-234.

- 135 Shah, V.N., Cook, R.D. and Huang, T.C.,** "Loads moving on beam supported by layered elastic foundation," *ASME Journal of Mechanical Design*, 1980, **102**, 295-302.
- 136 Shaw, M., de Josez, B. and Griffin, K.,** "Track/train dynamics," *Report No. TP-11251E*, Research and Development Department, CP Rail System, Vol 8, 1992.
- 137 Shen, Z.Y., Hedrick, J.K. and Elkins, J.A.,** "A comparison of alternative creep force models for rail vehicle dynamics analysis. *Proc. of 8th IAVSD Symposium*, Cambridge, MA, 1983, pp.591-605.
- 138 Singh, V.V. and Deepak, D.,** "Evaluation of track stiffness and track damping. *J. of Sound and vibration*, 1984, **97**(1), 129-135.
- 139 Smith, C.C. and Wormley, D.J.,** "Response of continuous periodically supported guideway beams to traveling vehicle loads," *J. Dyn. Syst., Measurement, and Control*, 1975, **97**, pp.21-29.
- 140 Smith, R.E. Bullock, R.L. and Lin, M.W.,** "Track/train interaction-resonance as a cause of structural failure," *RTD-Vol 6, Rail transportation, ASME*. 1993, 53-59.
- 141 Srinivasan, M.,** Modern permanent way. *Somaiya Publications Pvt Ltd, Bombay*, 1969, pp. 399-408.
- 142 Steele, C.R.,** "The Timoshenko beam with a moving load," *J. of Applied Mechanics*, 1968, **35**.
- 143 Stewart, H. E.,** "Measurement and prediction of vertical track modulus," *Transportation Research Record* 1022, U.S.A.
- 144 Sueoka, A., Ayabe, T., Kawakami, M. and Tamura, H.,** "An approximate model with an infinite number of vehicles for analysis of coupled vibrations between railway vehicle wheels and rail in the vertical direction," *JSME International Journal*, 1988, **31**(4), 739-747.
- 145 Sueoka, A., Ayabe, T., Kawakami, M. and Yamamoto, N.,** "Coupled vibrations between railway vehicle wheels and the rail," *Bull. JSME*, 1986, **29**, 4344.
- 146 Taheri, M. R., Ting, E. C. and Kukreti, A. R.,** "Vehicle-guideway interactions: a literature review," *Shock Vib. Dig.*, 1990, **22**(6), 3-9.

- 147 Tassilly, E. and Vincent, N.,** "A linear model for the corrugation of rails," *J. of Sound and Vibration*, 1991, **150**(1), 25-45.
- 148 Thomas, J. and Abbas, B.A.H.,** Finite element model for dynamic analysis of Timoshenko beam. *J. of Sound and Vibration*, 1975, **41**(3), 291-299.
- 149 Thompson, D. J.,** "Theoretical modelling of wheel-rail noise generation," *Proceedings of Institution of Mechanical Engineers, Part F*, 1991, **205**, 137-149.
- 150 Ting, E. C., Genin, J. and Ginsberg, J. H.,** "A general algorithm for moving mass problems," *J. of Sound and Vibration*, 1974, **33**, 49-58.
- 151 Torby, B. J.,** "Deflection results from moving loads on a beam that rests upon an elastic foundation reacting in compression only," *Journal of Applied Mechanics*, 1975, 738-739.
- 152 Tunna, J. M.,** "Wheel/rail force due to wheel irregularities," *Proceedings Ninth International Wheelset Congress*, paper 6-2, Montreal, Canada, Oct. 1988.
- 153 Tuten, J.M. and Harrison, H.D.,** "Design, validation and application of a monitoring device for measuring dynamic wheel/rail loads," *ASME Paper No. 84-WART-10*, 1984.
- 154 Weitsman, Y.,** "On foundations that react in compression only," *J. of Applied Mechanics*, December 1970, 1019-1030.
- 155 Wilkinson, J.H.,** The algebraic eigenvalue problem Oxford, Clarendon Press, 1965.
- 156 Williams, F.W. and Wittrick, W.H.,** "An automatic computational procedure for calculating natural frequencies of skeletal structures," *International Journal of Mechanical Sciences*, 1970, **12**(9), 781-791.
- 157 Williams, S., Ahlbeck, D.R. and Harrison, H.D.,** "Railroad bearing performance under the wheel impact load environment," *ASME Winter Annual Meeting, Session RT-2*, December 16, 1987.
- 158 Zhai, W. and Sun, X.,** "A detailed model for investigating vertical interaction between railway vehicle and track," *Proc. of 13th IAVSD-Symposium on the Dynamics of Vehicle on Roads and on tracks*, Chengdu, China, Aug. 1993.

- 159 Darglos, J.,"Opening speech" 4th International Conference of Wheel/Rail Wear and Contact Mechanics, Vancouver, Canada, July 1994.**
- 160 Grassie, S.L. and Kalousek, J., "Rail corrugation: characteristics, causes and treatments" Proc. Inst. Mech Engrs, Part F, 1993.**